

Study on Uncertainty Modeling and
Sampling Scheme with Focus on Tail
Distribution Applied to Biomechanics
Simulation of Pressure Ulcer

September 2014

Samuel Susanto Slamet

DISSERTATION

*Submitted to the School of Science for Open and Environmental Systems, Keio
University, in partial fulfillment of the requirements for the degree of Doctor of
Philosophy*

ABSTRACT

In the field of computational mechanics, ever since the publication of guideline for validation of finite element analysis by the American Society of Mechanical Engineers in 2006, uncertainty modeling is becoming an important issue not only in the industries but also in the academic research because they require huge computational cost when Monte Carlo simulation is used. The uncertainties of input parameters for finite element analysis are usually expressed by probability density function (pdf). However, epistemic uncertainty is lacking in accuracy of pdf and confidence. In other words, there remains a problem in the uncertainty modeling when it is hardly expressed by pdf. Also in the Monte Carlo simulation, the prediction of the critical value of quantity of interest (QoI) is not easy and the case with very low frequency is hard to be validated because it will rarely happen in real life situation.

Hence, this thesis proposed practical sampling scheme for Monte Carlo simulation with focus on QoI in the tail distribution, which was named as stepwise limited sampling (SLS) method. The uncertainty parameters with and without defined pdf were considered in this study. Mathematical description of those uncertainty parameters and every computational procedure were presented. This method consists of three steps. The first step is the convergence check of the expected value of QoI. New methodology for convergence check was proposed and verified. The second step is the definition of limited sampling zone. The parameters in this limited sampling zone may result in a critical value of QoI. It was approximated by polygon after choosing two parameters among many

parameters, which contributed to the automatic processing in the computer program and also for the projection process to reduce the number of uncertainty parameters. The third step is the analysis of tail distribution by generating random numbers in the limited sampling zone.

This proposed method was then applied to biomechanics analysis of pressure ulcer with assumption that tiny damage in fibril tissue at the bone-muscle interface in human buttock is the trigger of this disease. Seven parameters were taken into consideration including Young's modulus of fat and muscle, shear modulus of fat, volume fraction of fat and muscle, loading condition, length and location of fibril tissue damage modeled by cutout in finite element method. Three parameters with respect to the mechanical properties of fat and muscle were expressed by pdf. On the other hand, pdf was not given to other four parameters. The proposed SLS method could successfully analyze the tail distribution and critical combination of parameters were obtained that result in very high shear strain value at the cutout tip at the bone-muscle interface following the prediction of occurrence of pressure ulcer. The biomechanics analysis could also explain the reoccurrence of pressure ulcer even after the surgical treatment. Through this demonstration of SLS method, the reliability and usefulness of the obtained tail distribution were proven together with its cost-effectiveness to be used in wide engineering fields.

ACKNOWLEDGEMENT

First of all, I would like to express my sincere gratitude to my advisor Prof. Naoki Takano, for making my study in Japan possible. His continuous support, patience, motivation, and enthusiasm with my study and research for 5 years in Japan from Master degree to Ph.D. has been very helpful. I'm very grateful to have him as my advisor.

Besides my advisor, I would like to thank the rest of my thesis committee: Prof. Kenji Oguni, Assoc. Prof. Masayuki Kohiyama, and Assoc. Prof. Masaki Omiya for their time, hard questions, criticisms, and advices during the hearing and private discussions.

My thanks also goes to Prof. Tomohisa Nagasao and Dr. Asako Hatano from Keio University Hospital for sharing their knowledge and CT-image data regarding pressure ulcer.

For the financial support, I would like to thank the Japanese Government (Monbukagakusho), the Keio Leading-edge Laboratory (KLL) and Grants-in-Aid for Scientific Research (KAKENHI).

I would also like to thank my lab mates, especially those who helped in the process of my thesis: Yoshiyuki Tanabe, Kohta Okamoto, Kyohei Hatano, Yuta Shimizu, Nobuhito Ibaraki and all the other lab members for sharing the ups and downs in the laboratory with me. Also thanks to my Indonesian friends in Japan, Aryabhima, Anditto, Heryanto and Sandy.

Finally, I would like to acknowledge the support and encouragement provided by my family during my studies in Japan.

TABLE OF CONTENT

CHAPTER 1.....	1
INTRODUCTION	1
1.1 MOTIVATION	1
1.2 ORGANIZATION OF THESIS	7
CHAPTER 2.....	10
LITERATURE REVIEW	10
2.1 STOCHASTIC FINITE ELEMENT METHOD	10
2.2 STOCHASTIC RESPONSE SURFACE METHOD	11
2.3 MOST PROBABLE POINT METHOD	12
2.4 MONTE CARLO SIMULATION	12
CHAPTER 3.....	15
COMPUTATIONAL METHOD OF TAIL DISTRIBUTION ANALYSIS BY STEPWISE LIMITED SAMPLING .15	
3.1 SETUP OF UNCERTAINTY PARAMETERS	15
3.2 CONVERGENCE CHECK	18
3.3 DEFINITION OF LIMITED SAMPLING ZONE AND ITS PROJECTION	19
3.4 ANALYSIS OF TAIL DISTRIBUTION	21
CHAPTER 4.....	22
BIOMECHANICS PROBLEM SETTING OF PRESSURE ULCER	22
4.1 BACKGROUND AND LITERATURE REVIEW	22
4.2 ASSUMPTION OF BIOMECHANICS	25
4.3 UNCERTAINTIES IN INPUT PARAMETERS	26
4.4 EXPERIMENTAL MODEL	30
4.5 FINITE ELEMENT DISCRETIZATION AND QUANTITY OF INTEREST	38
4.6 PREDICTION RULE OF PRESSURE ULCER OCCURRENCE	43
CHAPTER 5.....	50
NUMERICAL RESULTS	50
5.1 DEFORMATION AND STRAIN DISTRIBUTION	50

5.2 CONVERGENCE OF EXPECTED VALUE	54
5.3 LIMITED SAMPLING ZONE	55
5.4 PROJECTION OF LIMITED SAMPLING ZONE	64
5.5 RESULTS OF TAIL DISTRIBUTION ANALYSIS	71
CHAPTER 6.....	74
DISCUSSIONS	74
CHAPTER 7.....	77
CONCLUSIONS.....	77
7.1 FINDINGS	77
7.2 LIST OF ASSUMPTIONS AND LIMITATION	79
7.3 FUTURE WORKS	80
APPENDIX A.....	82
CONVERGENCE CHECK, PREDICTION RULE OF PRESSURE ULCER OCCURRENCE AND LIMITED SAMPLING ZONE.....	82
APPENDIX B.....	137
LIST OF PUBLICATIONS.....	137
ARTICLES ON PERIODICALS	137
ARTICLES ON INTERNATIONAL CONFERENCE PROCEEDINGS	137
PRESENTATIONS AT INTERNATIONAL CONFERENCES	138
PRESENTATIONS AT DOMESTIC CONFERENCES	138
REFERENCES.....	140

LIST OF FIGURES

Figure 1.1: Phases of modeling and simulation and the role of verification and validation.
 3

Figure 1.2 Very rare case x is located at $QoIx \geq QoIc$. The sampling scheme in this thesis
 is to find a sampling point $x \in (QoIx \geq QoIc)$ 4

Figure 1.3: Steps in probabilistic study. 6

Figure 1.4: A graphical representation of the Stepwise Limited Sampling (SLS) method.
 The method starts with the setup of uncertainty parameters in Chapter 3.1. 7

Figure 1.5: Hierarchical approach and respective chapters in this thesis. 9

Figure 2.1: The basic analysis on Monte Carlo simulation (Schenk and Schuëller, 2005)
 14

Figure 3.1 Approximation of pdf performed when the data is not enough 16

Figure 3.2 Case where the histogram to generate the pdf is mostly flat. 16

Figure 3.3: An illustration of the uncertainty parameters considered in the analysis. The
 description for each parameter can be seen in Eq. (3.1) and Eq. (3.2). $y_n = y_w$ is the
 location of where the tail distribution will be analyzed and will be explained more
 in Chapter 3.4. 17

Figure 3.4: Concept of definition of limited sampling zone for two input parameters with
 pdf notated by x_i and x_j that are independent to each other. Examples of the
 approximation equations forming the limited zones by polygon are shown in the
 green and yellow areas. 20

Figure 3.5: An illustration of a projection of $LSZ_{ij}(y_k, y_l)$ following Eq. (3.6). 20

Figure 4.1: CT image of a human buttock showing the loose fibril tissue. It is a simplified numerical modeling by assuming that the initial damage occurs at the interface between bone and muscle by the loose fibril tissue damage.	26
Figure 4.2: Typical human buttock with mathematical parameters showing material properties, contour shape, cutout location and boundary condition.....	27
Figure 4.3: Items used in the experiment	30
Figure 4.4: Supine position into complete lateral position A.....	31
Figure 4.5: Supine position into complete lateral position B.	32
Figure 4.6: Supine position into complete lateral position C.	32
Figure 4.7: Experiment with and without the bed sheet for supine position into complete lateral position A and supine position into complete lateral position B.....	33
Figure 4.8: Experiment with and without the bed sheet for supine position into complete lateral position C.....	33
Figure 4.9: Contact area during supine position.....	35
Figure 4.10: Measured length during supine position.	35
Figure 4.11: Contact area during lateral position.	36
Figure 4.12: Measured length during lateral position.....	36
Figure 4.13: Contact area during movement from supine to lateral position.....	36
Figure 4.14: Measured length during position change from supine to lateral position. .	37
Figure 4.15: Comparison of areas during position change from supine to lateral position. The difference can be seen in the red area.....	38
Figure 4.16: Finite element mesh used for the analysis. Evaluation of interface strains at cutout tips is also shown in the bottom left. The goal is to find QoI for normalized strains ε_n and γ_m w.r.t parameters on left and right tips of cutout. The evaluation of strain was done using extrapolation.....	40

Figure 4.17: The location of loading area during supine position.....	41
Figure 4.18: The location of loading area during lateral position. The left picture is for lateral-A position and the right picture is for lateral-B position.....	42
Figure 4.19: Finite element model of damaged interface for the healthy model.....	43
Figure 4.20: Finite element model of damaged interface for the after surgery model...	44
Figure 4.21: ε_n for the healthy body model with cutout.	45
Figure 4.22: $ \gamma_m $ for the healthy body model with cutout.....	46
Figure 4.23: ε_n for the after surgery model with cutout.....	46
Figure 4.24: $ \gamma_m $ for the after surgery model with cutout.	47
Figure 4.25: Typical result for the extrapolation of strains for the healthy model with cutout.	48
Figure 4.26: Typical result for the extrapolation of strains for the after surgery model with cutout.	48
Figure 4.27: Flowchart of prediction rule of pressure ulcer.....	49
Figure 5.1: Deformation of the mesh from original deformation value to 5x deformation value.	50
Figure 5.2: Strain distribution of ε_x , ε_y and γ_{xy} with supine loading condition for $a_{mid1} = 42.34$ mm.....	51
Figure 5.3: Strain distribution of ε_x , ε_y and γ_{xy} with supine loading condition for $a_{mid2} = 104.38$ mm.....	52
Figure 5.4: Strain distribution of ε_x , ε_y and γ_{xy} with supine loading condition for $a_{mid3} = 166.63$ mm.....	53
Figure 5.5: A convergence check example for $\bar{s}(E_{muscle}, E_{fat}, G_{fat} 9.69, \text{supine}, 4, 104.38)$.	
Following Eq. (3.4), the left hand side of the equation is shown in the blue line and	

the right hand side of the equation is shown in the red line. The red circle shows the area where the equation is satisfied three times continuously..... 54

Figure 5.6: Prediction rule of pressure ulcer occurrence at $s(G_{fat}, 9.69, lateral-A, 8, 104.38)$.
..... 56

Figure 5.7: Mathematical form used to determine automatic limited sampling zone. 58

Figure 5.8: Example of defining the limited sampling zone of $s(G_{fat}, I_{fm} = 9.69, b = lateral - A, L_a = 8, a_{mid} = 104.38 | E_{muscle}, E_{fat}; p_a E_{muscle} + q_a E_{fat} + r_a \geq 0 \forall a)$ 59

Figure 5.9: Limited sampling zone at $s(G_{fat}, I_{fm} = 9.69, b = lateral - A, L_a = 8, a_{mid} = 104.38)$.
The limit is defined in the material properties in Table 3.1. 59

Figure 5.10: In order to make the projection, the related LSZ for all $L_a = 4$ and $a_{mid} = 104.38$ are unioned into a single LSZ. The figure here shows an example for the projection for $s(G_{fat}, L_a = 4, a_{mid} = 104.38 | E_{muscle}, E_{fat}, I_{fm}, b; p_a E_{muscle} + q_a E_{fat} + r_a \geq 0 \forall a)$ 65

Figure 5.11: Projection result for $s(G_{fat}, L_a = 4, a_{mid} = 104.38 | E_{muscle}, E_{fat}, I_{fm}, b; p_a E_{muscle} + q_a E_{fat} + r_a \geq 0 \forall a)$ as shown in the multi dimension figure. The dashed line for I_{fm} and b means that those parameters has been projected into L_a and a_{mid} .
..... 65

Figure 5.12: This figure shows the location of the sampling point to be analyzed in the yellow box. Currently the 4 surrounding LSZ are the only known LSZ as shown in the figure above. Rather than restarting the analysis from the beginning to find the LSZ at $L_a = 4$ mm and $a_{mid} = 70.88$, a linear interpolation is performed. 66

Figure 5.13: The initial sampling points with limited sampling zone that was created. This figure also shows the location of sampling points that are going to be analyzed... 67

Figure 5.14: A general form for linear interpolation calculation. The process involves changing the equation of polygon in y_u and y_v into points and then performing the interpolation into y_w from those points. After the interpolation of the points, the polygon is then regenerated in y_w 67

Figure 5.15: The first two interpolation process were performed for $LSZ_{E_{muscle} \& E_{fat}}(\mathbf{I}_{fm}, \mathbf{b})^{a_{mid}=70.88 \& L_a=4}$ and $LSZ_{E_{muscle} \& E_{fat}}(\mathbf{I}_{fm}, \mathbf{b})^{a_{mid}=70.88 \& L_a=8}$ 69

Figure 5.16: The second interpolation process was performed at the sampling points to be analyzed for $LSZ_{E_{muscle} \& E_{fat}}(\mathbf{I}_{fm}, \mathbf{b})^{a_{mid}=70.88 \& L_a=6}$ 69

Figure 5.17: Tail distribution of pressure ulcer occurrence at $L_a = 6$ mm and $a_{mid} = 70.88$ mm showing the highest $|\gamma_m|$ values at b_2 (supine). Verification points are also shown in this figure showing 2 verification location. 71

LIST OF TABLES

Table 4.1: Material properties based on linear isotropic model.	29
Table 4.2: Calculated length during supine position as shown in Fig. 4.10.	35
Table 4.3: Calculated length during lateral position as shown in Fig. 4.12.	36
Table 4.4: Calculated length during movement from supine to lateral position as shown in Fig. 4.14.	37
Table 4.5: Boundary conditions for three positions including load value, angle, loaded area and constraint.	42
Table 5.1: Convergence check results for 54 discrete combination of sampling points.	55
Table 5.2: Equations that shapes the polygon that governs the limited sampling zone of pressure ulcer occurrence at $s(G_{fat}, I_{fm} = 9.69, b = lateral-A, L_a = 8, a_{mid} = 104.38)$.	59
Table 5.3: All governing equations for all 54 combination of discrete sampling points.	61
Table 5.4: Equations that shapes the polygon that governs the limited sampling zone of pressure ulcer occurrence at $L_a = 6$ mm and $a_{mid} = 70.88$ mm.	70
Table 5.5: Obtained combination of parameters related to the highest strain value in the tail distribution of pressure with verification.	70

CHAPTER 1

Introduction

1.1 Motivation

The quality assurance of engineering simulation is essential ever since the American Society of Mechanical Engineers (ASME) published the guidelines for verification and validation (The American Society of Mechanical Engineers, 2006, 2009, 2012). In Japan, The Japan Society for Computational Engineering and Science (JSCES) published two standards on the quality management and model procedure for engineering simulation (The Japan Society for Computational Engineering and Science, 2011a, 2011b). These two JSCES standards followed ISO and NAFEMS (Hellen, 2004) in the United Kingdom. The main concern of verification and validation is to assess the accuracy of a computational simulation, which is required to provide confidence that the results from the computational models are accurate and to solve the intended problem. It is important in engineering and biomechanics fields to obtain validation by creating a model that is an accurate representation of a real object. However, validation must be preceded by code and solution verification.

ASME (2012) defines verification as the process of determining that computer model accurately represents the underlying mathematical equations and their solution. The verification process has two aspects: code verification and calculation verification. Code verification is the process of ensuring that there are no programming errors and that

the numerical algorithms used will yield accurate solutions. Calculation verification is defined as the process of determining the solution accuracy of a particular calculation. Again, ASME (2012) defines validation as the process of determining the degree to which a computational model is an accurate representation of the real world from the perspective of the intended uses of the model. Validation process involves the comparison of computational results of the modeling and simulation process with experimental data from various sources (Oberkampf et al., 2004; American Institute of Aeronautics and Astronautics, 1998). A method proposed by Coleman and Stern (1997) uses the concept from experimental uncertainty modeling to consider the errors and uncertainties in both the solution and the data (The American Society of Mechanical Engineers, 2009).

A graphical representation of this verification and validation process can be seen in Fig. 1.1, which was made based on the figure made by Society for Computer Simulation (SCS) in 1979 (Oberkampf et al., 2004). The figure shows two types of model, conceptual and computerized model. The conceptual model contains mathematical modeling data and equations while the computerized model contains an operational computer program that implements the conceptual model itself. With the verification and validation, the accuracy of the conceptual and computerized model can be assessed.

Subsequently, the uncertainty modeling of practical problems in the engineering and biomechanics fields is becoming a matter of interest. In the experimental works, it is quite natural to consider the uncertainty. On the other hand, in the engineering simulation, the consideration of uncertainty usually requires huge computational cost and therefore most of the industries are hesitating to carry out the probabilistic and/or stochastic analysis. ASME (2012) described the numerical error in detail, but

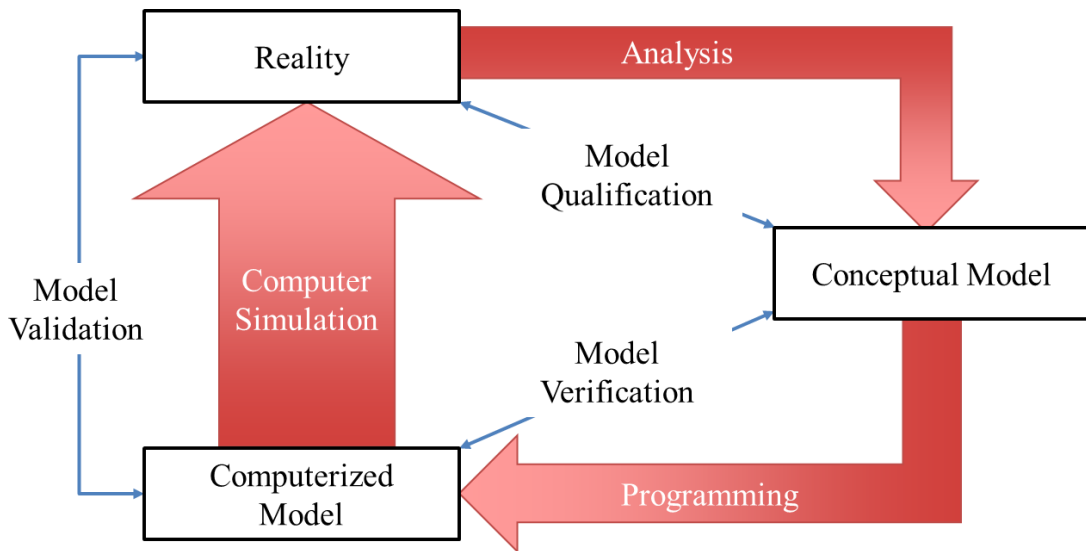


Figure 1.1: Phases of modeling and simulation and the role of verification and validation.

the practical computational methods are not discussed except very classical Monte Carlo method and Latin Hypercube Sampling (LHS). JSCES standards (The Japan Society for Computational Engineering and Science, 2011a, 2011b) described nothing about the uncertainty modeling and simulation. On the other hand, NAFEMS summarized more practical computational methods and many examples in industries (Thacker, 2008). Some more details on the state-of-the-art of probabilistic/stochastic finite element methods are discussed in Chapter 2.

However, there still remain many problems in the probabilistic/stochastic finite element analysis. The case with very low frequency is hard to validate because it will never happened in real life situation. Engineers have difficulties due to the lack of knowledge about some parts of a process and as such it is difficult to describe the true behavior of real-world system with sufficient accuracy (Rauh, 2011). Meanwhile, an accurate prediction of tail distribution is important especially when human life is put into consideration. Risk can be minimized but not eliminated completely (Haldar and Mahadevan, 2000). Serious accident can happen in very rare case of combination from

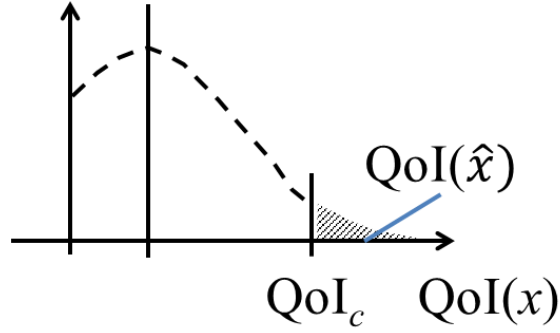


Figure 1.2 Very rare case \hat{x} is located at $QoI(\hat{x}) \geq QoI_c$. The sampling scheme in this thesis is to find a sampling point $\hat{x} \in (QoI(x) \geq QoI_c)$.

internal and external parameters. The missing combination of very rare case can be found in the tail region. Shown in Fig. 1.2, tail region is defined as the region where the quantity of interest (QoI) of input parameter x is larger than or equal to QoI_c . The probability function of QoI in the tail region is the tail distribution and the integral in the tail is the tail probability as shown in the following equation:

$$\int_{QoI(x) \geq QoI_c} f(QoI(x)) dx \quad (1.1)$$

The practical and effective computational scheme for tail distribution analysis is still an open problem. This thesis will give a methodology to resolve that problem.

In this thesis, the term “tail distribution analysis” or “analysis of tail distribution” was defined by finding a very rare case \hat{x} where $\hat{x} \in (QoI(x) \geq QoI_c)$. After that, the sampling points are analyzed by FEM. The probability is not calculated but the term tail region is not a clear term so tail distribution is used. The term in the thesis title “sampling scheme with focus on tail distribution” means how to find this very rare sampling case of \hat{x} . The term tail distribution was used because there was known term for the above group of $(QoI(\hat{x}) \geq QoI_c)$.

Uncertainties in engineering design are unavoidable and it is important for current industry to have a method that can handle very large number of uncertainty parameters with high accuracy and low computational cost. This in turn will help the industry to

make a better decision in design. Measures of uncertainty is difficult to obtain but uncertainty in software can still be measured (Dienstfrey, 2012). ASME (2006) and NAFEMS (2008) defines two kinds of uncertainties, irreducible uncertainties (aleatory) and reducible uncertainties (epistemic). In finite element analysis and Monte Carlo simulation, reducible (epistemic) uncertainties are often discussed now. Both of these uncertainties can be defined in the form of a probability density function (pdf) by mean values and standard deviation but not all uncertainties can be defined in pdf form, because there are some cases that the uncertainties cannot represent the situation in pdf form correctly. In that case, discrete sample points are instead defined for that particular uncertainties. The necessary statistical information can be extracted following Fig. 1.3 for steps in probabilistic study based on Haldar and Mahadevan (2000).

The probability density function (pdf) is a function to express the scattered data, which is defined by the histogram of raw data with always some assumption or approximation. Even if the number of raw data is enough, it is not good to assume the normal distribution, which is also written in ASME (2006). In the past project on the skin biomechanics study for microneedle array design, mixed Weibull distribution was assumed. In that experience, the accuracy of the assumed pdf is not good especially in the area leading to the tail distribution of QoI. This thesis does not give guide when pdf should be used and when histogram should be used in the definition of input parameters with pdf and without defined pdf, which is up to the users.

Currently, there are several known methods to analyze uncertainties in modeling such as stochastic finite element method (Stochastic FEM), stochastic response surface method (SRSM), and most probable point uncertainty analysis (MPPUA). These methods will be discussed more in Chapter 2.

Another known method is the Monte Carlo simulation that can perform uncertainty analysis regardless of the complexity of the model but has a drawback of a very high computational cost to solve it (Schenk and Schuëller, 2005; Gamerman and Lopes, 2006; Rubinstein and Kroese, 2008; Sakata et al., 2013b). In this thesis, a computational procedure is proposed to obtain both sufficiently accurate expected value of the quantity of interest and the tail distribution in the Monte Carlo simulation with finite element analysis. This method consists of three-step procedures. First, the Monte Carlo simulation is suspended when the expected value of quantity of interest reaches the convergence. Second, the limited sampling zone is determined by the calculated results

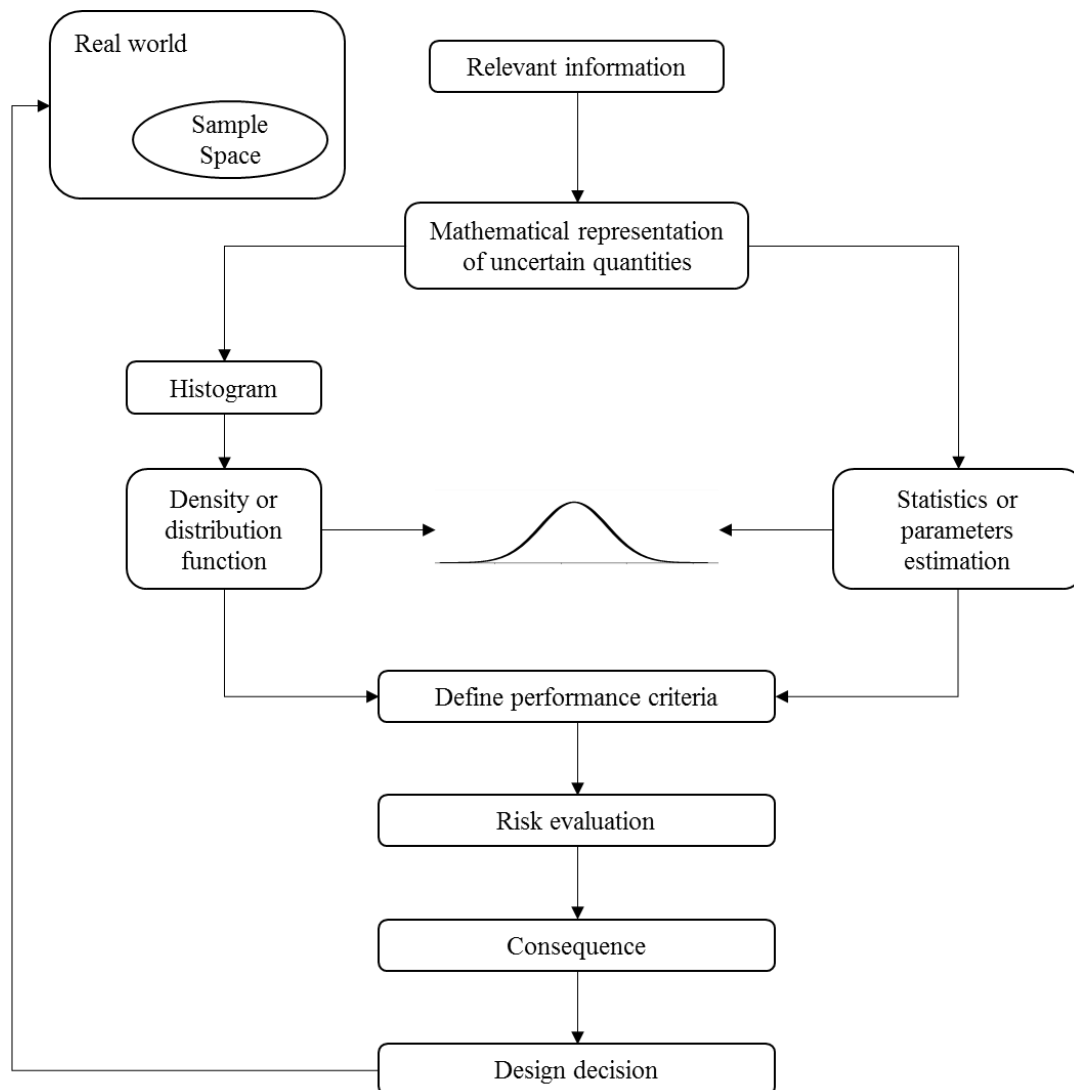


Figure 1.3: Steps in probabilistic study.

in the first step so that the probable combination of input parameters in this zone will lead to critical results. Variety of uncertainty parameters are considered and some of them are not expressed by probability density function. A projection scheme is proposed in the second step for those parameters without defined probability density function, which contributes to the reduction of number of parameters. Finally, the second Monte Carlo simulation is performed to analyze the tail distribution using only the random sample points in the limited zone. This three-step scheme is named the stepwise limited sampling (SLS) method. See Fig. 1.4 for a graphical representation of this SLS method.

This method was then applied to analyze the tail distribution analysis of pressure ulcer. Pressure ulcer is a disease that occurs in the human body and involves human life.

1.2 Organization of Thesis

This thesis is organized into seven chapters. The introduction shown in Chapter 1 here focused on drawing the whole view of the current activities for verification and validation of engineering simulation as a motivation of this research work. Following it, more detailed literature review from the academic viewpoint in the finite element method,

Stepwise Limited Sampling

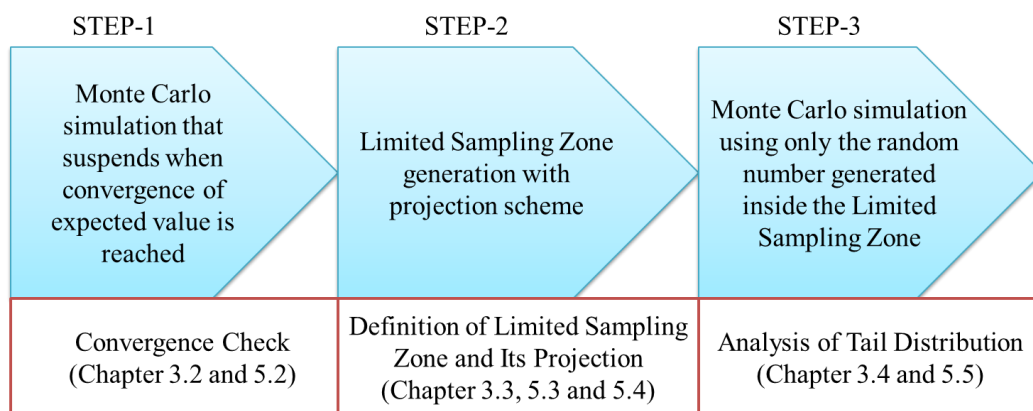


Figure 1.4: A graphical representation of the Stepwise Limited Sampling (SLS) method. The method starts with the setup of uncertainty parameters in Chapter 3.1.

several uncertainty analysis methods, and Monte Carlo simulation are introduced in Chapter 2. The main contribution of this thesis is the development of the new sampling scheme for practical Monte Carlo simulation highlighting on the tail distribution, named as stepwise limited sampling (SLS) method, which is presented in Chapter 3.

Chapters 4 and 5 are devoted to the application of the proposed method to a biomechanics problem of pressure ulcer. Chapter 4 describes the problem setting beginning with the background from medical viewpoint, assumption of biomechanics, uncertainty parameters and finite element modeling. The numerical results and discussion are shown in Chapter 5. Note here that a biomechanics analysis is one of the difficult problems from the standpoint of validation, because *in-vivo* experiments are hardly carried out or in many cases impossible. Therefore, there is a growing need for computational biomechanics simulation. The applicability of the proposed methodology to a biomechanics problem is worth discussing in this paper.

Following this demonstrative example, the overall discussion on the proposed computational scheme is given in Chapter 6. Findings, limitations and future works are summarized in Chapter 7. A graphical representation of the organization of thesis can be seen in Fig. 1.5.

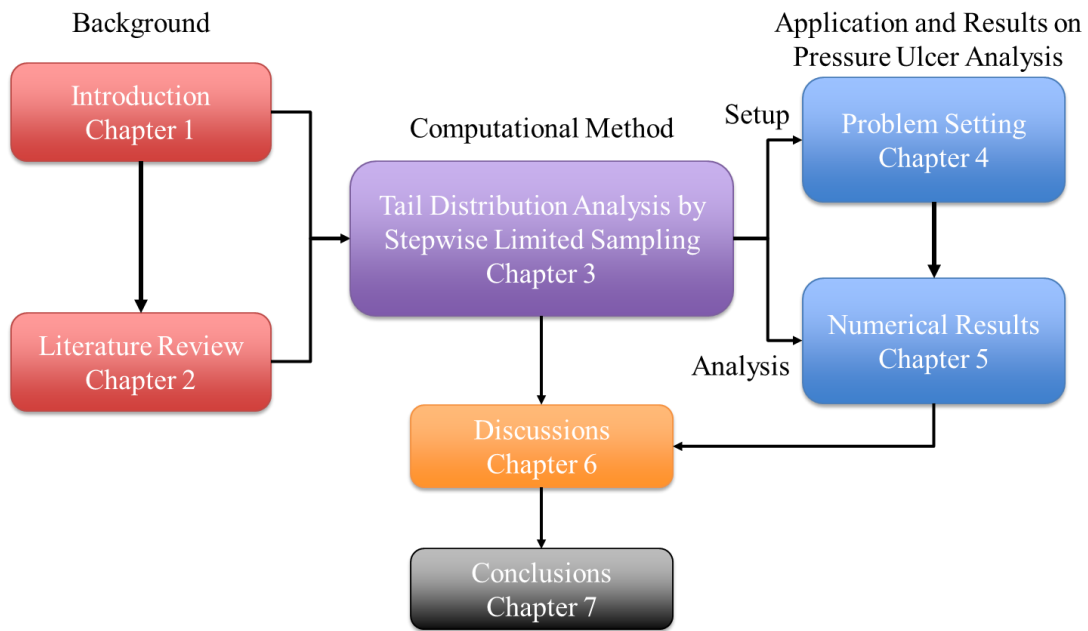


Figure 1.5: Hierarchical approach and respective chapters in this thesis.

CHAPTER 2

Literature Review

2.1 Stochastic Finite Element Method

As mentioned in Chapter 1, there are several ways to perform the analysis in uncertainty modeling. The first method discussed in this literature review is the stochastic finite element method. This method is an extension of the classical deterministic finite element approach to the stochastic framework i.e. to the solution of static and dynamic problems involving finite elements whose properties are random (Stefanou, 2009). The method is a broad and sophisticated reliability analysis method that can be used for both explicit and implicit performance functions (Haldar and Mahadevan, 2000).

An analysis of multiscale stochastic stress analysis of the porous material considering a microscopic geometrical random variation has been studied (Sakata et al., 2013a).

The stochastic finite element analysis is considered to be a useful method in comparison with the conventional sampling method or Monte Carlo simulation when the computational cost is large (Basarudin et al., 2013). Since first-order or sometimes second-order perturbation with respect to an input parameter is used, however, the applications are limited to the uncertainty in material properties and moreover only a small fluctuation such as the shape and size of the target structure, the calculation of the

derivative of strain-displacement matrix in finite element method is not accurate enough due to the nature of the finite difference approximation.

2.2 Stochastic Response Surface Method

Stochastic response surface method (SRSM) constructs a polynomial closed-form approximation. This method involves in the approximation of both input and output of an uncertain system. The propagation of input uncertainty through a model using SRSM is accomplished by expressing input uncertainties in terms of a set of random variables, then assume a functional form for selected outputs and finally the parameters of the functional approximation are determined (Isukapalli et al., 1998). Further savings in the computer resources for SRSM has been performed (Isukapalli et al., 2000). The major advantage of SRSM is that it allows existing deterministic numerical code to be used as a “black-box” within the method. However, the application of stochastic response surface method to reliability problems has not been investigated sufficiently due to reason such as computational complexity (Li et al., 2011).

According to Datta and Kushwaha (2011), the SRSM is adopted to achieve the goal in which the number of model simulations for adequate estimation of uncertainty is substantially reduced compared to conventional simulation. In that study, an analysis for a non-linear problem was demonstrated with the groundwater model, in which the injection of a tracer chemical and its corresponding concentration as a function of time and distance was presented. The SRSM is based on polynomial chaos theory and in that study the Polynomial Chaos Expansion (PCE) was applied for quantification and propagation of the uncertainty of the model output with a limited number of model run.

It seems that the success of SRSM is strongly dependent on the sampling scheme to form an accurate response surface. The difficulty always lies in the trade-off between computational cost and accuracy.

2.3 Most Probable Point Method

The most probable point method is widely used for engineering reliability analysis and reliability-based design (Du et al., 2010). It has a good balance between accuracy and efficiency. The concept of this method to analyze uncertainty analysis is to utilize the cumulative distribution function of a system output by evaluating probability estimates at a serial of limit states across a range of output performance (Du and Chen, 2001).

Reliability analysis based approaches have better accuracy compared to sensitivity based approximations and response surface modeling. Reliability analysis method are characterized by the use of analytical techniques to find a particular point in design space that can be related or approximated to the probability of system failure. This point is referred to as most probable point. The method itself has a way to improve the locating of the most probable point by employing a better search algorithm and strategy (Du and Chen, 2001).

Compared to the most probable point method, this thesis put highlight on the tail distribution region including the most probable point. In that sense, the proposed method in this paper may be categorized as an extension of the most probable point method.

2.4 Monte Carlo Simulation

Monte Carlo simulation is another method that can perform uncertainty analysis regardless of the complexity of the model but with a drawback of very high computational cost. The computational cost increases with respect to the complexity of the model.

Another close example to Monte Carlo simulation is the Latin Hypercube method. The difference between the two methods is that uncertainty distribution of every single parameter in Monte Carlo must be specified while in Latin Hypercube method the distribution is divided into a series of non-overlapping intervals of equal probability (Bieda, 2012). The Latin Hypercube was described by McKay et al. (2000) and it was said that it has an advantage when the output is dominated by only a few components. This method ensures that each of the components represented in a fully stratified manner without considering the importance.

Another very common method used in Monte Carlo simulation is the Markov Chain Monte Carlo method which can be used to approximate sample generation from an arbitrary distribution. Markov Chain is one part of Markov process. Markov process are stochastic processes whose futures are conditionally independent of their pasts given their present value. A Markov process with a discrete set is called Markov Chain and Markov process with a discrete state space and continuous index set is called Markov jump process (Rubinstein and Kroese, 2008). The Markov chain is a special type of stochastic process which deals with characterization of sequences of random variables (Gamerman and Lopes, 2006).

Important sampling is a technique to reduce the standard deviation found in an advanced Monte Carlo simulation for estimating properties of a particular distribution. It is one of the most effective variance reduction techniques other than conditional Monte Carlo (Rubinstein and Kroese, 2008). The reduction is very dramatic that sometimes it goes to the order of millions. However, the understanding is that, importance sampling is used when such combination of parameters are already obtained or provided. The importance sampling itself did not discuss on how to obtain the combination of parameters.

The Markov Chain Monte Carlo (MCMC) was proposed by Metropolis et al. (1953) when they had the idea to generating Markov chain with limits in distribution equal to the desired target distribution when handling problem in statistical physics. Some modification of the Metropolis algorithm includes the one made by Hastings (Hastings, 1970). The main idea of the Metropolis-Hastings algorithm is to simulate a Markov Chain such that the stationary distribution of this chain coincides with the target distribution (Rubinstein and Kroese, 2008).

Fig. 2.1 describes the basic principle of Monte Carlo simulation based on Schenk and Schuëller (2005). Statistics are used to give information on variability of the response. The system is described by L and set of random input variables is in vector \mathbf{x} defined in an m -dimensional vector space mapped to the r -dimensional output \mathbf{y} .

In a typical stochastic simulation, randomness is introduced into simulation models via independent uniformly distributed random variables (Rubinstein and Kroese, 2008). The accuracy of Monte Carlo simulation is very dependent on the random number algorithm generation and the number of computational cases. Using the Mersenne Twister to generate 10,000 random sampling points is not good enough for the reliability to analyze the tail distribution. Therefore, an accurate and practical sampling scheme is needed for the tail distribution analysis.

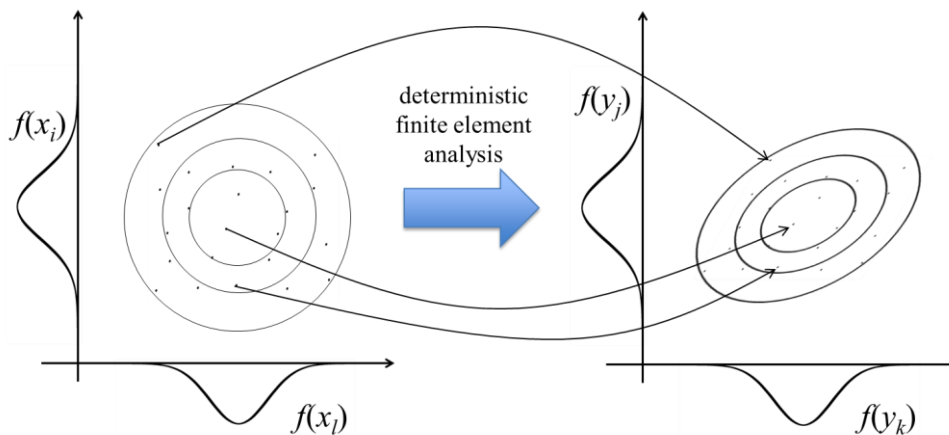


Figure 2.1: The basic analysis on Monte Carlo simulation (Schenk and Schuëller, 2005)

CHAPTER 3

Computational Method of Tail Distribution Analysis by Stepwise Limited Sampling

3.1 Setup of Uncertainty Parameters

In uncertainty modeling, there can be two kinds of input parameters: parameters with probability density function (pdf) with total parameters m_1 and parameters without defined pdf with total parameters m_2 .

An input parameter without defined probability density function (pdf) means that the pdf of this parameter is not created accurately from the histogram of measured data due to the lack of enough number of data as shown in Fig. 3.1. Note that pdf is created by approximating the histogram of measured data. Even when more number of measured data exist, we cannot assume the normal distribution. Therefore, when the number of measured data is small, which are often encounter, the proposed modeling framework allows the users to choose whether that they want to use assumed pdf or that they treat it as a parameter without defined pdf.

In this thesis, when a combination of parameters leading to critical value of QoI is obtained, the probability of that combination of parameters is not a concern. Therefore, the probability of a sampling point with respect to a parameter without defined pdf is not referred, where the sampling point will be chosen from the measured data in Fig. 3.1.

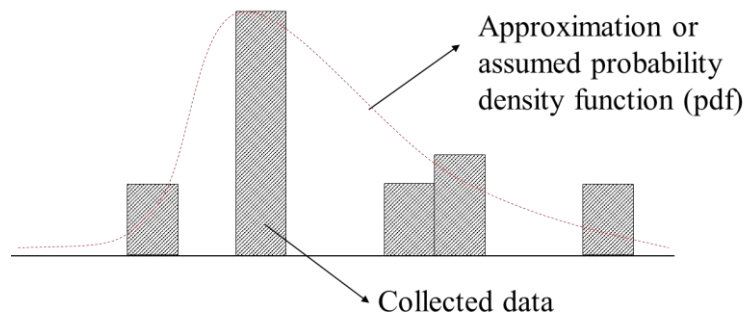


Figure 3.1 Approximation of pdf performed when the data is not enough

Histogram is mostly flat

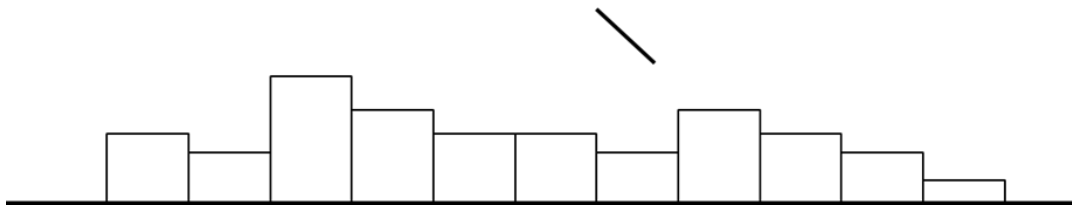


Figure 3.2 Case where the histogram to generate the pdf is mostly flat.

The histogram of the measured data and the pdf are quite different. The parameter without defined pdf should be determined based on the histogram of measured data. Note that, we do not prohibit to assume pdf if users want to use assumed pdf in the simulation.

There are some cases for parameters without defined pdf such as:

1. When histogram is not measured and the input parameter is not a single value.
2. When histogram was given by measurement but the number of data is not enough.

The user then decided not to assume the pdf.

Another good example of such parameter that cannot be approximated by pdf can be seen in Fig. 3.2. In this case, the scattering of measured data is very large and the histogram is preventing the finding of pdf. This is mostly true in inter-individual difference in biomechanical data. Even if samples were added, the histogram will be mostly flat.

The parameters with pdf are random parameters because they have histogram. When one sampling point was taken, then the sampling point can be treated as a

deterministic parameter until the union of that limited sampling zone was performed in the projection step. Since the probability of finally obtained combination of parameters leading to critical value of QoI is not a matter of concern in SLS method, the probability of each sampling points is not referred in the simulation.

In this method, s is the collection of sampling with

$$s = (\mathbf{x}, \mathbf{y}) = (x_1, \dots, x_{m_1}, \mathbf{y}_1, \dots, \mathbf{y}_{m_2}) \quad (3.1)$$

where \mathbf{x} is the parameters with pdf and \mathbf{y} is the parameters without defined pdf and instead has discrete sampling cases $N(\mathbf{y})$ or $N(\mathbf{y}_i)$. The parameters \mathbf{y} and \mathbf{y}_i are written in bold lettering because they are in the form of vectors of the parameters without defined pdf and of discrete sampling cases respectively. The parameter \mathbf{x} is written in bold lettering because it is a vector of the parameters x_i with pdf. This setup can manage large amount of input parameters that include both parameters with pdf and without defined pdf as seen in Fig. 3.3. The total number of combination of discrete sampling cases is determined as follows:

$$\prod (N(\mathbf{y})) \equiv \prod (N(\mathbf{y}_1), \dots, N(\mathbf{y}_{m_2})) = N(\mathbf{y}_1) N(\mathbf{y}_2) \dots N(\mathbf{y}_{m_2}) \quad (3.2)$$

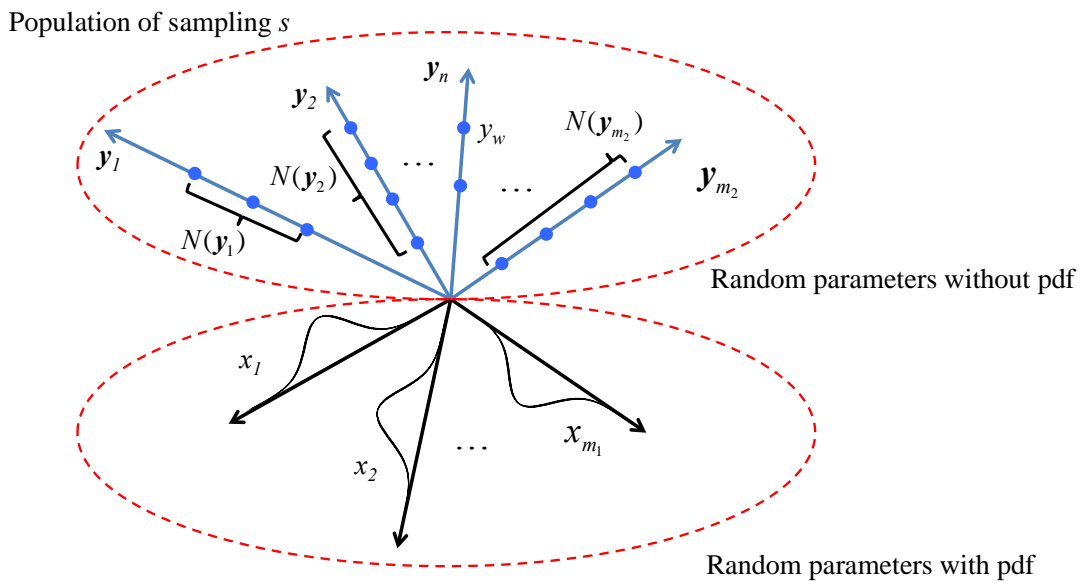


Figure 3.3: An illustration of the uncertainty parameters considered in the analysis. The description for each parameter can be seen in Eq. (3.1) and Eq. (3.2). $\mathbf{y}_n = \mathbf{y}_w$ is the location of where the tail distribution will be analyzed and will be explained more in Chapter 3.4.

The bound for parameter \mathbf{y} should be defined when determining the parameters. It is very common to have a bound and the more sampling points is preferable because the response surface will not be linear inside that particular range. In order to define this bound, the user should ask opinion of experts that can help the user to define the bound from the experience of those experts.

3.2 Convergence Check

The Monte Carlo simulation is performed with parameters \mathbf{x} for fixed parameters $\mathbf{y}_1, \dots, \mathbf{y}_{m_2}$ which is denoted by the collection of sampling \bar{s} as follows:

$$\bar{s} = \bar{s}(x_1, \dots, x_{m_1} | \mathbf{y}_1, \dots, \mathbf{y}_{m_2}) \quad (3.3)$$

Note, in this thesis, the fixed parameters are shown after the symbol “|” in the equation.

The number of combination of fixed parameters is $\prod (N(\mathbf{y}))$.

The convergence of the expected value is, in general, more easily obtained than the standard deviation (Takano et al., 2012). This is because the quality of random numbers generated in the tail distribution is not good enough using 10,000 random numbers. The convergence can be obtained if Eq. (3.4) is satisfied three times continuously because the expected value oscillates as the increase of analyses in Monte Carlo simulation (Takano et al., 2012).

$$EV(\bar{s}_{(100g)}) - EV(\bar{s}_{(100(g-1))}) \leq \frac{SD(\bar{s}_{(100)})}{EV(\bar{s}_{(100)})\sqrt{n_{max}}} \quad (3.4)$$

where $EV(\bar{s})$ denotes the expected value of QoI, $SD(\bar{s})$ the standard deviation and $g = 1, \dots, 100$ in order to stop the Monte Carlo simulation with maximum sampling points $n_{max} = 10,000$. The number of necessary sampling points is defined as $MC_{conv}(i)$ ($i = 1, \dots, \prod (N(\mathbf{y}))$). This procedure is automated in the computer program.

3.3 Definition of Limited Sampling Zone and Its Projection

The purpose of this section is to choose the possible combination of parameters leading to critical value of QoI by investigating the obtained results whose expected value is converged. Even if there are a number of input parameters, it is easy to study about sets of two parameters among all parameters. The possible zone of tail distribution can be illustrated in 2D plane with respect to the selected set of two parameters as shown in Fig. 3.4. When two parameters x_i and x_j where $i < j$ are selected, this zone is called in this thesis a limited sampling zone, LSZ_{ij} . If the zone is approximated by polygon, the zone is then bounded by multiple linear equations. Thus, LSZ_{ij} is defined by the following equation:

$$LSZ_{ij} = \{s; p_a x_i + q_a x_j + r_a \geq 0 \forall a\} \\ = s(x_1, \dots, x_{i-1}, x_{i+1}, \dots, x_{j-1}, x_{j+1}, \dots, x_{m_1}, y_1, \dots, y_{m_2} | x_i, x_j; p_a x_i + q_a x_j + r_a \geq 0 \forall a) (i < j) \quad (3.5)$$

where p_a , q_a and r_a are the coefficient factors of linear equations. In the equation, the symbol “;” denotes the condition of collection sampling. This procedure to define LSZ_{ij} can be automated because of the approximation by polygon.

The number of (x_i, x_j) planes is a combination of ${}_m C_2$ for each QoI and each $N(\mathbf{y})$. Those planes can be collected by the following procedure called projection in this thesis. The limited sampling zone, LSZ_{ij} , is individually defined in x_i - x_j plane for fixed sampling points of each \mathbf{y} . Since the same x_i - x_j plane is used, it is easy to overlap all limited sampling zone and to take a union, which is called as projection in my thesis. Figure 3.5 illustrates the concept of projection that uses union operation and is described by the following equation for a typical case where two parameters y_k and y_l without defined pdf where $k < l$ are concerned:

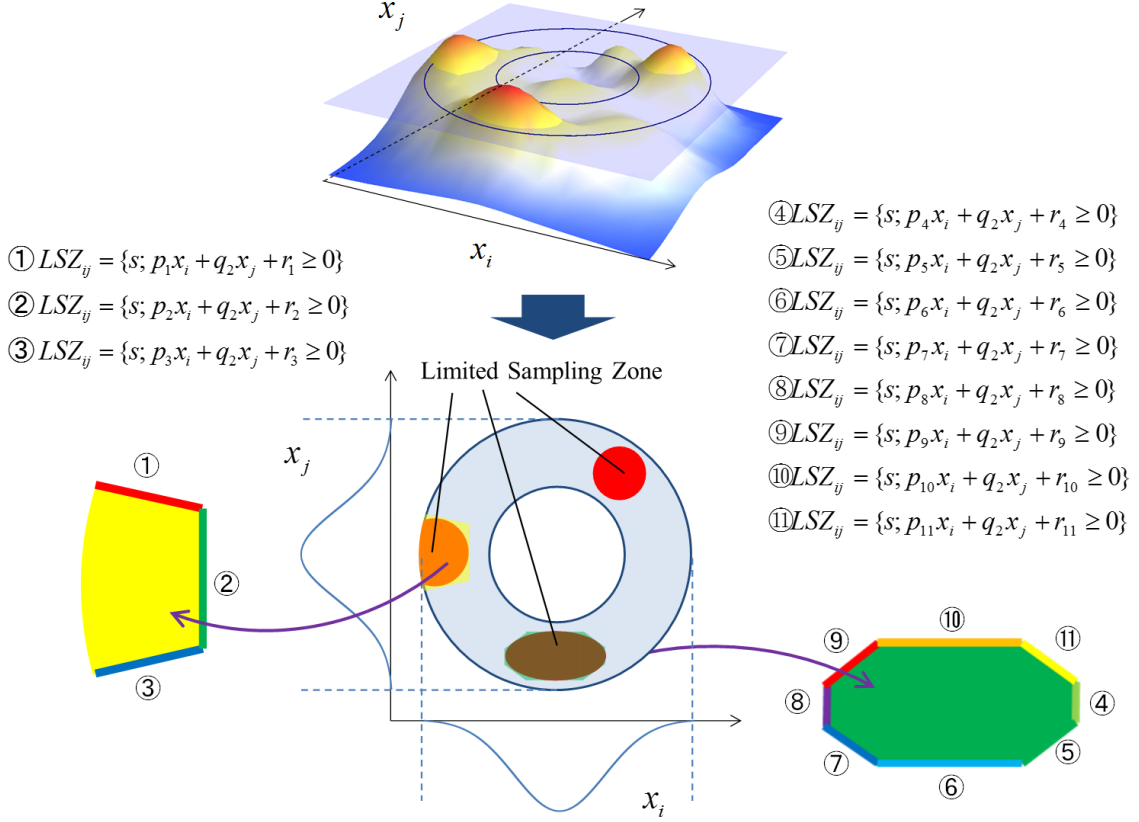


Figure 3.4: Concept of definition of limited sampling zone for two input parameters with pdf notated by x_i and x_j that are independent to each other. Examples of the approximation equations forming the limited zones by polygon are shown in the green and yellow areas.

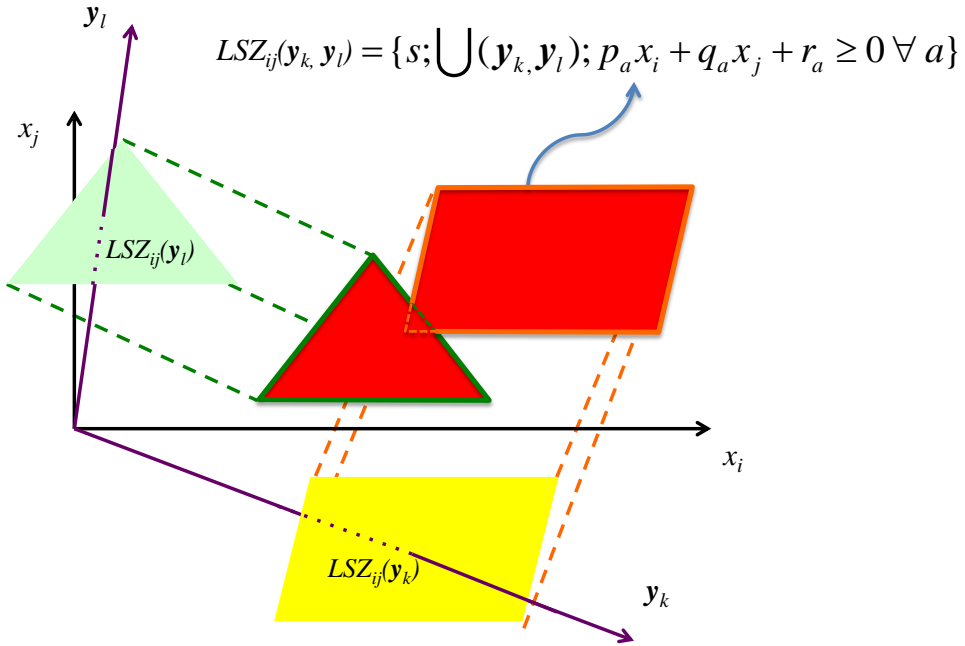


Figure 3.5: An illustration of a projection of $LSZ_{ij}(y_k, y_l)$ following Eq. (3.6).

$$\begin{aligned}
LSZ_{ij}(\mathbf{y}_k, \mathbf{y}_l) &= \{s; \bigcup (\mathbf{y}_k, \mathbf{y}_l); p_a x_i + q_a x_j + r_a \geq 0 \forall a\} \\
&= s(x_1, \dots, x_{i-1}, x_{i+1}, \dots, x_{j-1}, x_{j+1}, \dots, x_{m_1}, \mathbf{y}_1, \dots, \mathbf{y}_{k-1}, \mathbf{y}_{k+1}, \dots, \mathbf{y}_{l-1}, \mathbf{y}_{l+1}, \dots, \mathbf{y}_{m_2} \\
&\quad | x_i, x_j, \mathbf{y}_k, \mathbf{y}_l; p_a x_i + q_a x_j + r_a \geq 0 \forall a) (i < j, k < l)
\end{aligned} \quad (3.6)$$

The projection procedure can reduce the number of combination parameters. That is, in the case of Eq. (3.6), both $N(\mathbf{y}_k)$ and $N(\mathbf{y}_l)$ are reduced to 1.

In order to analyze the problem in multi-dimensional parameter space, ${}_{m_1} C_2$ number of 2D cross sections are considered. That is, 2D cross sections are taken with respect to all axes in multi-dimensional parameter space. This was performed by simply following the mathematical formula. There is no need to recognize the surface in the multi-dimensional space because it is very difficult to visualize.

3.4 Analysis of Tail Distribution

With the limited sampling zone projected to 2D planes with respect to two parameters with pdf, the sampling points are generated only in this limited sampling zone using, for instance, a rejection method and are then used for the 2nd Monte Carlo simulation. In the sense, the proposed method is called stepwise limited sampling (SLS) method. The re-analysis of tail distribution with a fixed point $\mathbf{y}_n = \mathbf{y}_w$ as shown in Fig. 3.3 is performed using the collection of sampling determined as follows:

$$s = \{s \subset LSZ_{ij}(\mathbf{y}_k, \mathbf{y}_l)^{\mathbf{y}_n = \mathbf{y}_w}\} \quad (3.7)$$

In SLS, the 1st Monte Carlo simulation provides the expected value of QoI and the 2nd simulation is devoted to analyze the tail distribution very accurately and not missing a possibility of combination of parameters leading to critical value of QoI. The most notable feature of SLS lies in the definition of limited sampling zone in 2D planes approximated by polygon and its projection to reduce the number of parameters.

CHAPTER 4

Biomechanics Problem Setting of Pressure Ulcer

4.1 Background and Literature Review

Pressure ulcer is a disease caused by prolonged pressure that cuts off the blood supply to cells and/or organs (Bansal et al., 2005). This cut off of blood causes the surrounding skin cells to die. Only 2 hours of continuous physical pressure is enough to cause a pressure ulcer (Reddy et al., 2006). Low quality mechanical tissue properties can cause pressure ulcer, which are known to be caused by aging, wet conditions and a lack of nutrition (Schoonhoven et al., 2002). The changes in tissue properties are hard to understand, and as a result most current research is focused more on treatment after a pressure ulcer occurs and designing special mattresses rather than studying the biomechanism even though it is very important for the prevention of pressure ulcers.

Pressure ulcers are classified into 4 stages in the medical field with Stage IV as the worst case (Brem and Lyder, 2004):

- Stage I: A reddened area on the skin that does not turn white when pressed. This indicates that a pressure ulcer is starting to develop.
- Stage II: The skin blisters or forms an open sore. The area around the sore may be red and irritated.

- Stage III: The skin breakdown now looks like a crater. There is damage to the tissue below the skin.
- Stage IV: The pressure ulcer has become so deep that there is damage to the muscle and bone, and sometimes to tendons and joints.

Most pressure ulcers occur in situations where the subject is prone to a continuous mechanical load for a very long time i.e. bedridden people or people who are dependent on using a wheel chair (Makhsous et al., 2007). The human buttock is always used to support their weight, and the fact that the human buttock has very little fat over the bone (Linder-Ganz et al., 2007) shows that the human buttock is the most prone area for pressure ulcer. Determining the correct nursing care is important in order to reduce the chance of pressure ulcers occurrences. In this thesis, the application of the SLS method is performed in order to find the nursing strategy to prevent the pressure ulcer from occurring by analyzing the critical combination in the tail distribution.

It has been found that internal damage in deep muscle layers covering bony prominences can result in fatal pressure ulcer (Maeda, 2006; Bouten et al., 2003). However, the initial location of that damage has not yet been found. Since it is important to know the local internal strain/stress regions under external pressure, some numerical studies using CT/MRI image-based FEM have been reported. However, Bouten et al. (2003) claimed that FEM is not familiar method to clinical and nursing staff. Therefore, this study aims at developing a practical simulation methodology. Each person has different material properties that were influenced by age, gender, nutrition intake, and wet or dry skin. These differences will effect on how the nursing method should be performed and what positioning will be best for each individual patient.

Some studies on pressure ulcer were performed using the finite element method varying from 2D to 3D analyses. The 3D analysis did not always have a very good

accuracy. Makhsous (Makhsous et al., 2007) used the Mooney-Rivlin model, and a uniform contact pressure of 20.34 kPa was applied to the 3D model. The differences between FEM and measurement from MRI images were compared. The measured displacement at a certain point was 16.8 ± 16.5 mm, while the numerical prediction was 10.7 ± 8.0 mm. In another region, the measured value was 36.6 ± 9.0 mm, while the predicted one was 18.1 ± 5.8 mm. The accuracy was not very good probably because of the Neumann condition. On the other hand, the prediction by Linder-Ganz et al. (2007) was very accurate. The Neo-Hookean model, Prony series expansion type viscoelastic model and Dirichlet condition using the measured deformation by MRI were adopted. The measured pressure was 17 ± 4 kPa, and the predicted value was 18 ± 3 kPa. Yamamoto et al. (2008) used a 2D model and Ogden model, but a multi-scale analysis was carried out to predict not only the strain distribution but also capillary deformation and cutaneous blood flow. The correlation between blood flow and contact pressure was compared qualitatively with experimental measurement. It should be noted that Yamamoto's model was 2D, but novel advanced simulation was conducted.

An interesting result by Linder-Ganz et al. (2007) was that large inter-individual differences were seen among 6 subjects. The maximum von Mises stress ranged from 20 to 53 kPa in gluteus muscle and 14 to 25 kPa in enveloping fat. Makhsous et al. (2007) also noted that the stresses reported by many others showed great variation, which may be due to differences of the configurations, material parameters, loading and boundary conditions. We postulate that the consideration of uncertainty parameters in the simulation is a critical issue, but we can find no literature on this point.

Another interesting result from the work by Linder-Ganz et al. (2007) were the reported values for maximum shear stress. The values ranged from 12 to 30 kPa in gluteus muscle among 6 subjects and 7 to 13 kPa in fat, where inter-individual differences were

again seen. It was found that if severe shear loading is repeatedly applied to a patient, pressure ulcer may occur as a result of mode II type fibril tissue damage and damaged area propagation in either mode I or mode II. More on this will be discussed in the prediction rule of pressure ulcer occurrence in Chapter 4.6.

This thesis itself will employ 2D model. The consideration of uncertainty parameters is also a matter of concern in the pressure ulcer analysis because there are many parameters to be considered in order to predict the occurrence of pressure ulcer but no literature can be found on this point. Furthermore, in this thesis, seven parameters are considered, some of which are not expressed in pdf. Also note that the geometrical parameter is newly considered. In the stochastic finite element analysis, for instance, the numerical method to include the geometrical parameter using finite difference method has a problem in the accuracy (Sakata et al., 2013a).

4.2 Assumption of Biomechanics

In the very early stage of pressure ulcer formation, the tissues inside the body are damaged even though skin surface looks normal. The initial damage that leads to pressure ulcer occurs in deep muscle layers, however, the initial damaged location has not been clarified. Therefore, assumption that the tiny damage of fibril tissues at the interface between bone and muscle in human buttock becomes the trigger of muscle damage. The tension and/or shear strain first damages loose fibril tissue between the bone and muscle and that propagation of the damaged area leads to more serious stages. The bio-mechanism assumption of interface fibril tissue damage is employed in this thesis. Figure 4.1 shows a typical CT image of healthy human buttock. The fibril tissue deforms due to the external load. Bone, muscle, fat and skin are the main tissues, and the center part is the target region where muscle covering bony prominences is seen.

In the finite element analysis, a cutout models the interface damage, because the exact size of the tiny damage of fibril tissues is unknown at this moment, as it was never measured. The strains were evaluated at both tips of the cutout. Note here that the skin was neglected because it was reported that the deformation of skin was much smaller than that of muscle and fat (Makhsous et al., 2007).

4.3 Uncertainties in Input Parameters

The first step to determine the uncertainties in input parameters is to determine the mathematical parameters in the model that are going to be analyzed. Figure 4.2 shows a typical image of a healthy human buttock showing the mathematical parameters considered in the analysis.

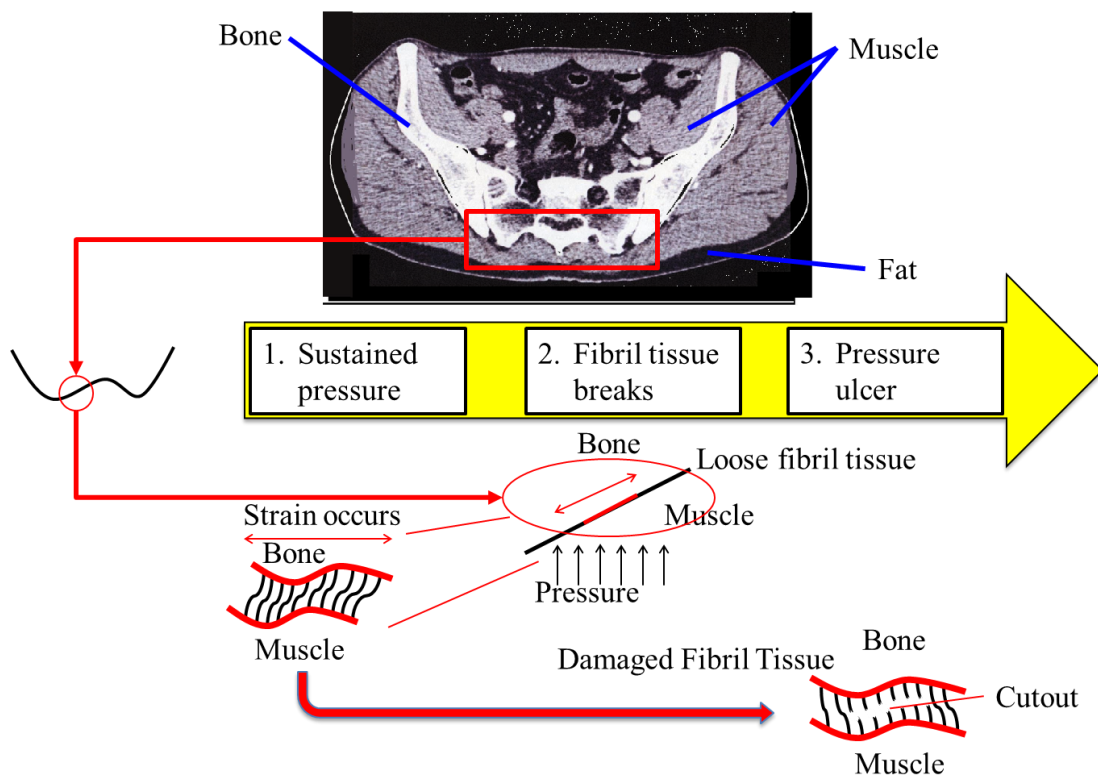


Figure 4.1: CT image of a human buttock showing the loose fibril tissue. It is a simplified numerical modeling by assuming that the initial damage occurs at the interface between bone and muscle by the loose fibril tissue damage.

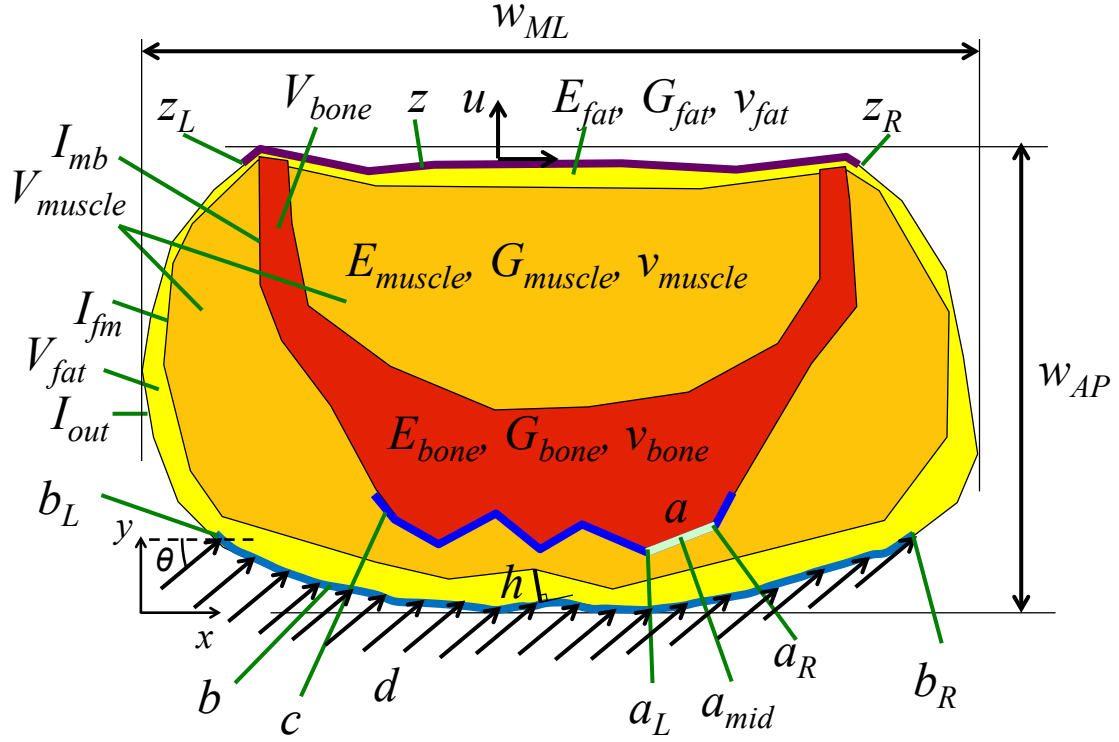


Figure 4.2: Typical human buttock with mathematical parameters showing material properties, contour shape, cutout location and boundary condition.

Concerning the material properties, Young's moduli, Poisson's ratios and shear moduli of bone, fat and muscle are considered represented by E_{fat} , E_{muscle} , and E_{bone} for the Young's moduli of fat, muscle and bone, ν_{fat} , ν_{muscle} and ν_{bone} for their Poisson's ratios and G_{fat} , G_{muscle} and G_{bone} for the shear moduli. The bone is much stiffer than the others. Hence, the properties of fat and muscle, i.e., E_{fat} , E_{muscle} and G_{fat} , are considered as uncertainty parameters, which will be described in more detail later.

The dimensions of the model are defined as w_{AP} in anterior-posterior direction and w_{ML} in medial-lateral direction respectively. They are 266 mm and 468 mm respectively. The curved shape of the model is defined as I_{out} , I_{fm} , and I_{mb} where each represents outer contour, interface between fat and muscle, and interface between muscle and bone. I_{out} is used to define the boundary condition and I_{mb} is used to define the interface damage modeled by a cutout. The outer shape I_{out} is fixed for simplicity because it is very influential on the boundary condition. Contact area or loading area is defined as

$b = [b_L, b_R] \subset I_{out}$ and the constraints as $z = [z_L, z_R] \subset I_{out}$. The loading value is assumed to be constant on b and denoted as d . The loading angle θ is defined as $\theta = \pi/2$ for supine case, $\theta = 0$ or $\theta = \pi$ for two lateral cases. The direction of the constraints is defined as u with $u_x = 0$ when the model is constraint in the x -direction and $u_y = 0$ when the model is constraint in the y -direction. In this thesis, \mathbf{b} is considered as a parameter without defined pdf associated with the positioning of a patient. Supine position and two lateral positions are considered.

The volume fraction of fat is defined as V_{fat} , that of muscle as V_{muscle} and that of bone as V_{bone} . The volume fractions of fat and muscle are considered. Then, \mathbf{I}_{fm} is one of the parameters without defined pdf. To quantify the feature of \mathbf{I}_{fm} , which will be used as a measure of the axis \mathbf{I}_{fm} in the parameter space, the distance of \mathbf{I}_{fm} is defined as $f(\mathbf{I}_{fm})$ by the following relation:

$$f(\mathbf{I}_{fm}) = \alpha V_{fat} + (1 - \alpha) SD_{fat} \quad (4.1)$$

where α is the weighting factor and SD_{fat} is standard deviation of the thickness of fat h defined in Fig. 4.2. In this thesis, three types of configuration, i.e., muscle-rich, fat-rich and very fat-rich cases, are considered. Those are assumed to be represented quantitatively by only V_{fat} , then $\alpha = 1$ is assumed in Eq. (4.1).

The fibril tissue damage was modeled by a cutout and the possible location of cutout is defined as $c \subset I_{mb}$, and the cutout region is defined as $a \subset c$. The center location of a is denoted as a_{mid} , its length is denoted as L_a and the location of left and right edges as a_L and a_R . The local curved coordinate system along c is used to measure those parameters L_a , a_{mid} , a_L and a_R . Among them, L_a and a_{mid} are considered as uncertainty parameters without defined pdf.

Table 4.1: Material properties based on linear isotropic model.

(a) Young's modulus showing mean value, standard deviation and lower/upper limit.

Material name	Young's modulus, E (MPa)			
	Mean value	Standard deviation	Lower limit	Upper limit
Fat	8.0×10^{-2}	8.0×10^{-3}	4.0×10^{-2}	1.2×10^{-1}
Muscle	7.5×10^{-2}	7.5×10^{-3}	3.75×10^{-2}	1.125×10^{-1}
Bone	2.0×10^4	-	-	-

(b) Shear modulus showing mean value, standard deviation and lower/upper limit.

Material name	Shear modulus, G (MPa)			
	Mean value	Standard deviation	Lower limit	Upper limit
Fat	2.857×10^{-2}	2.857×10^{-3}	1.429×10^{-2}	4.286×10^{-2}
Muscle	2.517×10^{-2}	-	-	-
Bone	7.692×10^3	-	-	-

In summary, seven parameters, E_{fat} , E_{muscle} , G_{fat} , I_{fm} , \mathbf{b} , L_a and \mathbf{a}_{mid} are considered as uncertainty parameters. Three parameters, E_{fat} , E_{muscle} , G_{fat} , are assumed to be in normal distribution, whilst pdf are not determined for the other four parameters. That is, the number of parameters with and without defined pdf are $m_1 = 3$ and $m_2 = 4$.

Table 4.1 shows the material properties based on linear isotropic model (Yamamoto et al., 2008; Elsner et al., 2002; Agache and Humbert, 2004) and normal distribution is simply assumed. Note that the Young's moduli and/or shear moduli for muscle and fat are scattered. The coefficient of correlation between Young's modulus and shear modulus for fat was determined so that the Poisson's ratio does not exceed 0.5. For muscle, only the variation of Young's modulus was considered because its Poisson's ratio is close to 0.5.

The number of discrete sampling cases that were used for parameters without defined pdf are as follows: location of cutout (\mathbf{a}_{mid}) with 3 different sampling locations $\{a_{mid1} = 42.34 \text{ mm}, a_{mid2} = 104.38 \text{ mm}, a_{mid3} = 166.63 \text{ mm}\}$ bounded between a_{mid1} and a_{mid3} , length of cutout (L_a) with 2 different sampling lengths $\{L_{a1} = 4 \text{ mm}, L_{a2} = 8 \text{ mm}\}$ bounded between L_{a1} and L_{a2} , loading condition (\mathbf{b}) with 3 different loading sampling $\{b_1 = \text{lateral-A}, b_2 = \text{supine}, b_3 = \text{lateral-B}\}$ bounded between b_1 and b_3 , and configuration

of muscle and fat (I_{fm}) with 3 different sampling configurations $\{I_{fm1} = 9.69\%, I_{fm2} = 15.20\%, I_{fm3} = 22.92\%\}$ following Eq. (4.1) bounded between I_{fm1} and I_{fm3} . Following Eq. (4.2), the combinations of discrete sampling points gave a total discrete model of:

$$\prod(N(y)) = \prod(N(I_{fm}), N(\mathbf{b}), N(L_a), N(\mathbf{a}_{mid})) = \prod(3,3,2,3) = 54 \quad (4.2)$$

4.4 Experimental Model

Before going into the finite element discretization, a positioning change experiment was performed in order to understand more about the boundary conditions. The first experiment was performed to find which area of the patient has the largest force, whether it was painful or not, and also to find out whether the existence of a bed sheet has any effects.

The experiment uses the following items as shown in Fig. 4.3:

- 2 tables large for moving the patient.
- 2 pillows used for nursing.
- Cushion for nursing, one large and one small.
- Bed sheet made from 100% cotton.



Figure 4.3: Items used in the experiment

The experiment starts by finding out the ways to move a patient from supine position to lateral position. There are 3 ways to move the patient as follows:

- Supine position into complete lateral position (Right side of the body is underneath) A shown in Fig. 4.4.
- Supine position into complete lateral position (Right side of the body is underneath) B shown in Fig. 4.5
- Supine position into complete lateral position (Right side of the body is underneath) C shown in Fig. 4.6.

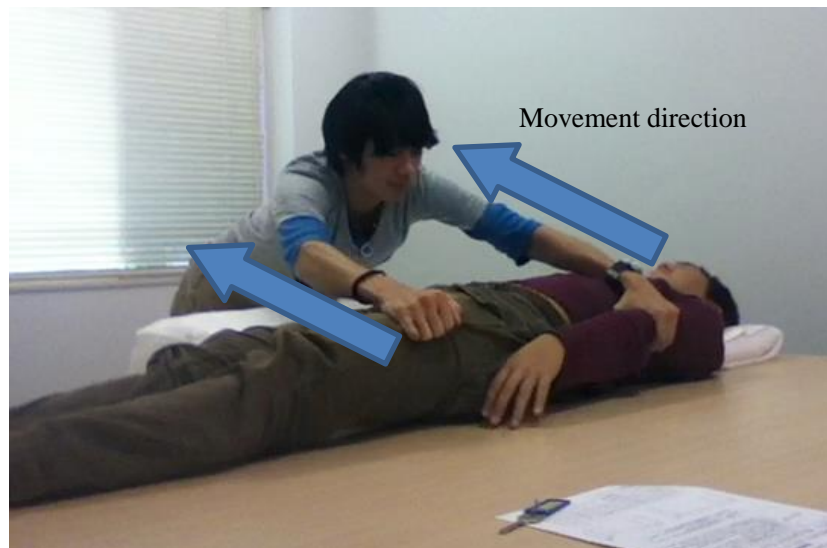


Figure 4.4: Supine position into complete lateral position A.

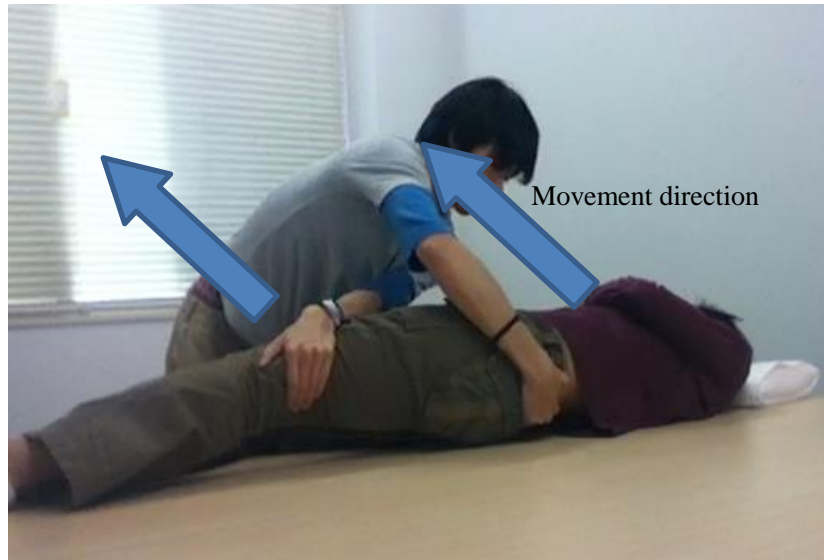


Figure 4.5: Supine position into complete lateral position B.



Figure 4.6: Supine position into complete lateral position C.

The impression from the patient after position change shows that the area where the bone comes out has large pressure especially for old and slim people will have a very high pressure locally in that area. During the position change, when the patient body was grabbed, the force needed to lift the body is much influenced by the patient itself. There is also some shear force involved between the patient body and the bed. Also, not related with the position change, after the patient is put into the lateral position and the cushion was not used then a very strong pressure can be felt at the left knee, right shoulder, and

right pelvis. If the cushion was used, then the very strong pressure can be felt at the right shoulder, right pelvis, right side of the buttocks and right rib.

The next step was to confirm the effect of the bed sheet to the patient during position change. For the method A and B, the results are almost the same and can be seen in Fig. 4.7. For patient with a thick buttocks, without the bed sheet the buttocks will slide over and with the bed sheet it did not slide. During the rotation, the right side of the buttock becomes fixed at the edge and it remains the same even after. Also, it can be felt that without the bed sheet the shear force was smaller. For patient with a thinner buttock felt the same way with or without the bed sheet and there was no burden felt in the pelvis area.



Figure 4.7: Experiment with and without the bed sheet for supine position into complete lateral position A and supine position into complete lateral position B.

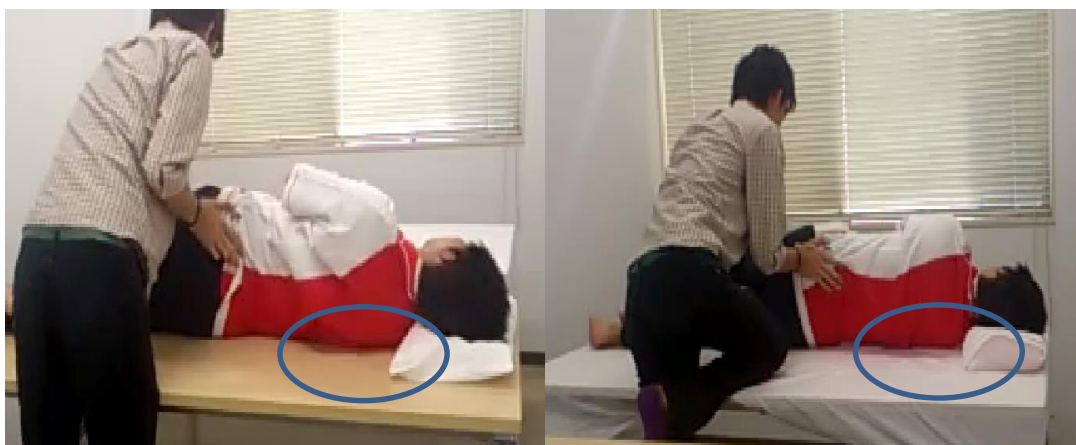


Figure 4.8: Experiment with and without the bed sheet for supine position into complete lateral position C.

However, the patient felt that the body was being dragged to the outside when the rotation just started and it also happens with and without the bed sheet.

Regarding the pressure that influence to the buttock, the results for method C are the same as method A and B shown in Fig. 4.8. Without the bed sheet, the friction between the table and the body are small and so the body will slide and during the rotation the lower body part of the right shoulder has a small burden of pressure. With the bed sheet, the friction becomes larger and so the body did not slide as easily but also the right shoulder had more burden. Also with and without the bed sheet, when the body was pushed, the patient can felt the pressure on the outer part just like before. However, these impression for method C does not differ between patients with thicker or thinner buttocks.

The second experiment was performed to find the contact area between the buttock and the bed during supine and lateral position. The experiments were performed by putting sands on the table and then letting the patients lay on top of them.

- Finding the contact area for patient during supine position.
- Finding the contact area for patient during lateral position.
- Finding the contact area for patient that was moved from supine to lateral position.



Figure 4.9: Contact area during supine position.

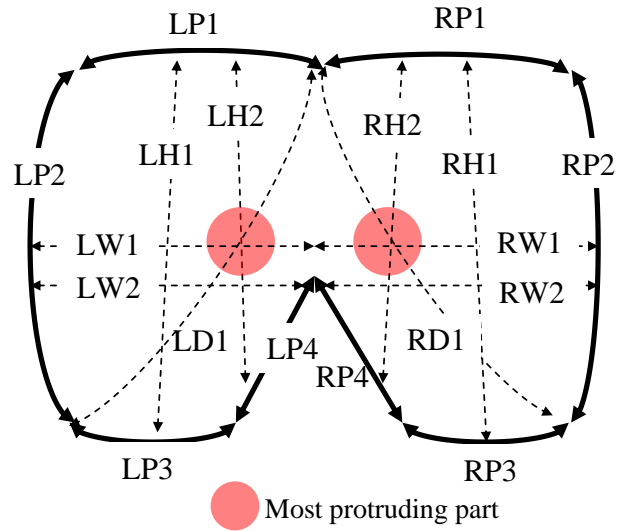


Figure 4.10: Measured length during supine position.

Table 4.2: Calculated length during supine position as shown in Fig. 4.10.

	Length (cm)		Length (cm)
LH1	24.8	RH1	26.6
LH2	20.4	RH2	21.3
LW1	16.1	RW1	16.7
LW2	16.5	RW2	16.9
LD1	29.3	RD1	29.0
LP1	9.7	RP1	11.5
LP2	27.5	RP2	27.0
LP3	5.7	RP3	3.9
LP4	13.5	RP4	16.9

Fig. 4.9 shows the picture of the patient buttocks right after the experiment to find the contact area for patient during supine position. The area where the sand sticks to the patient buttocks is shown in Fig. 4.10 with the calculated length shown in Table 4.2. The contact area was 553.5 cm^2 with the longest width $LW1+RW1 = 32.8 \text{ cm}$.

Fig. 4.11 shows the picture of the patient buttocks right after the experiment to find the contact area for patient during lateral position. The area where the sand sticks to the patient buttocks is shown in Fig. 4.12 with the calculated length shown in Table 4.3. The contact area was 434.8 cm^2 with the longest width $SW1 = 16.6 \text{ cm}$.



Figure 4.11: Contact area during lateral position.

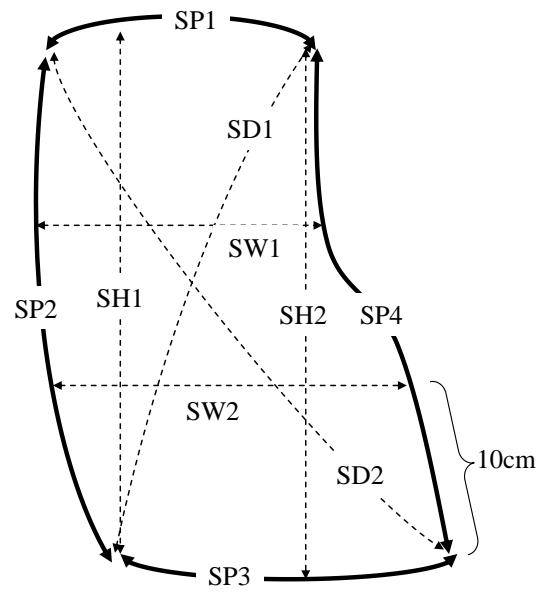


Figure 4.12: Measured length during lateral position.

Table 4.3: Calculated length during lateral position as shown in Fig. 4.12.

	Length (cm)		Length (cm)
SH1	32.5	SP1	10.5
SH2	29.1	SP2	34.0
SW1	16.6	SP3	17.6
SW2	17.5	SP4	30.0
SD1	31.6		
SD2	37.6		



Figure 4.13: Contact area during movement from supine to lateral position.

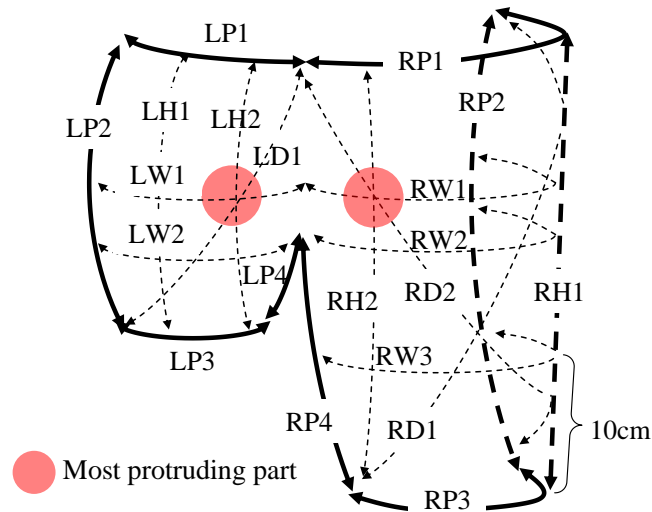


Figure 4.14: Measured length during position change from supine to lateral position.

Table 4.4: Calculated length during movement from supine to lateral position as shown in Fig. 4.14.

	Length (cm)		Length (cm)
LH1	24.8	RH1	40.9
LH2	20.4	RH2	37.5
LW1	16.1	RW1	33.5
LW2	16.5	RW2	29.8
LD1	29.3	RW3	22.0
LP1	9.7	RD1	39.0
LP2	27.5	RD2	55.0
LP3	5.7	RP1	24.2
LP4	13.5	RP2	41.8
		RP3	20.4
		RP4	27.7



Figure 4.15: Comparison of areas during position change from supine to lateral position. The difference can be seen in the red area.

Fig. 4.13 shows the picture of the patient buttocks right after the experiment to find the contact area for patient that was moved from supine to lateral position. The area where the sand sticks to the patient buttocks is shown in Fig. 4.14 with the calculated length shown in Table 4.4. The contact area was 1333.3 cm^2 with the longest width $LW1+RW1 = 46.6 \text{ cm}$.

Figure 4.15 shows the comparison of areas during position change from supine to lateral position. The red area shows the area where the sand sticks during position change but not during lateral position only. This happens because during the nursing process the patient right knee was hold down by the nurse.

4.5 Finite Element Discretization and Quantity of Interest

Following the biomechanical assumption and mathematical definition, the finite element models were generated as shown in Fig. 4.16 independently for muscle-rich case ($I_{fm1} = 9.69\%$), fat-rich case ($I_{fm2} = 15.20\%$) and very fat-rich case ($I_{fm3} = 22.92\%$). Total number of four-noded elements and nodes were 77,334 and 77,397 respectively for three models. Regular and fine mesh was prepared carefully along the interface $c \subset I_{mb}$ between

bone and muscle in order to calculate the interface strain as in the magnified view in Fig. 4.16. The mesh allows us to set the cutout represented by a_{mid} everywhere in c in the Monte Carlo simulation with SLS method. Also in this particular setup following Chapter 4.3, the cutout shown in Fig. 4.16 was located at $a_{mid1} = 42.34$ mm, $a_{mid2} = 104.38$ mm, and $a_{mid3} = 166.63$ mm, with the length of cutout of $L_{a1} = 4$ mm and $L_{a2} = 8$ mm for each cutout location.

The interface normal and shear strains were evaluated as QoIs at the cutout tips. The local coordinate system, i.e., normal (n) and tangential (t) coordinate system, was defined element-wise along I_{mb} as shown in Fig. 4.16. The strains ε_n and γ_{tn} at the cutout tips were extrapolated from the values at Gauss points in the cutout elements. Concerning normal strain ε_n , it was assumed that only tensile strain contributed to the breakage of fibril tissue and propagation of damage area. The cutout elements were in the muscle region and the Young's modulus was 10^{-5} times smaller than the mean Young's modulus of muscle.

Using the second experiment result in chapter 4.4, the boundary condition of the model can be defined for when the patient is laying on supine position and both lateral position.

For the supine position, the length of the finite element model was determined in Chapter 4.3 as $w_{ML} = 468$ mm while the experiment model has w_{ML} of 368.50 mm. From here, it was found that the finite element model is larger by 1.27 in comparison to the experiment model. The experiment result shown the contact area to be 553.5 cm^2 which means the contact area for the finite element model is $553.5 \text{ cm}^2 \times (1.27 \times 1.27) = 892.74 \text{ cm}^2$. The CT image that was used for the finite element modeling is a slice of a human buttock where the most protruding part is $LW1+RW1 = 32.8$ cm and so the length of the contact that should be used in the finite element model is $32.8 \text{ cm} \times 1.27 = 41.6$ cm.

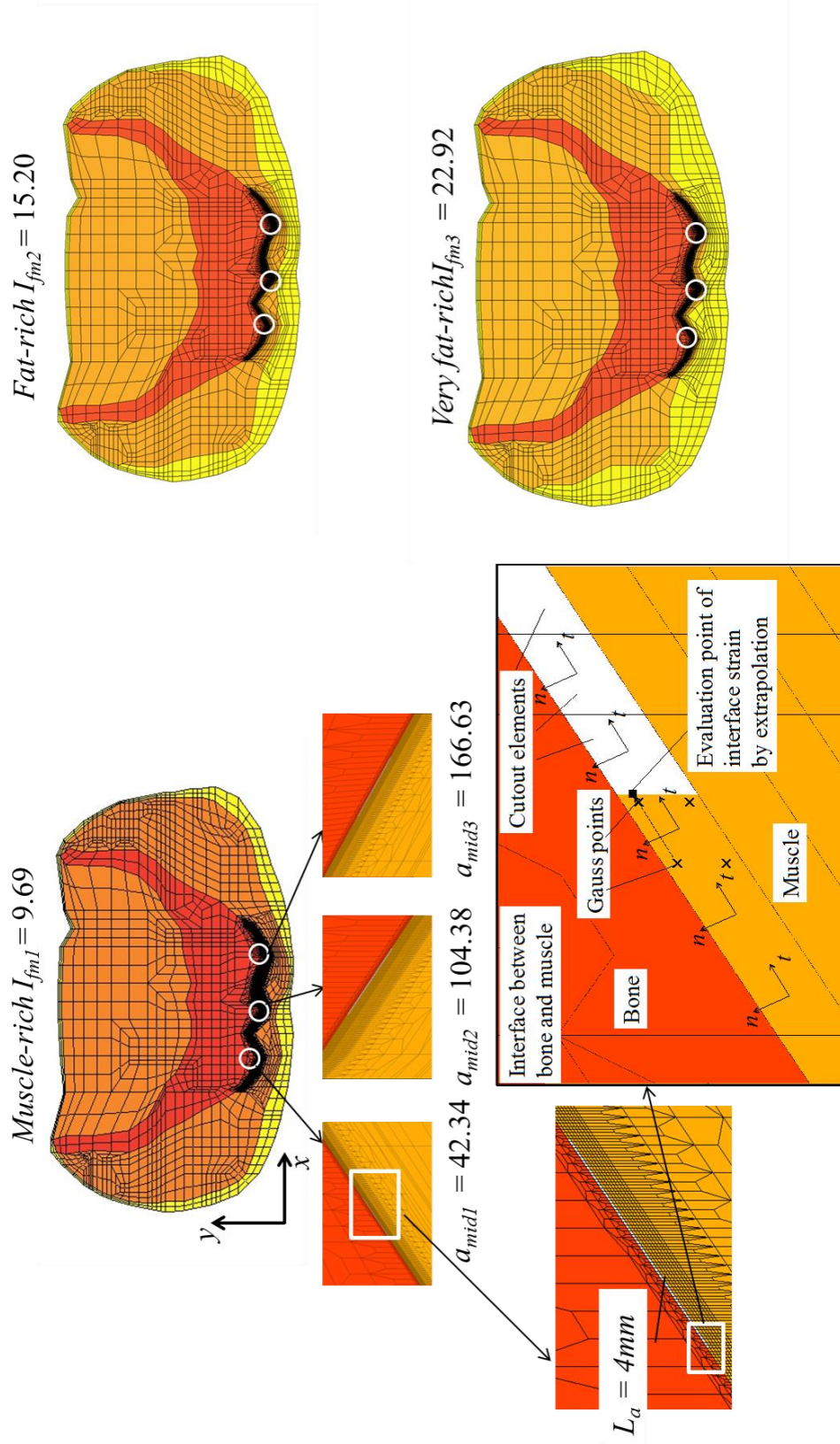


Figure 4.16: Finite element mesh used for the analysis. Evaluation of interface strains at cutout tips is also shown in the bottom left. The goal is to find QoI for normalized strains ϵ_n and γ_m w.r.t parameters on left and right tips of cutout. The evaluation of strain was done using extrapolation.

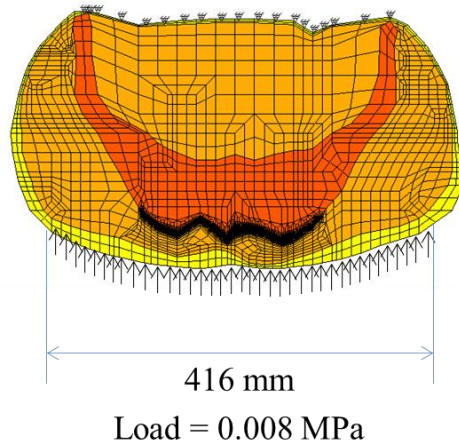


Figure 4.17: The location of loading area during supine position.

Using these information and assuming the weight of human body of 70 kg for the finite element model and a gravity of 10 m/s^2 the load value can then be found as $\frac{700 \text{ N}}{89,274 \text{ mm}^2} = 0.008 \text{ MPa}$ for the length of 416 mm. These can be seen in Fig. 4.17 and Table 4.5 for supine position.

For the both lateral position of A and B, the length of the finite element model was determined in Chapter 4.3 as $w_{AP} = 266 \text{ mm}$ while the experiment model has w_{AP} of 260 mm. From here, it was found that the finite element model is larger by 1.02 in comparison to the experiment model. It was also found that the supine and lateral position had a difference in the comparison. In order to get an equality result between supine and lateral position, only the length of the contact will be used from the experiment result while the load value will assume the same 0.008 MPa as the supine. However, since the length is different the load value will also change following the length. The CT image that was used for the finite element modeling is a slice of a human buttock where the most protruding part is $SW1 = 16.6 \text{ cm}$ and so the length of the contact that should be used in the finite element model is $16.6 \text{ cm} \times 1.02 = 17 \text{ cm}$. The load value is determined as $\frac{0.008 \text{ MPa} \times 41.6 \text{ cm}}{17 \text{ cm}} = 0.018 \text{ MPa}$. These can be seen in Fig. 4.18 and Table 4.5 for lateral position.

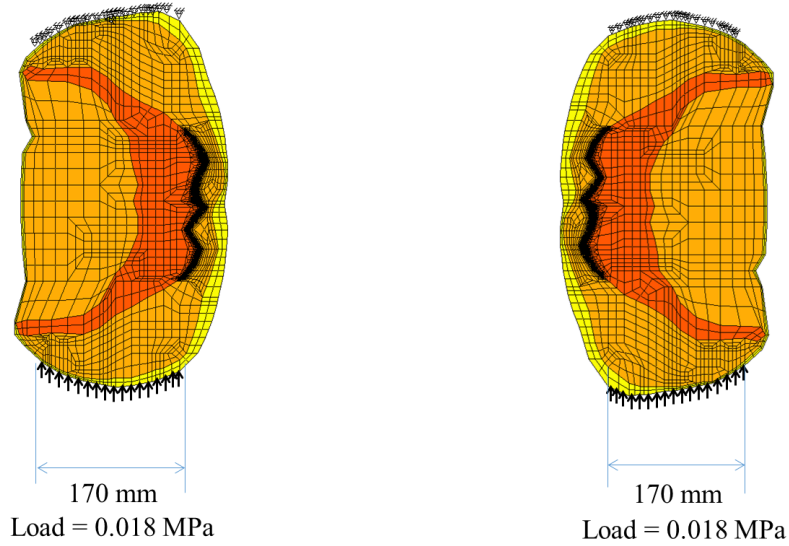


Figure 4.18: The location of loading area during lateral position. The left picture is for lateral-A position and the right picture is for lateral-B position.

Table 4.5: Boundary conditions for three positions including load value, angle, loaded area and constraint.

Position	d (N/mm ²)	θ	$b \setminus I_{out}$		u	$z \setminus I_{out}$	
			b_L (mm)	b_R (mm)		z_L (mm)	z_R (mm)
Supine	8.0×10^{-3}	$\pi/2$	(31, 49)	(439, 48)	$u_y = 0$	(66, 266)	(392, 260)
Lateral-A	1.8×10^{-2}	0	(20, 60)	(30, 230)	$u_x = 0$	(422, 36)	(436, 220)
Lateral-B	1.8×10^{-2}	π	(456, 60)	(430, 230)	$u_x = 0$	(29, 70)	(66, 266)

Due to the simplified constraint condition where only one node was fixed in the x -direction and in order to escape the singularity of the model, a regularization technique was used as shown in Eq. 4.3 (Kikuchi and Oden, 1988; Takano et al., 2001).

$$(K + \lambda \int_V N^T N dV) u = f \quad (4.3)$$

K and N are the stiffness matrix and shape function and u and f are the displacement and force vectors. The regularization was applied after diagonal scaling in the scaled conjugate gradient (SCG) solver. The coefficient factor $\lambda = 10^{-10}$ was determined from sensitivity analysis.

4.6 Prediction Rule of Pressure Ulcer Occurrence

The prediction rule was based on the maximum strain criteria rather than the Mises or the Tresca type criterion because the measurement of the interaction between strain components at the fibril tissue is impossible at this moment. The analysis to determine this prediction rule and involves an analysis of two numerical models. One is a model of a healthy person as seen in Fig. 4.19 while the other is a model of a patient with surgical treatment as seen in Fig. 4.20. Notice the difference in the meshing in Fig. 4.19 and Fig. 4.20 at the interface between bone and muscle. Also, different from the finite element model shown in Chapter 4.5, the prediction rule analysis only focused on one cutout location. There were several surgical methods available to treat pressure ulcer and for this particular analysis the bone cut and surgical flap method was chosen (Romanelli et al., 2006). A surgical flap is made to cover a wound caused by a pressure ulcer using muscle from a different body part. Surgical treatment is used to treat patients with pressure ulcers, especially patients with stage IV pressure ulcers. Treatment for these patients is more aggressive since the process involves cleaning and dressing the diseased area and continued surgical repair, and then the surgical flap comes into place. The surgical flap is used because the muscle retains its own blood supply, thus aiding the recovery process.

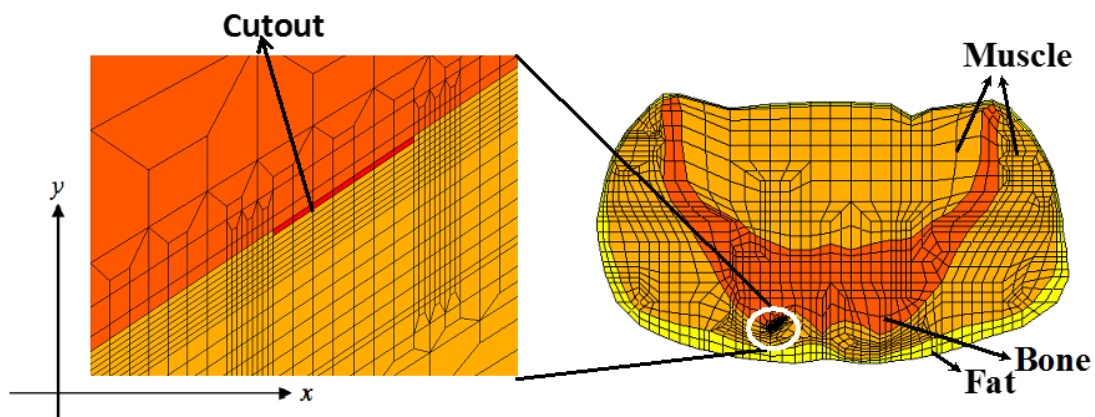


Figure 4.19: Finite element model of damaged interface for the healthy model.

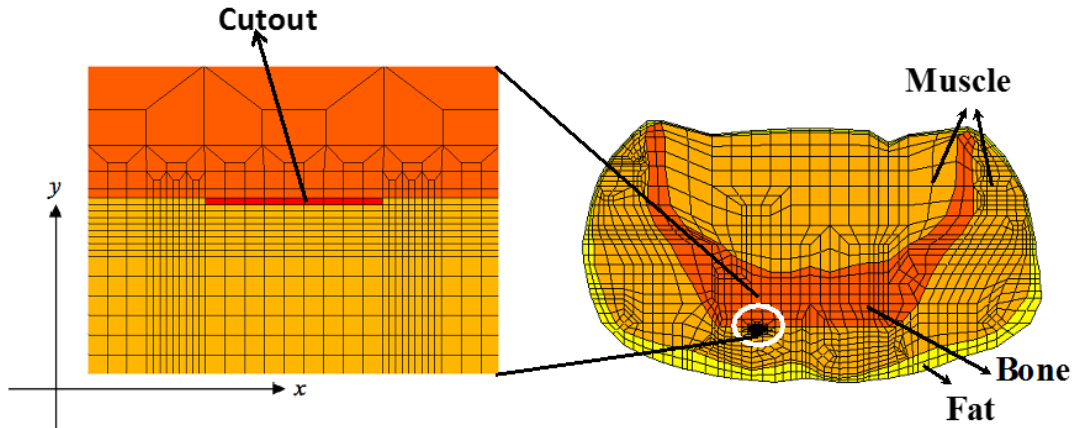


Figure 4.20: Finite element model of damaged interface for the after surgery model.

In this prediction rule analysis, the analyzed strains were also transformed into the t and n -directions following the explanation in Fig. 4.16. The strain was analyzed with various loading cases ranging from 0° (shear) to 90° (perpendicular) for supine position only. Then, the maximum strain values for the load cases in the reference model were modified and denoted by $\varepsilon_n^{\text{reference}}_{\text{max}}$ and $|\gamma_m^{\text{reference}}|_{\text{max}}$. These values were used as reference criteria because they were lower than the real strength of the fibril tissue and because the damaged zone in the healthy body was not supposed to propagate with these values. Here, the values were determined from the result under supine loading condition with $\theta = 0^\circ$ of healthy model with no cutout. The tiny damage modeled by cutout in FEM will be self-healed for a healthy person, and so the model with cutout was compared with a model without cutout and the strain value of a model without cutout was used in the prediction rule.

The strains at the tips of the cutout in the target body are denoted by $\varepsilon_n^{\text{target}}$ and $|\gamma_m^{\text{target}}|$. If $\varepsilon_n^{\text{reference}}_{\text{max}} \leq \varepsilon_n^{\text{target}}$, then mode I propagation is possible. If $|\gamma_m^{\text{reference}}|_{\text{max}} \leq |\gamma_m^{\text{target}}|$, then mode II propagation is possible.

The target will be the healthy model with cutout and after surgery model with cutout for both the element next to the left cutout tip shown in blue line and the element next to the right cutout tip shown in red line in Figs. 4.21 to 4.24. The yellow bars indicate

the strains at the same location for a healthy model with no cutout. Note that the strain values uses the value at center point of the element rather than extrapolation.

For Fig. 4.21 and 4.22, the result explains the fact that pressure ulcers can occur even in a healthy person if the fibril tissues between the bone and muscle are damaged and the damaged zone propagates. When the θ is close to 0 which is when shear force is applied, tensile ε_n happens which shows that the ε_n can be the reason of fracture. For $|\gamma_m|$ the figure shows that if the consideration is looked at as a whole, the danger happens when the shear force of 30° or lower is applied. However, when analyzing the loading case by case, the left tip of $|\gamma_m|$ is always higher than the $|\gamma_m^{\text{nocutout}}|$ for that same loading angle. There is no sure way to say which is more dominant because there is no tendency here, but both ε_n and $|\gamma_m|$ is dominant and can cause the propagation of pressure ulcer. This also explains the cutout model shown in Fig. 4.1.

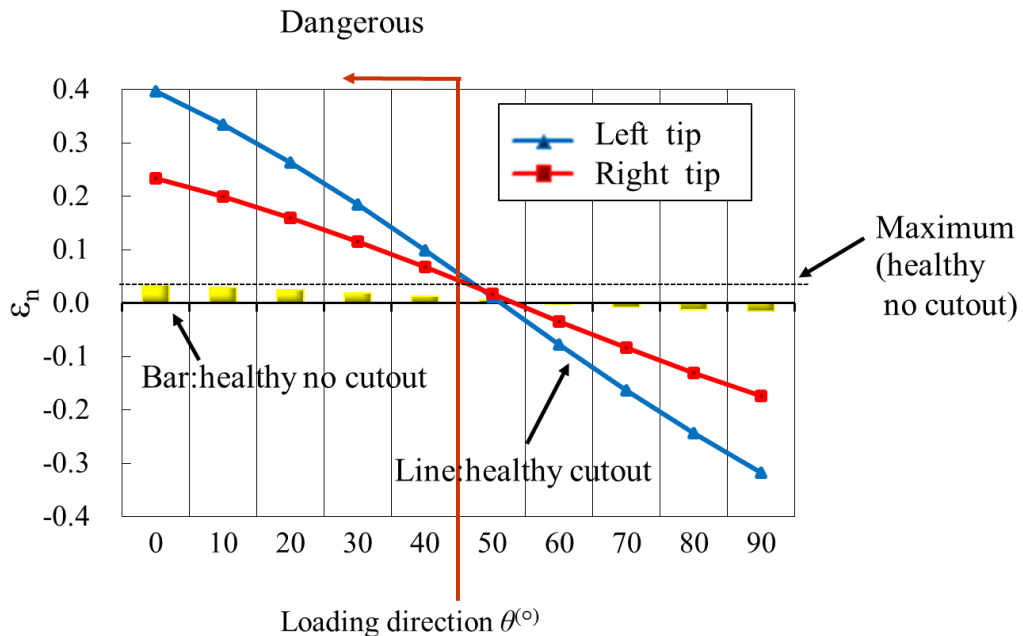


Figure 4.21: ε_n for the healthy body model with cutout.

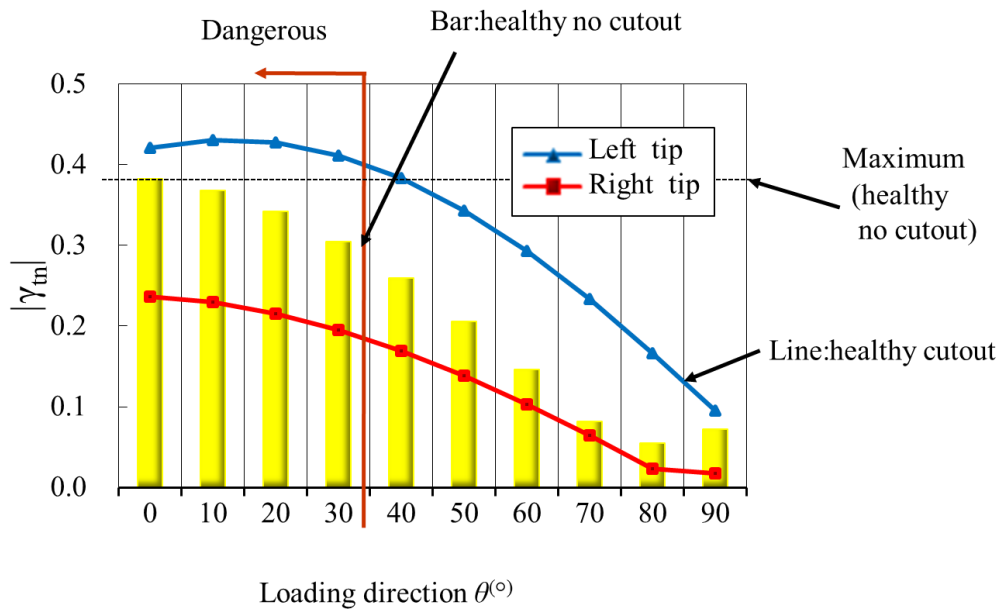


Figure 4.22: $|\gamma_m|$ for the healthy body model with cutout.

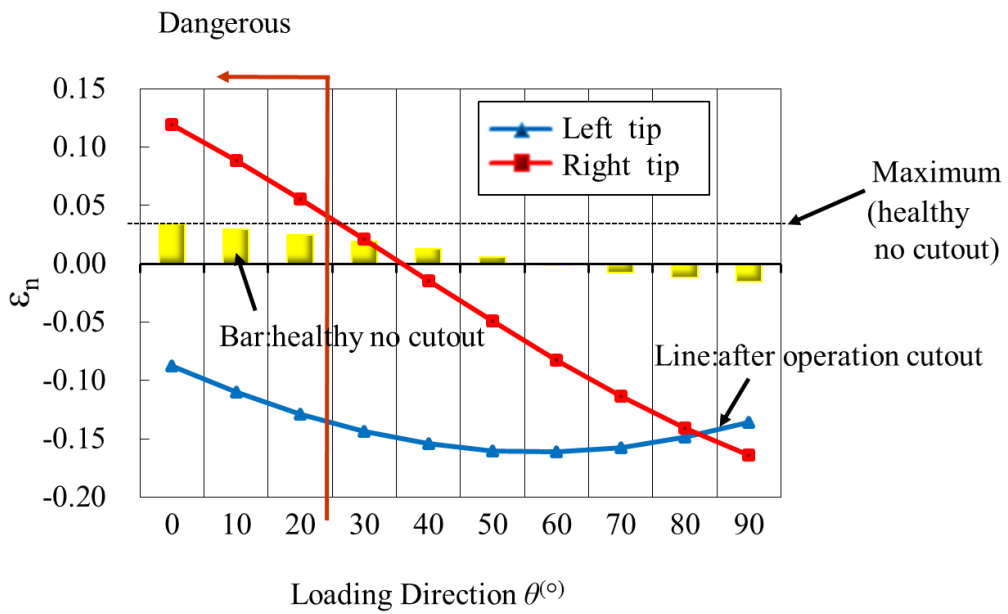


Figure 4.23: ϵ_n for the after surgery model with cutout.

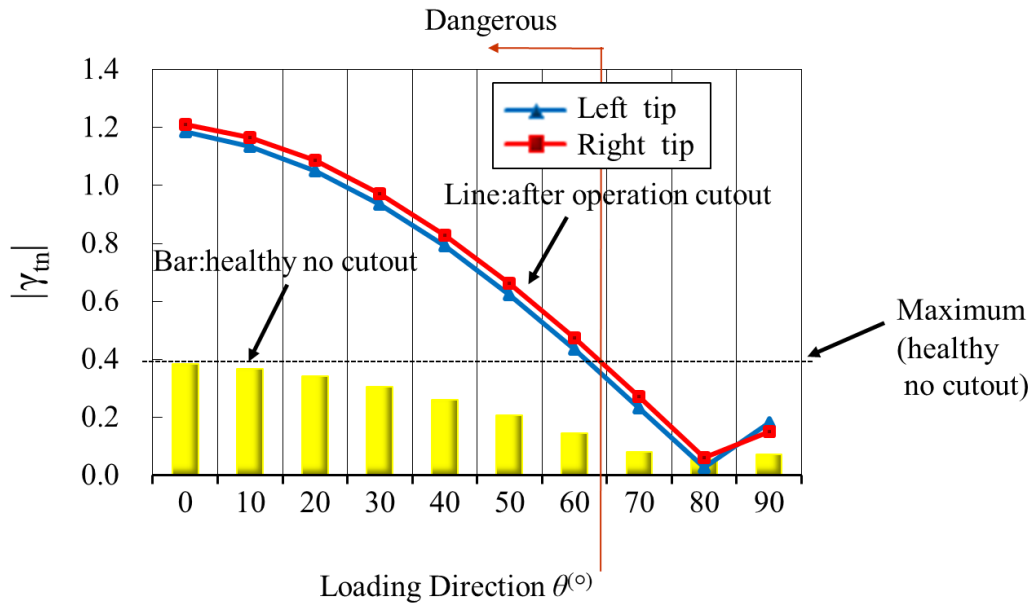


Figure 4.24: $|\gamma_m|$ for the after surgery model with cutout.

For Fig. 4.23 and 4.24, the result shows that axial strain was mostly negative, but relatively high tensile strain was found at the right tip of the cutout under sever shear loading condition. This implies mode I propagation. Moreover, very high strain was observed for wider loading angle range, which implies mode II propagation.

Of course, the target values should be obtained by extrapolating the strain distribution along the interface as seen in Fig. 4.3 but during this prediction rule analysis they were replaced by the strain values at the center point of the neighboring element the cutout because the post processing was easier. The extrapolation of strains for healthy model with cutout can be seen in Fig. 4.25 and after surgery model with cutout in Fig. 4.26 for both case with $\theta = 0^{\circ}$.

For Fig. 4.26, the absolute values of the extrapolated strains were larger or almost the same which means that the choice of the extrapolated value or the value of the neighboring element did not influence the conclusion. However, the importance of extrapolation value is shown in Fig. 4.25 were it was seen that the absolute values of the extrapolated strains were generally higher than the plotted ones except the shear strain for

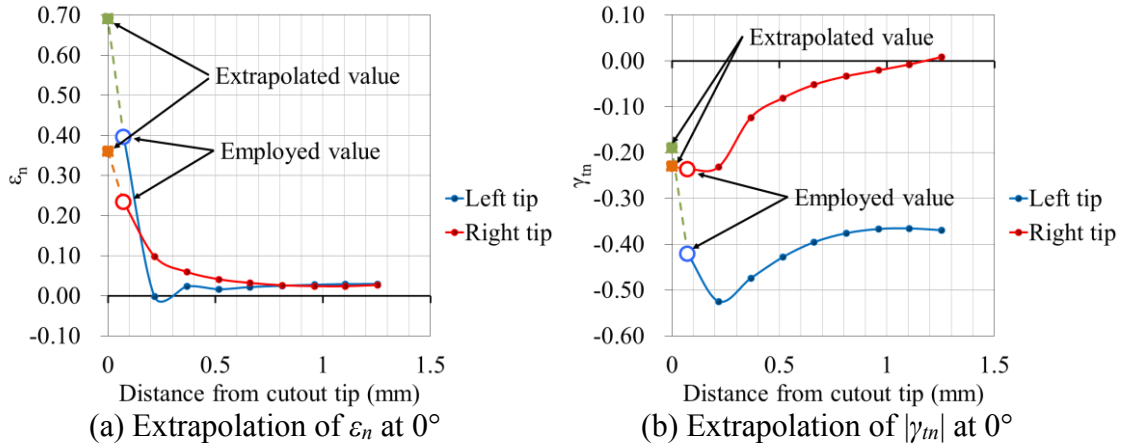


Figure 4.25: Typical result for the extrapolation of strains for the healthy model with cutout.

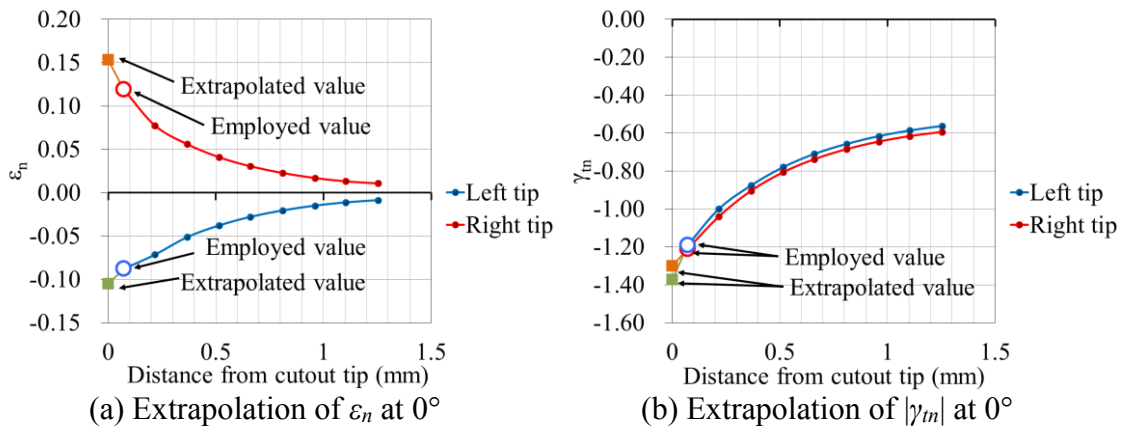


Figure 4.26: Typical result for the extrapolation of strains for the after surgery model with cutout.

$\theta = 0^\circ$ shown in Fig. 4.25(b). Because of this, in the demonstrative example of the SLS method here, the extrapolation value was used.

In the first paper as shown from Fig. 4.21 to Fig. 4.24 in the main thesis, only the load angle was put into consideration while in the application of SLS to pressure ulcer analysis, many uncertainty parameters were also put into consideration. In Fig. 4.21 to Fig. 4.24, the maximum strain value was defined as a threshold. But, in SLS considering many uncertainty parameters, the histogram was obtained when expected value is converged, which means that the standard deviation and probability density function are not reliable because the number of sampling points is not enough in the Monte Carlo simulation. Hence, the maximum value should not be determined. Instead the overlap of

the histogram was looked into. In this sense, the comparison of the overlap looks qualitative. However, in this study the judgment was done manually.

In the SLS analysis, the prediction rule analysis was performed following the same procedure. As the threshold, the interface strains for a case without cutout $\varepsilon_n^{\text{nocutout}}$ and $|\gamma_m|^{\text{nocutout}}$, are calculated. This is easy because the same mesh in Fig. 4.16 can be used. Next, the target value is found by assuming the cutout, if ε_n or $|\gamma_m|$ is higher than $\varepsilon_n^{\text{nocutout}}$ or $|\gamma_m|^{\text{nocutout}}$, then it is supposed that the fibril tissue damage may propagate. $\varepsilon_n^{\text{nocutout}}$ and $|\gamma_m|^{\text{nocutout}}$ are evaluated at the same location of the cutout model. A graphical representation of the prediction rule for the pressure ulcer analysis using SLS method can be seen in Fig. 4.27.

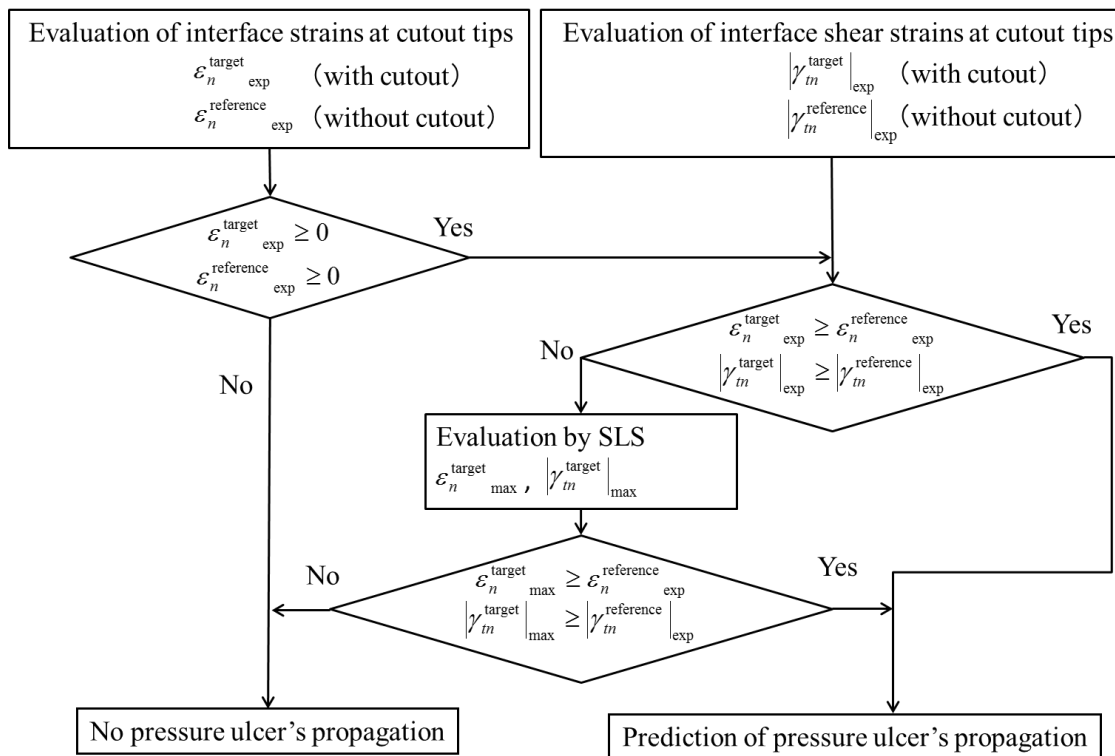


Figure 4.27: Flowchart of prediction rule of pressure ulcer.

CHAPTER 5

Numerical Results

5.1 Deformation and Strain Distribution

Before going into the analysis of the strains at the interface, the model was confirmed by looking at the deformation and strain distribution. The deformation under supine loading condition can be seen in Fig. 5.1 from original to 5x deformation.

The strain distribution of ϵ_x , ϵ_y and γ_{xy} is shown in Fig. 5.2, 5.3 and 5.4 for a case with and without a cutout under the supine loading condition for all three different cutout location. These strain distributions confirmed that the effect of the cutout was only seen near the cutout.

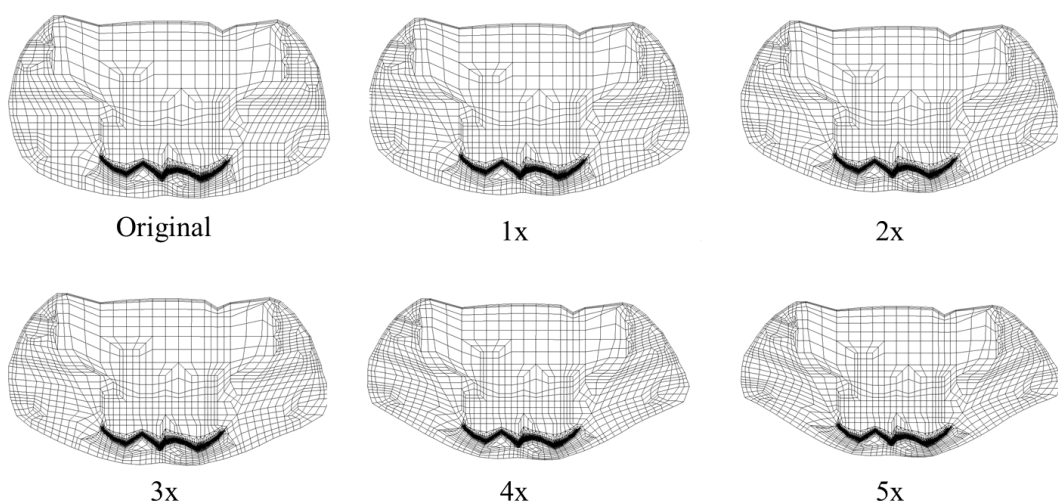


Figure 5.1: Deformation of the mesh from original deformation value to 5x deformation value.

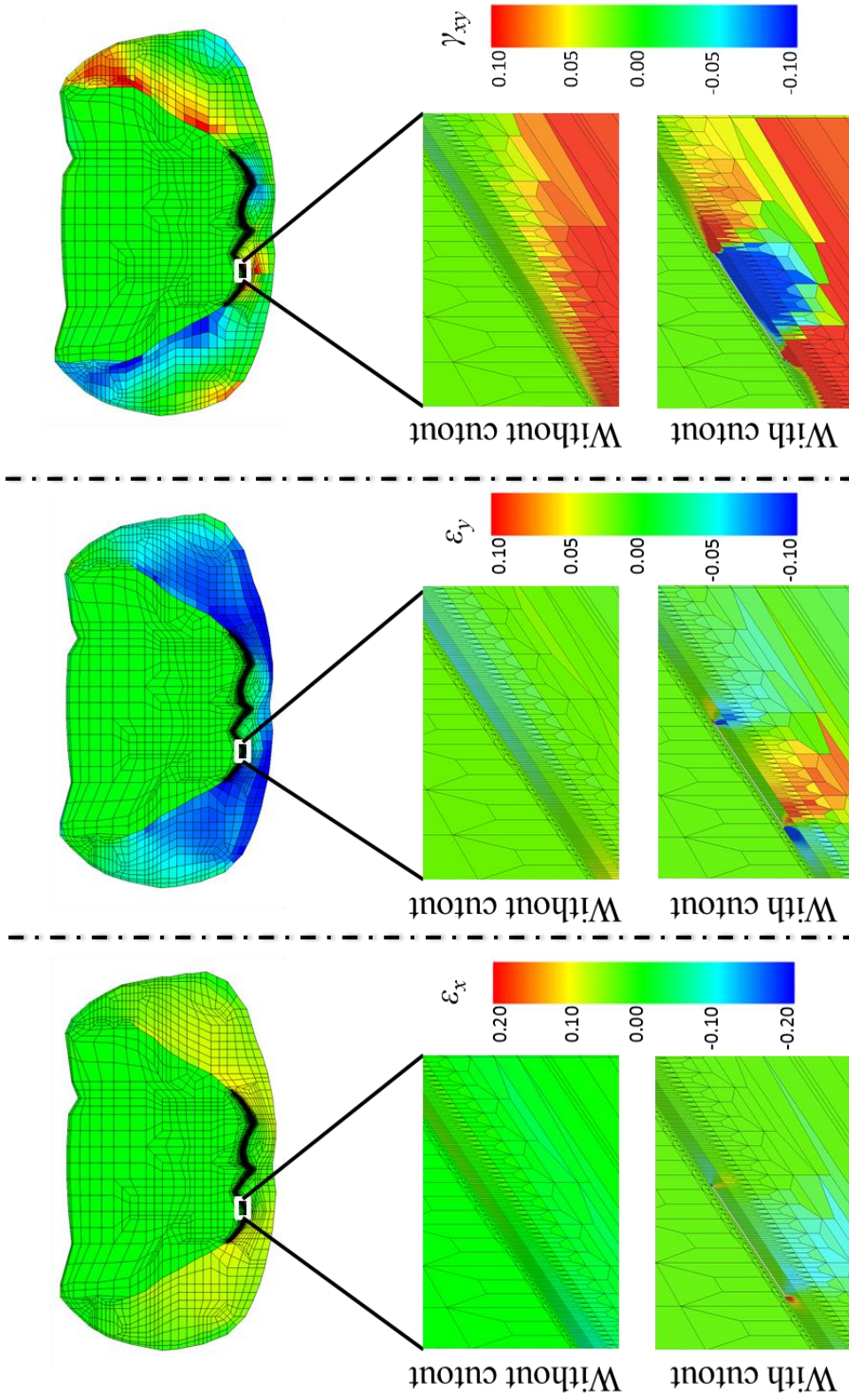


Figure 5.2: Strain distribution of ϵ_x , ϵ_y and γ_{xy} with supine loading condition for $a_{mid} = 42.34$ mm.

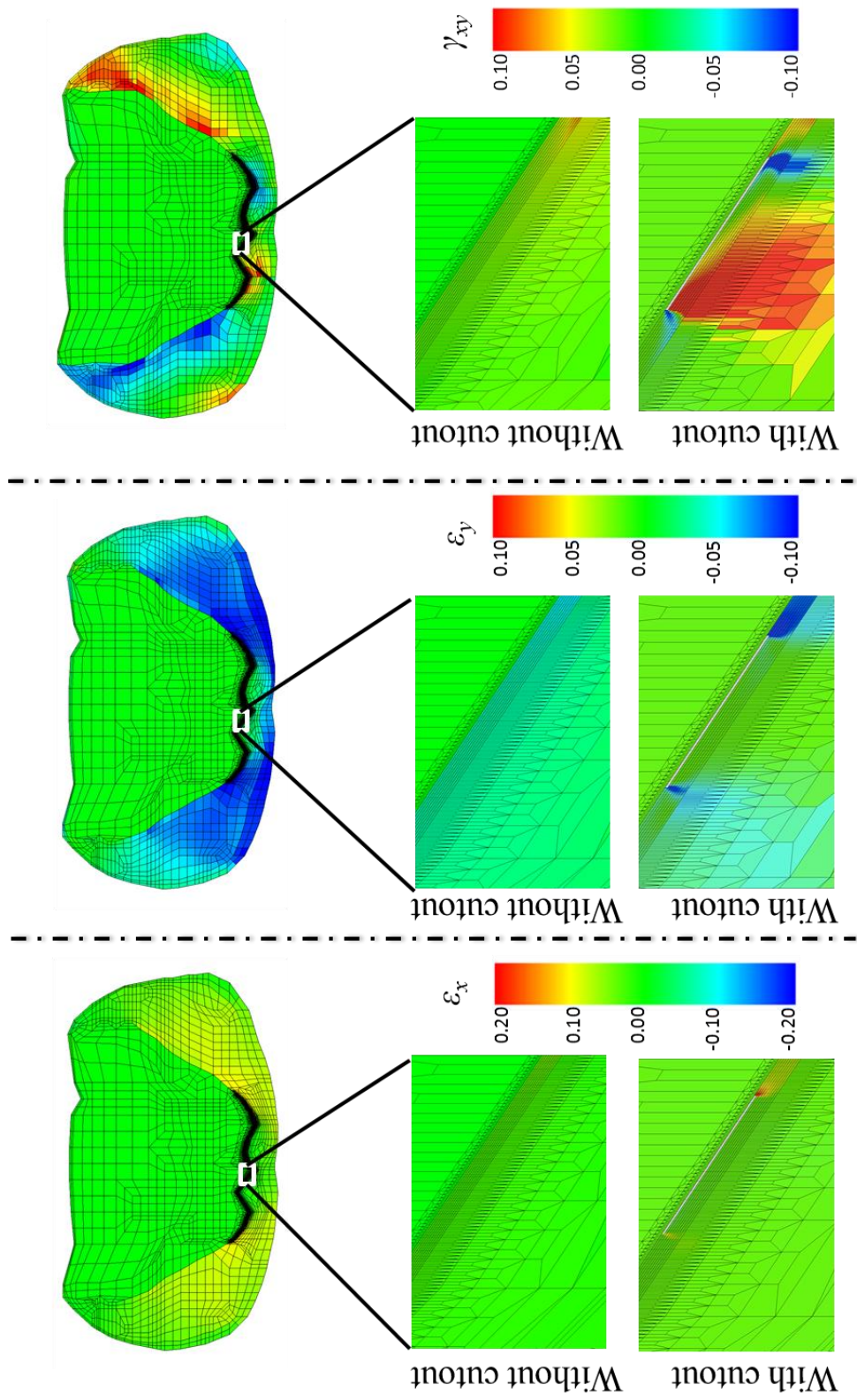


Figure 5.3: Strain distribution of ϵ_x , ϵ_y and γ_{xy} with supine loading condition for $a_{mid2} = 104.38$ mm.

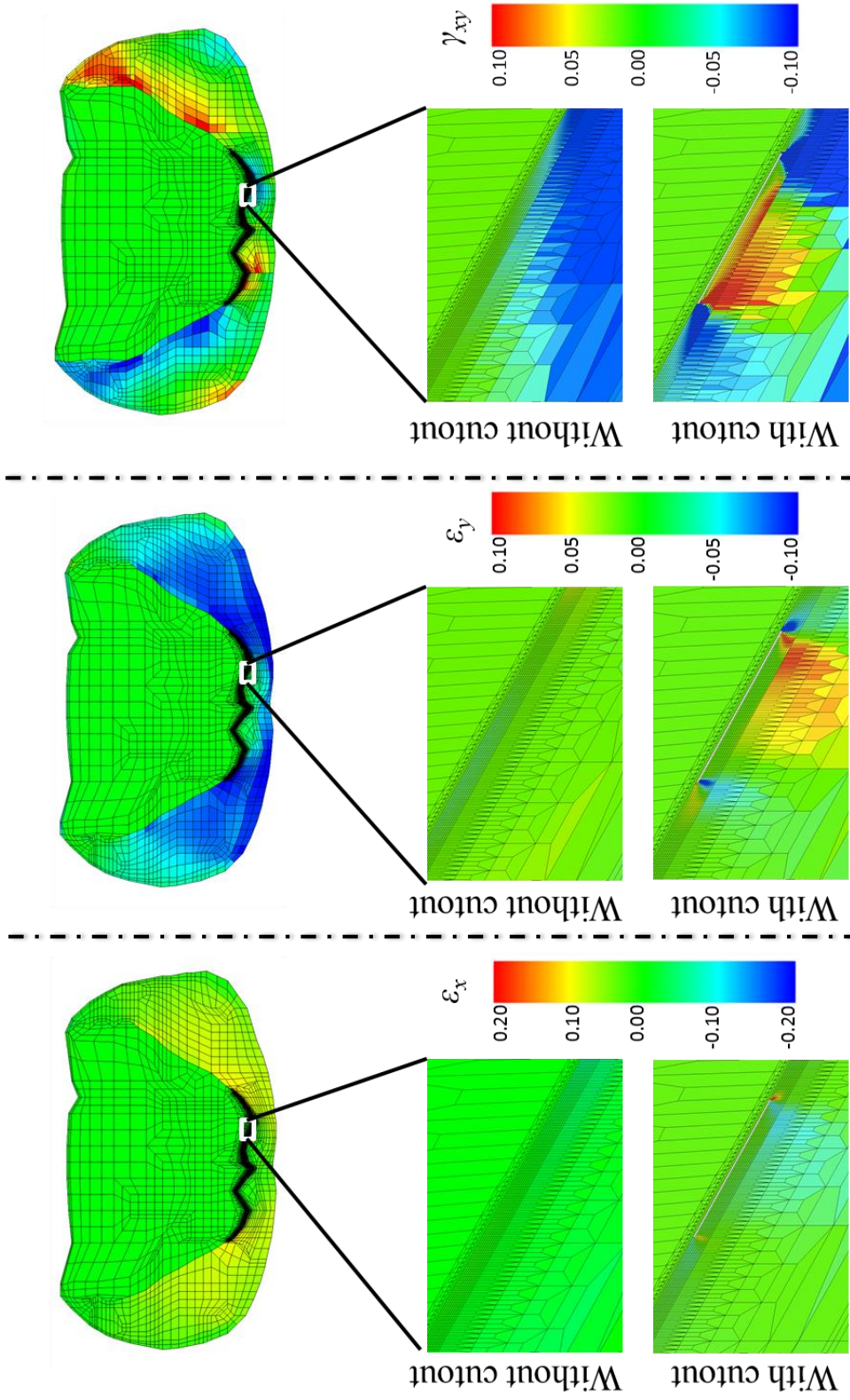


Figure 5.4: Strain distribution of ϵ_x , ϵ_y and γ_{xy} with supine loading condition for $a_{mid3} = 166.63$ mm.

5.2 Convergence of Expected Value

In the standard Monte Carlo simulation considering the normal distribution of material properties, the expected values of strains at the left and right tips of the cutout were monitored after every 100 analyses. Following Eq. (3.3), we determined the collection of sampling for convergence check as follow:

$$\bar{s} = \bar{s}(E_{muscle}, E_{fat}, G_{fat} | I_{fm}, \mathbf{b}, \mathbf{L}_a, \mathbf{a}_{mid}) \quad (5.1)$$

The number of QoIs is 4 for each analysis. Let $EV(\bar{s})_j$ and $SD(\bar{s})_j$ be the expected value and standard deviation for the collection of sampling \bar{s} at j , then the convergence is calculated as:

$$MC_{conv}(i) = \max_j [MC_{conv}(I_{fm}, \mathbf{b}, \mathbf{L}_a, \mathbf{a}_{mid})_i]_j \quad (5.2)$$

where $i = 1, \dots, 54$. The convergence check then follows the rules in Eq. (3.4).

An example of the convergence check is shown in Fig. 5.5 for $\bar{s}(E_{muscle}, E_{fat}, G_{fat} | 9.69, \text{supine}, 4, 104.38)$. In this example, the convergence was found to be 2,000 cases for $j = 1$. The other convergence check can be seen in Appendix A.

Table 5.1 shows the convergence check for all discrete combination of sampling points where it is shown that the convergence varies from 700 to 4,900 cases.

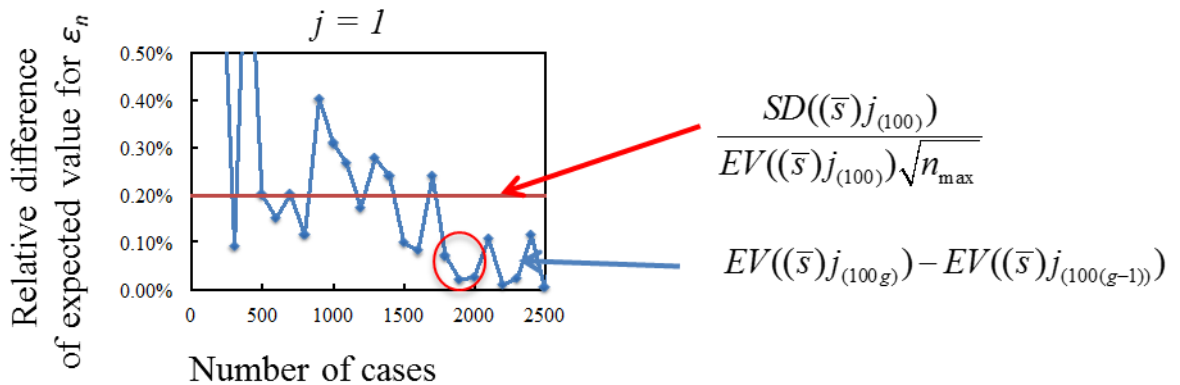


Figure 5.5: A convergence check example for $\bar{s}(E_{muscle}, E_{fat}, G_{fat} | 9.69, \text{supine}, 4, 104.38)$. Following Eq. (3.4), the left hand side of the equation is shown in the blue line and the right hand side of the equation is shown in the red line. The red circle shows the area where the equation is satisfied three times continuously.

Table 5.1: Convergence check results for 54 discrete combination of sampling points.

i	I_{fm}	b	L_a	a_{mid}	MC_{conv}	i	I_{fm}	b	L_a	a_{mid}	MC_{conv}
1	9.69	supine	4	42.23	2000	28	15.2	lateral-A	8	42.23	1400
2	9.69	supine	4	104.38	2000	29	15.2	lateral-A	8	104.38	1500
3	9.69	supine	4	166.63	2000	30	15.2	lateral-A	8	166.63	1400
4	9.69	supine	8	42.23	1700	31	15.2	lateral-B	4	42.23	1300
5	9.69	supine	8	104.38	2000	32	15.2	lateral-B	4	104.38	1300
6	9.69	supine	8	166.63	2000	33	15.2	lateral-B	4	166.63	1500
7	9.69	lateral-A	4	42.23	1400	34	15.2	lateral-B	8	42.23	1300
8	9.69	lateral-A	4	104.38	1500	35	15.2	lateral-B	8	104.38	1300
9	9.69	lateral-A	4	166.63	1400	36	15.2	lateral-B	8	166.63	4900
10	9.69	lateral-A	8	42.23	1400	37	22.92	supine	4	42.23	2000
11	9.69	lateral-A	8	104.38	1400	38	22.92	supine	4	104.38	2000
12	9.69	lateral-A	8	166.63	1400	39	22.92	supine	4	166.63	2000
13	9.69	lateral-B	4	42.23	1300	40	22.92	supine	8	42.23	700
14	9.69	lateral-B	4	104.38	1500	41	22.92	supine	8	104.38	2000
15	9.69	lateral-B	4	166.63	1500	42	22.92	supine	8	166.63	2000
16	9.69	lateral-B	8	42.23	1300	43	22.92	lateral-A	4	42.23	1400
17	9.69	lateral-B	8	104.38	1500	44	22.92	lateral-A	4	104.38	1400
18	9.69	lateral-B	8	166.63	1500	45	22.92	lateral-A	4	166.63	1100
19	15.2	supine	4	42.23	2000	46	22.92	lateral-A	8	42.23	1100
20	15.2	supine	4	104.38	2000	47	22.92	lateral-A	8	104.38	1100
21	15.2	supine	4	166.63	2300	48	22.92	lateral-A	8	166.63	1100
22	15.2	supine	8	42.23	2000	49	22.92	lateral-B	4	42.23	1300
23	15.2	supine	8	104.38	2000	50	22.92	lateral-B	4	104.38	1300
24	15.2	supine	8	166.63	2000	51	22.92	lateral-B	4	166.63	1300
25	15.2	lateral-A	4	42.23	1400	52	22.92	lateral-B	8	42.23	1300
26	15.2	lateral-A	4	104.38	1400	53	22.92	lateral-B	8	104.38	1300
27	15.2	lateral-A	4	166.63	1400	54	22.92	lateral-B	8	166.63	1600

5.3 Limited Sampling Zone

Prediction rule of pressure ulcer occurrence was then performed in order to determine whether the QoI is considered dangerous or not and to define the limited sampling zone. The prediction rule follows the rules in Fig. 4.27 and the result for $s(G_{fat}, I_{fm} = 9.69, b = lateral-A, L_a = 8, a_{mid} = 104.38)$ can be seen in Fig. 5.6 and the prediction rule can be analyzed as follows. The red line shows the histogram for case with cutout at the convergence and the blue line shows the histogram for case without cutout at the convergence.

- 1) The top left figure of left tip ε_n shows that the red line is below 0 and following the prediction rule this means that the case is not dangerous. Using the same figure here, if the case here is at positive value, then this is a very clear case

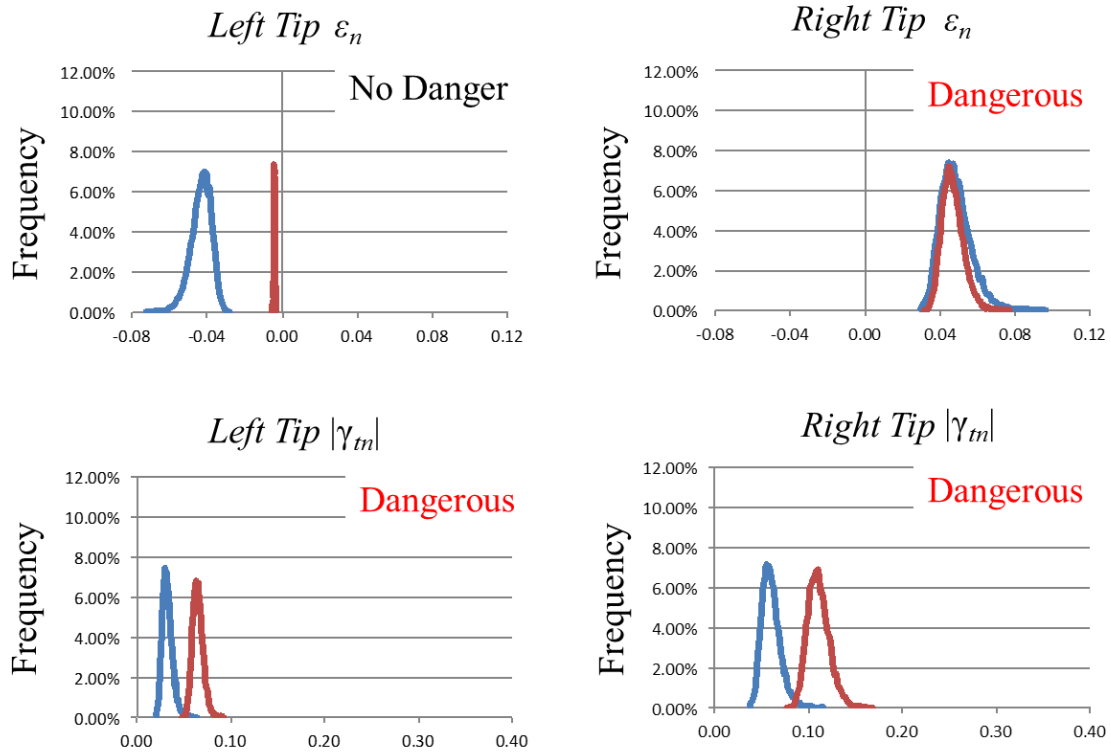


Figure 5.6: Prediction rule of pressure ulcer occurrence at $s(G_{fat}, 9.69, lateral-A, 8, 104.38)$.

when the overlap of the histogram is not seen and the case will be decided as dangerous.

- 2) For the top right figure of right tip ε_n shows that the histogram with and without cutout overlaps. This is an example of a case where the case is considered dangerous because we do not want to miss a single case that can lead to a higher strain. The computational cost for the third step of SLS is not high, so including this case is not costly.
- 3) For the bottom two figures of left and right tip $|\gamma_{tm}|$ shows that the overlap is on some part but the histogram for case with cutout can be higher, which means these cases should be considered dangerous.

The figure in the prediction rule as seen in Fig. 5.6 is not a pdf but just a histogram. The decision to use a contour line of the histogram rather than bars as in the usual form of histogram is to escape the invisible histogram. There are 54 prediction rule performed

in the analysis and each has 4 different location (left and right cutout tip of ε_n and $|\gamma_m|$) and can be seen in Appendix A. In order to see the prediction rule clearly, the scaling of the graph was put into the same range (the bottom axis/strain values) which caused some graphs to become smaller and rendering it invisible if bars were used.

There are possible cases where the strain value with cutout becomes smaller than the case without cutout. The first possibility is when the deformation mode changes. Another possibility is when the compression of the strain at the normal direction occurs. This can be seen in the prediction rule of pressure ulcer occurrence in Fig. 5.6 in the top left showing the prediction rule of left tip ε_n . It was clearly shown that the compression occurs which explains that the very flexible fibril tissue is not damaged.

Using this prediction rule, it was found that the supine loading condition is dominant in $|\gamma_m|$ only and the ε_n does not give any danger to the patient. However, this still means that the patient needs to be moved, and the movement of the patient in shear direction can cause pressure ulcer as shown in the prediction rule in Chapter 4.6. Good care of the patient when moving is needed. However, the lateral position shows both dominant in ε_n and $|\gamma_m|$ with a more dominant shown in $|\gamma_m|$.

The algorithm to develop the limited sampling zone $LSZ_{E_{muscle}\&E_{fat}}$ in the case for demonstration of pressure ulcer analysis involves in the definition of regression lines as shown in the red lines in Fig. 5.7 and explained by the following equation:

$$p_a^A x_i + q_a^A x_j + r_a^A = 0 \quad (5.3)$$

where for two parameters of x_i and x_j , A and B are points above the threshold and C are points below the threshold. Each two points of A are used to generate the lines then the generated lines needs to be checked with the other points of C. The rules for the limited sampling zone line is to find lines from two points of A that fulfils $p_a^A x_i^B + q_a^A x_j^B + r_a^A \geq 0$ but not $p_a^A x_i^C + q_a^A x_j^C + r_a^A \geq 0$.

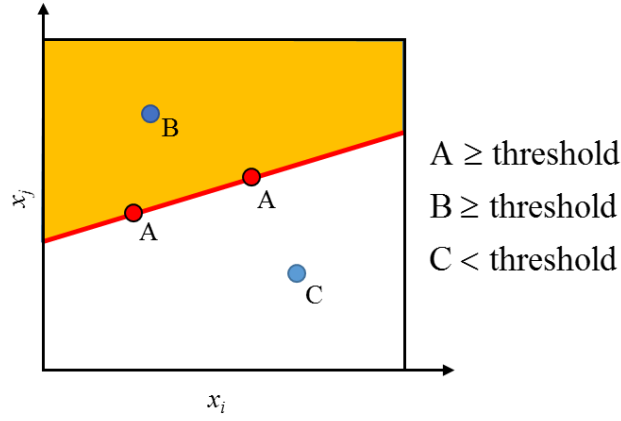


Figure 5.7: Mathematical form used to determine automatic limited sampling zone.

The threshold for the limited sampling zone in the analysis of pressure ulcer is assumed to be in the points above $\mu + 3\sigma$ shown in the red dots, where μ denotes the expected value and σ the standard deviation. In the case of Fig. 5.8, the wrong example of the line is shown in the left figure and the correct one on the right figure. Multiple linear equations using Eq. (3.5) were determined in the three-dimensional space of input parameters, E_{fat} , G_{fat} and E_{muscle} . In this analysis, the limited sampling zone could be defined by the combinations of $E_{fat} - G_{fat}$ and $E_{fat} - E_{muscle}$, but could not be defined for $E_{muscle} - G_{fat}$. In the end, only the correlation between $E_{fat} - E_{muscle}$ was found by combining all results from $E_{fat} - G_{fat}$ and $E_{fat} - E_{muscle}$. In one of the result in Fig. 5.8, it was shown that the governing lines were found to be $\{-0.985E_{muscle} - 0.158E_{fat} + 0.067 \geq 0\}$ and $\{E_{fat} - 0.061 \geq 0\}$.

The result is then also limited to the lower and upper limit as defined in Table 4.1. An example of the final limited sampling zone for $s(G_{fat}, I_{fm} = 9.69, b = lateral-A, L_a = 8, a_{mid} = 104.38)$ can be seen in Table 5.2 and Fig. 5.9 showing the following limited sampling zone:

$$\begin{aligned}
 LSZ_{E_{muscle} \& E_{fat}} &= s(G_{fat}, \mathbf{I}_{fm}, \mathbf{b}, \mathbf{L}_a, \mathbf{a}_{mid} | E_{muscle}, E_{fat}; p_a E_{muscle} + q_a E_{fat} + r_a \geq 0 \forall a) \\
 &= s(G_{fat}, 9.69, lateral-A, 4, 104.38 | E_{muscle}, E_{fat}; p_a E_{muscle} + q_a E_{fat} + r_a \geq 0 \forall a)
 \end{aligned}
 \tag{5.4}$$

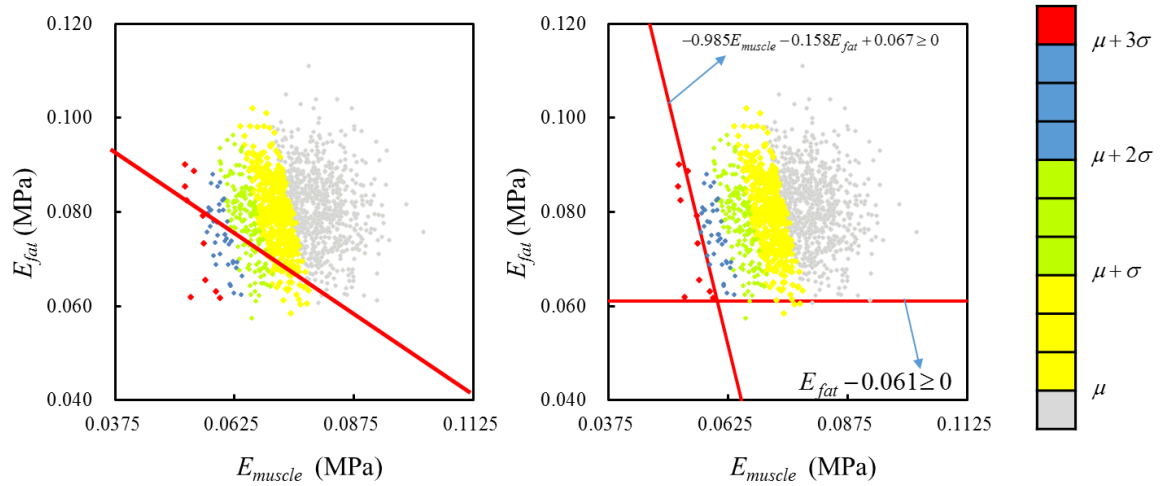


Figure 5.8: Example of defining the limited sampling zone of $s(G_{fat}, I_{fm} = 9.69, b = \text{lateral-A}, L_a = 8, a_{mid} = 104.38 | E_{muscle}, E_{fat}; p_a E_{muscle} + q_a E_{fat} + r_a \geq 0 \forall a)$

Table 5.2: Equations that shapes the polygon that governs the limited sampling zone of pressure ulcer occurrence at $s(G_{fat}, I_{fm} = 9.69, b = \text{lateral-A}, L_a = 8, a_{mid} = 104.38)$.

a	p_a	q_a	r_a
1	-0.970	-0.234	0.073
2	-0.985	-0.158	0.067
3	-0.989	0.138	0.045
4	0.000	1.000	-0.061

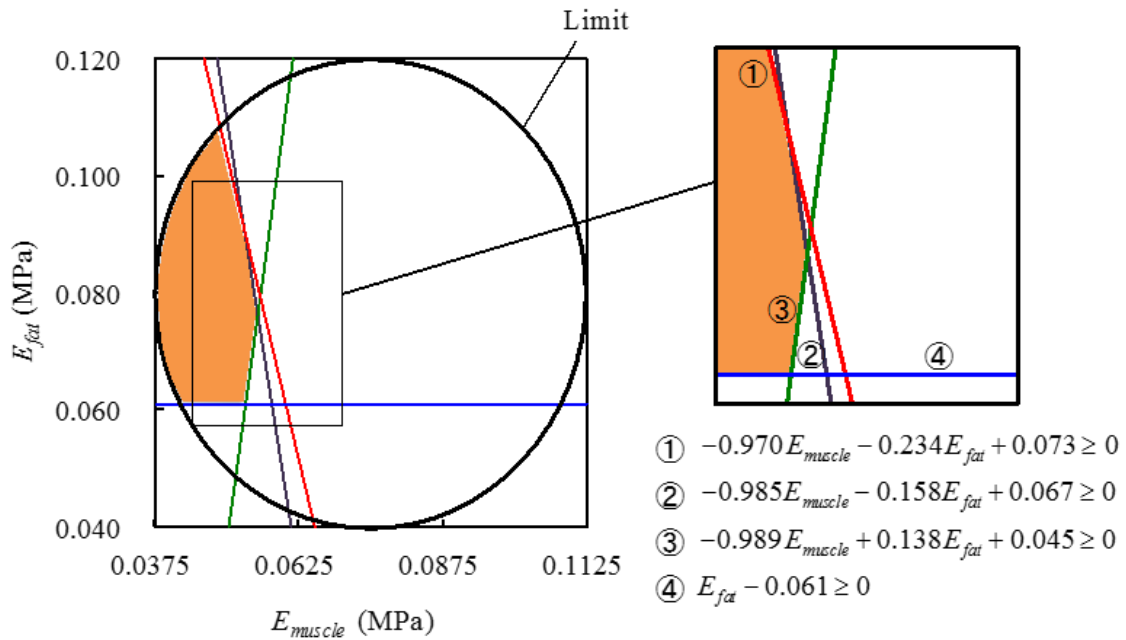


Figure 5.9: Limited sampling zone at $s(G_{fat}, I_{fm} = 9.69, b = \text{lateral-A}, L_a = 8, a_{mid} = 104.38)$. The limit is defined in the material properties in Table 3.1.

The limited sampling zone for all 54 combinations of sampling points can be seen in Table 5.3 and Appendix A showing the correlation between $E_{fat} - E_{muscle}$ after

combining all results from $E_{fat} - G_{fat}$ and $E_{fat} - E_{muscle}$. The number of lines generating the polygon varies from 2 to 5 lines. This number of lines comes from the prediction rule of pressure ulcer occurrence for each of the combination of sampling points. This polygon is also limited by the lower and upper limit of E_{fat} and E_{muscle} described in Table 4.1.

Table 5.3: All governing equations for all 54 combination of discrete sampling points.

i	I_{fm}	b	L_a	a_{mid}	a	p_a	q_a	r_a
1	9.69	supine	4	42.23	1	-0.881	-0.466	0.084
					2	-0.955	-0.287	0.076
					3	0.000	1.000	-0.064
2	9.69	supine	4	104.38	1	-0.911	-0.404	0.081
					2	-0.955	-0.287	0.076
					3	0.000	1.000	-0.064
3	9.69	supine	4	166.63	1	-0.996	0.067	0.051
					2	-0.833	-0.546	0.085
					3	0.000	1.000	-0.068
4	9.69	supine	8	42.23	1	-0.955	-0.287	0.076
					2	0.000	1.000	-0.064
5	9.69	supine	8	104.38	1	-0.881	-0.465	0.085
					2	-0.955	-0.287	0.076
					3	0.000	1.000	-0.064
6	9.69	supine	8	166.63	1	-0.996	0.067	0.052
					2	-0.955	-0.287	0.076
					3	0.000	1.000	-0.068
7	9.69	lateral-A	4	42.23	1	-0.985	-0.158	0.067
					2	-0.971	-0.228	0.072
					3	-0.970	-0.234	0.073
					4	-0.957	0.287	0.030
					5	0.000	1.000	-0.079
8	9.69	lateral-A	4	104.38	1	-0.970	-0.234	0.073
					2	-0.985	-0.158	0.067
					3	-0.876	-0.474	0.089
					4	0.000	1.000	-0.061
9	9.69	lateral-A	4	166.63	1	-0.961	0.275	0.032
					2	0.000	1.000	-0.082
10	9.69	lateral-A	8	42.23	1	-0.970	-0.234	0.073
					2	-0.957	-0.287	0.030
					3	-0.818	0.575	0.004
					4	0.000	1.000	-0.081
11	9.69	lateral-A	8	104.38	1	-0.970	-0.234	0.073
					2	-0.985	-0.158	0.067
					3	-0.989	0.138	0.045
					4	0.000	1.000	-0.061
12	9.69	lateral-A	8	166.63	1	-0.961	0.275	0.032
					2	-0.970	0.242	0.035
					3	0.000	1.000	-0.079
13	9.69	lateral-B	4	42.23	1	-0.998	-0.020	0.060
					2	0.000	1.000	-0.075
14	9.69	lateral-B	4	104.38	1	-0.989	0.139	0.045
					2	-0.980	0.196	0.039
					3	-0.819	0.573	-0.001
					4	0.000	1.000	-0.075
15	9.69	lateral-B	4	166.23	1	-0.998	-0.033	0.062
					2	-0.971	0.238	0.040
					3	-0.997	-0.040	0.063
					4	-0.991	0.120	0.051
					5	0.000	1.000	-0.071

i	I_{fm}	b	L_a	a_{mid}	a	p_a	q_a	r_a
16	9.69	lateral-B	8	42.23	1	-0.979	-0.196	0.059
					2	-0.948	-0.316	0.028
					3	0.000	1.000	-0.075
17	9.69	lateral-B	8	104.38	1	-0.994	-0.088	0.064
					2	-0.993	0.110	0.047
					3	0.000	1.000	-0.065
18	9.69	lateral-B	8	166.63	1	-0.998	-0.010	0.060
					2	-0.857	0.514	0.011
					3	0.000	1.000	-0.078
19	15.2	supine	4	42.23	1	-0.683	-0.726	0.087
					2	0.000	1.000	-0.068
20	15.2	supine	4	104.38	1	-0.955	-0.287	0.076
					2	0.000	1.000	-0.064
21	15.2	supine	4	166.63	1	-0.985	0.165	0.048
					2	-0.891	-0.445	0.091
					3	0.000	1.000	-0.064
22	15.2	supine	8	42.23	1	-0.911	-0.404	0.081
					2	-0.968	-0.242	0.073
					3	0.000	1.000	-0.064
23	15.2	supine	8	104.38	1	-0.955	-0.287	0.076
					2	-0.905	-0.418	0.081
					3	0.000	1.000	-0.064
24	15.2	supine	8	166.63	1	-0.996	0.067	0.052
					2	-0.970	-0.226	0.084
					3	0.000	1.000	-0.068
25	15.2	lateral-A	4	42.23	1	-0.985	-0.158	0.067
					2	-0.985	0.168	0.043
					3	-0.894	0.447	0.013
					4	0.000	1.000	-0.081
26	15.2	lateral-A	4	104.38	1	-0.971	-0.228	0.072
					2	-0.962	-0.263	0.075
					3	-0.752	0.658	-0.015
					4	0.000	1.000	-0.082
27	15.2	lateral-A	4	166.63	1	-0.999	0.020	0.050
					2	0.000	1.000	0.079
28	15.2	lateral-A	8	42.23	1	-0.985	-0.158	0.067
					2	0.000	1.000	-0.081
29	15.2	lateral-A	8	104.38	1	-0.985	-0.158	0.067
					2	-0.962	-0.263	0.075
					3	-0.970	0.242	0.031
					4	0.000	1.000	-0.079
30	15.2	lateral-A	8	166.63	1	-0.961	0.275	0.032
					2	-0.970	0.242	0.035
					3	0.000	1.000	-0.079
31	15.2	lateral-B	4	42.23	1	-0.703	-0.703	0.111
					2	0.000	1.000	-0.075
32	15.2	lateral-B	4	104.38	1	-0.853	0.523	0.004
					2	-0.852	0.524	0.004
					3	0.000	1.000	-0.075

i	I_{fm}	b	L_a	a_{mid}	a	p_a	q_a	r_a
33	15.2	lateral-B	4	166.63	1	-0.971	0.238	0.040
					2	-0.957	0.287	0.033
					3	-0.997	-0.040	0.063
					4	-0.994	0.097	0.053
					5	0.000	1.000	-0.065
34	15.2	lateral-B	8	42.23	1	-0.961	0.274	0.032
					2	-0.948	-0.316	0.028
					3	0.000	1.000	-0.060
35	15.2	lateral-B	8	104.38	1	-0.998	-0.020	0.060
					2	-0.985	0.165	0.042
					3	0.000	1.000	-0.075
36	15.2	lateral-B	8	166.63	1	-0.995	-0.080	0.062
					2	-0.862	0.507	0.009
					3	0.000	1.000	-0.074
37	22.92	supine	4	42.23	1	-0.996	0.067	0.052
					2	0.000	1.000	-0.068
38	22.92	supine	4	104.38	1	-0.874	-0.479	0.085
					2	0.000	1.000	0.064
39	22.92	supine	4	166.63	1	-0.994	0.101	0.050
					2	-0.998	0.020	0.055
					3	0.000	1.000	-0.068
40	22.92	supine	8	42.23	1	-0.997	-0.047	0.061
					2	0.000	1.000	-0.068
41	22.92	supine	8	104.38	1	-0.997	-0.053	0.061
					2	0.000	1.000	-0.068
42	22.92	supine	8	166.63	1	-0.939	0.344	0.023
					2	-0.997	0.050	0.052
					3	0.000	1.000	-0.075
43	22.92	lateral-A	4	42.23	1	-0.998	-0.038	0.059
					2	-0.970	0.242	0.035
					3	0.000	1.000	-0.079
44	22.92	lateral-A	4	104.38	1	-0.962	-0.263	0.075
					2	0.000	1.000	-0.061
45	22.92	lateral-A	4	166.63	1	-0.973	0.230	0.036
					2	-0.923	0.385	0.020
					3	0.000	1.000	-0.079
46	22.92	lateral-A	8	42.23	1	-0.973	0.230	0.036
					2	-0.989	0.143	0.044
					3	0.000	1.000	-0.079
47	22.92	lateral-A	8	104.38	1	-0.970	0.242	0.035
					2	0.000	1.000	-0.079
48	22.92	lateral-A	8	166.63	1	-0.970	0.242	0.035
					2	-0.973	0.230	0.036
					3	0.000	1.000	-0.079
49	22.92	lateral-B	4	42.23	1	-0.952	0.306	0.028
					2	-0.975	0.220	0.038
					3	0.000	1.000	-0.075
50	22.92	lateral-B	4	104.38	1	-0.995	0.092	0.049
					2	-0.988	0.148	0.043
					3	0.000	1.000	-0.075
51	22.92	lateral-B	4	166.63	1	-0.952	0.306	0.028
					2	-0.997	0.055	0.051
					3	0.000	1.000	-0.075
52	22.92	lateral-B	8	42.23	1	-0.952	0.306	0.028
					2	-0.975	0.220	0.038
					3	0.000	1.000	-0.075

i	I_{fm}	b	L_a	a_{mid}	a	p_a	q_a	r_a
53	22.92	lateral-B	8	104.38	1	-0.942	0.336	0.024
					2	-0.989	0.142	0.044
					3	0.000	1.000	-0.075
54	22.92	lateral-B	8	166.63	1	-0.957	0.287	0.031
					2	0.000	1.000	-0.065

5.4 Projection of Limited Sampling Zone

After the process of convergence check and deciding the limited sampling zone for all 54 models as seen in Eq. (4.2), the results from those seven-dimensional spaces are then put into a two-dimensional space by projection following Eq. (3.6). The 54 limited sampling zones were projected onto one plane forming a single limited sampling zone with the same combination of x_i and x_j , or in the demonstration E_{fat} and E_{muscle} . In this demonstrative analysis, the tail distribution is analyzed for two fixed parameters without defined pdf as $L_a = 6$ mm and $a_{mid} = 70.88$ mm. Then, the other two parameters without defined pdf, I_{fm} and b are eliminated by projection following equation.

$$\begin{aligned}
LSZ_{E_{muscle} \& E_{fat}}(I_{fm}, b) &= \{s; \bigcup I_{fm}, \bigcup b; p_a E_{muscle} + q_a E_{fat} + r_a \geq 0 \forall a\} \\
&= s(G_{fat}, L_a, a_{mid} | E_{muscle}, E_{fat}, I_{fm}, b; p_a E_{muscle} + q_a E_{fat} + r_a \geq 0 \forall a)
\end{aligned} \tag{5.5}$$

An example of the projection for $s(G_{fat}, L_a = 4, a_{mid} = 104.38 | E_{muscle}, E_{fat}, I_{fm}, b; p_a E_{muscle} + q_a E_{fat} + r_a \geq 0 \forall a)$ can be seen in Fig. 5.10 and the resulted projection can be seen in Fig. 5.11. Because the projection is performed in L_a and a_{mid} , the other two parameter without defined pdf are all combined which is $3 \times 3 = 9$ limited sampling zone which are $s(G_{fat}, I_{fm} = 9.69, b = \text{supine}, L_a = 4, a_{mid} = 104.38)$, $s(G_{fat}, I_{fm} = 9.69, b = \text{lateral-A}, L_a = 4, a_{mid} = 104.38)$, $s(G_{fat}, I_{fm} = 9.69, b = \text{lateral-B}, L_a = 4, a_{mid} = 104.38)$, $s(G_{fat}, I_{fm} = 15.2, b = \text{supine}, L_a = 4, a_{mid} = 104.38)$, $s(G_{fat}, I_{fm} = 15.2, b = \text{lateral-A}, L_a = 4, a_{mid} = 104.38)$, $s(G_{fat}, I_{fm} = 15.2, b = \text{lateral-B}, L_a = 4, a_{mid} = 104.38)$, $s(G_{fat}, I_{fm} = 22.92, b = \text{supine}, L_a = 4, a_{mid} = 104.38)$, $s(G_{fat}, I_{fm} = 22.92, b = \text{lateral-A}, L_a = 4, a_{mid} = 104.38)$, $s(G_{fat}, I_{fm} = 22.92, b = \text{lateral-B}, L_a = 4, a_{mid} = 104.38)$.

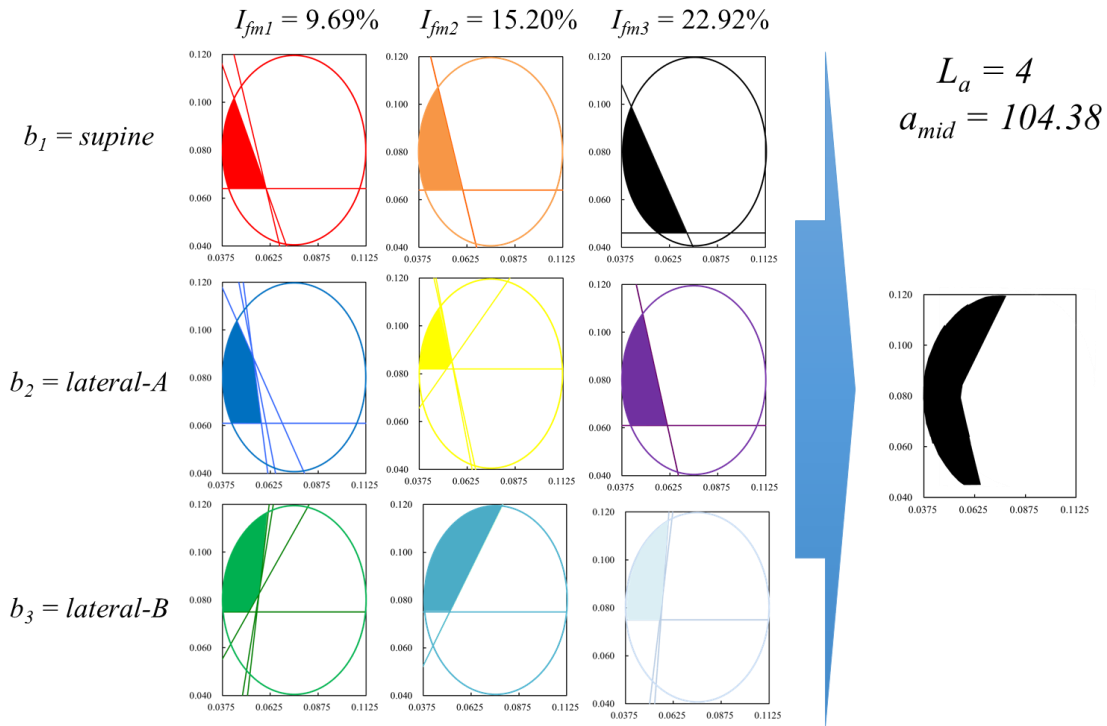


Figure 5.10: In order to make the projection, the related LSZ for all $L_a = 4$ and $a_{mid} = 104.38$ are unioned into a single LSZ. The figure here shows an example for the projection for $s(G_{fat}, L_a = 4, a_{mid} = 104.38 | E_{muscle}, E_{fat}, I_{fm}, b; p_a E_{muscle} + q_a E_{fat} + r_a \geq 0 \forall a)$.

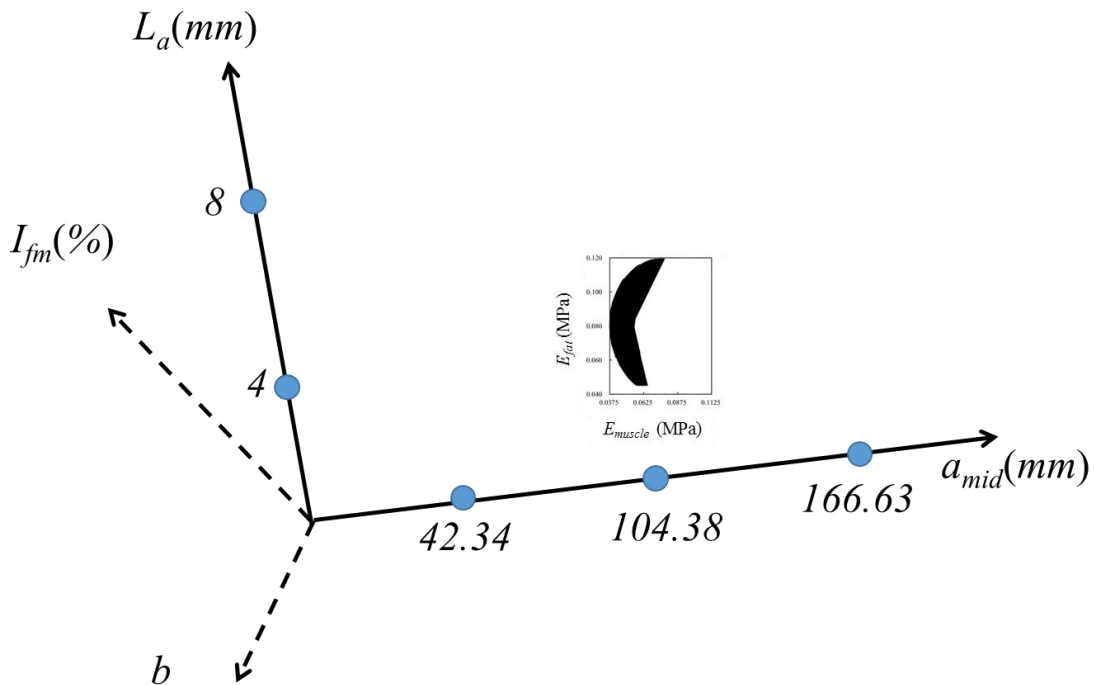


Figure 5.11: Projection result for $s(G_{fat}, L_a = 4, a_{mid} = 104.38 | E_{muscle}, E_{fat}, I_{fm}, b; p_a E_{muscle} + q_a E_{fat} + r_a \geq 0 \forall a)$ as shown in the multi dimension figure. The dashed line for I_{fm} and b means that those parameters has been projected into L_a and a_{mid} .

Using the same projection procedure, the limited sampling zones for combination of $L_a = 4$ mm and 8 mm and $a_{mid} = 42.23$ mm and 104.38 mm are obtained as shown in Fig. 5.12. The same figure also shows the limited sampling zone of the sampling point to be analyzed, which is $LSZ_{E_{muscle} \& E_{fat}}(\mathbf{I}_{fm}, \mathbf{b})^{a_{mid}=70.88 \& L_a=6}$ with the zoomed view of the red area can be seen in Fig. 5.13. In order to find this limited sampling, an interpolation procedure was used. Extrapolation should not be used since the bounds has been determined and there is no sure way to say that unexpected events can happen outside the bounds. There are several interpolation method such as linear interpolation, 2nd order interpolation, and bilinear interpolation. However, to perform 2nd order interpolation, at least 3 points with the same interval are needed and it is impossible to perform bilinear interpolation because a new multiplication type is needed to explain the mathematical process. A linear interpolation of polygon was performed for corresponding polygon nodes. For those parameters to which the interpolation is applied, a linear measure to describe the distance between sampling points is necessary. The mathematical formula for the linear interpolation can be explain using Fig. 5.14 and the following equation:

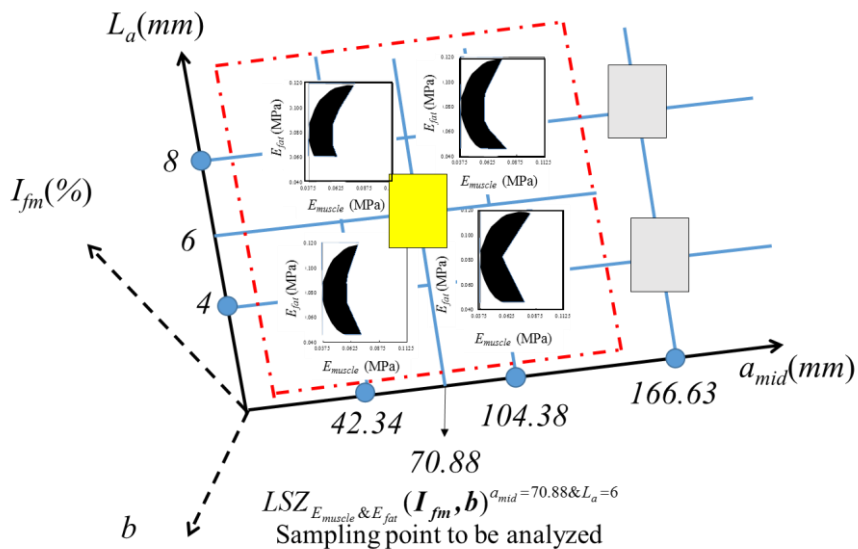


Figure 5.12: This figure shows the location of the sampling point to be analyzed in the yellow box. Currently the 4 surrounding LSZ are the only known LSZ as shown in the figure above. Rather than restarting the analysis from the beginning to find the LSZ at $L_a = 4$ mm and $a_{mid} = 70.88$, a linear interpolation is performed.

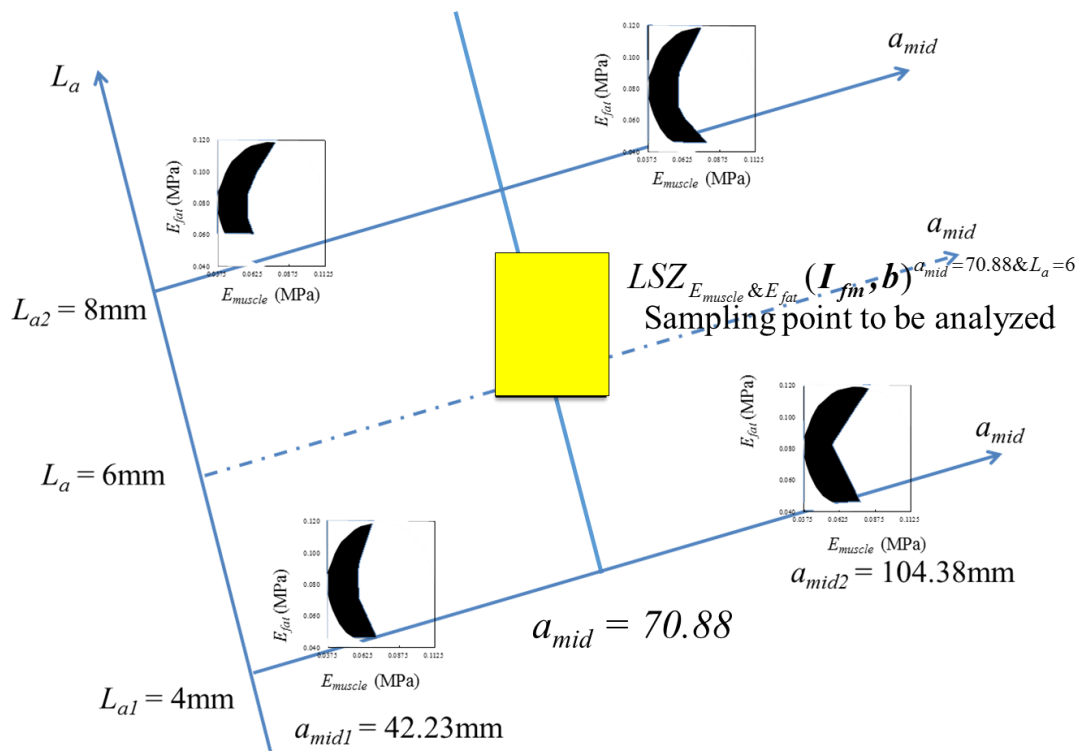


Figure 5.13: The initial sampling points with limited sampling zone that was created. This figure also shows the location of sampling points that are going to be analyzed.

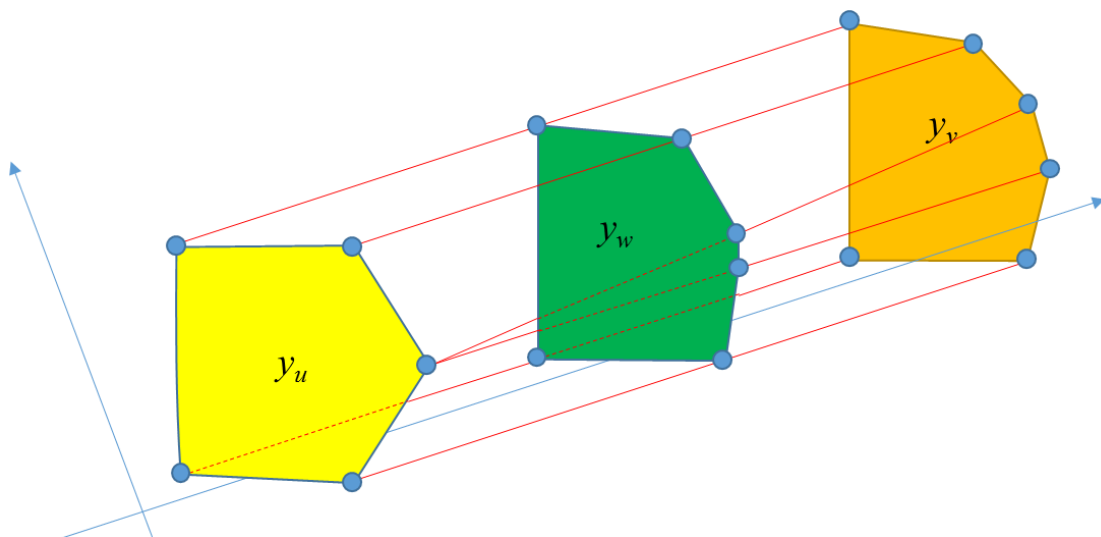


Figure 5.14: A general form for linear interpolation calculation. The process involves changing the equation of polygon in y_u and y_v into points and then performing the interpolation into y_w from those points. After the interpolation of the points, the polygon is then regenerated in y_w .

$$\begin{aligned}
LSZ_{ij}(\mathbf{y}_k)^{y_n=y_w} &= \{s \mid \bigcup \mathbf{y}_k, y_n = y_w; p_a x_i + q_a x_j + r_a \geq 0 \forall a\} \\
&= s(x_1, \dots, x_{i-1}, x_{i+1}, \dots, x_{j-1}, x_{j+1}, \dots, x_{m_1}, \mathbf{y}_1, \dots, \\
&\quad \mathbf{y}_{k-1}, \mathbf{y}_{k+1}, \dots, \mathbf{y}_{n-1}, \mathbf{y}_{n+1}, \dots, \mathbf{y}_{m_2} \mid x_i, x_j, \bigcup \mathbf{y}_k, \\
&\quad y_n = y_w; p_a x_i + q_a x_j + r_a \geq 0 \forall a) (i < j) (k < n) \\
&= \frac{|y_u| - |y_w|}{|y_v| - |y_u|} \otimes LSZ_{ij}(\mathbf{y}_k)^{y_n=y_u} \oplus \frac{|y_v| - |y_w|}{|y_v| - |y_u|} \otimes LSZ_{ij}(\mathbf{y}_k)^{y_n=y_v}
\end{aligned} \tag{5.6}$$

where \otimes and \oplus are the operators applied to the polygon nodes. In this example, the measures for L_a and a_{mid} are straightforward. Using Eq. (5.6) the interpolation procedure is described in the following equation:

$$\begin{aligned}
LSZ_{E_{muscle} \& E_{fat}}(\mathbf{I}_{fm}, \mathbf{b})^{a_{mid}=70.88 \& L_a=6} &= \frac{1}{2} \otimes LSZ_{E_{muscle} \& E_{fat}}(\mathbf{I}_{fm}, \mathbf{b})^{a_{mid}=70.88 \& L_a=4} \oplus \frac{1}{2} \otimes LSZ_{E_{muscle} \& E_{fat}}(\mathbf{I}_{fm}, \mathbf{b})^{a_{mid}=70.88 \& L_a=8} \\
&= \frac{1}{2} \otimes \left\{ \frac{1}{2} \otimes LSZ_{E_{muscle} \& E_{fat}}(\mathbf{I}_{fm}, \mathbf{b})^{a_{mid}=42.23 \& L_a=4} \oplus \frac{1}{2} \otimes LSZ_{E_{muscle} \& E_{fat}}(\mathbf{I}_{fm}, \mathbf{b})^{a_{mid}=104.38 \& L_a=4} \right\} \\
&\quad \oplus \frac{1}{2} \otimes \left\{ \frac{1}{2} \otimes LSZ_{E_{muscle} \& E_{fat}}(\mathbf{I}_{fm}, \mathbf{b})^{a_{mid}=42.23 \& L_a=8} \oplus \frac{1}{2} \otimes LSZ_{E_{muscle} \& E_{fat}}(\mathbf{I}_{fm}, \mathbf{b})^{a_{mid}=104.38 \& L_a=8} \right\}
\end{aligned} \tag{5.7}$$

The factors before the operator \otimes denotes the weighting factor and they are all $\frac{1}{2}$ in this case because the target sampling point is at the middle point of the discrete sampling points.

The first interpolation was performed twice and can be seen in Fig. 5.15 with the equation shown in Eq. (5.8) for $LSZ_{E_{muscle} \& E_{fat}}(\mathbf{I}_{fm}, \mathbf{b})^{a_{mid}=70.88 \& L_a=4}$ and Eq. (5.9) for $LSZ_{E_{muscle} \& E_{fat}}(\mathbf{I}_{fm}, \mathbf{b})^{a_{mid}=70.88 \& L_a=8}$. The second interpolation can be seen in Fig. 5.16 with the equation shown in Eq. (5.10) for $LSZ_{E_{muscle} \& E_{fat}}(\mathbf{I}_{fm}, \mathbf{b})^{a_{mid}=70.88 \& L_a=6}$.

$$\begin{aligned}
LSZ_{E_{muscle} \& E_{fat}}(\mathbf{I}_{fm}, \mathbf{b})^{a_{mid}=70.88 \& L_a=4} &= \frac{1}{2} \otimes LSZ_{E_{muscle} \& E_{fat}}(\mathbf{I}_{fm}, \mathbf{b})^{a_{mid}=42.23 \& L_a=4} \\
&\quad \oplus \frac{1}{2} \otimes LSZ_{E_{muscle} \& E_{fat}}(\mathbf{I}_{fm}, \mathbf{b})^{a_{mid}=104.38 \& L_a=4}
\end{aligned} \tag{5.8}$$

$$\begin{aligned}
LSZ_{E_{muscle} \& E_{fat}}(\mathbf{I}_{fm}, \mathbf{b})^{a_{mid}=70.88 \& L_a=8} &= \frac{1}{2} \otimes LSZ_{E_{muscle} \& E_{fat}}(\mathbf{I}_{fm}, \mathbf{b})^{a_{mid}=42.23 \& L_a=8} \\
&\quad \oplus \frac{1}{2} \otimes LSZ_{E_{muscle} \& E_{fat}}(\mathbf{I}_{fm}, \mathbf{b})^{a_{mid}=104.38 \& L_a=8}
\end{aligned} \tag{5.9}$$

$$\begin{aligned}
LSZ_{E_{muscle} \& E_{fat}}(\mathbf{I}_{fm}, \mathbf{b})^{a_{mid}=70.88 \& L_a=6} &= \frac{1}{2} \otimes LSZ_{E_{muscle} \& E_{fat}}(\mathbf{I}_{fm}, \mathbf{b})^{a_{mid}=70.88 \& L_a=4} \\
&\quad \oplus \frac{1}{2} \otimes LSZ_{E_{muscle} \& E_{fat}}(\mathbf{I}_{fm}, \mathbf{b})^{a_{mid}=70.88 \& L_a=8}
\end{aligned} \tag{5.10}$$

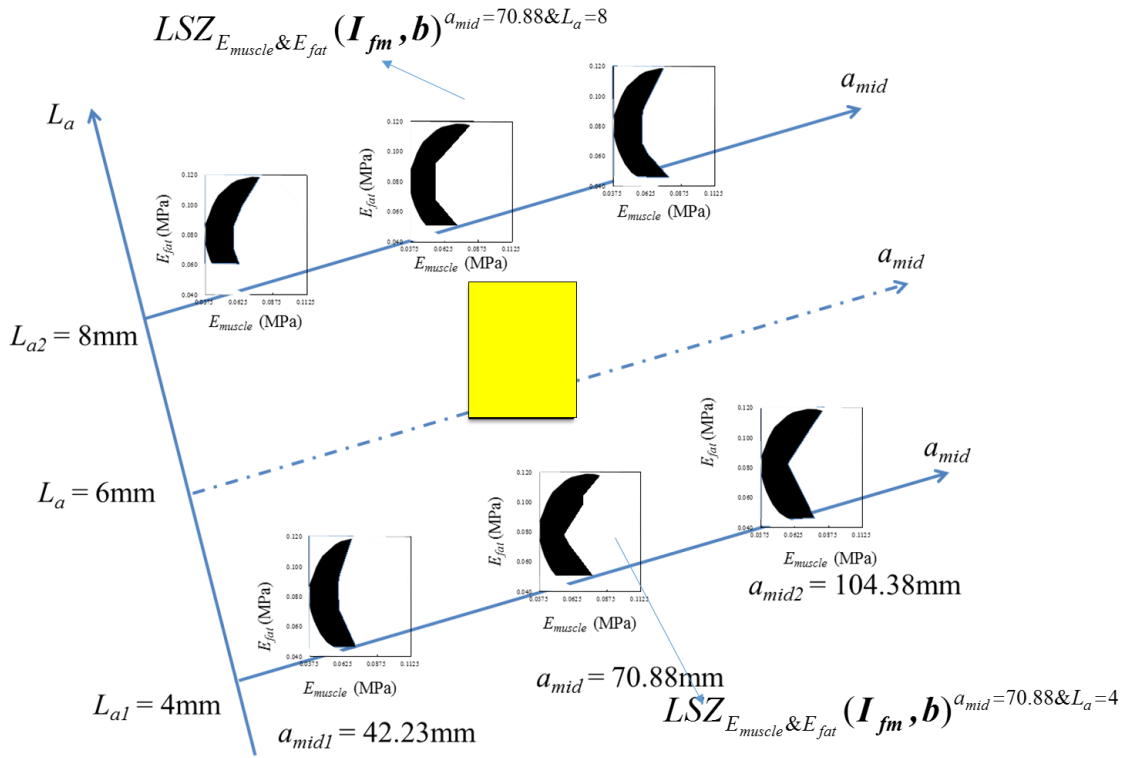


Figure 5.15: The first two interpolation process were performed for $LSZ_{E_{muscle} & E_{fat}}(I_{fm}, b)^{a_{mid}=70.88 & L_a=4}$ and $LSZ_{E_{muscle} & E_{fat}}(I_{fm}, b)^{a_{mid}=70.88 & L_a=8}$.

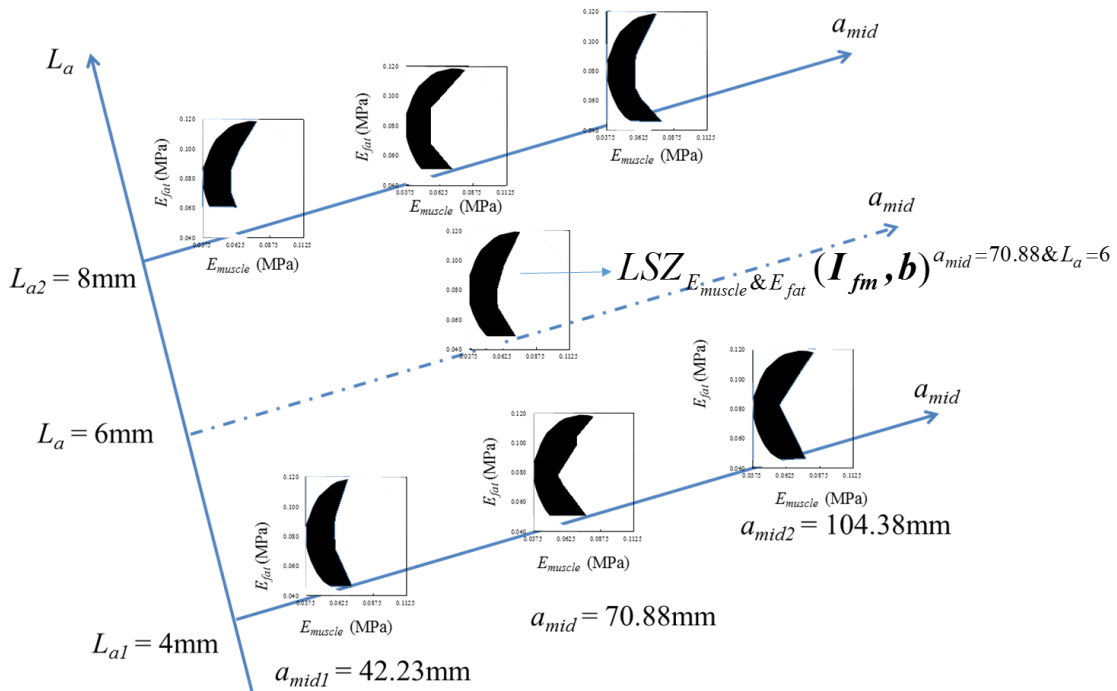


Figure 5.16: The second interpolation process was performed at the sampling points to be analyzed for $LSZ_{E_{muscle} & E_{fat}}(I_{fm}, b)^{a_{mid}=70.88 & L_a=6}$.

The finally obtained limited sampling zone at $L_a = 6$ mm and $a_{mid} = 70.88$ mm was bounded by 6 equations as shown in Table 5.4 and Fig. 5.17.

In this demonstration, looking at the finally obtained results in Fig. 5.17, the green triangle and yellow square have the same E_{fat} and E_{muscle} but different parameter with respect to I_{fm} , the pdf of which is not defined. In this 2D figure, the same points gave different strain values because the parameter without defined pdf (I_{fm}) is different. This demonstrative example may clearly show how the projection was performed. Note that when the projection or union operation is performed, previously obtained linear equations forming each polygon can be used as they are, and there is no need to re-define the polygon after union operation.

Table 5.4: Equations that shapes the polygon that governs the limited sampling zone of pressure ulcer occurrence at $L_a = 6$ mm and $a_{mid} = 70.88$ mm.

a	p_a	q_a	r_a
1	-0.866	0.500	0.007
2	-0.914	0.406	0.019
3	-0.948	0.316	0.029
4	-0.997	-0.047	0.062
5	-0.823	-0.562	0.088
6	0.000	1.000	-0.050

Table 5.5: Obtained combination of parameters related to the highest strain value in the tail distribution of pressure with verification.

Input parameters with pdf			Input parameters without defined pdf				QoI
Young's modulus of fat (MPa)	Shear modulus of fat (MPa)	Young's modulus of muscle (MPa)	Length of cutout (mm)	Location of cutout (mm)	Configuration of fat and muscle	Loading area	$ \gamma_m $ (%)
5.15×10^{-2}	1.85×10^{-2}	6.20×10^{-2}	6	70.88	<i>Very fat-rich</i>	<i>Supine</i>	13.2
5.15×10^{-2}	1.84×10^{-2}	4.19×10^{-2}	6	70.88	<i>Very fat-rich</i>	<i>Supine</i>	12.3
1.13×10^{-2}	4.03×10^{-2}	4.19×10^{-2}	6	70.88	<i>Very fat-rich</i>	<i>Supine</i>	4.2
5.15×10^{-2}	1.85×10^{-2}	6.20×10^{-2}	6	70.88	<i>Muscle-rich</i>	<i>Supine</i>	5.26
5.15×10^{-2}	1.84×10^{-2}	4.19×10^{-2}	6	70.88	<i>Muscle-rich</i>	<i>Supine</i>	4.73
1.13×10^{-2}	4.03×10^{-2}	4.19×10^{-2}	6	70.88	<i>Muscle-rich</i>	<i>Supine</i>	0.86
5.33×10^{-2}	1.90×10^{-2}	6.89×10^{-2}	6	70.88	<i>Fat-rich</i>	<i>Supine</i>	4.62
5.15×10^{-2}	1.84×10^{-2}	4.19×10^{-2}	6	70.88	<i>Fat-rich</i>	<i>Supine</i>	3.47
1.13×10^{-2}	4.03×10^{-2}	4.19×10^{-2}	6	70.88	<i>Fat-rich</i>	<i>Supine</i>	2.38

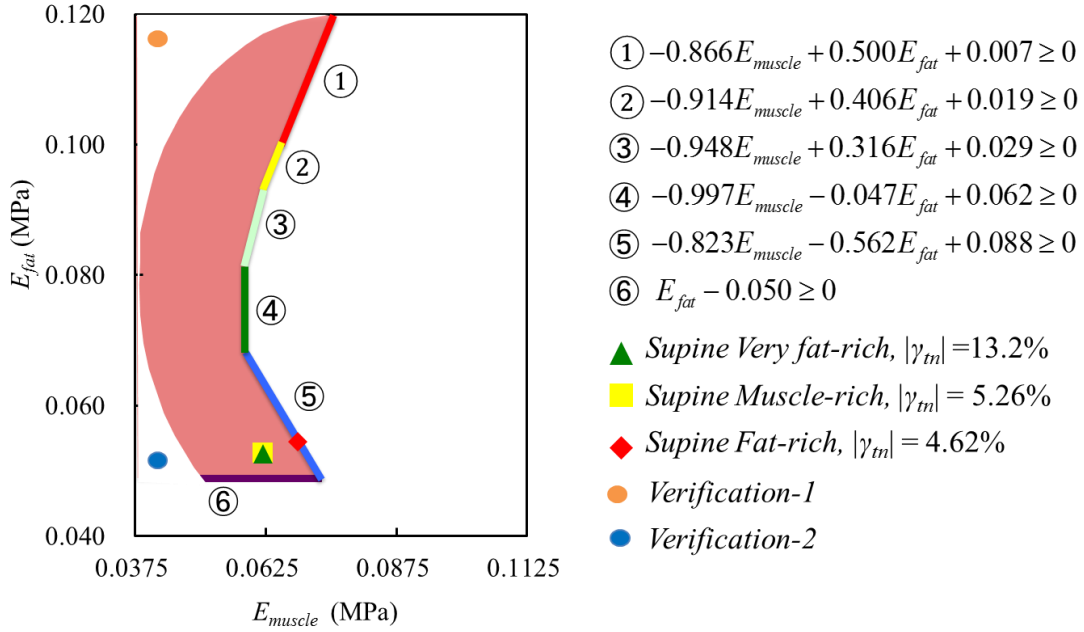


Figure 5.17: Tail distribution of pressure ulcer occurrence at $L_a = 6$ mm and $a_{mid} = 70.88$ mm showing the highest $|\gamma_{tm}|$ values at b_2 (supine). Verification points are also shown in this figure showing 2 verification location.

5.5 Results of Tail Distribution Analysis

Following Eq. (3.7), the new collection of sampling for the re-analysis in pressure ulcer analysis could be determined as follows:

$$s = \{s \subset LSZ_{E_{muscle} \& E_{fat}}(\mathbf{I}_{fm}, \mathbf{b})^{a_{mid}=70.88 \& L_a=6}\} \quad (5.11)$$

The total number of cases is 9 with respect to \mathbf{I}_{fm} and \mathbf{b} . The number of samples for each case is 1,000 in the following.

Three cases with very high strains among all results in the limited sampling zone in Fig. 5.17 are summarized in Table 5.5. It was found that high shear strain values appeared under supine position, although two lateral positions were also analyzed. The material properties of fat and muscle for three cases are plotted in Fig. 5.17.

Generally speaking, the result shows that high strains occur when the patient under supine position has low E_{muscle} and low E_{fat} . If the patient is in very fat-rich

condition, very high strain may occur. Except this special case, the volume fraction of fat or muscle seems to be not sensitive to the strain value.

One interesting result is that shear strains were higher than normal strains. Normal strains will lead to the breakage of loose fibril tissue under tension, but the result implies that damage due to shear deformation is more likely. Although linear problem was considered, it is easy to understand that repeated shear deformation applied to the loose fibril tissue may probably lead to fatigue fracture. As was shown in the prediction rule of pressure ulcer in Chapter 4.5, the loading angle was influential on the deformation mode at the interface. This thesis fixed the load as pressure supposing the patient lying on bed, but if the shear force is applied to the patient during position change, then the high shear strain can occur more frequently. This point is worth discussing furthermore from clinical viewpoint to improve the nursing care.

There are two types of verification that can be performed. The first verification method is to check if a combination of input parameters leading to critical value of QoI is prepared in experimental work or in numerical work, SLS can obtain or predict the prepared combination. Since the SLS can find very rare case with very low probability, the preparation of such a rare case is very hard. One master course student who very recently could apply my SLS to very simple engineering problem verified that SLS could find a very rare case but classical Monte Carlo simulation could not even after 500,000 iterations. Only possible verification method is to fix the very rare case to the prepared one. To do this, reanalysis of the whole data is needed, which will take approximately 2-3 months.

Another way to perform the verification which has already been is to check if the obtained strain value in the pressure ulcer analysis is really higher than other cases whose sampling points are located outside of the Limited Sampling Zone.

Shown in Fig. 5.17, the first location of verification shown in orange circle is a case when the E_{fat} is very high and E_{muscle} is very low, the second location shown in blue circle is a case when both E_{fat} and E_{muscle} is very low. Both are outside of the limited sampling zone. The results can be seen in Table 5.2. This result means that the critical value of QoI does not correspond to the critical value of input parameter and the merit of SLS lies in this demonstration.

CHAPTER 6

Discussions

Uncertainty is unavoidable in the numerical modeling of real phenomena and the proposed uncertainty modeling in the tail distribution will become more important especially when human life is put into consideration. Pressure ulcer is a disease that has a direct relation with quality of life (QOL), which means that the biomechanics simulation of pressure ulcer is one of the problems where tail distribution analysis is important. When nursing patient with pressure ulcer, it is important to consider cases in the tail distribution area. With this demonstrative application, this chapter discusses the feature of the proposed method for uncertainty modeling and stepwise limited sampling (SLS) scheme.

The proposed uncertainty modeling strategy considers two types of parameters: parameter with probability density function and parameter without defined probability density function. In the analysis of pressure ulcer, the most notable feature lies in the parameterization of amount and shape of fat/muscle, which is hardly expressed by a probability density function. Including such typical parameter, the critical combination in input parameters gave a critical value of quantity of interest (QoI) when a large number of input parameters were considered. The setup of parameters in the SLS method had a significant impact on the analysis performed. Parameters with probability density function (pdf) can be projected which contributes to the simplification of the problem by

reducing the number of parameters. This 2nd step of the SLS method helps the visualization of the limited sampling zone as shown in Fig. 5.11.

The fluctuation of each parameter in the pressure ulcer analysis was not small, which means that the application of the stochastic finite element method is possible. The advantage of Monte Carlo method was that any kind of uncertainty parameters can be considered. But its disadvantage was the huge computational cost. The proposed method performed the tail distribution analysis with less number of sampling points than the usual 10,000 sampling points used in the Monte Carlo simulation as shown in Table 5.1. The accuracy of the obtained result by SLS was compared with standard Monte Carlo with 10,000 cases and both agreed quite well. This shows that the convergence check method in the first step of SLS was verified and it also shows that the SLS has a merit in reducing the computational cost. Table 5.1 shows that the total number of sampling points is 86,700 for 54 cases, which is only 16% compared to the conventional method of Monte Carlo simulation. Hence, the SLS could conquer the disadvantage of Monte Carlo simulation, and was expected to be applied to variety of biomechanical and/or industrial problems. In addition, the use of parallel computing for many sampling points will reduce the computational time (Takano et al., 2012).

In the third step of SLS, the tail distribution analysis was performed and combination of input parameters was found that led to high interface strain in the pressure ulcer analysis. Low frequency probability that was difficult to analyze can now be found. To verify the generation of sampling points in Fig. 5.17, additional finite element analyses were carried out for some additional points. It was proven that the obtained values were higher than any other point in the limited sampling zone.

The suspension of Monte Carlo simulation when the expected value converged means that the SLS does not provide a reliable probability density function of QoI.

However, finding the very rare case is more important than obtaining the standard deviation of QoI. In this example of application of SLS for pressure ulcer analysis, believing that the initial damage at the bone and muscle interface results in serious future pressure ulcer, the combination of physical parameters of patients will provide useful and new information to the nursing care. This knowledge also gives the biomedical researchers the inspiration to the future experimental work using animals because the proposed simulation could point out important parameters.

CHAPTER 7

Conclusions

7.1 Findings

In this section, all findings in both studies of the computational method of tail distribution and of its application to the biomechanics analysis of the pressure ulcer are summarized.

The main contribution of this thesis lies in the development of practical sampling scheme for Monte Carlo simulation with focus on critical value of QoI in the tail distribution, which was named as stepwise limited sampling (SLS) method. The expected value of QoI is obtained with moderate accuracy, but with much less computational cost than the conventional Monte Carlo simulation. The probability density function of QoI is ignored in the SLS method, but the combination of input parameters that lead to an critical value of QoI is obtained very accurately, but with moderate computational cost. The SLS method consists of three steps. The first step is the convergence check of the expected value. The second step is the definition of limited sampling zone. The parameters in this limited sampling zone may result in an critical value of QoI. The third step is the analysis of tail distribution.

The findings in this study of SLS are listed as follows:

1. Mathematical description of the three steps in SLS was presented. The general formulation is useful when SLS is applied to variety of engineering problems.

2. The proposed rule for the convergence check in the first step was verified through comparison with classical Monte Carlo simulation using 10,000 analyses.
3. Two types of uncertainty parameters were considered, with and without defined probability density function (pdf). For those parameters without defined pdf, some discrete sampling points were analyzed and the limited sampling zones were projected. It contributed to the reduction of the number of parameters and enabled the visualization the limited sampling zones.
4. To define the limited sampling zones, two parameters were chosen among many parameters, which were enabled automatically in a computer program.
5. The limited sampling zone was approximated by polygon, which contributed not only to the automatic processing in a computer program but also to the projection process.
6. In the demonstrative analysis of pressure ulcer, the cost-effectiveness and reliability of the obtained combination of parameters that led to the really critical value were proven. In addition to the projection of the limited sampling zone, the interpolation procedure was proposed by virtue of the polygon approximation.

In addition, the findings from biomechanical and biomedical viewpoints in the study of pressure ulcer are summarized as follows:

7. For patients with low Young's moduli of fat and muscle with very fat-rich buttock lying on bed in supine position can have higher chance of occurrence of pressure ulcer due to high shear strain at the bone-muscle interface.

8. Even after the surgical treatment, external shear force during position change in nursing may cause high shear strain at the bone-muscle interface and may lead to reoccurrence of pressure ulcer.
9. There is no experimental evidence for the above results, but the obtained combination of parameters contributes much for biomechanics researchers to the planning of future animal experiments to clarify the biomechanics of pressure ulcer. Such numerical simulation may open new door to the biomechanics research.

7.2 List of Assumptions and Limitation

In the biomechanics simulation of pressure ulcer in this thesis, there remain the following limitations:

1. The numerical model is in 2D linear. 3D nonlinear problem considering large deformation and contact between buttock and bed should be solved. The load condition should be the body force due to self-weight.
2. Dynamic analysis should be carried out simulating the position change in nursing.
3. The interpolation of the limited sampling zone in the second step of SLS should be verified.
4. Further study on finding other automated algorithm should be conducted in order to make it universally applicable to any kind of problems.
5. It is possible to have an island-like shape limited sampling zone within my framework and the previously described automated algorithm may hopefully work with minor change of the computer program, but it was never

encountered in the demonstration of pressure ulcer analysis and therefore it has not yet been verified.

For future 3D and dynamic analysis, our research group have succeeded in 3D image-based modeling using commercial software Simpleware and DYNA3D, but at this moment the maximum number of elements is limited.

7.3 Future Works

The proposed SLS method should be applied to engineering problems with more parameters, which can be validated by comparison with experimental measurement. One of the attempt in our research group is the tensile test of a flat plate with multiple holes. The specimen is made by laser processing which will cause the geometrical fluctuation with respect to the size of the holes. At this moment, the accuracy of the convergence check in the first step of SLS was verified. It was also confirmed that the definition of limited sampling zones were automatically performed in computer program. The comparison with classical Monte Carlo simulation proved that even 100,000 sampling in the classical Monte Carlo simulation could not find a critical value of QoI which was very easily found by SLS method. This result shows the effectiveness of the proposed method. As a near future work, it is expected that the validity of the proposed method is proven from an experimental measurement.

After the above work on the validation, it is expected that the SLS procedure is implemented in commercial software so that many industries can use the merit of the tail distribution analysis.

A research work on the synthesis to avoid the critical value of QoI should follow as a feedback of tail distribution analysis to the design. The uncertainty of the input parameter in the analysis should be regarded as a design parameter in the framework of

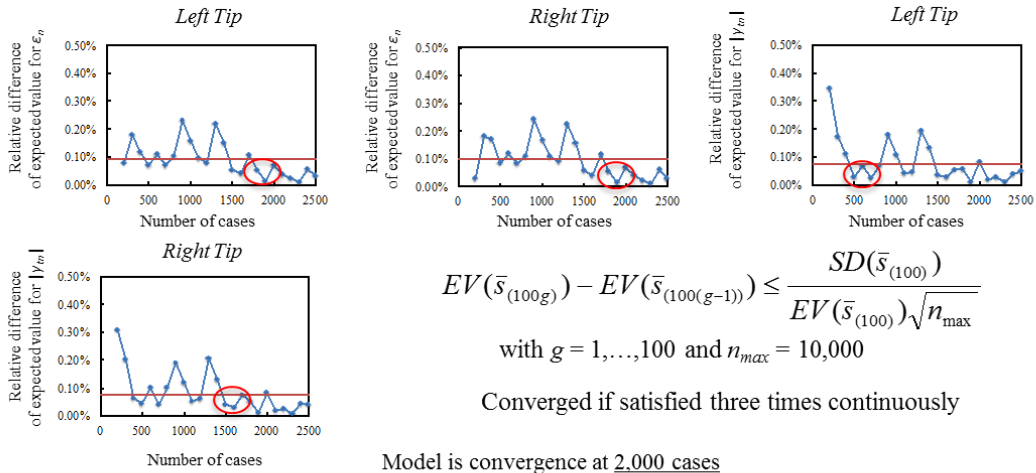
synthesis procedure. Other reliability evaluation method such as the prediction rule of pressure ulcer occurrence estimation should be cooperated in the synthesis. It will enable the design of highly reliable and sustainable products in the future.

Further study on finding other automated algorithm to find the limited sampling zone should be conducted in the future. Also, the verification of the proposed SLS method is an important issue as pointed out in Chapter 5 and it should be appended as one of the future works.

APPENDIX A

Convergence Check, Prediction Rule of Pressure Ulcer Occurrence and Limited Sampling Zone

$$I_{fm} = 9.69 \quad b = \text{supine} \quad L_a = 4 \quad a_{mid} = 42.23$$

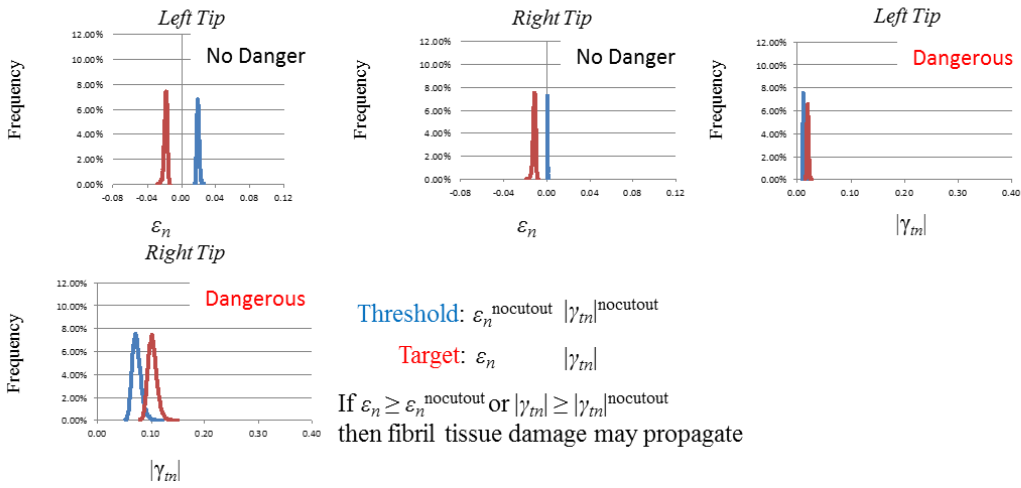


$$EV(\bar{s}_{(100g)}) - EV(\bar{s}_{(100(g-1))}) \leq \frac{SD(\bar{s}_{(100)})}{EV(\bar{s}_{(100)})\sqrt{n_{max}}}$$

with $g = 1, \dots, 100$ and $n_{max} = 10,000$

Converged if satisfied three times continuously

Model is convergence at 2,000 cases



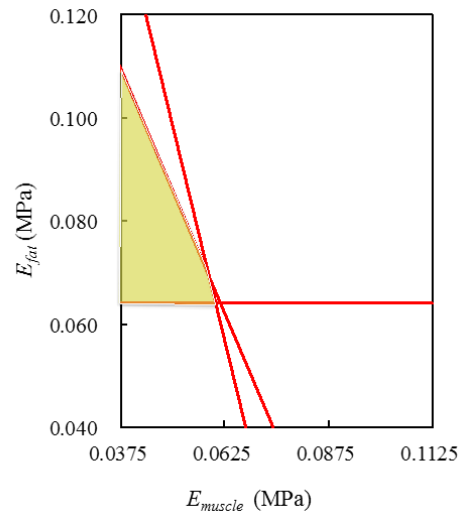
Threshold: $\epsilon_n^{nocutout} \quad |\gamma_m|^{nocutout}$

Target: $\epsilon_n \quad |\gamma_m|$

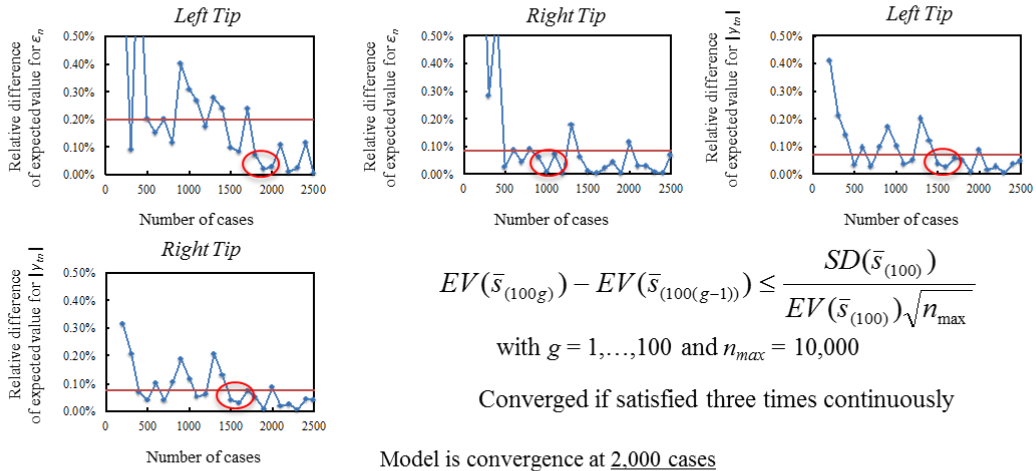
If $\epsilon_n \geq \epsilon_n^{nocutout}$ or $|\gamma_m| \geq |\gamma_m|^{nocutout}$
then fibril tissue damage may propagate

$$LSZ_{E_{muscle}E_{fat}} = \{s; p_a E_{muscle} + q_a E_{fat} + r_a \geq 0 \forall a\}$$

a	p_a	q_a	r_a
1	-0.881	-0.466	0.084
2	-0.955	-0.287	0.076
3	0	1	-0.064



$$I_{fm} = 9.69 \quad b = \text{supine} \quad L_a = 4 \quad a_{mid} = 104.38$$

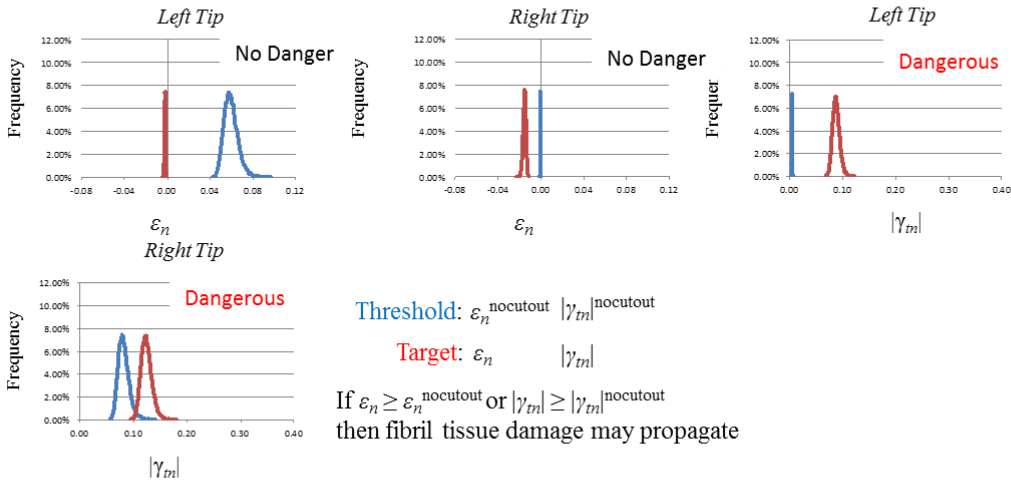


$$EV(\bar{s}_{(100g)}) - EV(\bar{s}_{(100(g-1))}) \leq \frac{SD(\bar{s}_{(100)})}{EV(\bar{s}_{(100)})\sqrt{n_{max}}}$$

with $g = 1, \dots, 100$ and $n_{max} = 10,000$

Converged if satisfied three times continuously

Model is convergence at 2,000 cases



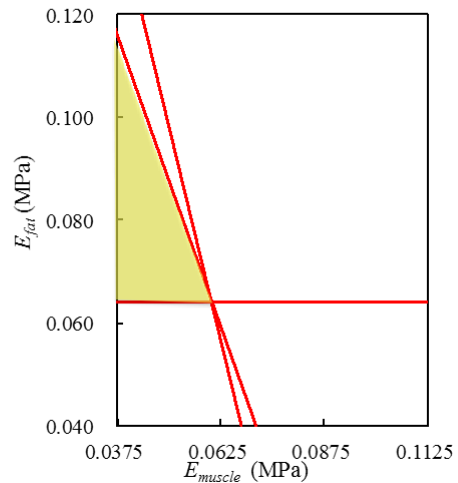
Threshold: $\epsilon_n^{nocutout} \quad |\gamma_m|^{nocutout}$

Target: $\epsilon_n \quad |\gamma_m|$

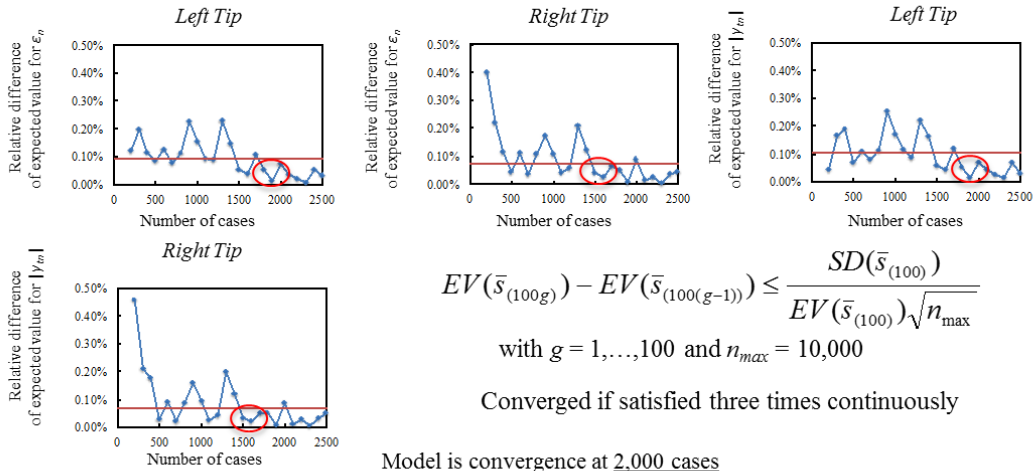
If $\epsilon_n \geq \epsilon_n^{nocutout}$ or $|\gamma_m| \geq |\gamma_m|^{nocutout}$
then fibril tissue damage may propagate

$$LSZ_{E_{muscle} E_{fat}} = \{s; p_a E_{muscle} + q_a E_{fat} + r_a \geq 0 \forall a\}$$

a	p_a	q_a	r_a
1	-0.911	-0.404	0.081
2	-0.955	-0.287	0.076
3	0	1	-0.064



$$I_{fm} = 9.69 \quad b = \text{supine} \quad L_a = 4 \quad a_{mid} = 166.63$$

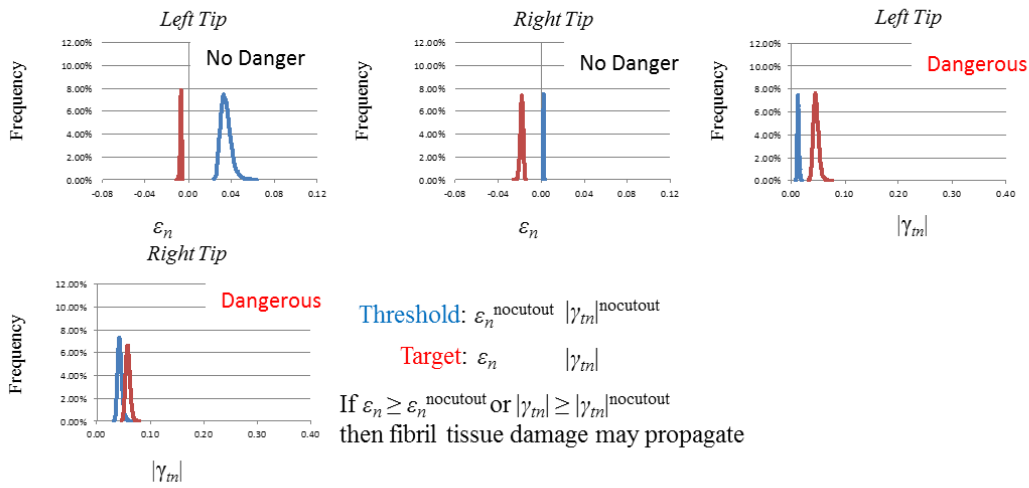


$$EV(\bar{s}_{(100g)}) - EV(\bar{s}_{(100(g-1))}) \leq \frac{SD(\bar{s}_{(100)})}{EV(\bar{s}_{(100)})\sqrt{n_{max}}}$$

with $g = 1, \dots, 100$ and $n_{max} = 10,000$

Converged if satisfied three times continuously

Model is convergence at 2,000 cases



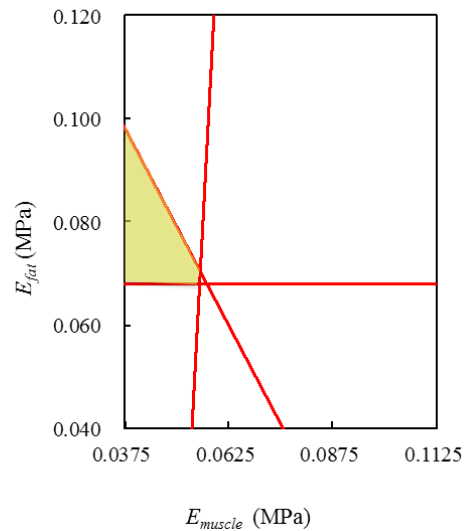
Threshold: $\epsilon_n^{nocutout} \quad |\gamma_m|^{nocutout}$

Target: $\epsilon_n \quad |\gamma_m|$

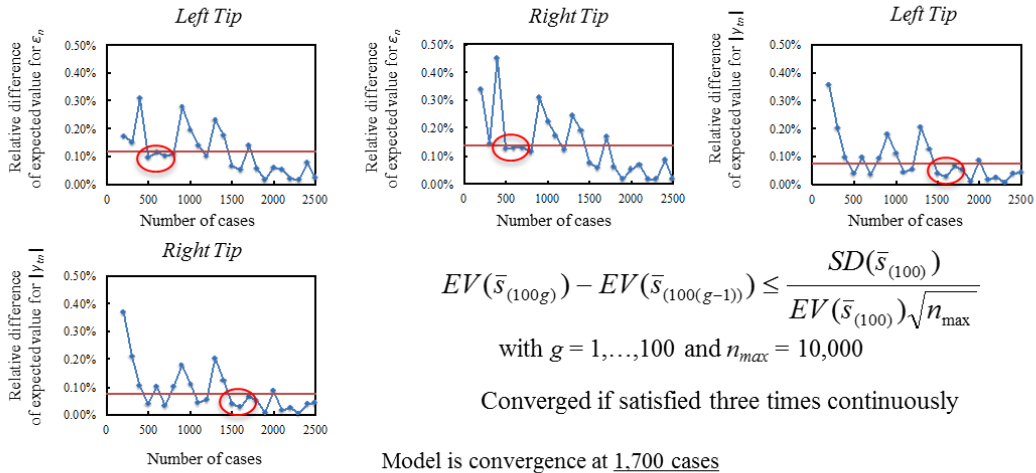
If $\epsilon_n \geq \epsilon_n^{nocutout}$ or $|\gamma_m| \geq |\gamma_m|^{nocutout}$
then fibril tissue damage may propagate

$$LSZ_{E_{muscle} E_{fat}} = \{s; p_a E_{muscle} + q_a E_{fat} + r_a \geq 0 \forall a\}$$

a	p_a	q_a	r_a
1	-0.996	0.067	0.051
2	-0.833	-0.546	0.085
3	0	1	-0.068



$$I_{fm} = 9.69 \quad b = \text{supine} \quad L_a = 8 \quad a_{mid} = 42.23$$

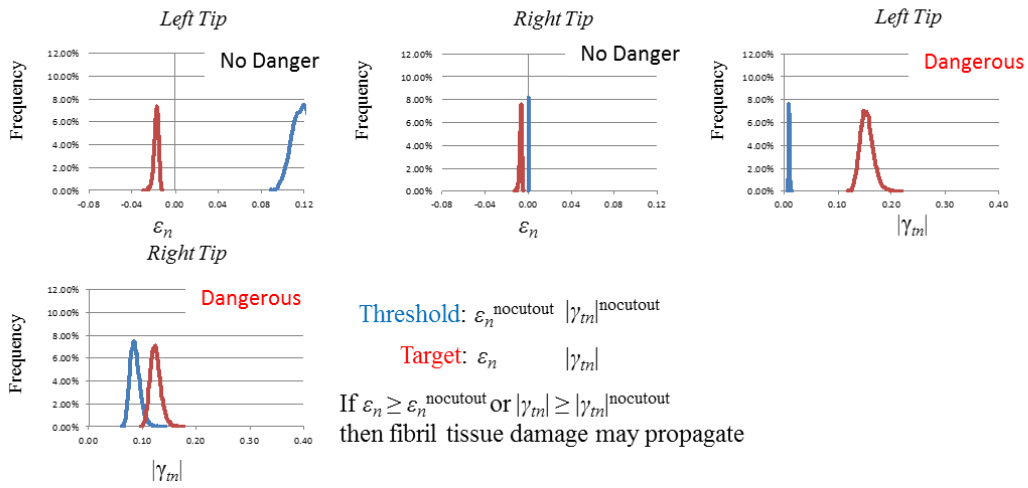


$$EV(\bar{s}_{(100g)}) - EV(\bar{s}_{(100(g-1))}) \leq \frac{SD(\bar{s}_{(100)})}{EV(\bar{s}_{(100)})\sqrt{n_{max}}}$$

with $g = 1, \dots, 100$ and $n_{max} = 10,000$

Converged if satisfied three times continuously

Model is convergence at 1.700 cases



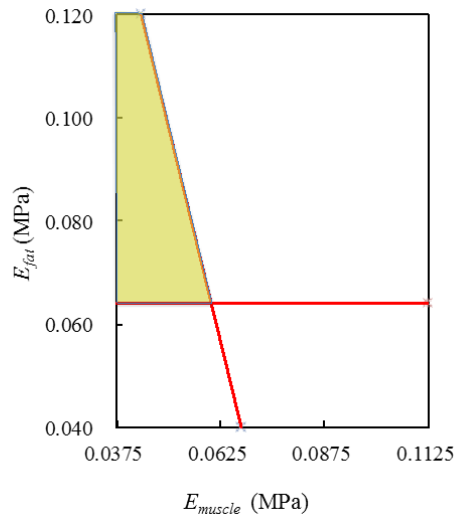
Threshold: $\epsilon_n^{\text{nocutout}} \quad |\gamma_m|^{\text{nocutout}}$

Target: $\epsilon_n \quad |\gamma_m|$

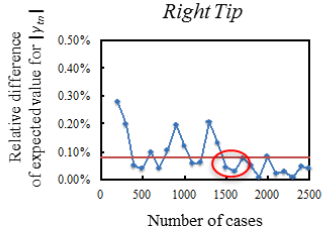
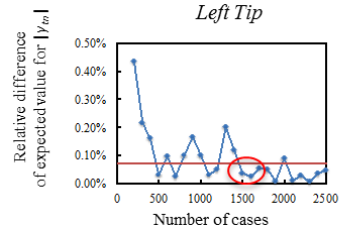
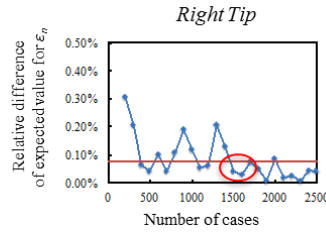
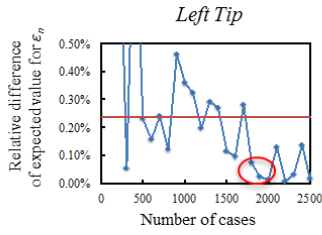
If $\epsilon_n \geq \epsilon_n^{\text{nocutout}}$ or $|\gamma_m| \geq |\gamma_m|^{\text{nocutout}}$
then fibril tissue damage may propagate

$$LSZ_{E_{muscle} E_{fat}} = \{s; p_a E_{muscle} + q_a E_{fat} + r_a \geq 0 \forall a\}$$

a	p_a	q_a	r_a
1	-0.955	-0.287	0.076
2	0	1	-0.064



$$I_{fm} = 9.69 \quad b = \text{supine} \quad L_a = 8 \quad a_{mid} = 104.38$$

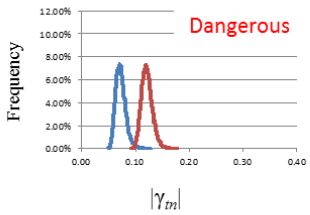
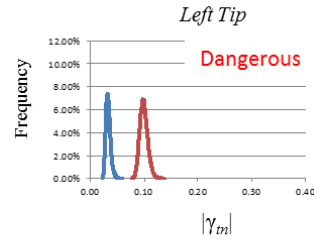
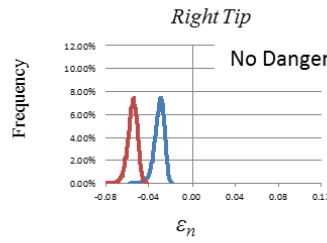
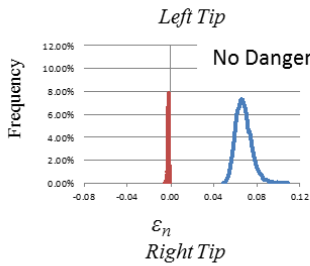


$$EV(\bar{s}_{(100g)}) - EV(\bar{s}_{(100(g-1))}) \leq \frac{SD(\bar{s}_{(100)})}{EV(\bar{s}_{(100)})\sqrt{n_{max}}}$$

with $g = 1, \dots, 100$ and $n_{max} = 10,000$

Converged if satisfied three times continuously

Model is convergence at 2,000 cases



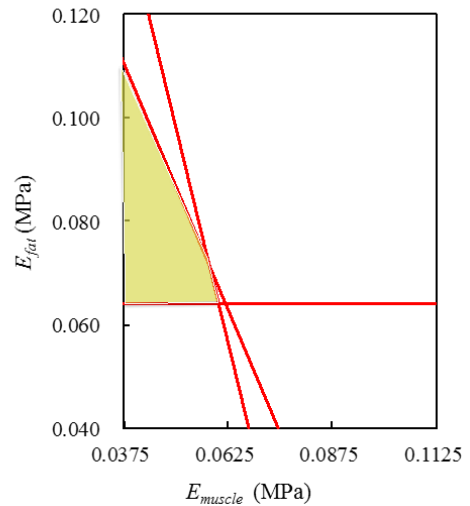
Threshold: $\epsilon_n^{\text{nocutout}} \quad |\gamma_m|^{\text{nocutout}}$

Target: $\epsilon_n \quad |\gamma_m|$

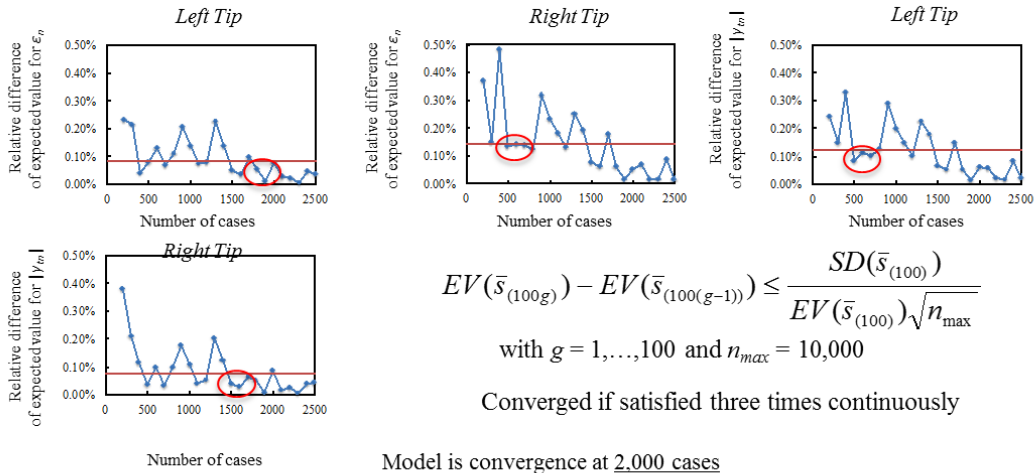
If $\epsilon_n \geq \epsilon_n^{\text{nocutout}}$ or $|\gamma_m| \geq |\gamma_m|^{\text{nocutout}}$
then fibril tissue damage may propagate

$$LSZ_{E_{muscle} E_{fat}} = \{s; p_a E_{muscle} + q_a E_{fat} + r_a \geq 0 \forall a\}$$

a	p_a	q_a	r_a
1	-0.881	-0.465	0.085
2	-0.955	-0.287	0.076
3	0	1	-0.064



$$I_{fm} = 9.69 \quad b = \text{supine} \quad L_a = 8 \quad a_{mid} = 166.63$$

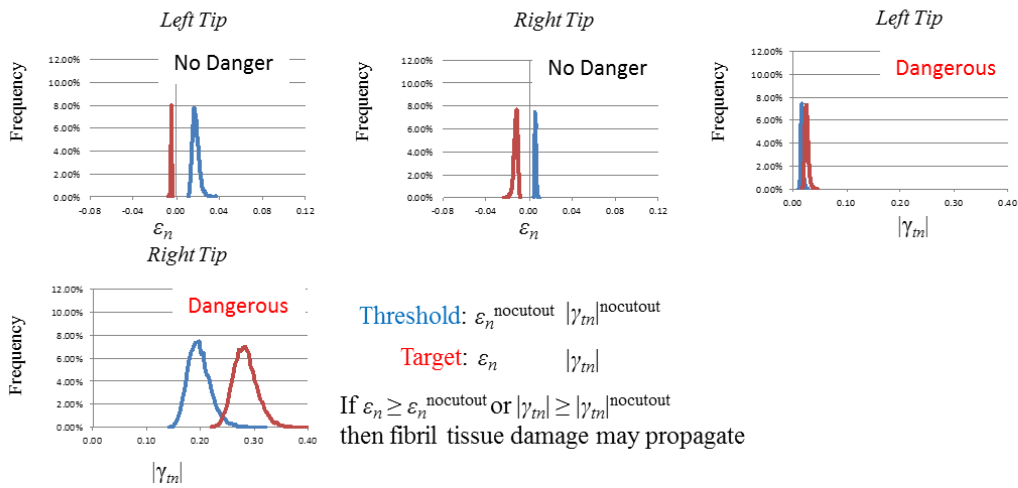


$$EV(\bar{s}_{(100g)}) - EV(\bar{s}_{(100(g-1))}) \leq \frac{SD(\bar{s}_{(100)})}{EV(\bar{s}_{(100)})\sqrt{n_{max}}}$$

with $g = 1, \dots, 100$ and $n_{max} = 10,000$

Converged if satisfied three times continuously

Model is convergence at 2,000 cases



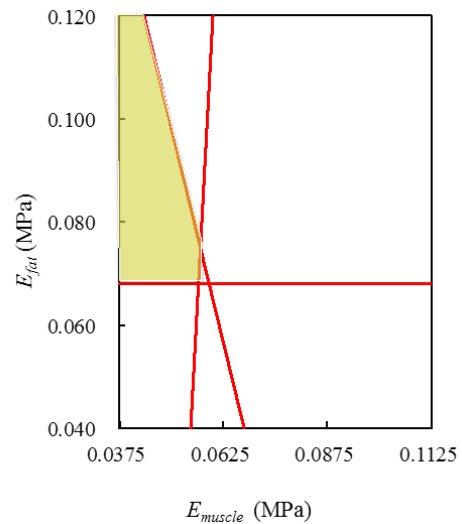
Threshold: $\epsilon_n^{nocutout} \quad |\gamma_m|^{nocutout}$

Target: $\epsilon_n \quad |\gamma_m|$

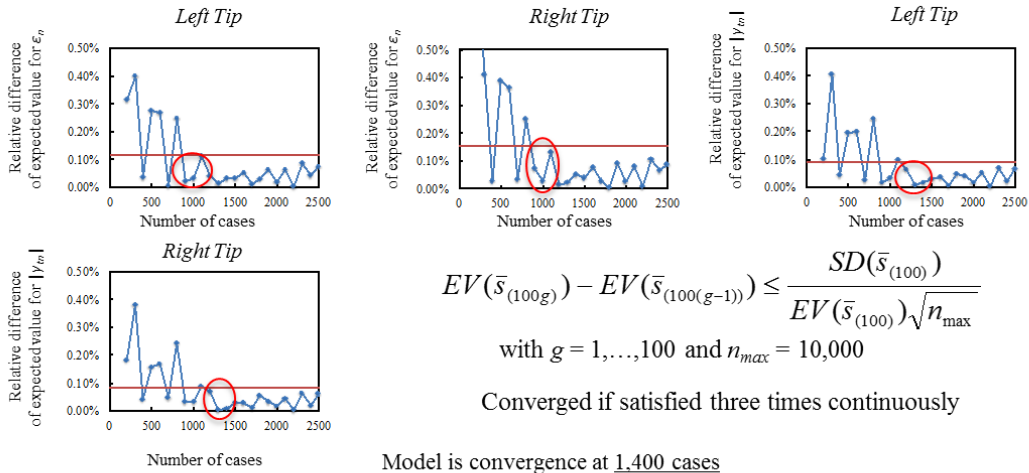
If $\epsilon_n \geq \epsilon_n^{nocutout}$ or $|\gamma_m| \geq |\gamma_m|^{nocutout}$
then fibril tissue damage may propagate

$$LSZ_{E_{muscle}E_{fat}} = \{s; p_a E_{muscle} + q_a E_{fat} + r_a \geq 0 \forall a\}$$

a	p_a	q_a	r_a
1	-0.996	0.067	0.052
2	-0.955	-0.287	0.076
3	0	1	-0.068



$$I_{fm} = 9.69 \quad b = \text{lateral-A} \quad L_a = 4 \quad a_{mid} = 42.23$$

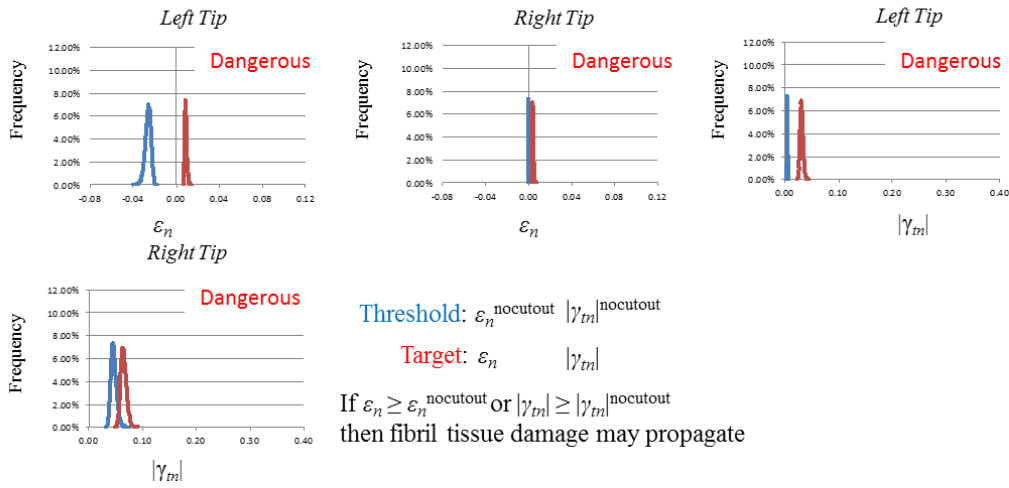


$$EV(\bar{s}_{(100g)}) - EV(\bar{s}_{(100(g-1))}) \leq \frac{SD(\bar{s}_{(100)})}{EV(\bar{s}_{(100)})\sqrt{n_{max}}}$$

with $g = 1, \dots, 100$ and $n_{max} = 10,000$

Converged if satisfied three times continuously

Model is convergence at 1400 cases



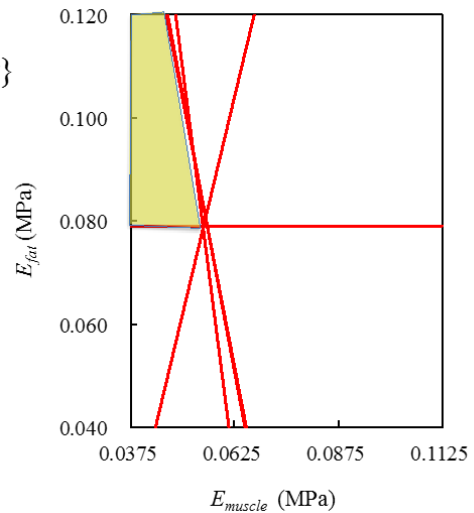
Threshold: $\epsilon_n^{nocutout} \quad |\gamma_m|^{nocutout}$

Target: $\epsilon_n \quad |\gamma_m|$

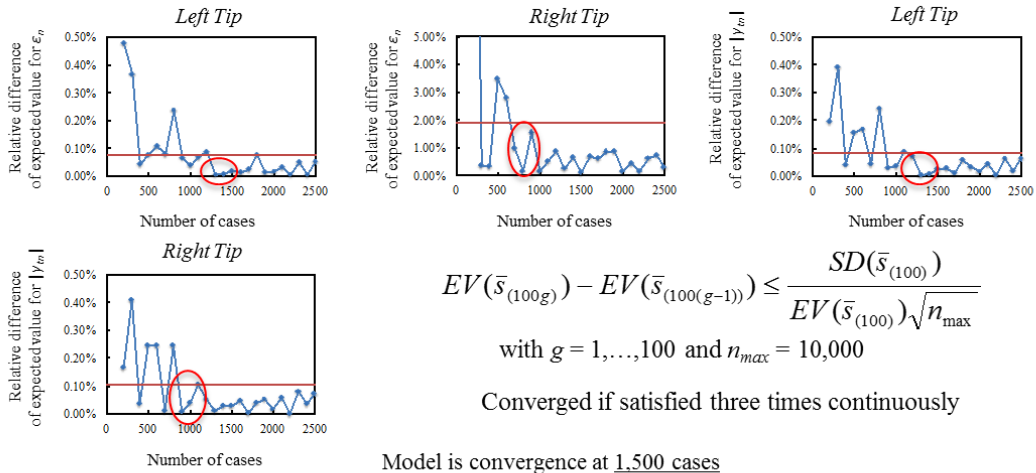
If $\epsilon_n \geq \epsilon_n^{nocutout}$ or $|\gamma_m| \geq |\gamma_m|^{nocutout}$
then fibril tissue damage may propagate

$$LSZ_{E_{muscle} E_{fat}} = \{s; p_a E_{muscle} + q_a E_{fat} + r_a \geq 0 \forall a\}$$

a	p_a	q_a	r_a
1	-0.985	-0.158	0.067
2	-0.971	-0.228	0.072
3	-0.97	-0.234	0.073
4	-0.957	0.287	0.03
5	0	1	-0.079



$$I_{fm} = 9.69 \quad b = \text{lateral-A} \quad L_a = 4 \quad a_{mid} = 104.38$$

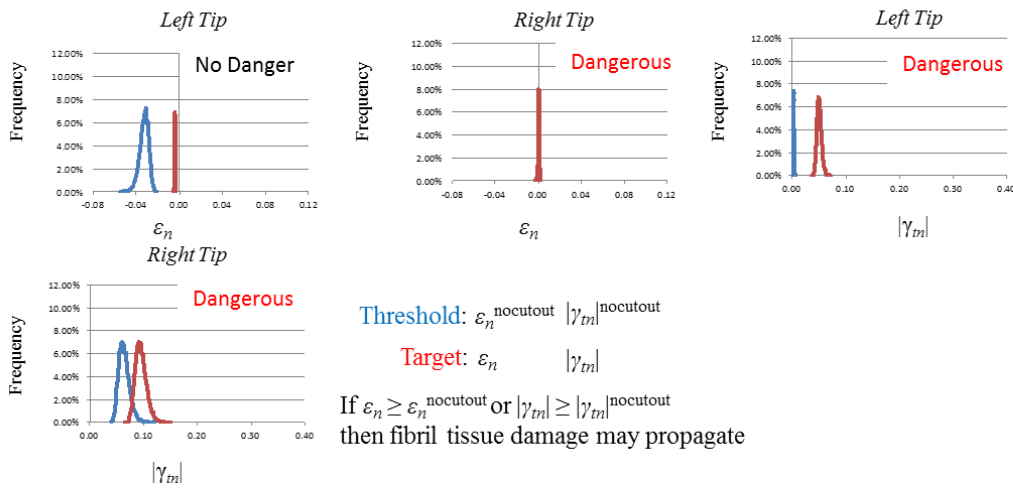


$$EV(\bar{s}_{(100g)}) - EV(\bar{s}_{(100(g-1))}) \leq \frac{SD(\bar{s}_{(100)})}{EV(\bar{s}_{(100)})\sqrt{n_{max}}}$$

with $g = 1, \dots, 100$ and $n_{max} = 10,000$

Converged if satisfied three times continuously

Model is convergence at 1,500 cases



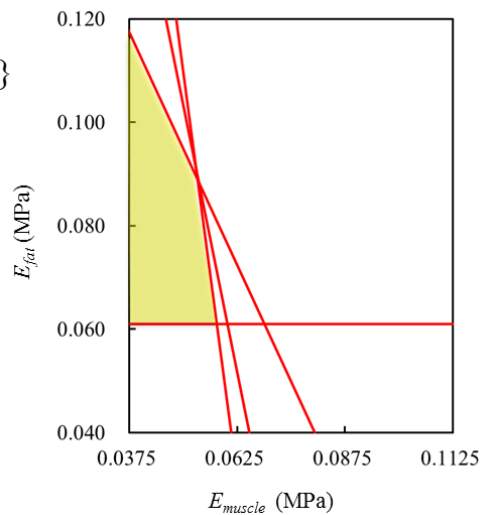
Threshold: $\epsilon_n^{nocutout} \quad |\gamma_m|^{nocutout}$

Target: $\epsilon_n \quad |\gamma_m|$

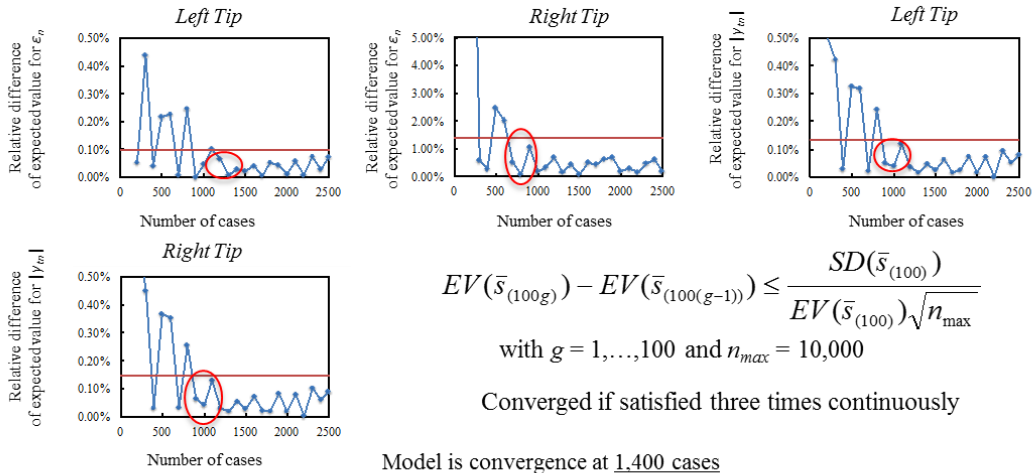
If $\epsilon_n \geq \epsilon_n^{nocutout}$ or $|\gamma_m| \geq |\gamma_m|^{nocutout}$
then fibril tissue damage may propagate

$$LSZ_{E_{muscle} E_{fat}} = \{s; p_a E_{muscle} + q_a E_{fat} + r_a \geq 0 \forall a\}$$

a	p_a	q_a	r_a
1	-0.97	-0.234	0.073
2	-0.985	-0.158	0.067
3	-0.876	-0.474	0.089
4	0	1	-0.061



$$I_{fm} = 9.69 \quad b = \text{lateral-A} \quad L_a = 4 \quad a_{mid} = 166.63$$

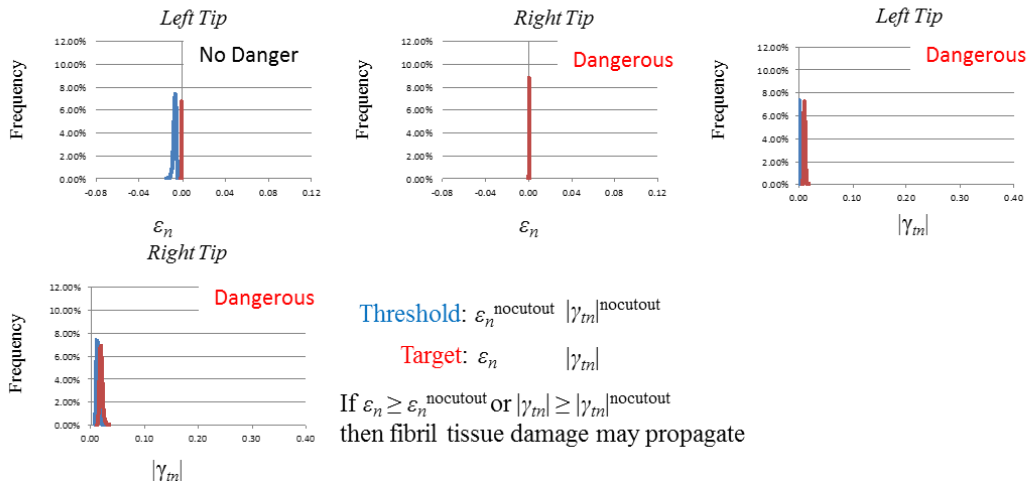


$$EV(\bar{s}_{(100g)}) - EV(\bar{s}_{(100(g-1))}) \leq \frac{SD(\bar{s}_{(100)})}{EV(\bar{s}_{(100)})\sqrt{n_{max}}}$$

with $g = 1, \dots, 100$ and $n_{max} = 10,000$

Converged if satisfied three times continuously

Model is convergence at 1,400 cases



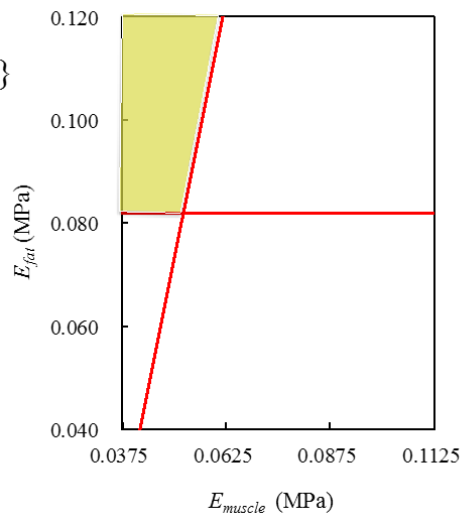
Threshold: $\epsilon_n^{nocutout} \quad |\gamma_m|^{nocutout}$

Target: $\epsilon_n \quad |\gamma_m|$

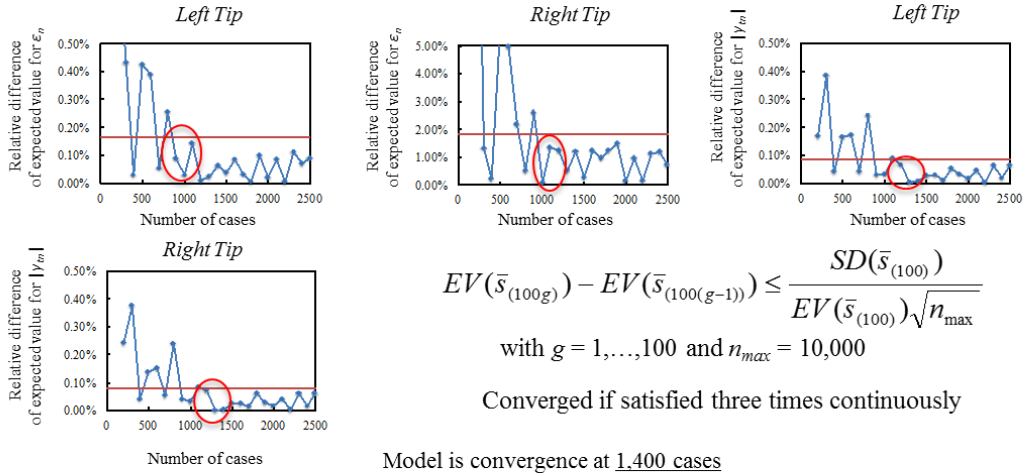
If $\epsilon_n \geq \epsilon_n^{nocutout}$ or $|\gamma_m| \geq |\gamma_m|^{nocutout}$
then fibril tissue damage may propagate

$$LSZ_{E_{muscle} E_{fat}} = \{s; p_a E_{muscle} + q_a E_{fat} + r_a \geq 0 \forall a\}$$

a	p_a	q_a	r_a
1	-0.961	0.275	0.032
2	0	1	-0.082



$$I_{fm} = 9.69 \quad b = \text{lateral-A} \quad L_a = 8 \quad a_{mid} = 42.23$$

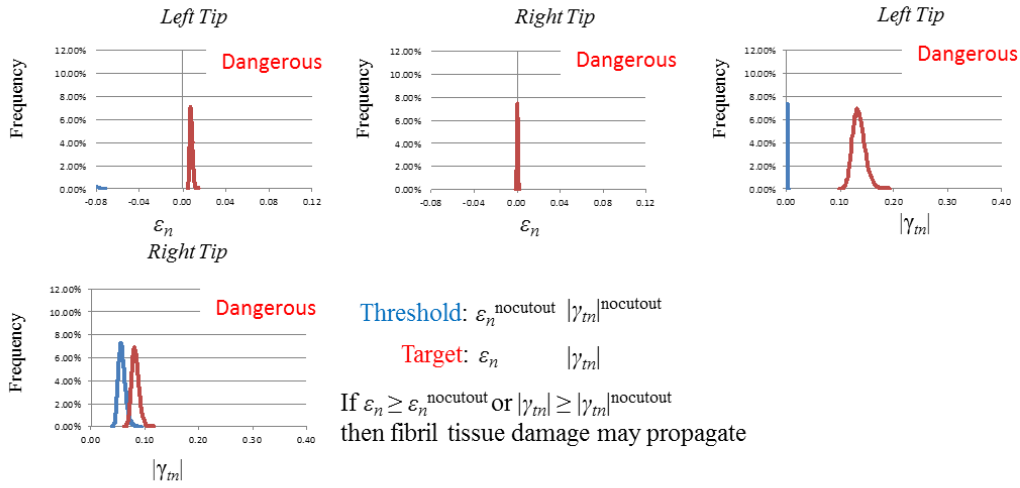


$$EV(\bar{s}_{(100g)}) - EV(\bar{s}_{(100(g-1))}) \leq \frac{SD(\bar{s}_{(100)})}{EV(\bar{s}_{(100)})\sqrt{n_{max}}}$$

with $g = 1, \dots, 100$ and $n_{max} = 10,000$

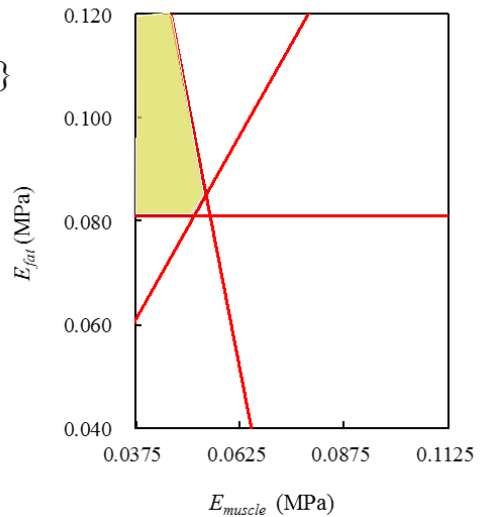
Converged if satisfied three times continuously

Model is convergence at 1,400 cases

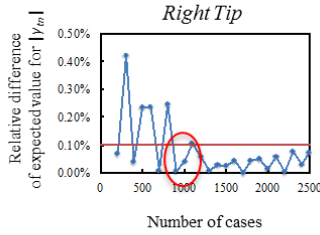
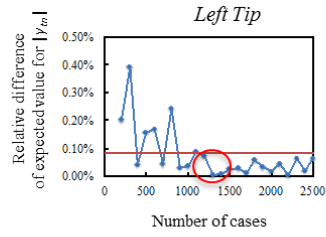
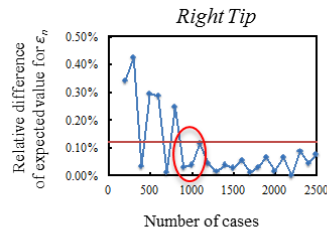
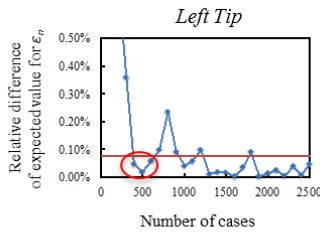


$$LSZ_{E_{muscle} E_{fat}} = \{s; p_a E_{muscle} + q_a E_{fat} + r_a \geq 0 \forall a\}$$

a	p_a	q_a	r_a
1	-0.97	-0.234	0.073
2	-0.957	-0.287	0.03
3	-0.818	0.575	0.004
4	0	1	-0.081



$$I_{fm} = 9.69 \quad b = \text{lateral-A} \quad L_a = 8 \quad a_{mid} = 104.38$$

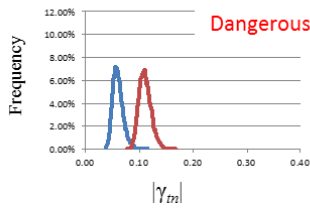
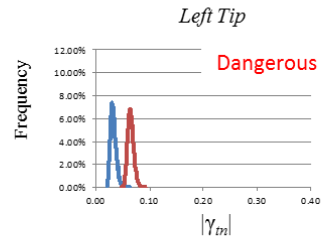
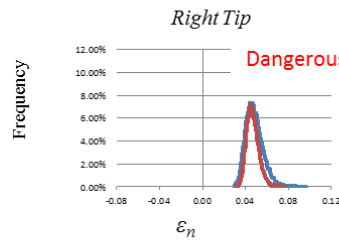
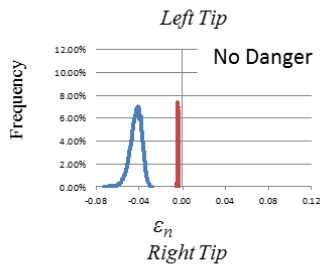


$$EV(\bar{s}_{(100g)}) - EV(\bar{s}_{(100(g-1))}) \leq \frac{SD(\bar{s}_{(100)})}{EV(\bar{s}_{(100)})\sqrt{n_{max}}}$$

with $g = 1, \dots, 100$ and $n_{max} = 10,000$

Converged if satisfied three times continuously

Model is convergence at 1,400 cases



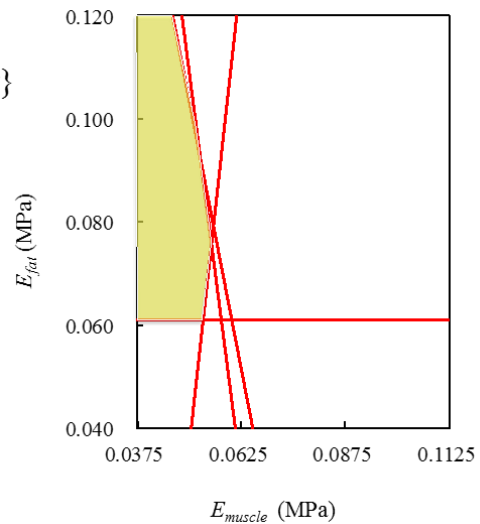
Threshold: $\varepsilon_n^{\text{nocutout}} \quad |\gamma_m|^{\text{nocutout}}$

Target: $\varepsilon_n \quad |\gamma_m|$

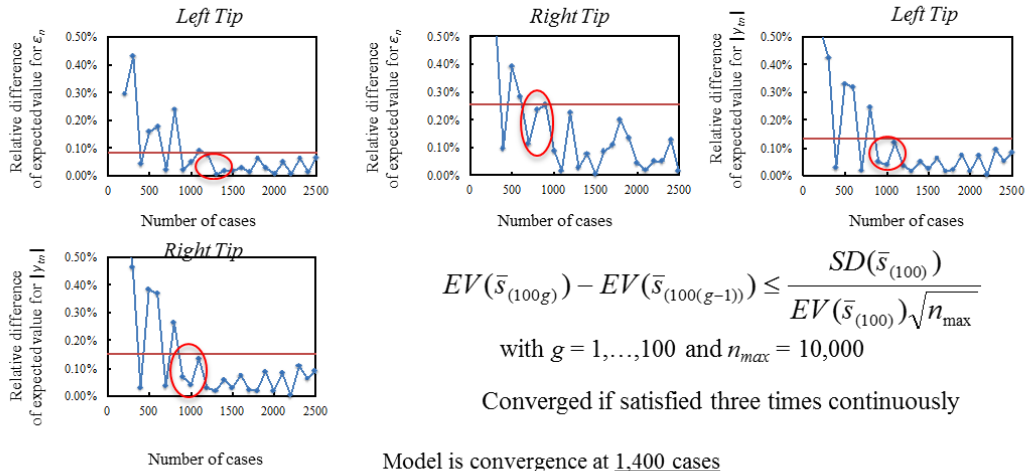
If $\varepsilon_n \geq \varepsilon_n^{\text{nocutout}}$ or $|\gamma_m| \geq |\gamma_m|^{\text{nocutout}}$
then fibril tissue damage may propagate

$$LSZ_{E_{muscle} E_{fat}} = \{s; p_a E_{muscle} + q_a E_{fat} + r_a \geq 0 \forall a\}$$

a	p_a	q_a	r_a
1	-0.97	-0.234	0.073
2	-0.985	-0.158	0.067
3	-0.989	0.138	0.045
4	0	1	-0.061



$$I_{fm} = 9.69 \quad b = \text{lateral-A} \quad L_a = 8 \quad a_{mid} = 166.63$$

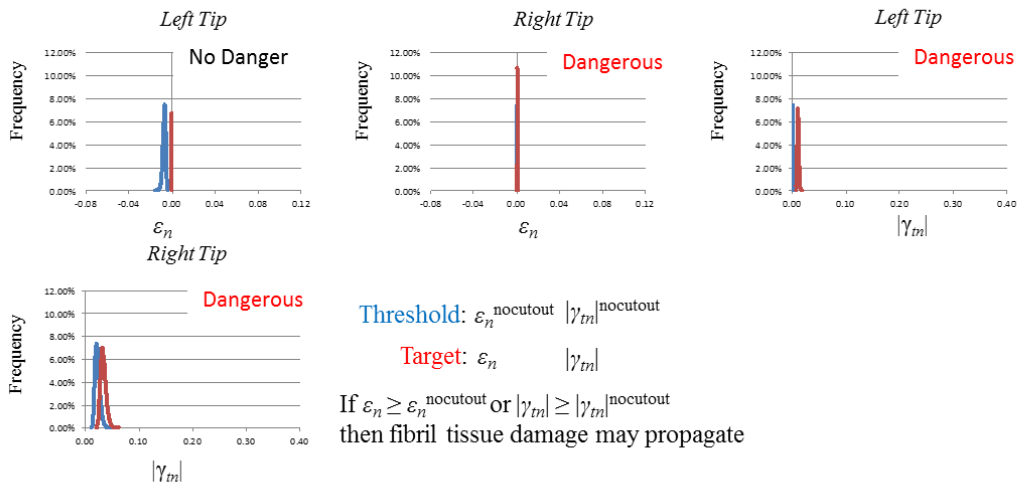


$$EV(\bar{s}_{(100g)}) - EV(\bar{s}_{(100(g-1))}) \leq \frac{SD(\bar{s}_{(100)})}{EV(\bar{s}_{(100)})\sqrt{n_{max}}}$$

with $g = 1, \dots, 100$ and $n_{max} = 10,000$

Converged if satisfied three times continuously

Model is convergence at 1,400 cases



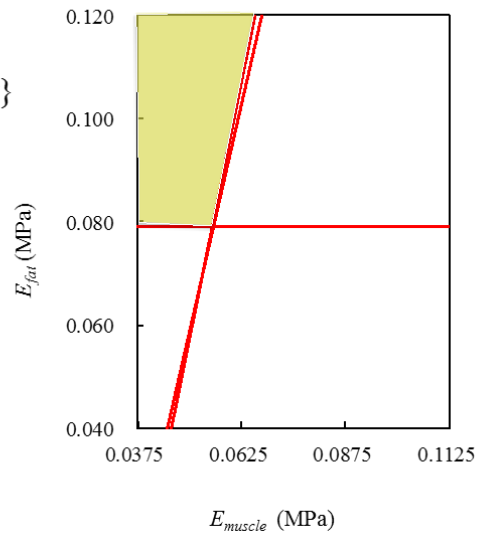
Threshold: $\epsilon_n^{nocutout} \quad |\gamma_m|^{nocutout}$

Target: $\epsilon_n \quad |\gamma_m|$

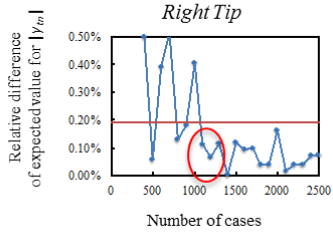
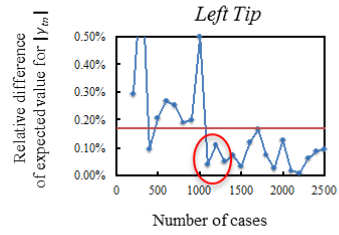
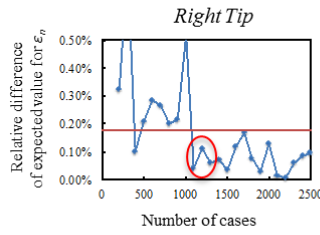
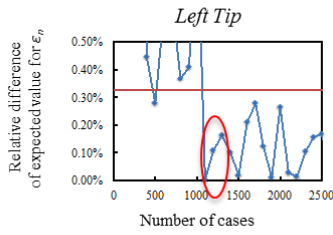
If $\epsilon_n \geq \epsilon_n^{nocutout}$ or $|\gamma_m| \geq |\gamma_m|^{nocutout}$
then fibril tissue damage may propagate

$$LSZ_{E_{muscle} E_{fat}} = \{s; p_a E_{muscle} + q_a E_{fat} + r_a \geq 0 \forall a\}$$

a	p_a	q_a	r_a
1	-0.961	0.275	0.032
2	-0.97	0.242	0.035
3	0	1	-0.079



$$I_{fm} = 9.69 \quad b = \text{lateral-B} \quad L_a = 4 \quad a_{mid} = 42.23$$

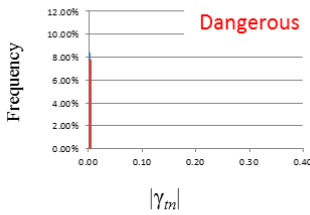
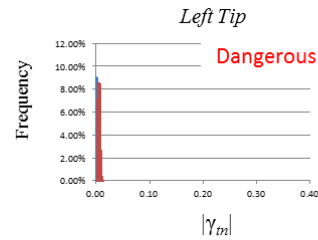
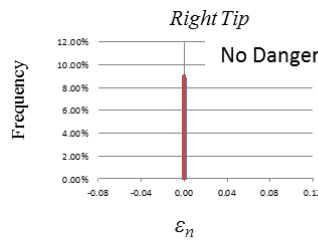
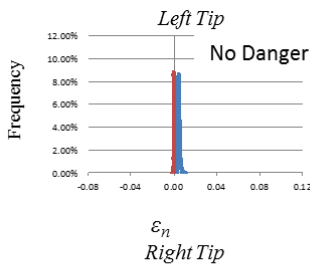


$$EV(\bar{s}_{(100g)}) - EV(\bar{s}_{(100(g-1))}) \leq \frac{SD(\bar{s}_{(100)})}{EV(\bar{s}_{(100)})\sqrt{n_{max}}}$$

with $g = 1, \dots, 100$ and $n_{max} = 10,000$

Converged if satisfied three times continuously

Model is convergence at 1,300 cases



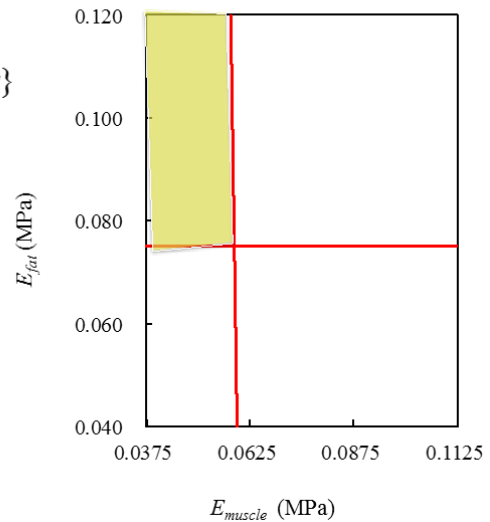
Threshold: $\varepsilon_n^{nocutout} \quad |\gamma_m|^{nocutout}$

Target: $\varepsilon_n \quad |\gamma_m|$

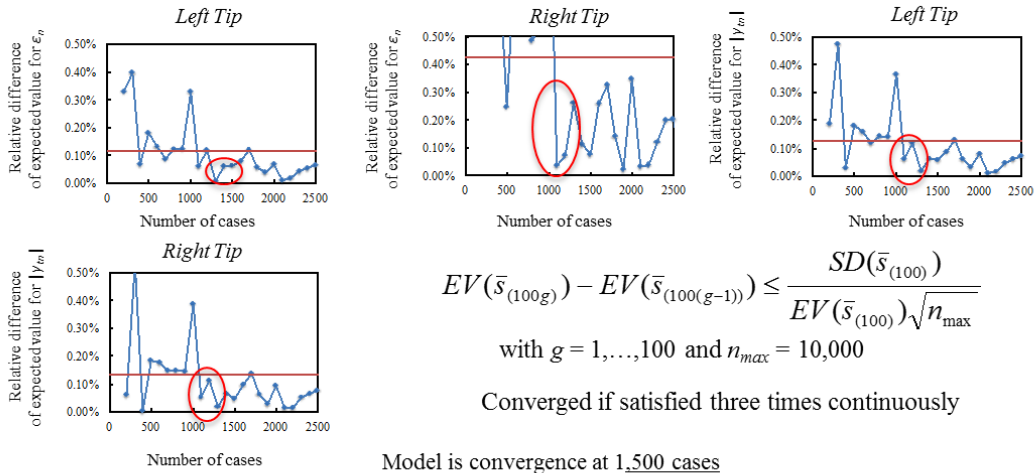
If $\varepsilon_n \geq \varepsilon_n^{nocutout}$ or $|\gamma_m| \geq |\gamma_m|^{nocutout}$
then fibril tissue damage may propagate

$$LSZ_{E_{muscle} E_{fat}} = \{s; p_a E_{muscle} + q_a E_{fat} + r_a \geq 0 \forall a\}$$

a	p_a	q_a	r_a
1	-0.998	-0.02	0.06
2	0	1	-0.075



$$I_{fm} = 9.69 \quad b = \text{lateral-B} \quad L_a = 4 \quad a_{mid} = 104.38$$

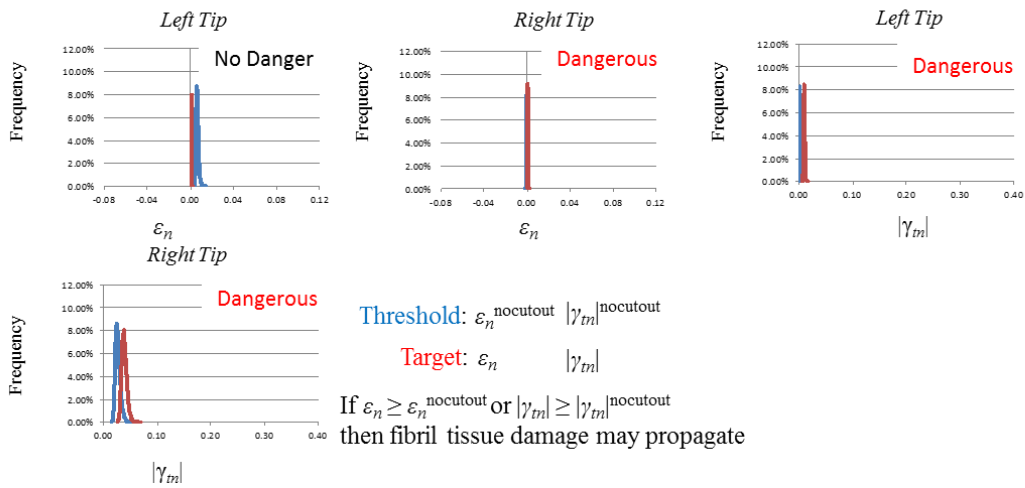


$$EV(\bar{s}_{(100g)}) - EV(\bar{s}_{(100(g-1))}) \leq \frac{SD(\bar{s}_{(100)})}{EV(\bar{s}_{(100)})\sqrt{n_{max}}}$$

with $g = 1, \dots, 100$ and $n_{max} = 10,000$

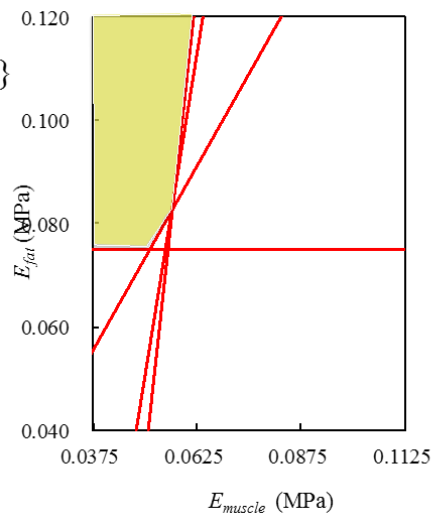
Converged if satisfied three times continuously

Model is convergence at 1,500 cases

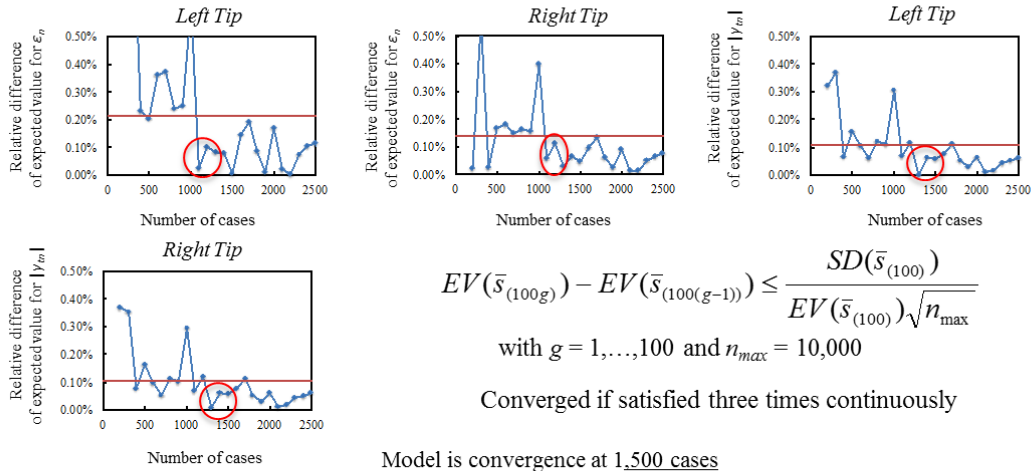


$$LSZ_{E_{muscle} E_{fat}} = \{s; p_a E_{muscle} + q_a E_{fat} + r_a \geq 0 \forall a\}$$

a	p_a	q_a	r_a
1	-0.989	0.139	0.045
2	-0.98	0.196	0.039
3	-0.819	0.573	-0.001
4	0	1	-0.075



$$I_{fm} = 9.69 \quad b = \text{lateral-B} \quad L_a = 4 \quad a_{mid} = 166.63$$

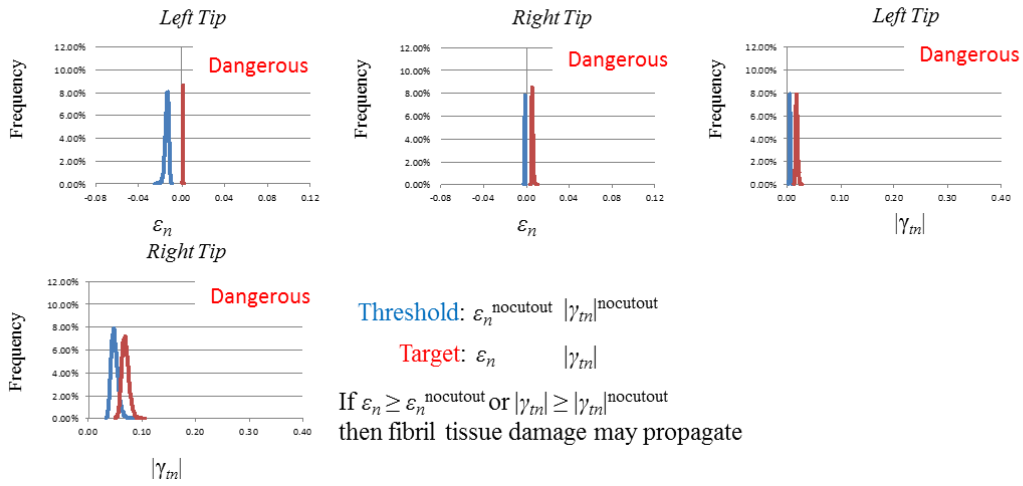


$$EV(\bar{s}_{(100g)}) - EV(\bar{s}_{(100(g-1))}) \leq \frac{SD(\bar{s}_{(100)})}{EV(\bar{s}_{(100)})\sqrt{n_{max}}}$$

with $g = 1, \dots, 100$ and $n_{max} = 10,000$

Converged if satisfied three times continuously

Model is convergence at 1,500 cases



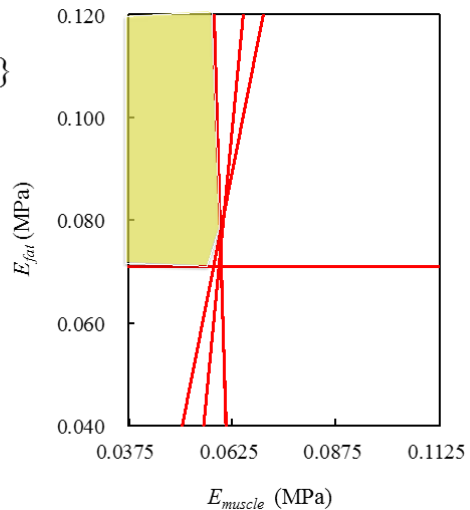
Threshold: $\epsilon_n^{nocutout} \quad |\gamma_{tm}|^{nocutout}$

Target: $\epsilon_n \quad |\gamma_{tm}|$

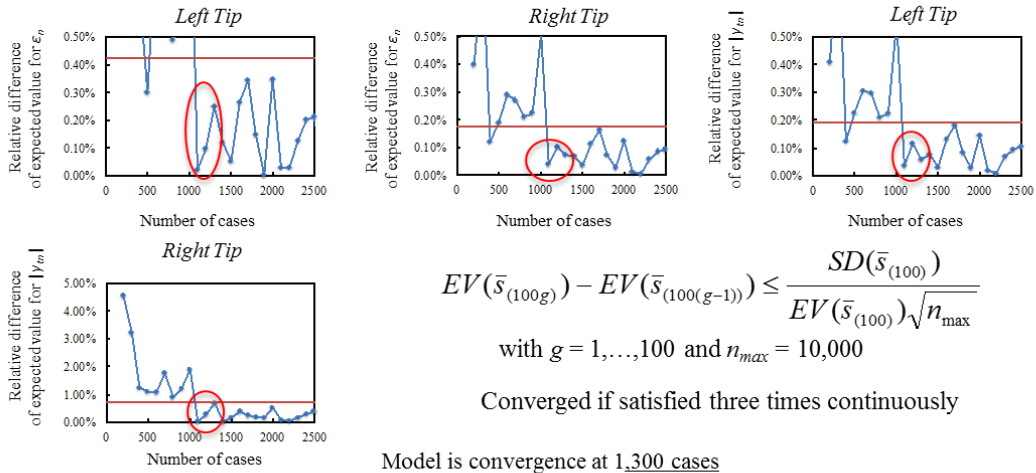
If $\epsilon_n \geq \epsilon_n^{nocutout}$ or $|\gamma_{tm}| \geq |\gamma_{tm}|^{nocutout}$ then fibril tissue damage may propagate

$$LSZ_{E_{muscle} E_{fat}} = \{s; p_a E_{muscle} + q_a E_{fat} + r_a \geq 0 \forall a\}$$

a	p_a	q_a	r_a
1	-0.998	-0.033	0.062
2	-0.971	0.238	0.04
3	-0.997	-0.04	0.063
4	-0.991	0.12	0.051
5	0	1	-0.071



$$I_{fm} = 9.69 \quad b = \text{lateral-B} \quad L_a = 8 \quad a_{mid} = 42.23$$

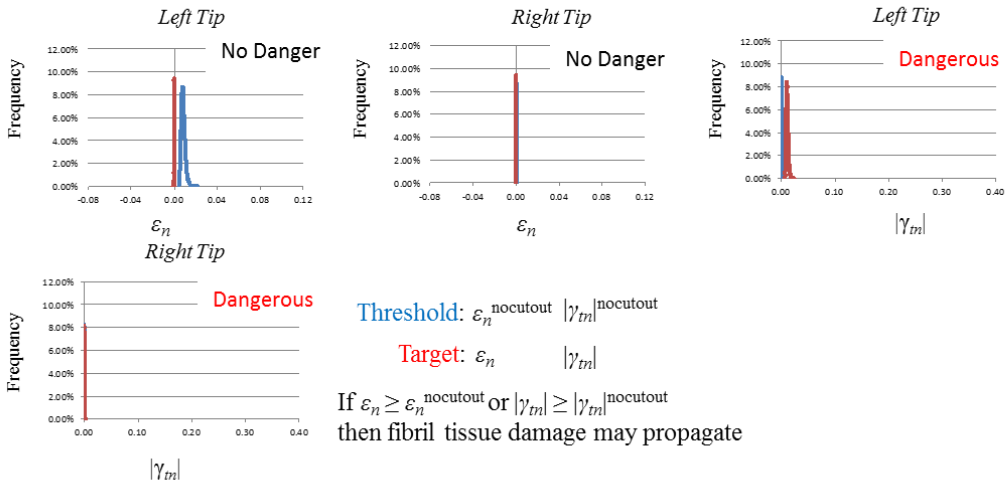


$$EV(\bar{s}_{(100g)}) - EV(\bar{s}_{(100(g-1))}) \leq \frac{SD(\bar{s}_{(100)})}{EV(\bar{s}_{(100)})\sqrt{n_{max}}}$$

with $g = 1, \dots, 100$ and $n_{max} = 10,000$

Converged if satisfied three times continuously

Model is convergence at 1,300 cases



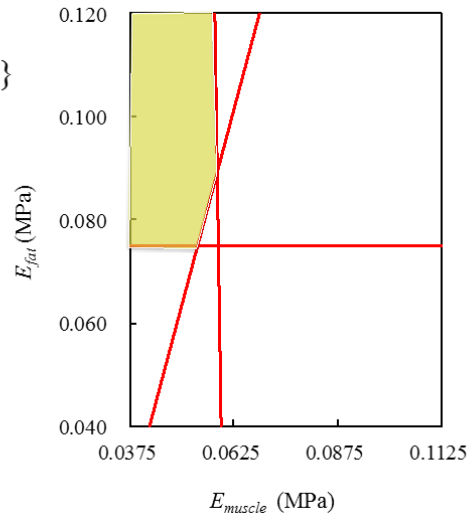
Threshold: $\varepsilon_n^{nocutout} \quad |\gamma_m|^{nocutout}$

Target: $\varepsilon_n \quad |\gamma_m|$

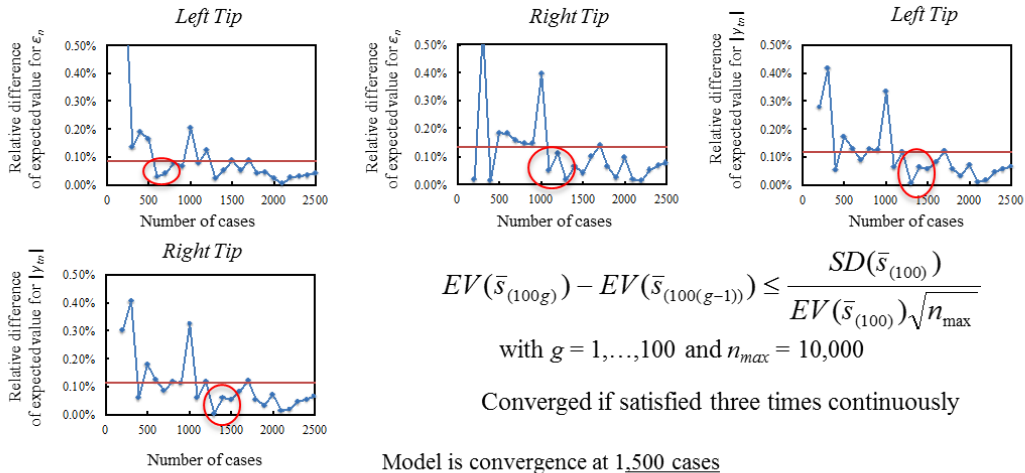
If $\varepsilon_n \geq \varepsilon_n^{nocutout}$ or $|\gamma_m| \geq |\gamma_m|^{nocutout}$
then fibril tissue damage may propagate

$$LSZ_{E_{muscle} E_{fat}} = \{s; p_a E_{muscle} + q_a E_{fat} + r_a \geq 0 \forall a\}$$

a	p_a	q_a	r_a
1	-0.979	-0.196	0.059
2	-0.948	-0.316	0.028
3	0	1	-0.075



$$I_{fm} = 9.69 \quad b = \text{lateral-B} \quad L_a = 8 \quad a_{mid} = 104.38$$

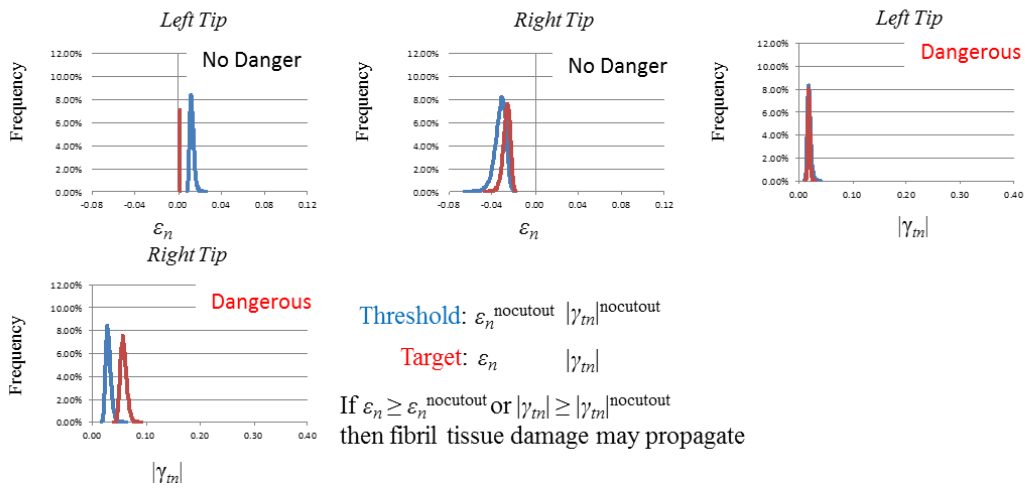


$$EV(\bar{s}_{(100g)}) - EV(\bar{s}_{(100(g-1))}) \leq \frac{SD(\bar{s}_{(100)})}{EV(\bar{s}_{(100)})\sqrt{n_{max}}}$$

with $g = 1, \dots, 100$ and $n_{max} = 10,000$

Converged if satisfied three times continuously

Model is convergence at 1,500 cases



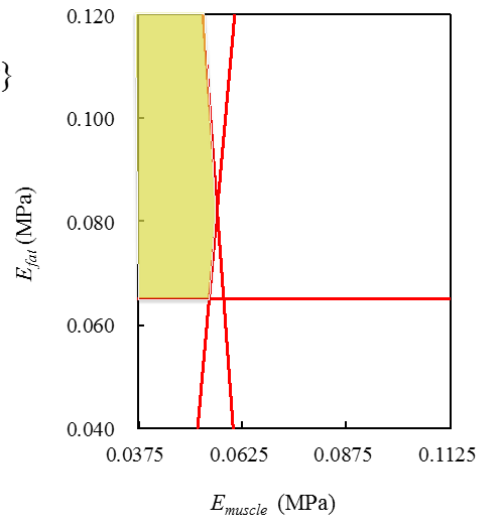
Threshold: $\epsilon_n^{nocutout} \quad |\gamma_m|^{nocutout}$

Target: $\epsilon_n \quad |\gamma_m|$

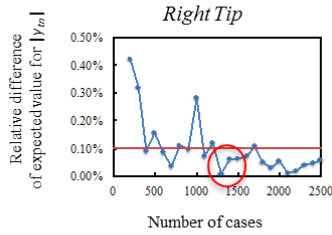
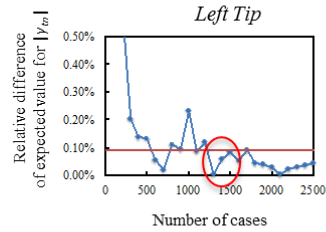
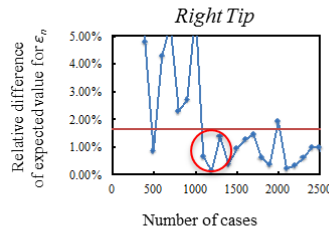
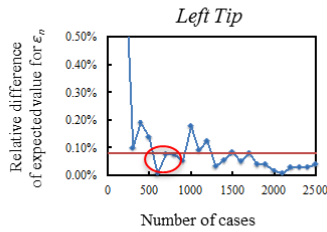
If $\epsilon_n \geq \epsilon_n^{nocutout}$ or $|\gamma_m| \geq |\gamma_m|^{nocutout}$
then fibril tissue damage may propagate

$$LSZ_{E_{muscle} E_{fat}} = \{s; p_a E_{muscle} + q_a E_{fat} + r_a \geq 0 \forall a\}$$

a	p_a	q_a	r_a
1	-0.994	-0.088	0.064
2	-0.993	0.11	0.047
3	0	1	-0.065



$$I_{fm} = 9.69 \quad b = \text{lateral-B} \quad L_a = 8 \quad a_{mid} = 166.63$$

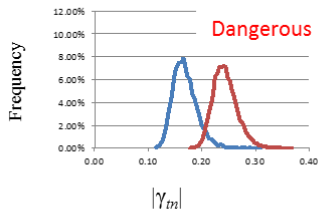
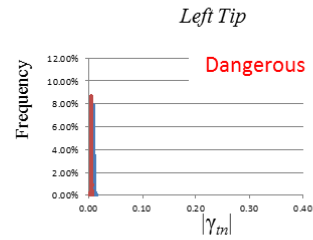
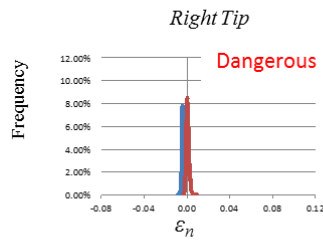
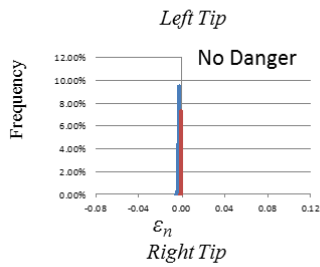


$$EV(\bar{s}_{(100g)}) - EV(\bar{s}_{(100(g-1))}) \leq \frac{SD(\bar{s}_{(100)})}{EV(\bar{s}_{(100)})\sqrt{n_{max}}}$$

with $g = 1, \dots, 100$ and $n_{max} = 10,000$

Converged if satisfied three times continuously

Model is convergence at 1,500 cases



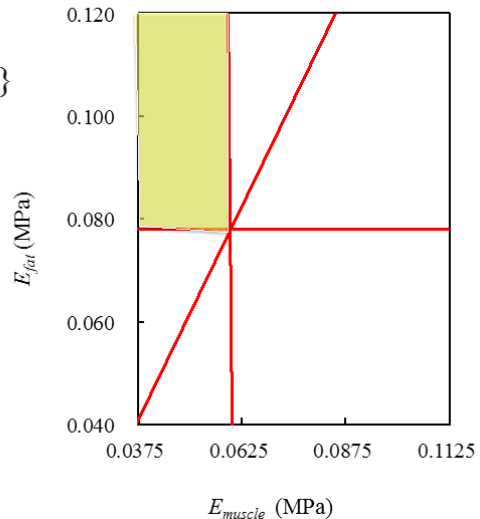
Threshold: $\varepsilon_n^{nocutout} \quad |\gamma_m|^{nocutout}$

Target: $\varepsilon_n \quad |\gamma_m|$

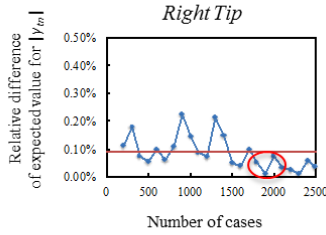
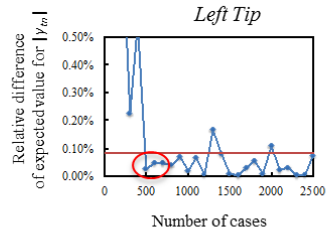
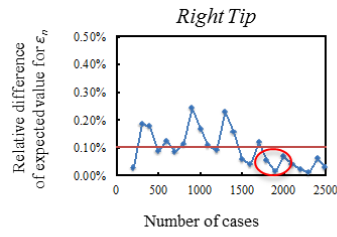
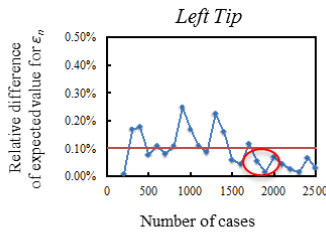
If $\varepsilon_n \geq \varepsilon_n^{nocutout}$ or $|\gamma_m| \geq |\gamma_m|^{nocutout}$
then fibril tissue damage may propagate

$$LSZ_{E_{muscle} E_{fat}} = \{s; p_a E_{muscle} + q_a E_{fat} + r_a \geq 0 \forall a\}$$

a	p_a	q_a	r_a
1	-0.998	-0.01	0.06
2	-0.857	0.514	0.011
3	0	1	-0.078



$$I_{fm} = 15.2 \quad b = \text{supine} \quad L_a = 4 \quad a_{mid} = 42.23$$

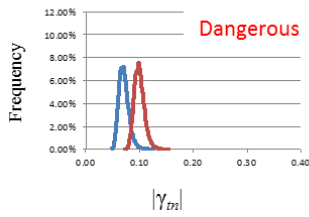
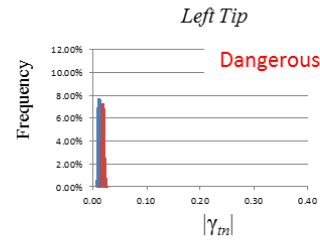
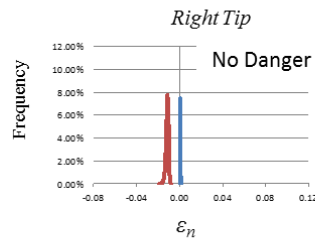
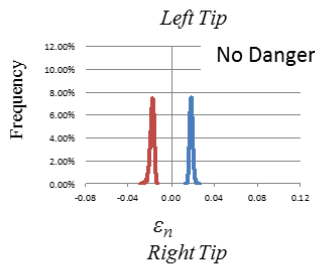


$$EV(\bar{s}_{(100g)}) - EV(\bar{s}_{(100(g-1))}) \leq \frac{SD(\bar{s}_{(100)})}{EV(\bar{s}_{(100)})\sqrt{n_{max}}}$$

with $g = 1, \dots, 100$ and $n_{max} = 10,000$

Converged if satisfied three times continuously

Model is convergence at 2,000 cases



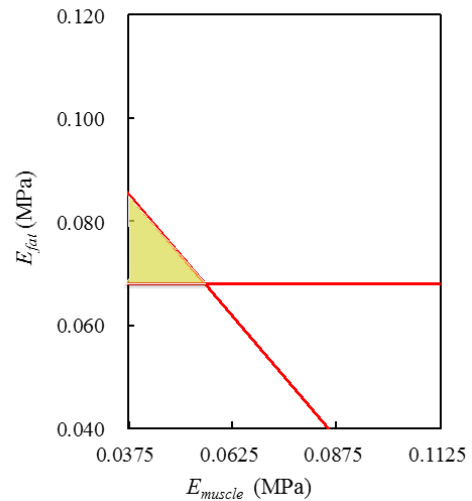
Threshold: $\varepsilon_n^{\text{nocutout}} \quad |\gamma_m|^{\text{nocutout}}$

Target: $\varepsilon_n \quad |\gamma_m|$

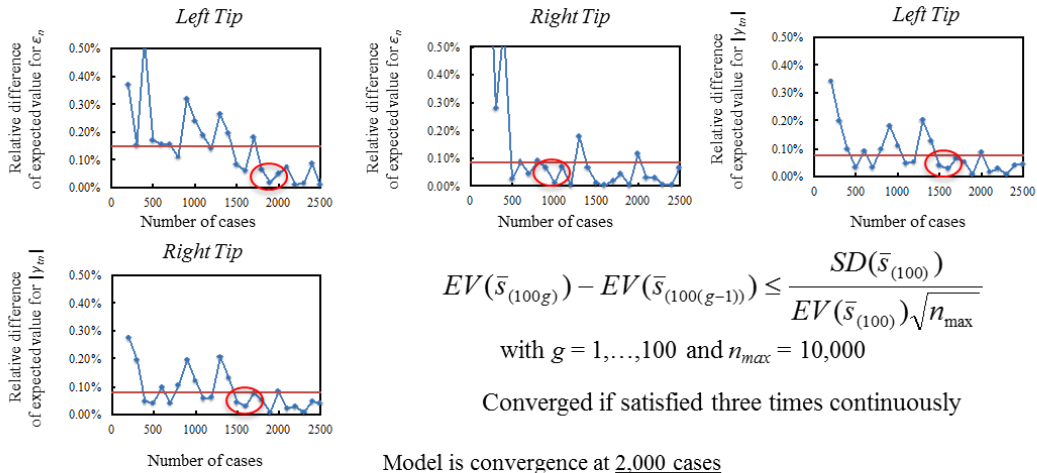
If $\varepsilon_n \geq \varepsilon_n^{\text{nocutout}}$ or $|\gamma_m| \geq |\gamma_m|^{\text{nocutout}}$
then fibril tissue damage may propagate

$$LSZ_{E_{muscle} E_{fat}} = \{s; p_a E_{muscle} + q_a E_{fat} + r_a \geq 0 \forall a\}$$

a	p_a	q_a	r_a
1	-0.683	-0.726	0.087
2	0	1	-0.068



$$I_{fm} = 15.2 \quad b = \text{supine} \quad L_a = 4 \quad a_{mid} = 104.38$$

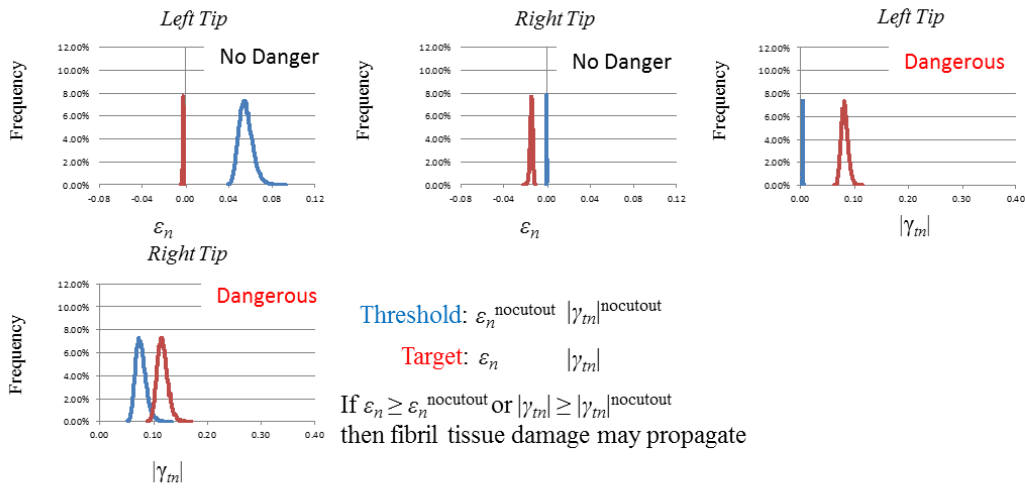


$$EV(\bar{s}_{(100g)}) - EV(\bar{s}_{(100(g-1))}) \leq \frac{SD(\bar{s}_{(100)})}{EV(\bar{s}_{(100)})\sqrt{n_{max}}}$$

with $g = 1, \dots, 100$ and $n_{max} = 10,000$

Converged if satisfied three times continuously

Model is convergence at 2,000 cases



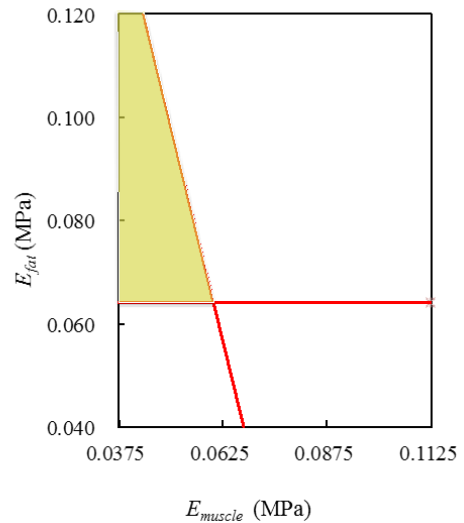
Threshold: $\epsilon_n^{nocutout} \quad |\gamma_m|^{nocutout}$

Target: $\epsilon_n \quad |\gamma_m|$

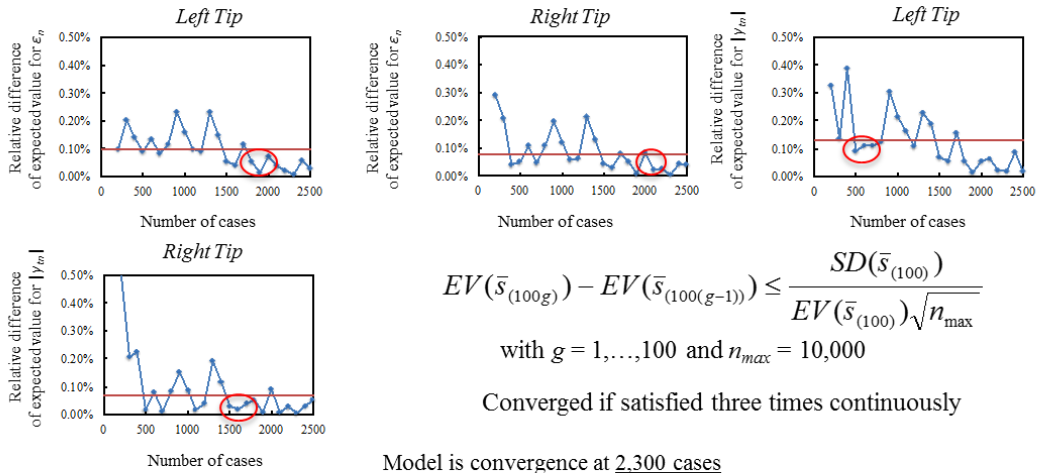
If $\epsilon_n \geq \epsilon_n^{nocutout}$ or $|\gamma_m| \geq |\gamma_m|^{nocutout}$
then fibril tissue damage may propagate

$$LSZ_{E_{muscle} E_{fat}} = \{s; p_a E_{muscle} + q_a E_{fat} + r_a \geq 0 \forall a\}$$

a	p_a	q_a	r_a
1	-0.955	-0.287	0.076
2	0	1	-0.064



$$I_{fm} = 15.2 \quad b = \text{supine} \quad L_a = 4 \quad a_{mid} = 166.63$$

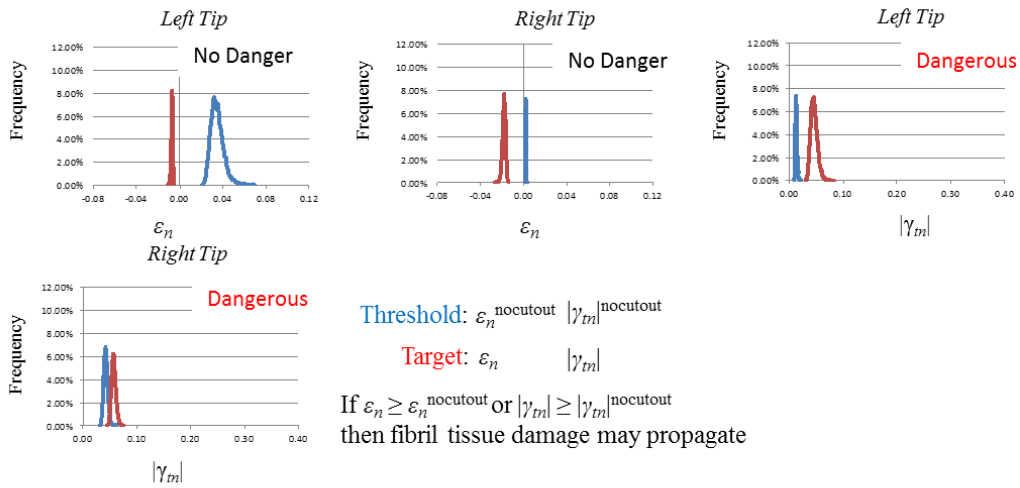


$$EV(\bar{s}_{(100g)}) - EV(\bar{s}_{(100(g-1))}) \leq \frac{SD(\bar{s}_{(100)})}{EV(\bar{s}_{(100)})\sqrt{n_{max}}}$$

with $g = 1, \dots, 100$ and $n_{max} = 10,000$

Converged if satisfied three times continuously

Model is convergence at 2,300 cases



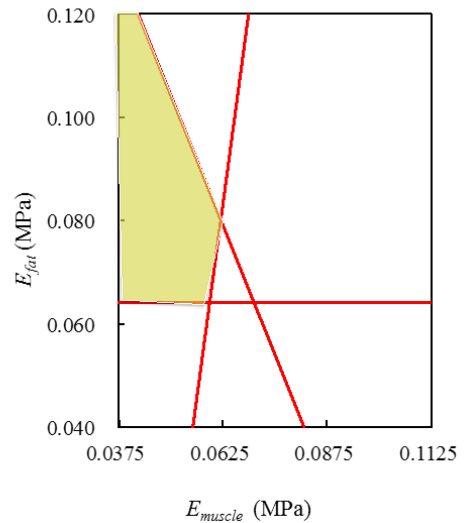
Threshold: $\epsilon_n^{nocutout} \quad |\gamma_m|^{nocutout}$

Target: $\epsilon_n \quad |\gamma_m|$

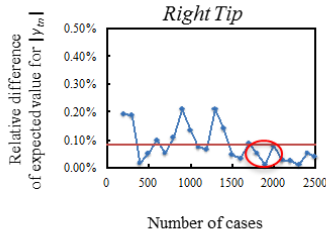
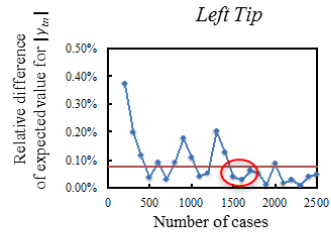
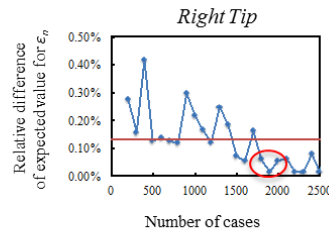
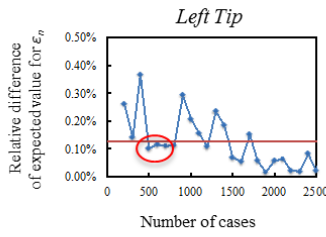
If $\epsilon_n \geq \epsilon_n^{nocutout}$ or $|\gamma_m| \geq |\gamma_m|^{nocutout}$
then fibril tissue damage may propagate

$$LSZ_{E_{muscle} E_{fat}} = \{s; p_a E_{muscle} + q_a E_{fat} + r_a \geq 0 \forall a\}$$

a	p_a	q_a	r_a
1	-0.985	0.165	0.048
2	-0.891	-0.445	0.091
3	0	1	-0.064



$$I_{fm} = 15.2 \quad b = \text{supine} \quad L_a = 8 \quad a_{mid} = 42.23$$

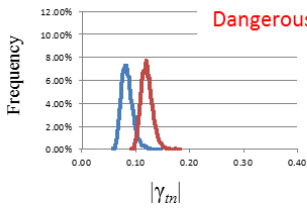
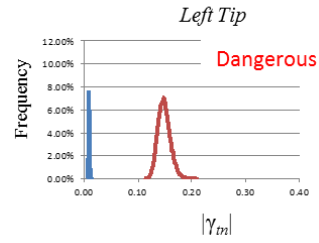
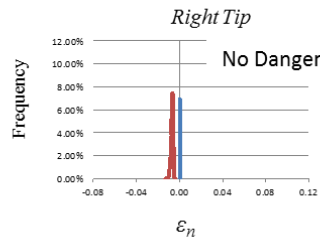
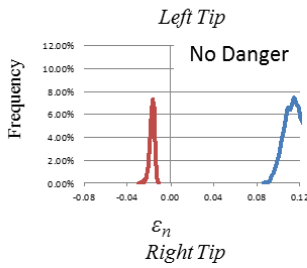


$$EV(\bar{s}_{(100g)}) - EV(\bar{s}_{(100(g-1))}) \leq \frac{SD(\bar{s}_{(100)})}{EV(\bar{s}_{(100)})\sqrt{n_{max}}}$$

with $g = 1, \dots, 100$ and $n_{max} = 10,000$

Converged if satisfied three times continuously

Model is convergence at 2,000 cases



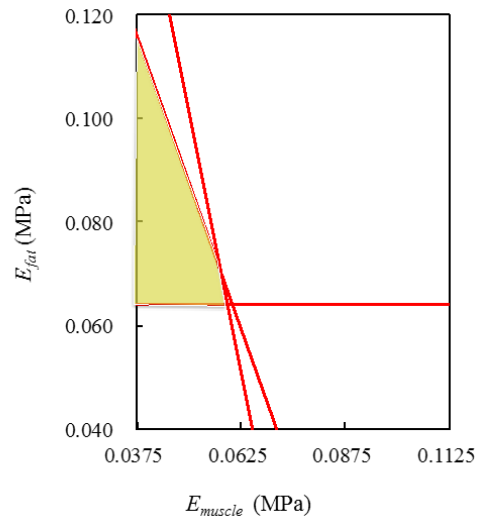
Threshold: $\varepsilon_n^{\text{nocutout}} \quad |\gamma_m|^{\text{nocutout}}$

Target: $\varepsilon_n \quad |\gamma_m|$

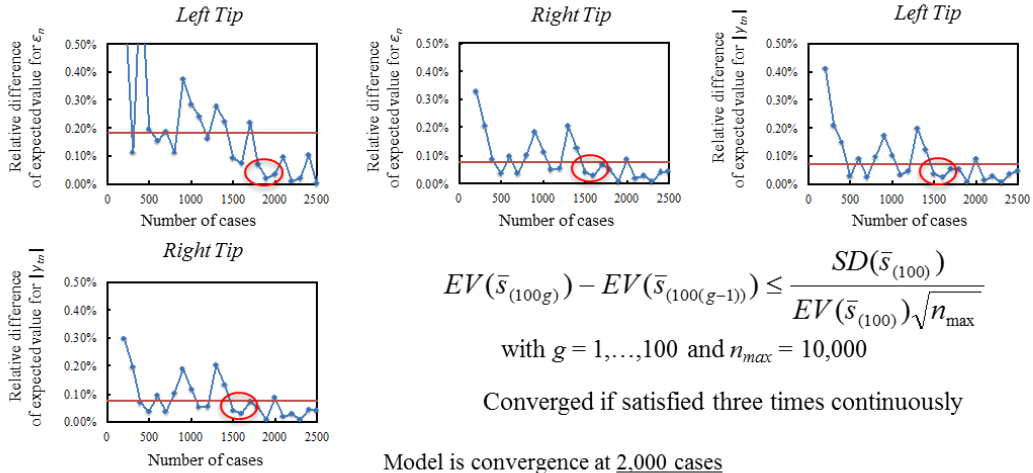
If $\varepsilon_n \geq \varepsilon_n^{\text{nocutout}}$ or $|\gamma_m| \geq |\gamma_m|^{\text{nocutout}}$
then fibril tissue damage may propagate

$$LSZ_{E_{muscle} E_{fat}} = \{s; p_a E_{muscle} + q_a E_{fat} + r_a \geq 0 \forall a\}$$

a	p_a	q_a	r_a
1	-0.911	-0.404	0.081
2	-0.968	-0.242	0.073
3	0	1	-0.064



$$I_{fm} = 15.2 \quad b = \text{supine} \quad L_a = 8 \quad a_{mid} = 104.38$$

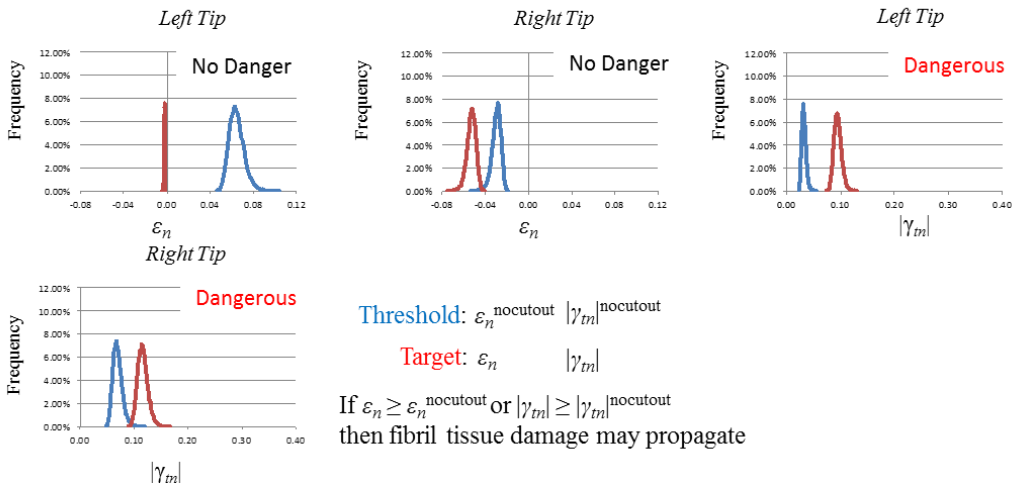


$$EV(\bar{s}_{(100g)}) - EV(\bar{s}_{(100(g-1))}) \leq \frac{SD(\bar{s}_{(100)})}{EV(\bar{s}_{(100)})\sqrt{n_{max}}}$$

with $g = 1, \dots, 100$ and $n_{max} = 10,000$

Converged if satisfied three times continuously

Model is convergence at 2.000 cases



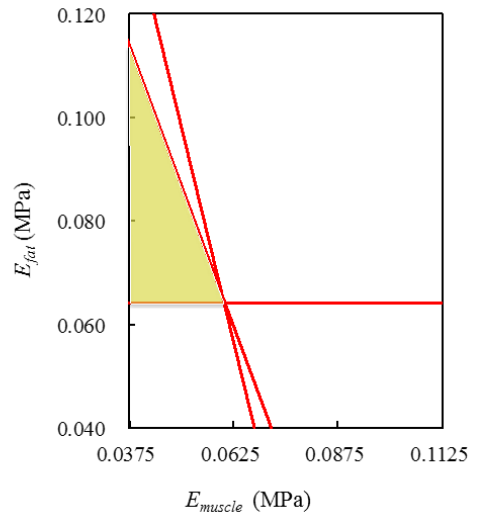
Threshold: $\varepsilon_n^{\text{nocutout}} \quad |\gamma_{fm}|^{\text{nocutout}}$

Target: $\varepsilon_n \quad |\gamma_{fm}|$

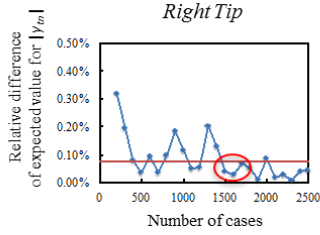
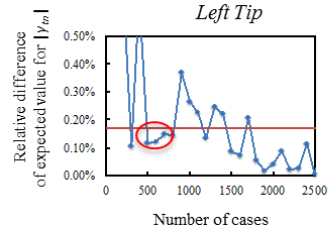
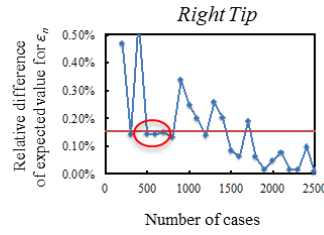
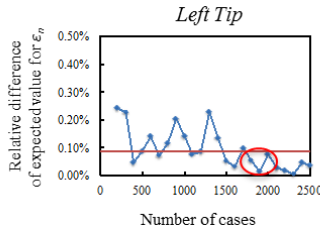
If $\varepsilon_n \geq \varepsilon_n^{\text{nocutout}}$ or $|\gamma_{fm}| \geq |\gamma_{fm}|^{\text{nocutout}}$
then fibril tissue damage may propagate

$$LSZ_{E_{muscle} E_{fat}} = \{s; p_a E_{muscle} + q_a E_{fat} + r_a \geq 0 \forall a\}$$

a	p_a	q_a	r_a
1	-0.955	-0.287	0.076
2	-0.905	-0.418	0.081
3	0	1	-0.064



$$I_{fm} = 15.2 \quad b = \text{supine} \quad L_a = 8 \quad a_{mid} = 166.63$$

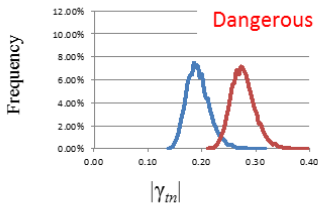
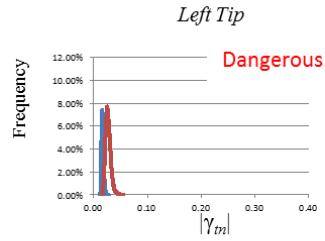
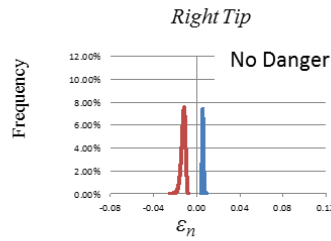
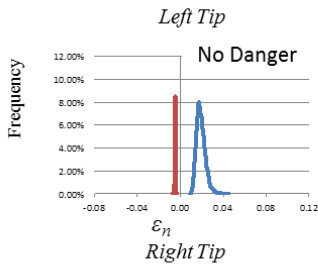


$$EV(\bar{s}_{(100g)}) - EV(\bar{s}_{(100(g-1))}) \leq \frac{SD(\bar{s}_{(100)})}{EV(\bar{s}_{(100)})\sqrt{n_{max}}}$$

with $g = 1, \dots, 100$ and $n_{max} = 10,000$

Converged if satisfied three times continuously

Model is convergence at 2,000 cases



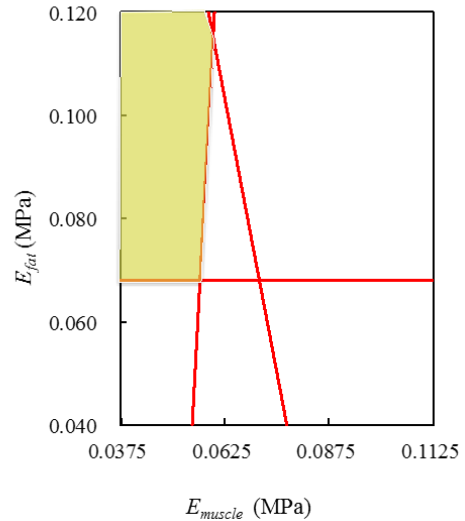
Threshold: $\varepsilon_n^{\text{nocutout}} \quad |\gamma_m|^{\text{nocutout}}$

Target: $\varepsilon_n \quad |\gamma_m|$

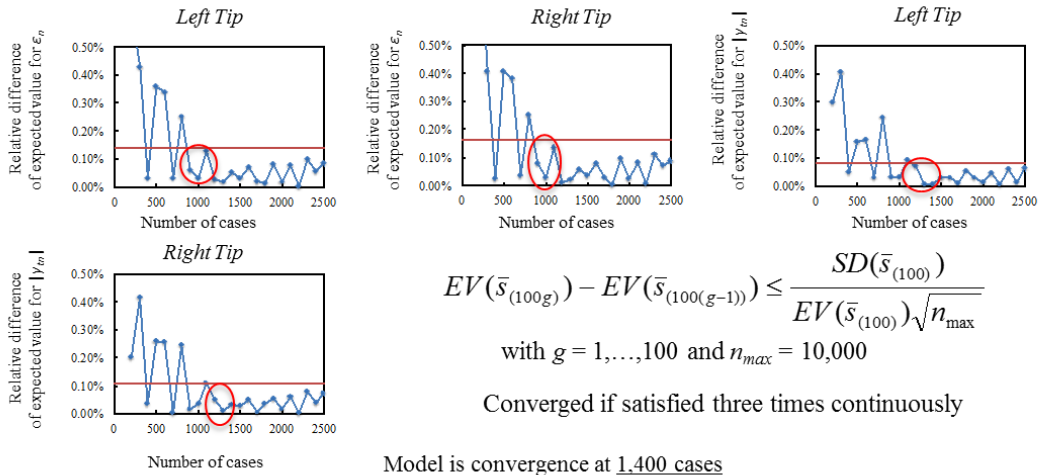
If $\varepsilon_n \geq \varepsilon_n^{\text{nocutout}}$ or $|\gamma_m| \geq |\gamma_m|^{\text{nocutout}}$
then fibril tissue damage may propagate

$$LSZ_{E_{muscle} E_{fat}} = \{s; p_a E_{muscle} + q_a E_{fat} + r_a \geq 0 \forall a\}$$

a	p_a	q_a	r_a
1	-0.996	0.067	0.052
2	-0.97	-0.226	0.084
3	0	1	-0.068



$$I_{fm} = 15.2 \quad b = \text{lateral-A} \quad L_a = 4 \quad a_{mid} = 42.23$$

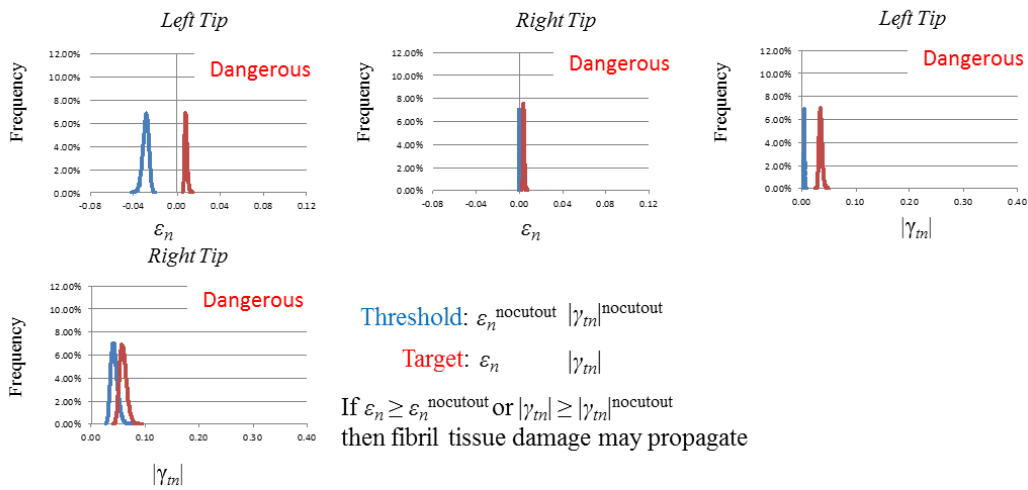


$$EV(\bar{s}_{(100g)}) - EV(\bar{s}_{(100(g-1))}) \leq \frac{SD(\bar{s}_{(100)})}{EV(\bar{s}_{(100)})\sqrt{n_{max}}}$$

with $g = 1, \dots, 100$ and $n_{max} = 10,000$

Converged if satisfied three times continuously

Model is convergence at 1,400 cases



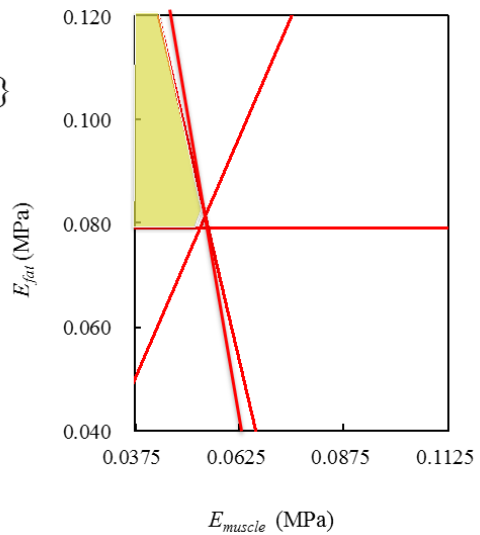
Threshold: $\epsilon_n^{nocutout} \quad |\gamma_m|^{nocutout}$

Target: $\epsilon_n \quad |\gamma_m|$

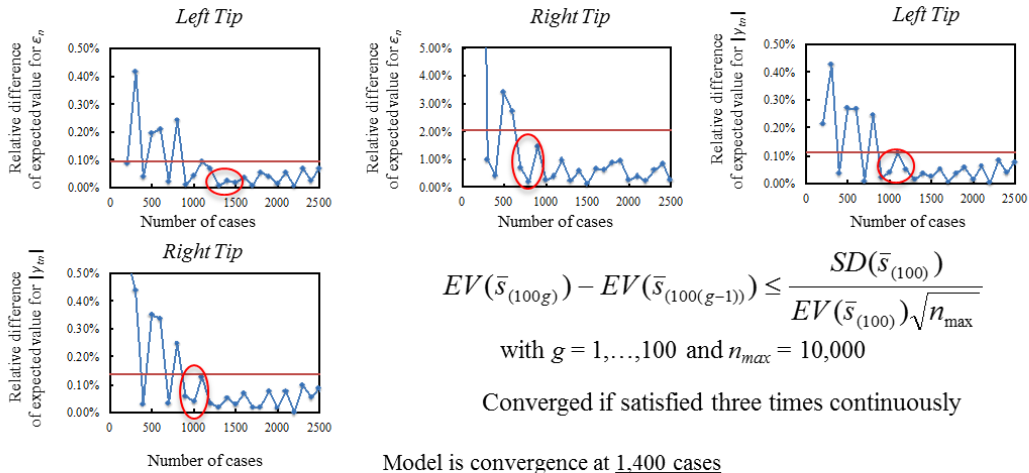
If $\epsilon_n \geq \epsilon_n^{nocutout}$ or $|\gamma_m| \geq |\gamma_m|^{nocutout}$
then fibril tissue damage may propagate

$$LSZ_{E_{muscle} E_{fat}} = \{s; p_a E_{muscle} + q_a E_{fat} + r_a \geq 0 \quad \forall a\}$$

a	p_a	q_a	r_a
1	-0.985	-0.158	0.067
2	-0.985	0.168	0.043
3	-0.894	0.447	0.013
4	0	1	-0.081



$$I_{fm} = 15.2 \quad b = \text{lateral-A} \quad L_a = 4 \quad a_{mid} = 104.38$$

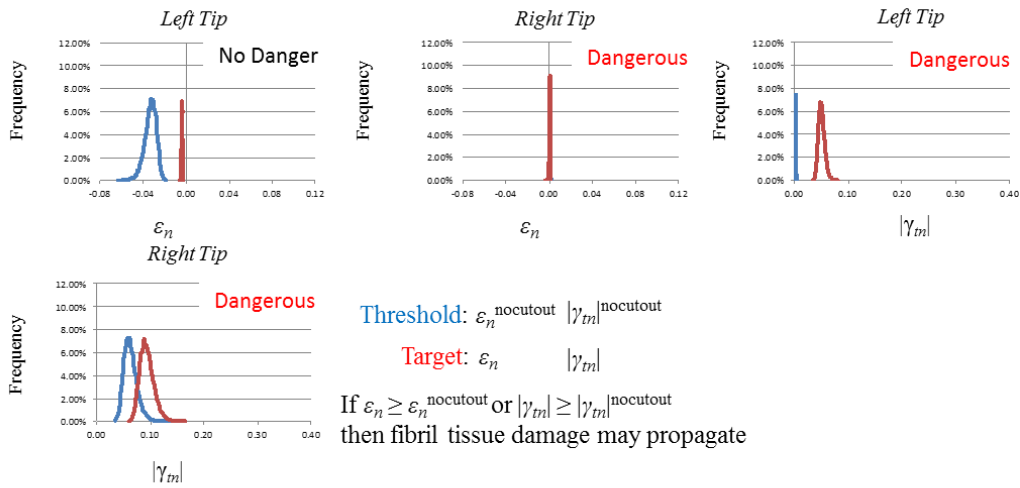


$$EV(\bar{s}_{(100g)}) - EV(\bar{s}_{(100(g-1))}) \leq \frac{SD(\bar{s}_{(100)})}{EV(\bar{s}_{(100)})\sqrt{n_{max}}}$$

with $g = 1, \dots, 100$ and $n_{max} = 10,000$

Converged if satisfied three times continuously

Model is convergence at 1,400 cases



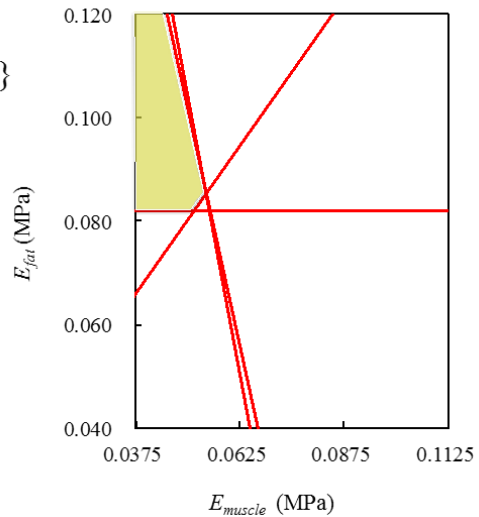
Threshold: $\epsilon_n^{nocutout} \quad |\gamma_m|^{nocutout}$

Target: $\epsilon_n \quad |\gamma_m|$

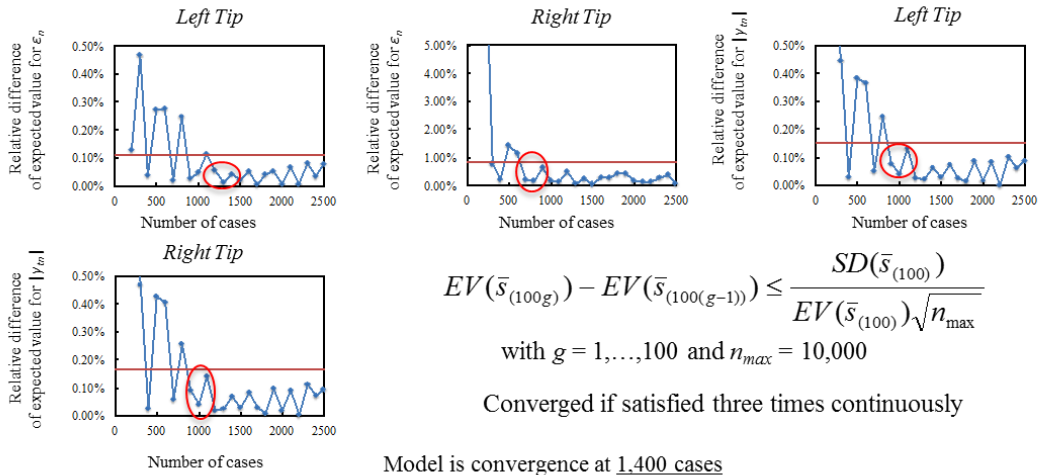
If $\epsilon_n \geq \epsilon_n^{nocutout}$ or $|\gamma_m| \geq |\gamma_m|^{nocutout}$
then fibril tissue damage may propagate

$$LSZ_{E_{muscle} E_{fat}} = \{s; p_a E_{muscle} + q_a E_{fat} + r_a \geq 0 \forall a\}$$

a	p_a	q_a	r_a
1	-0.971	-0.228	0.072
2	-0.962	-0.263	0.075
3	-0.752	0.658	-0.015
4	0	1	-0.082



$$I_{fm} = 15.2 \quad b = \text{lateral-A} \quad L_a = 4 \quad a_{mid} = 166.63$$

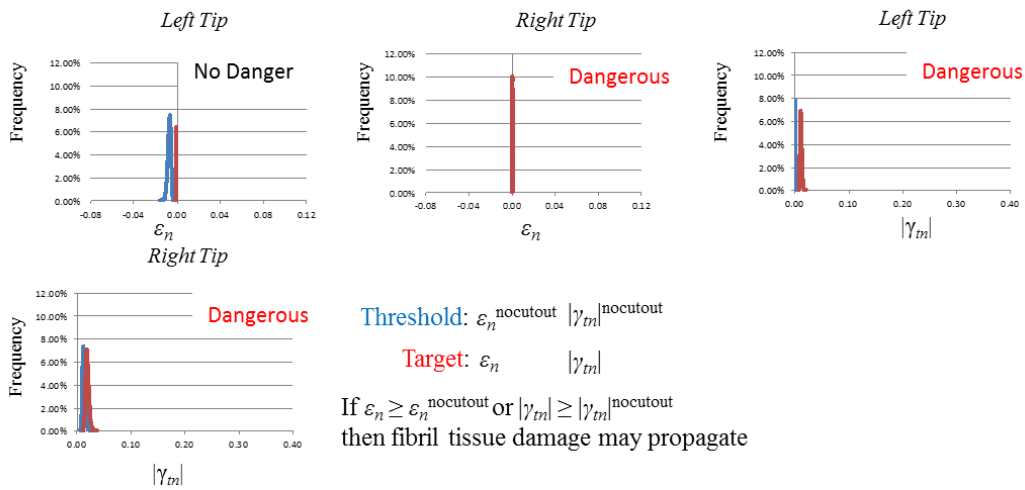


$$EV(\bar{s}_{(100g)}) - EV(\bar{s}_{(100(g-1))}) \leq \frac{SD(\bar{s}_{(100)})}{EV(\bar{s}_{(100)})\sqrt{n_{max}}}$$

with $g = 1, \dots, 100$ and $n_{max} = 10,000$

Converged if satisfied three times continuously

Model is convergence at 1,400 cases



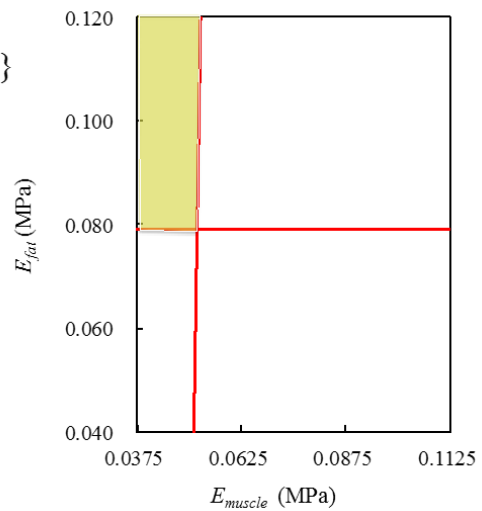
Threshold: $\epsilon_n^{nocutout} \quad |\gamma_{fm}|^{nocutout}$

Target: $\epsilon_n \quad |\gamma_{fm}|$

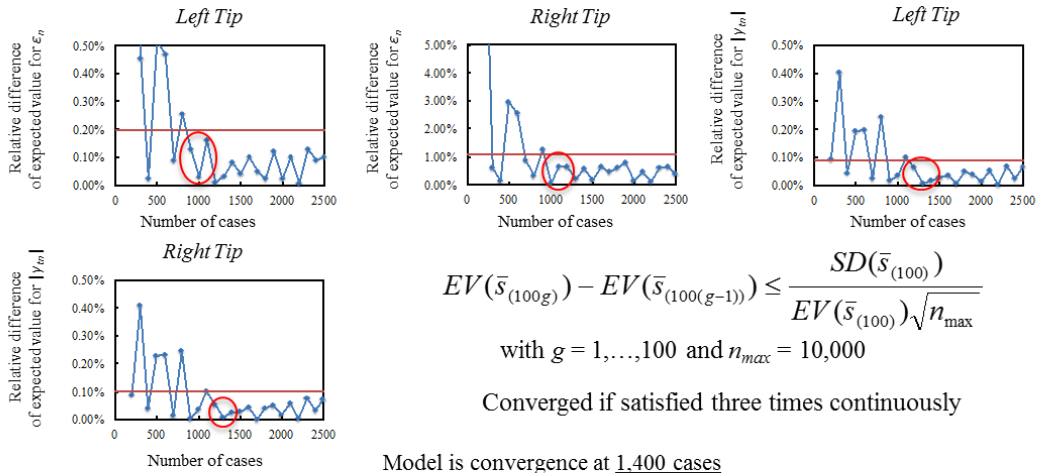
If $\epsilon_n \geq \epsilon_n^{nocutout}$ or $|\gamma_{fm}| \geq |\gamma_{fm}|^{nocutout}$
then fibril tissue damage may propagate

$$LSZ_{E_{muscle}E_{fat}} = \{s; p_a E_{muscle} + q_a E_{fat} + r_a \geq 0 \forall a\}$$

a	p_a	q_a	r_a
1	-0.999	0.02	0.05
2	0	1	0.079



$$I_{fm} = 15.2 \quad b = \text{lateral-A} \quad L_a = 8 \quad a_{mid} = 42.23$$

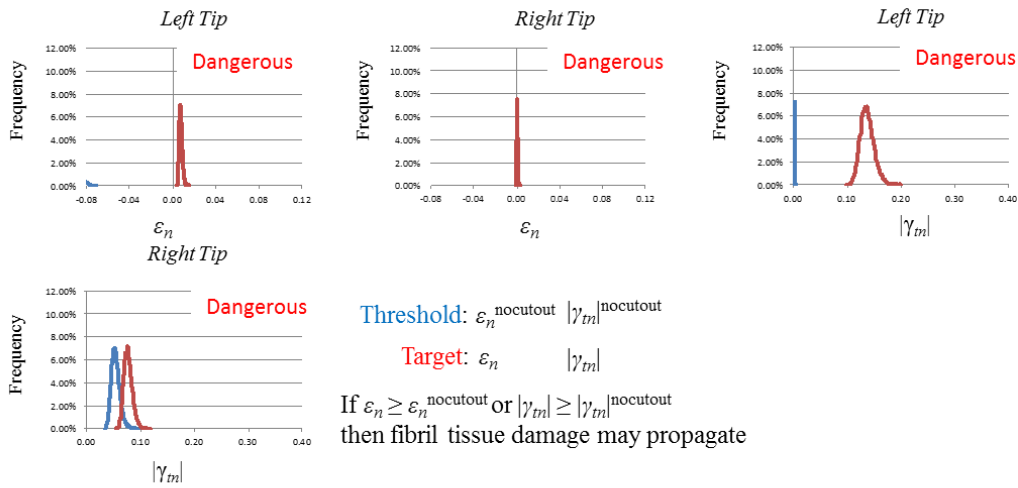


$$EV(\bar{s}_{(100g)}) - EV(\bar{s}_{(100(g-1))}) \leq \frac{SD(\bar{s}_{(100)})}{EV(\bar{s}_{(100)})\sqrt{n_{max}}}$$

with $g = 1, \dots, 100$ and $n_{max} = 10,000$

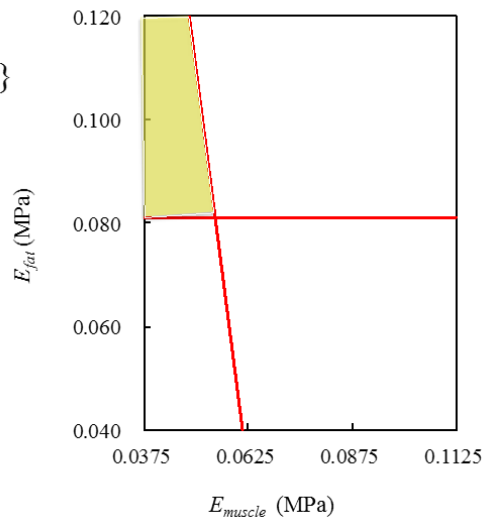
Converged if satisfied three times continuously

Model is convergence at 1,400 cases

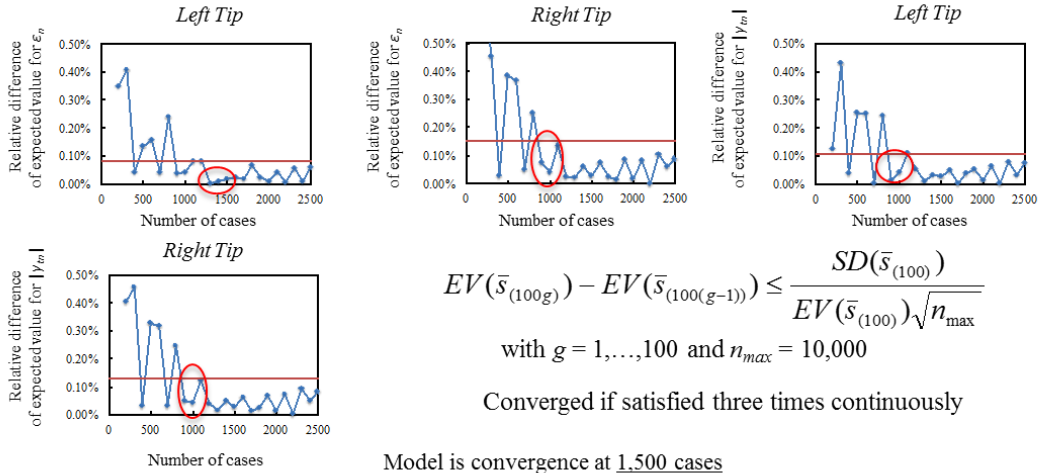


$$LSZ_{E_{muscle} E_{fat}} = \{s; p_a E_{muscle} + q_a E_{fat} + r_a \geq 0 \forall a\}$$

a	p_a	q_a	r_a
1	-0.985	-0.158	0.067
2	0	1	-0.081



$$I_{fm} = 15.2 \quad b = \text{lateral-A} \quad L_a = 8 \quad a_{mid} = 104.38$$

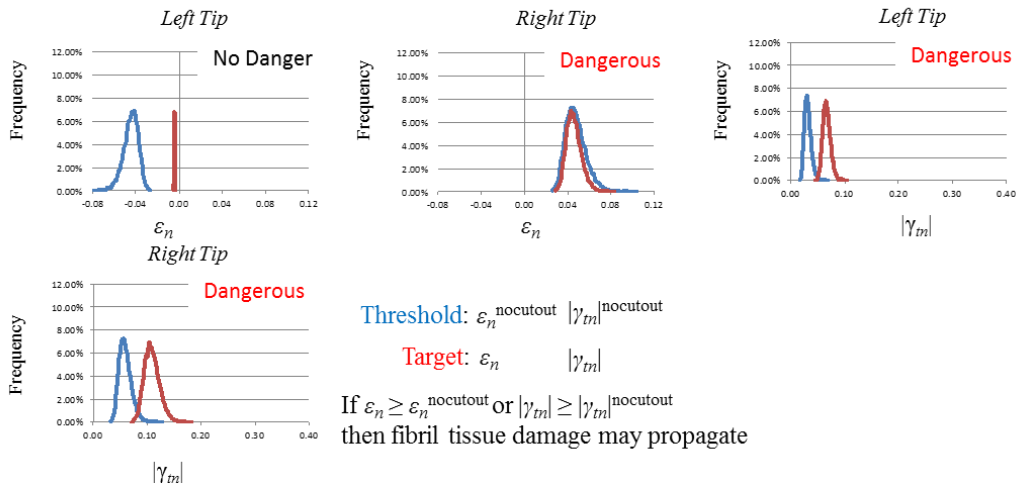


$$EV(\bar{s}_{(100g)}) - EV(\bar{s}_{(100(g-1))}) \leq \frac{SD(\bar{s}_{(100)})}{EV(\bar{s}_{(100)})\sqrt{n_{max}}}$$

with $g = 1, \dots, 100$ and $n_{max} = 10,000$

Converged if satisfied three times continuously

Model is convergence at 1.500 cases



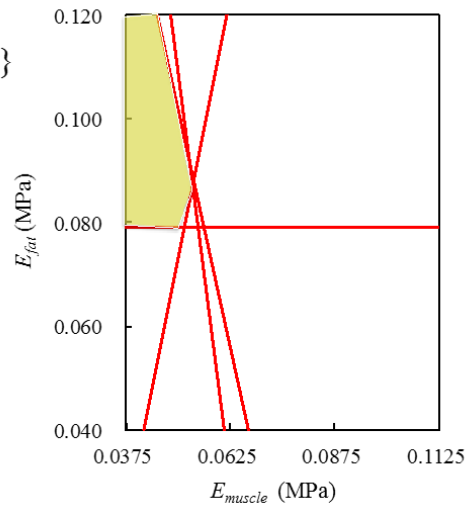
Threshold: $\epsilon_n^{nocutout} \quad |\gamma_m|^{nocutout}$

Target: $\epsilon_n \quad |\gamma_m|$

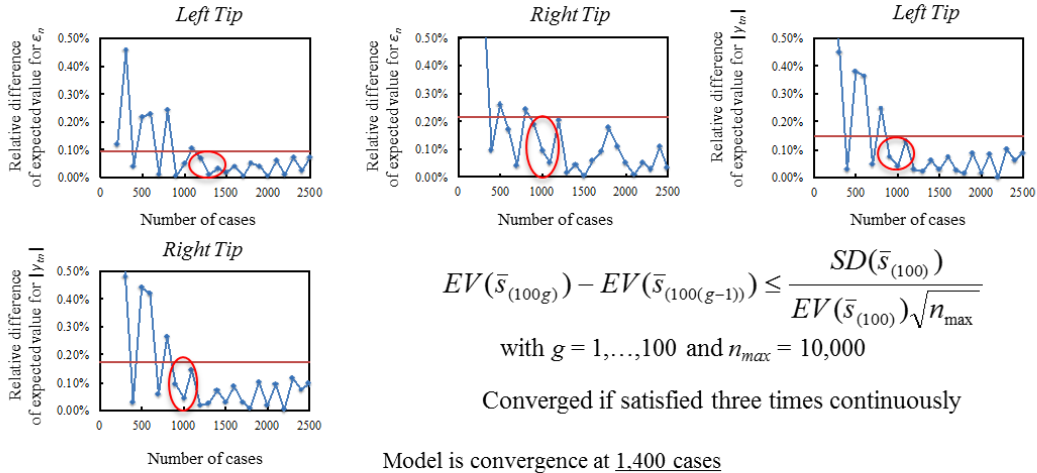
If $\epsilon_n \geq \epsilon_n^{nocutout}$ or $|\gamma_m| \geq |\gamma_m|^{nocutout}$
then fibril tissue damage may propagate

$$LSZ_{E_{muscle} E_{fat}} = \{s; p_a E_{muscle} + q_a E_{fat} + r_a \geq 0 \forall a\}$$

a	p_a	q_a	r_a
1	-0.985	-0.158	0.067
2	-0.962	-0.263	0.075
3	-0.97	0.242	0.031
4	0	1	-0.079



$$I_{fm} = 15.2 \quad b = \text{lateral-A} \quad L_a = 8 \quad a_{mid} = 166.63$$

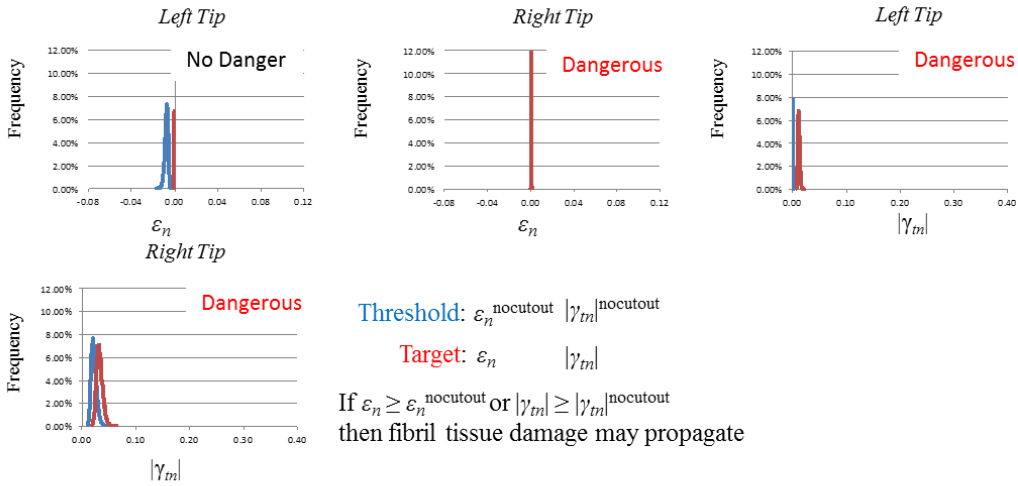


$$EV(\bar{s}_{(100g)}) - EV(\bar{s}_{(100(g-1))}) \leq \frac{SD(\bar{s}_{(100)})}{EV(\bar{s}_{(100)})\sqrt{n_{max}}}$$

with $g = 1, \dots, 100$ and $n_{max} = 10,000$

Converged if satisfied three times continuously

Model is convergence at 1,400 cases



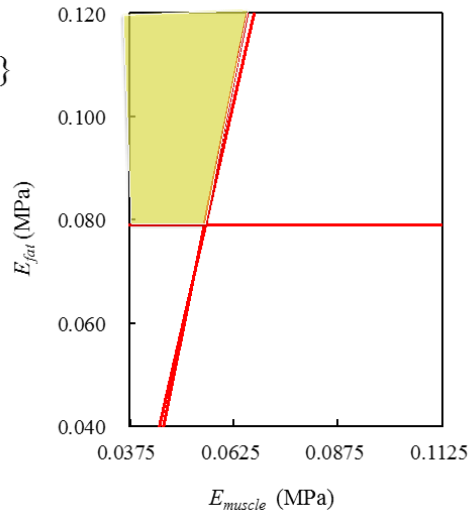
Threshold: $\epsilon_n^{nocutout} \quad |\gamma_m|^{nocutout}$

Target: $\epsilon_n \quad |\gamma_m|$

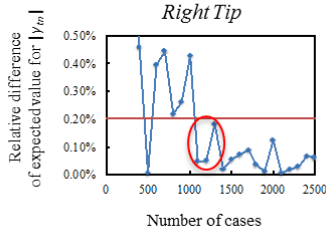
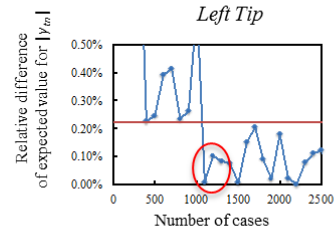
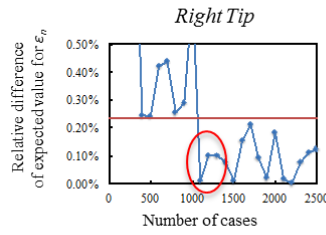
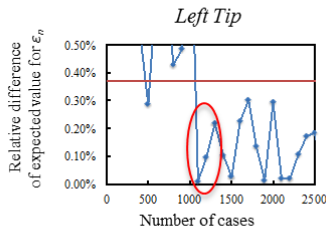
If $\epsilon_n \geq \epsilon_n^{nocutout}$ or $|\gamma_m| \geq |\gamma_m|^{nocutout}$
then fibril tissue damage may propagate

$$LSZ_{E_{muscle} E_{fat}} = \{s; p_a E_{muscle} + q_a E_{fat} + r_a \geq 0 \forall a\}$$

a	p_a	q_a	r_a
1	-0.961	0.275	0.032
2	-0.97	0.242	0.035
3	0	1	-0.079



$$I_{fm} = 15.2 \quad b = \text{lateral-B} \quad L_a = 4 \quad a_{mid} = 42.23$$

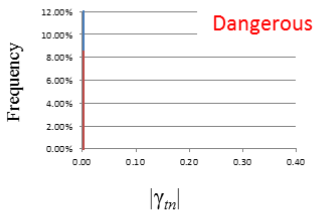
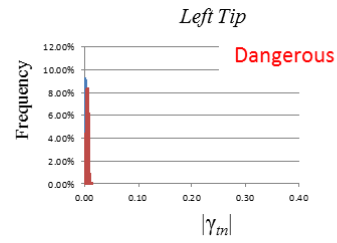
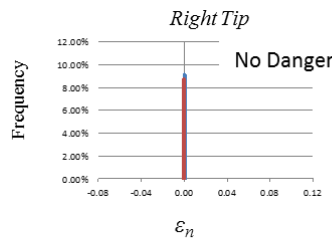
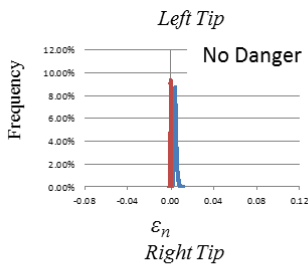


$$EV(\bar{s}_{(100g)}) - EV(\bar{s}_{(100(g-1))}) \leq \frac{SD(\bar{s}_{(100)})}{EV(\bar{s}_{(100)})\sqrt{n_{max}}}$$

with $g = 1, \dots, 100$ and $n_{max} = 10,000$

Converged if satisfied three times continuously

Model is convergence at 1,300 cases



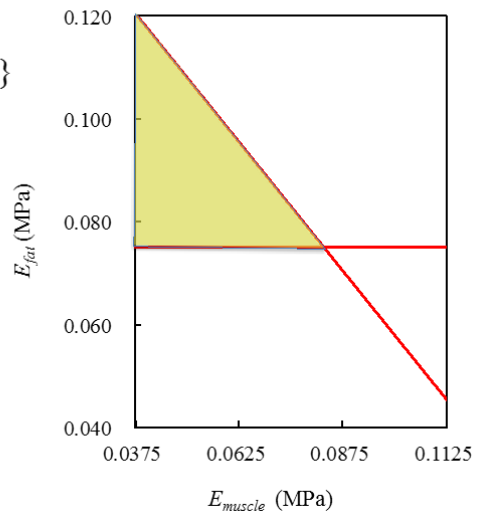
Threshold: $\varepsilon_n^{nocutout} \quad |\gamma_m|^{nocutout}$

Target: $\varepsilon_n \quad |\gamma_m|$

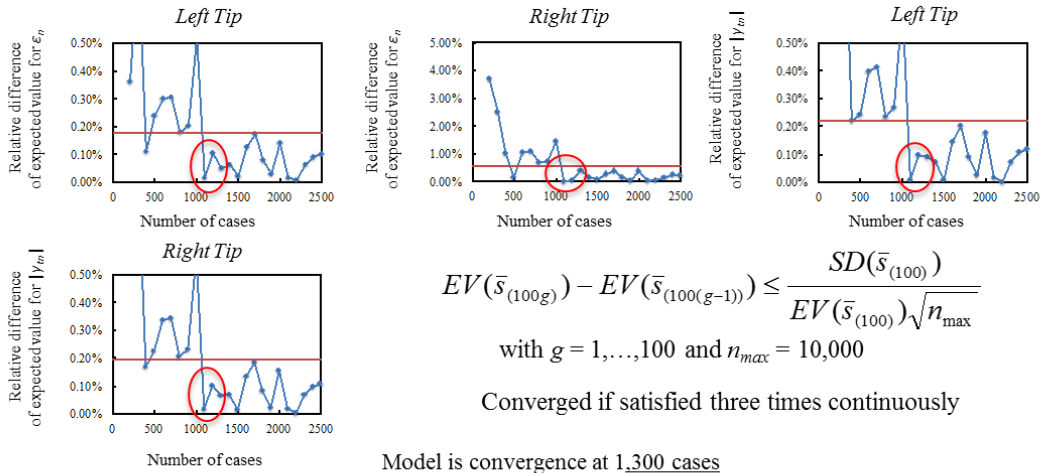
If $\varepsilon_n \geq \varepsilon_n^{nocutout}$ or $|\gamma_m| \geq |\gamma_m|^{nocutout}$
then fibril tissue damage may propagate

$$LSZ_{E_{muscle} E_{fat}} = \{s; p_a E_{muscle} + q_a E_{fat} + r_a \geq 0 \forall a\}$$

a	p_a	q_a	r_a
1	-0.703	-0.703	0.111
2	0	1	-0.075



$$I_{fm} = 15.2 \quad b = \text{lateral-B} \quad L_a = 4 \quad a_{mid} = 104.38$$

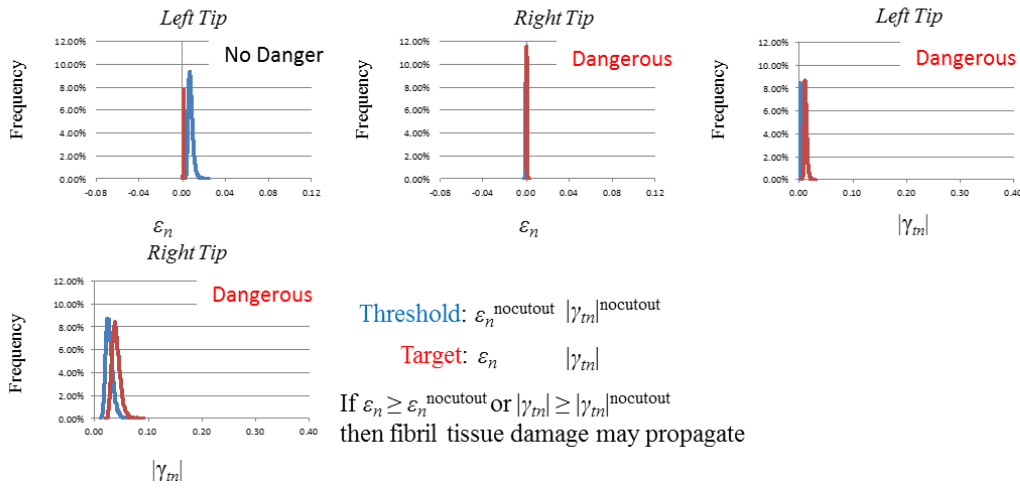


$$EV(\bar{s}_{(100g)}) - EV(\bar{s}_{(100(g-1))}) \leq \frac{SD(\bar{s}_{(100)})}{EV(\bar{s}_{(100)})\sqrt{n_{max}}}$$

with $g = 1, \dots, 100$ and $n_{max} = 10,000$

Converged if satisfied three times continuously

Model is convergence at 1,300 cases



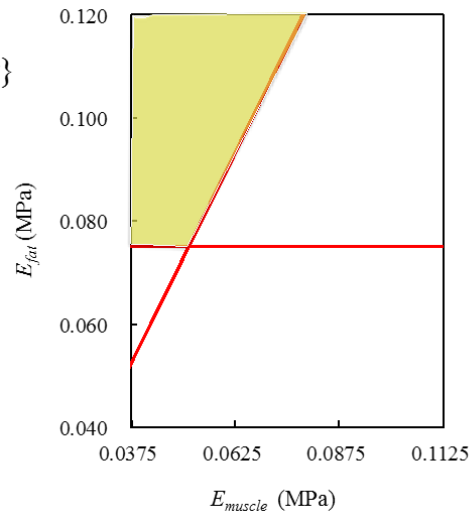
Threshold: $\epsilon_n^{nocutout} \quad |\gamma_m|^{nocutout}$

Target: $\epsilon_n \quad |\gamma_m|$

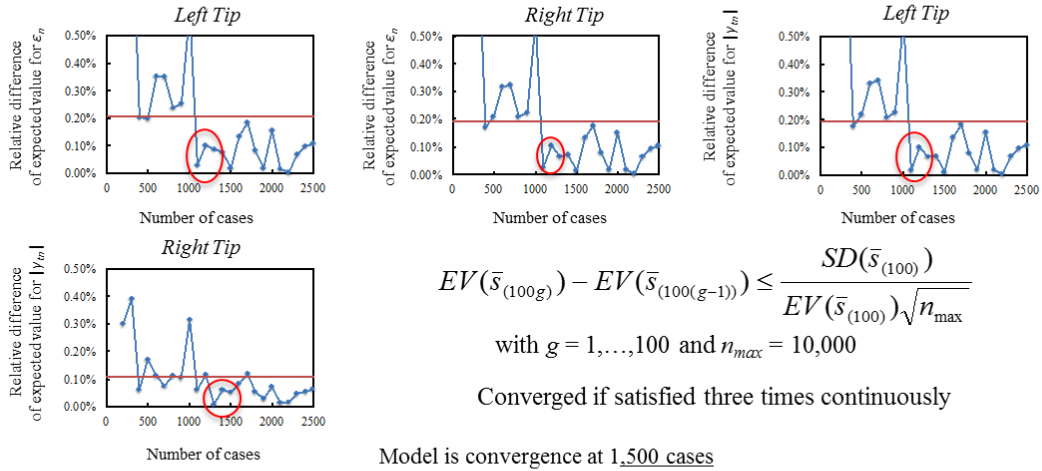
If $\epsilon_n \geq \epsilon_n^{nocutout}$ or $|\gamma_m| \geq |\gamma_m|^{nocutout}$
then fibril tissue damage may propagate

$$LSZ_{E_{muscle}E_{fat}} = \{s; p_a E_{muscle} + q_a E_{fat} + r_a \geq 0 \forall a\}$$

a	p_a	q_a	r_a
1	-0.853	0.523	0.004
2	-0.852	0.524	0.004
3	0	1	-0.075



$$I_{fm} = 15.2 \quad b = \text{lateral-B} \quad L_a = 4 \quad a_{mid} = 166.63$$

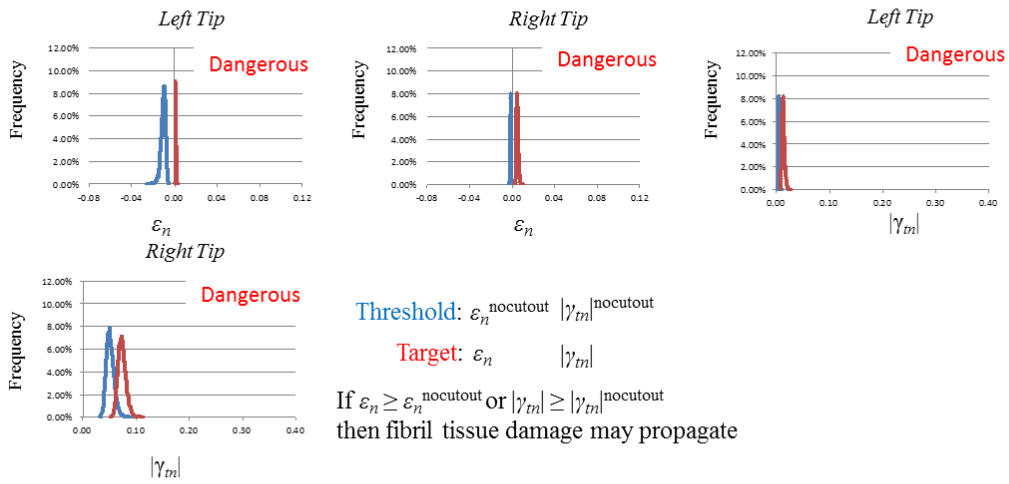


$$EV(\bar{s}_{(100g)}) - EV(\bar{s}_{(100(g-1))}) \leq \frac{SD(\bar{s}_{(100)})}{EV(\bar{s}_{(100)})\sqrt{n_{max}}}$$

with $g = 1, \dots, 100$ and $n_{max} = 10,000$

Converged if satisfied three times continuously

Model is convergence at 1,500 cases



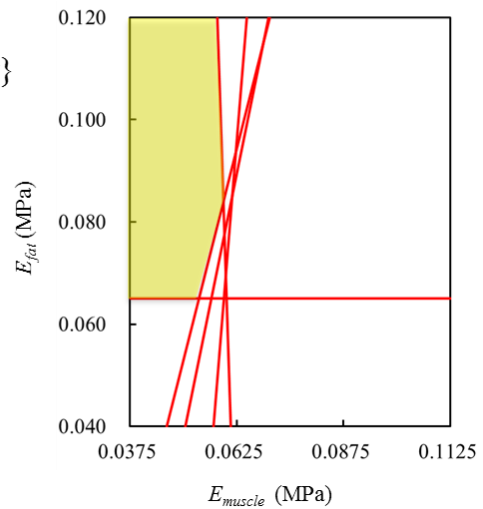
Threshold: $\epsilon_n^{nocutout} \quad |\gamma_{fm}|^{nocutout}$

Target: $\epsilon_n \quad |\gamma_{fm}|$

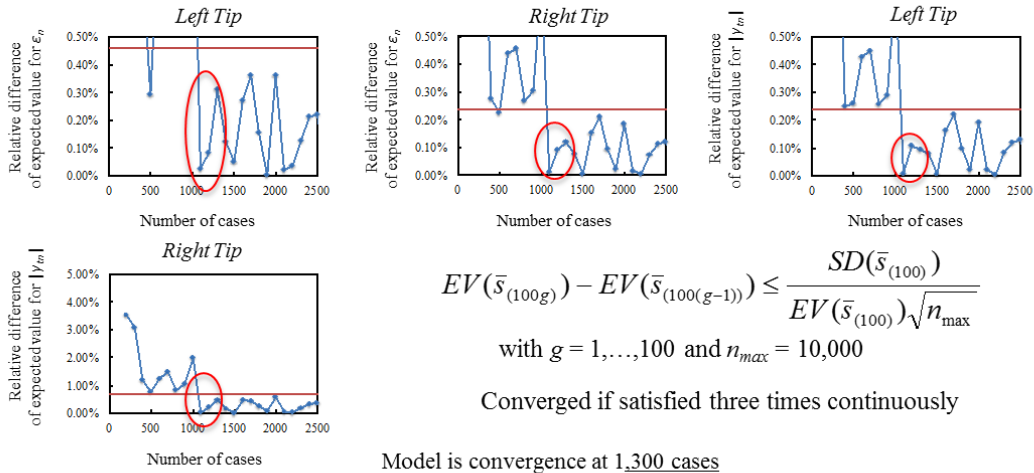
If $\epsilon_n \geq \epsilon_n^{nocutout}$ or $|\gamma_{fm}| \geq |\gamma_{fm}|^{nocutout}$
then fibril tissue damage may propagate

$$LSZ_{E_{muscle}E_{fat}} = \{s; p_a E_{muscle} + q_a E_{fat} + r_a \geq 0 \quad \forall a\}$$

a	p_a	q_a	r_a
1	-0.971	0.238	0.04
2	-0.957	0.287	0.033
3	-0.997	-0.04	0.063
4	-0.994	0.097	0.053
5	0	1	-0.065



$$I_{fm} = 15.2 \quad b = \text{lateral-B} \quad L_a = 8 \quad a_{mid} = 42.23$$

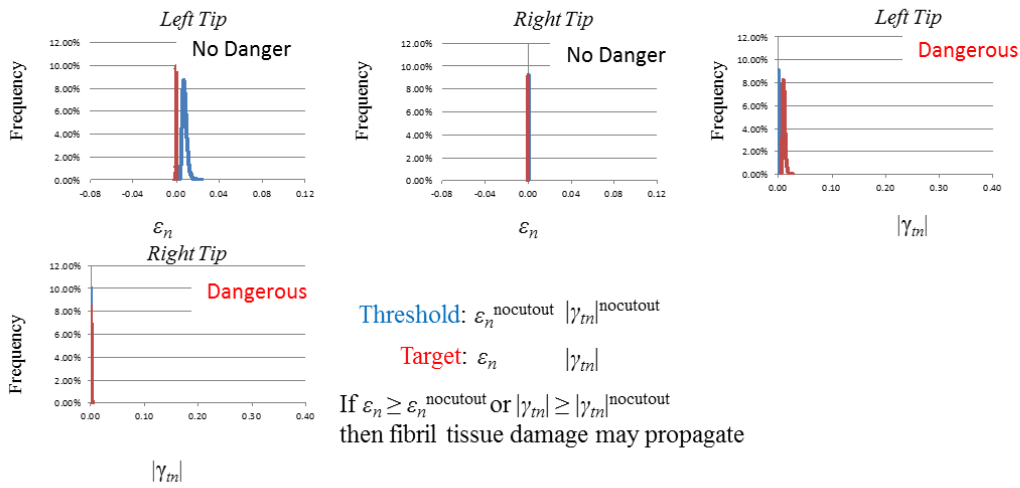


$$EV(\bar{s}_{(100g)}) - EV(\bar{s}_{(100(g-1))}) \leq \frac{SD(\bar{s}_{(100)})}{EV(\bar{s}_{(100)})\sqrt{n_{max}}}$$

with $g = 1, \dots, 100$ and $n_{max} = 10,000$

Converged if satisfied three times continuously

Model is convergence at 1,300 cases



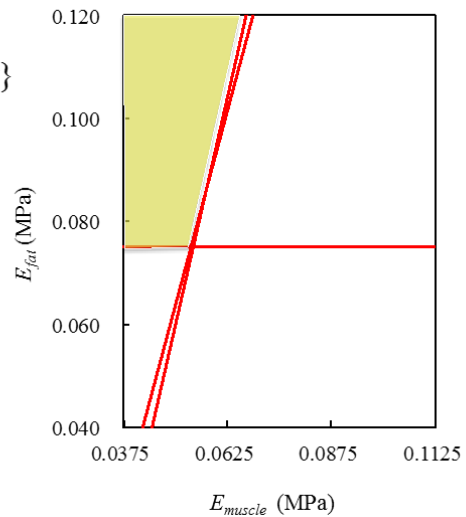
Threshold: $\epsilon_n^{nocutout} \quad |\gamma_m|^{nocutout}$

Target: $\epsilon_n \quad |\gamma_m|$

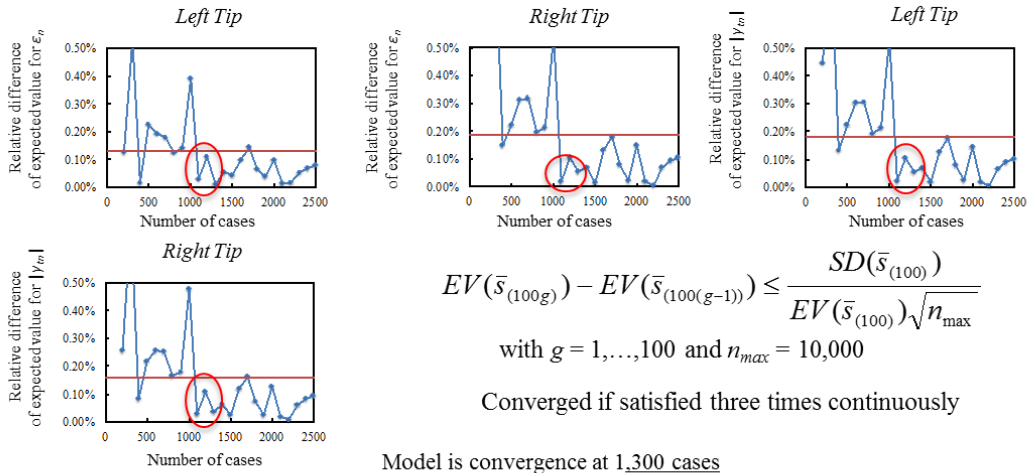
If $\epsilon_n \geq \epsilon_n^{nocutout}$ or $|\gamma_m| \geq |\gamma_m|^{nocutout}$
then fibril tissue damage may propagate

$$LSZ_{E_{muscle} E_{fat}} = \{s; p_a E_{muscle} + q_a E_{fat} + r_a \geq 0 \forall a\}$$

a	p_a	q_a	r_a
1	-0.961	0.274	0.032
2	-0.948	-0.316	0.028
3	0	1	-0.06



$$I_{fm} = 15.2 \quad b = \text{lateral-B} \quad L_a = 8 \quad a_{mid} = 104.38$$

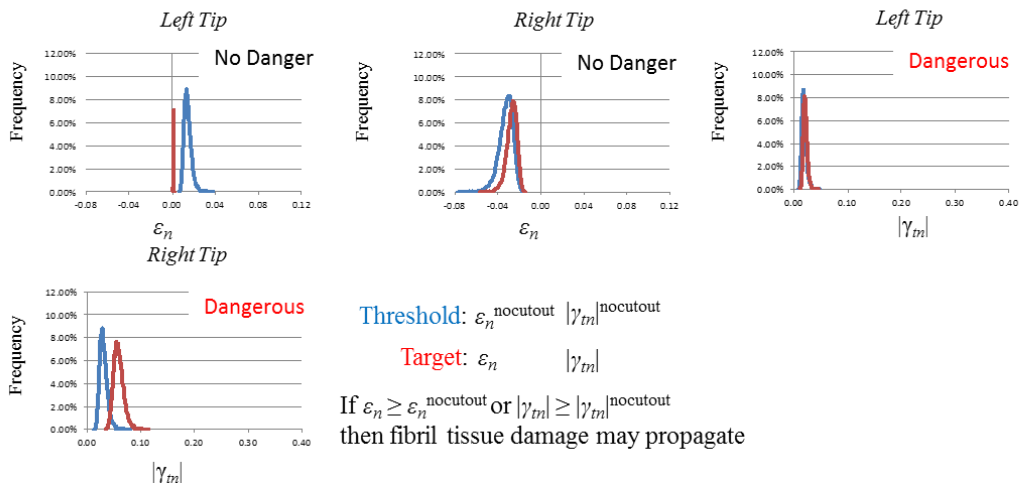


$$EV(\bar{s}_{(100g)}) - EV(\bar{s}_{(100(g-1))}) \leq \frac{SD(\bar{s}_{(100)})}{EV(\bar{s}_{(100)})\sqrt{n_{max}}}$$

with $g = 1, \dots, 100$ and $n_{max} = 10,000$

Converged if satisfied three times continuously

Model is convergence at 1,300 cases



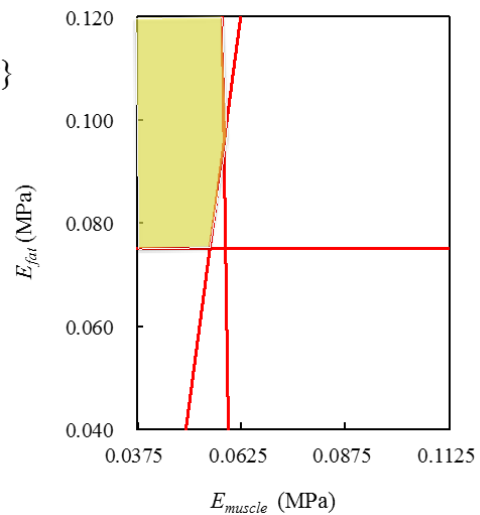
Threshold: $\epsilon_n^{nocutout} \quad |\gamma_m|^{nocutout}$

Target: $\epsilon_n \quad |\gamma_m|$

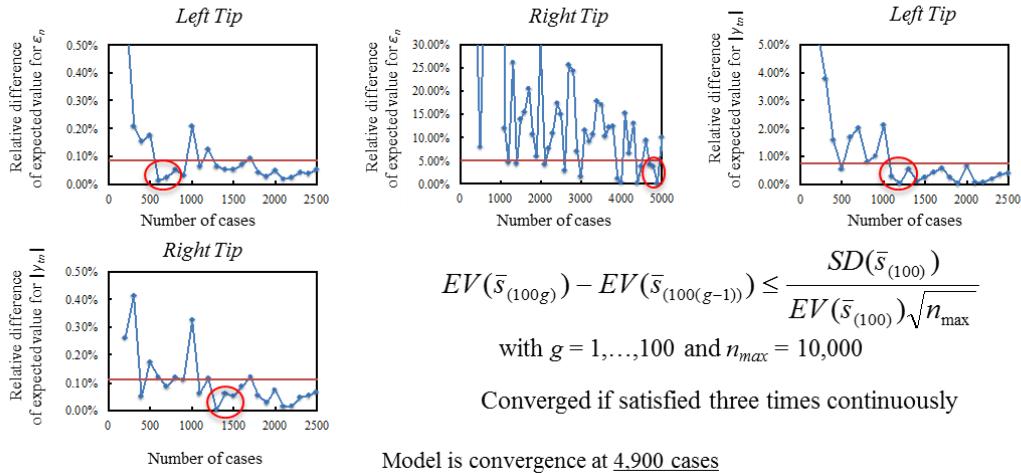
If $\epsilon_n \geq \epsilon_n^{nocutout}$ or $|\gamma_m| \geq |\gamma_m|^{nocutout}$
then fibril tissue damage may propagate

$$LSZ_{E_{muscle}E_{fat}} = \{s; p_a E_{muscle} + q_a E_{fat} + r_a \geq 0 \forall a\}$$

a	p_a	q_a	r_a
1	-0.998	-0.02	0.06
2	-0.985	0.165	0.042
3	0	1	-0.075



$$I_{fm} = 15.2 \quad b = \text{lateral-B} \quad L_a = 8 \quad a_{mid} = 166.63$$

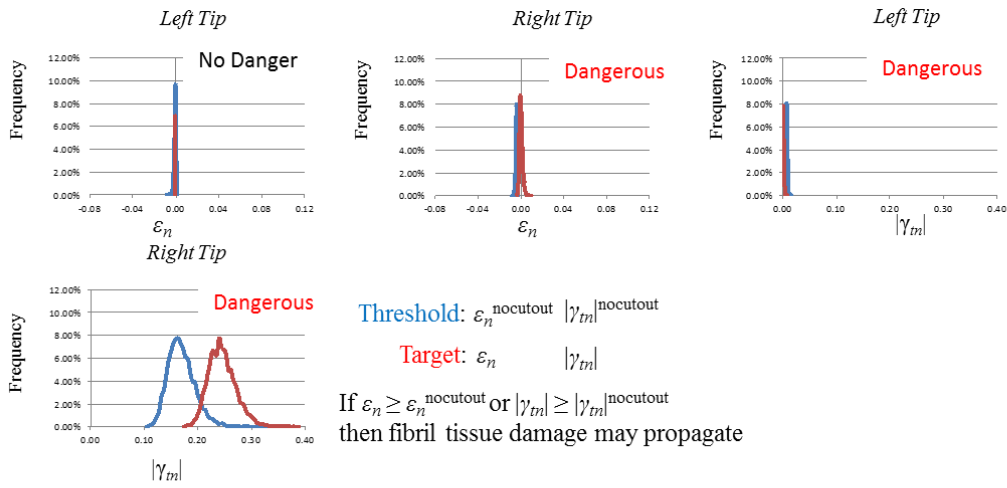


$$EV(\bar{s}_{(100g)}) - EV(\bar{s}_{(100(g-1))}) \leq \frac{SD(\bar{s}_{(100)})}{EV(\bar{s}_{(100)})\sqrt{n_{max}}}$$

with $g = 1, \dots, 100$ and $n_{max} = 10,000$

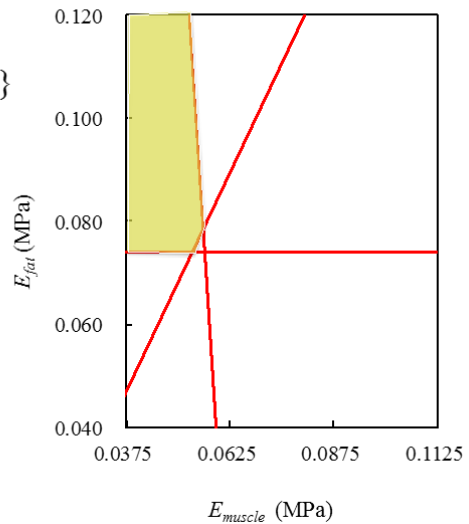
Converged if satisfied three times continuously

Model is convergence at 4,900 cases

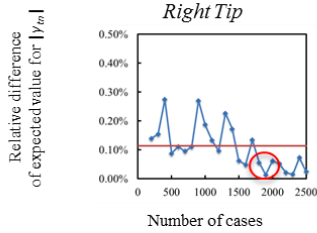
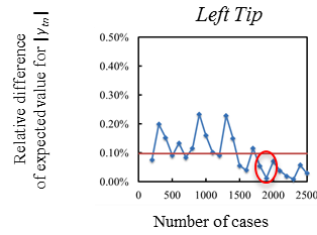
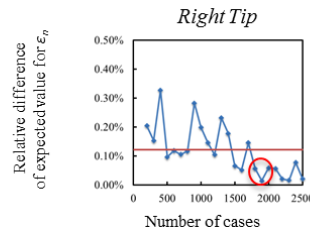
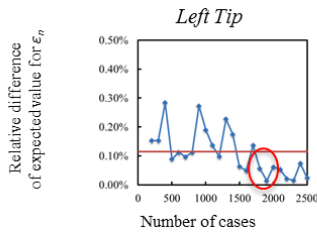


$$LSZ_{E_{muscle} E_{fat}} = \{s; p_a E_{muscle} + q_a E_{fat} + r_a \geq 0 \forall a\}$$

a	p_a	q_a	r_a
1	-0.995	-0.08	0.062
2	-0.862	0.507	0.009
3	0	1	-0.074



$$I_{fm} = 22.92 \quad b = \text{supine} \quad L_a = 4 \quad a_{mid} = 42.23$$

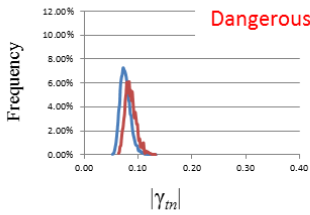
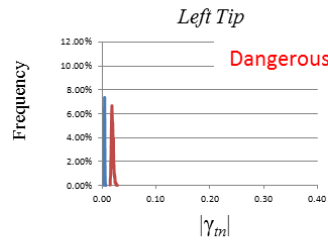
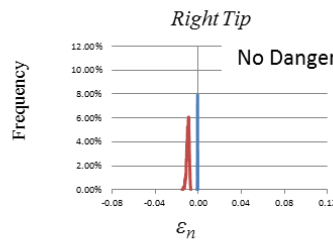
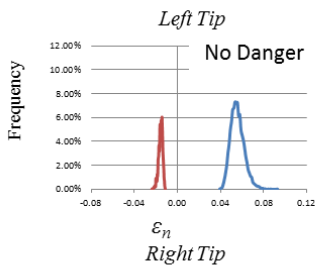


$$EV(\bar{s}_{(100g)}) - EV(\bar{s}_{(100(g-1))}) \leq \frac{SD(\bar{s}_{(100)})}{EV(\bar{s}_{(100)})\sqrt{n_{max}}}$$

with $g = 1, \dots, 100$ and $n_{max} = 10,000$

Converged if satisfied three times continuously

Model is convergence at 2,000 cases



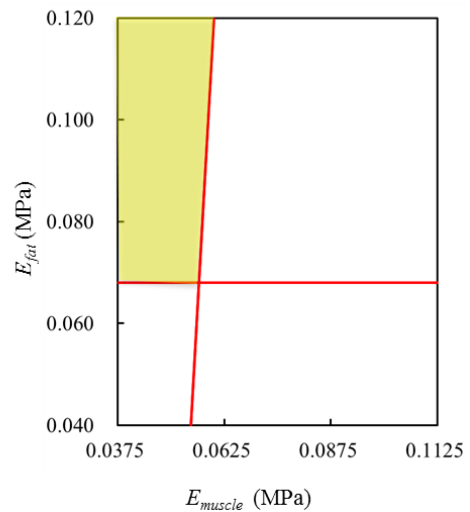
Threshold: $\varepsilon_n^{\text{nocutout}} \quad |\gamma_m|^{\text{nocutout}}$

Target: $\varepsilon_n \quad |\gamma_m|$

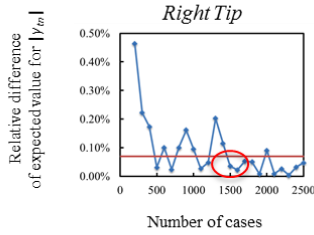
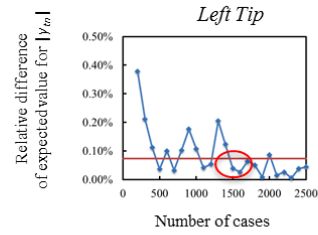
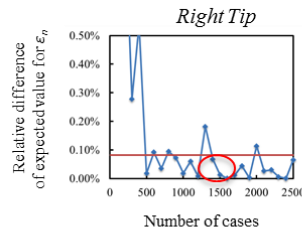
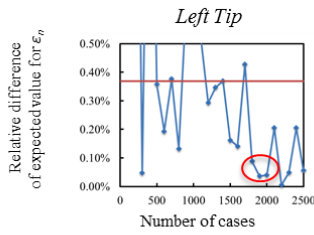
If $\varepsilon_n \geq \varepsilon_n^{\text{nocutout}}$ or $|\gamma_m| \geq |\gamma_m|^{\text{nocutout}}$
then fibril tissue damage may propagate

$$LSZ_{E_{muscle} E_{fat}} = \{s; p_a E_{muscle} + q_a E_{fat} + r_a \geq 0 \forall a\}$$

a	p_a	q_a	r_a
1	-0.996	0.067	0.052
2	0	1	-0.068



$$I_{fm} = 22.92 \quad b = \text{supine} \quad L_a = 4 \quad a_{mid} = 104.38$$

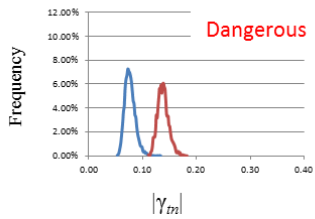
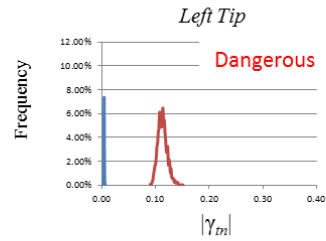
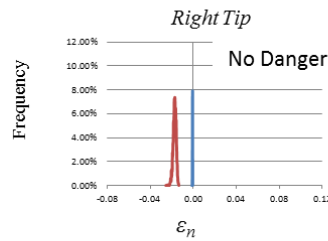
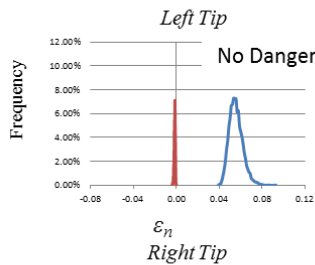


$$EV(\bar{s}_{(100g)}) - EV(\bar{s}_{(100(g-1))}) \leq \frac{SD(\bar{s}_{(100)})}{EV(\bar{s}_{(100)})\sqrt{n_{max}}}$$

with $g = 1, \dots, 100$ and $n_{max} = 10,000$

Converged if satisfied three times continuously

Model is convergence at 2,000 cases



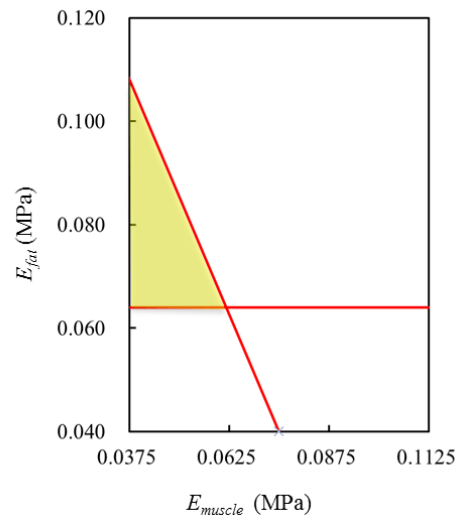
Threshold: $\varepsilon_n^{\text{nocutout}} \quad |\gamma_m|^{\text{nocutout}}$

Target: $\varepsilon_n \quad |\gamma_m|$

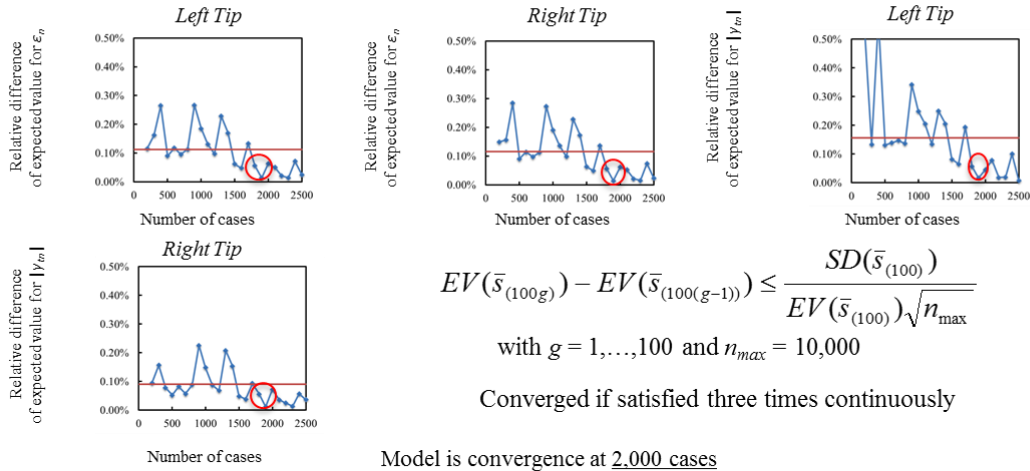
If $\varepsilon_n \geq \varepsilon_n^{\text{nocutout}}$ or $|\gamma_m| \geq |\gamma_m|^{\text{nocutout}}$
then fibril tissue damage may propagate

$$LSZ_{E_{muscle} E_{fat}} = \{s; p_a E_{muscle} + q_a E_{fat} + r_a \geq 0 \forall a\}$$

a	p_a	q_a	r_a
1	-0.874	-0.479	0.085
2	0	1	0.064



$$I_{fm} = 22.92 \quad b = \text{supine} \quad L_a = 4 \quad a_{mid} = 166.63$$

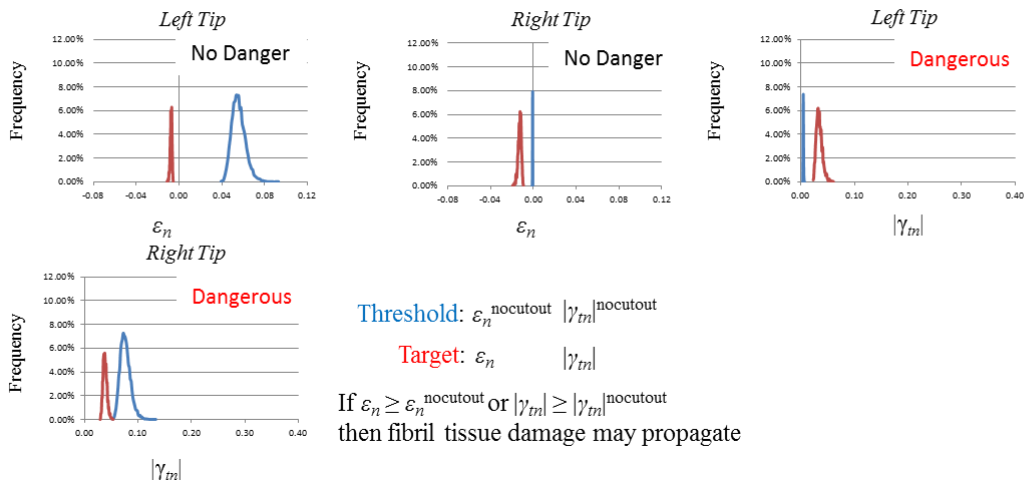


$$EV(\bar{s}_{(100g)}) - EV(\bar{s}_{(100(g-1))}) \leq \frac{SD(\bar{s}_{(100)})}{EV(\bar{s}_{(100)})\sqrt{n_{max}}}$$

with $g = 1, \dots, 100$ and $n_{max} = 10,000$

Converged if satisfied three times continuously

Model is convergence at 2.000 cases



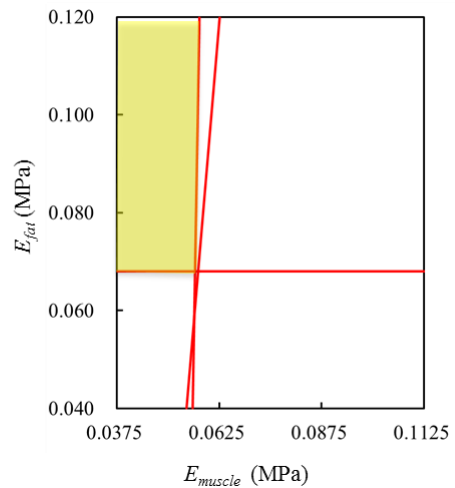
Threshold: $\epsilon_n^{nocutout} \quad |\gamma_{fm}|^{nocutout}$

Target: $\epsilon_n \quad |\gamma_{fm}|$

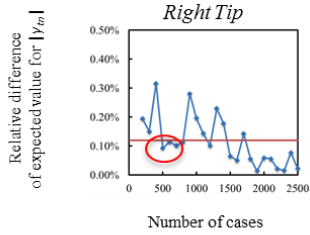
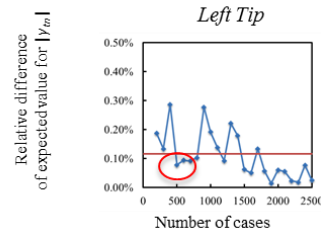
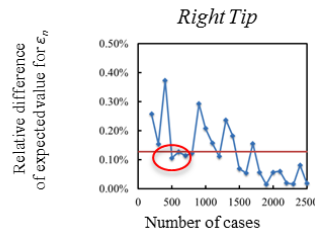
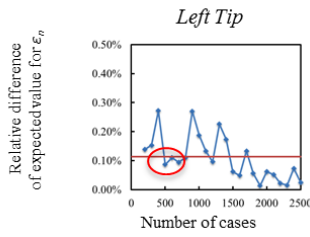
If $\epsilon_n \geq \epsilon_n^{nocutout}$ or $|\gamma_{fm}| \geq |\gamma_{fm}|^{nocutout}$
then fibril tissue damage may propagate

$$LSZ_{E_{muscle} E_{fat}} = \{s; p_a E_{muscle} + q_a E_{fat} + r_a \geq 0 \forall a\}$$

a	p_a	q_a	r_a
1	-0.994	0.101	0.05
2	-0.998	0.02	0.055
3	0	1	-0.068



$$I_{fm} = 22.92 \quad b = \text{supine} \quad L_a = 8 \quad a_{mid} = 42.23$$

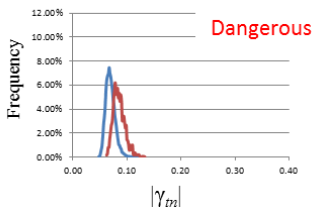
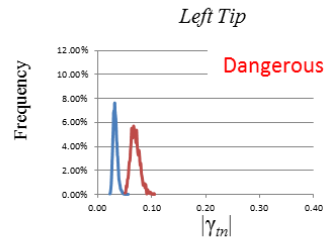
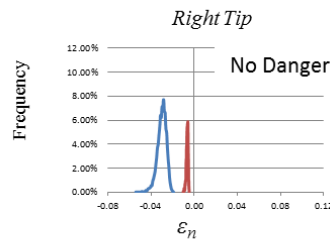
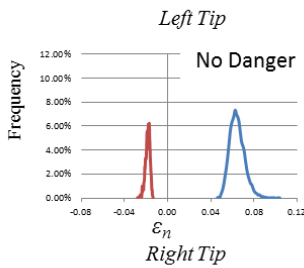


$$EV(\bar{s}_{(100g)}) - EV(\bar{s}_{(100(g-1))}) \leq \frac{SD(\bar{s}_{(100)})}{EV(\bar{s}_{(100)})\sqrt{n_{max}}}$$

with $g = 1, \dots, 100$ and $n_{max} = 10,000$

Converged if satisfied three times continuously

Model is convergence at 700 cases



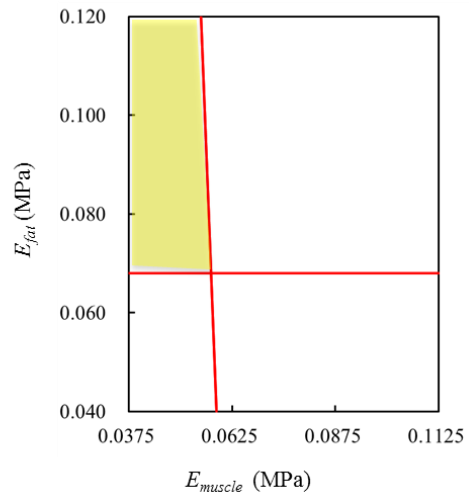
Threshold: $\epsilon_n^{\text{nocutout}} \quad |\gamma_m|^{\text{nocutout}}$

Target: $\epsilon_n \quad |\gamma_m|$

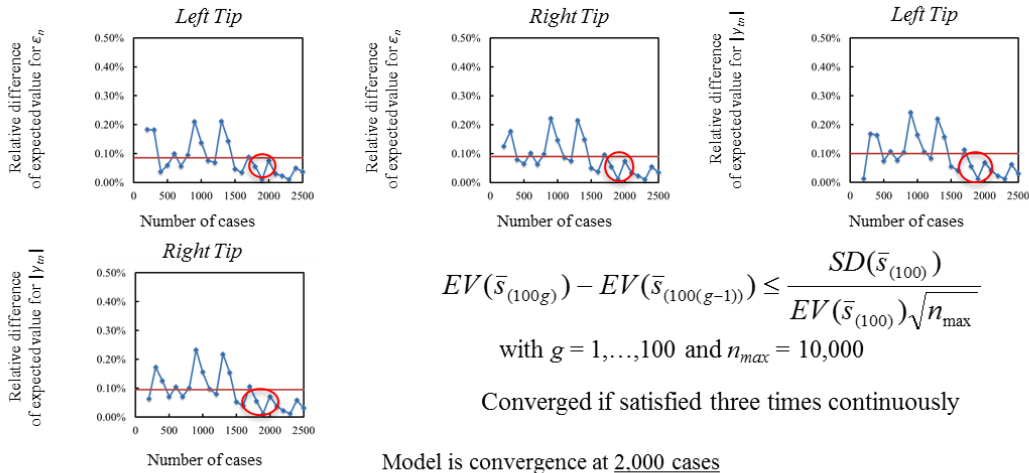
If $\epsilon_n \geq \epsilon_n^{\text{nocutout}}$ or $|\gamma_m| \geq |\gamma_m|^{\text{nocutout}}$
then fibril tissue damage may propagate

$$LSZ_{E_{muscle} E_{fat}} = \{s; p_a E_{muscle} + q_a E_{fat} + r_a \geq 0 \forall a\}$$

a	p_a	q_a	r_a
1	-0.997	-0.047	0.061
2	0	1	-0.068



$$I_{fm} = 22.92 \quad b = \text{supine} \quad L_a = 8 \quad a_{mid} = 104.38$$

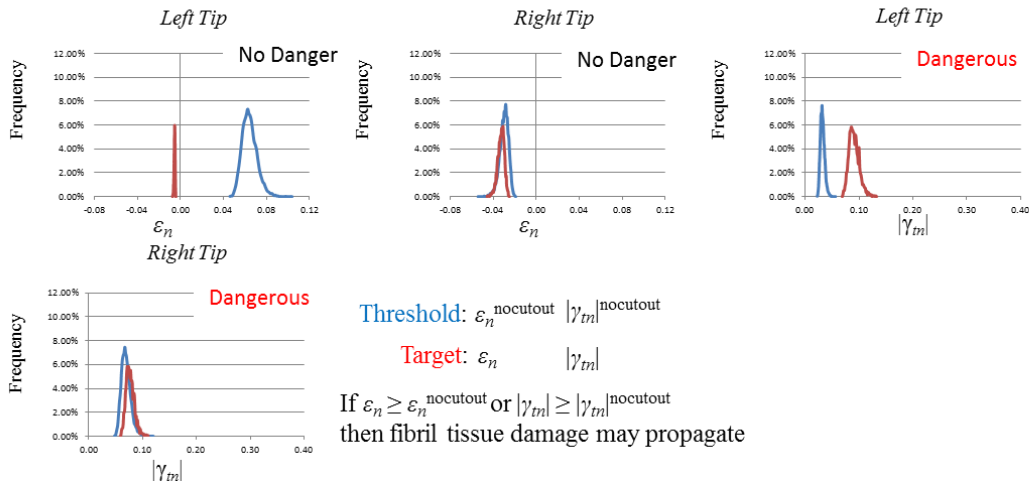


$$EV(\bar{s}_{(100g)}) - EV(\bar{s}_{(100(g-1))}) \leq \frac{SD(\bar{s}_{(100)})}{EV(\bar{s}_{(100)})\sqrt{n_{max}}}$$

with $g = 1, \dots, 100$ and $n_{max} = 10,000$

Converged if satisfied three times continuously

Model is convergence at 2,000 cases



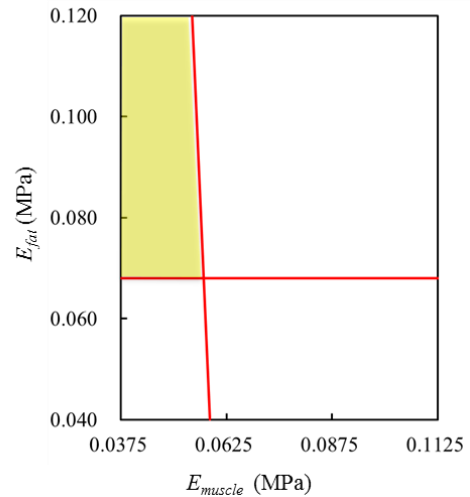
Threshold: $\epsilon_n^{\text{nocutout}} \quad |\gamma_m|^{\text{nocutout}}$

Target: $\epsilon_n \quad |\gamma_m|$

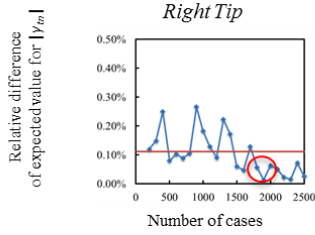
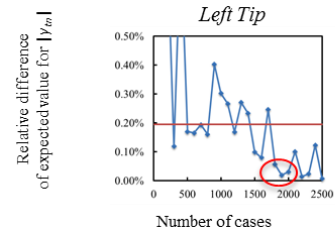
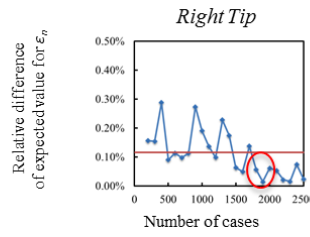
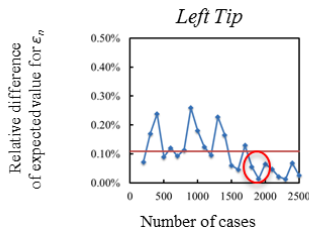
If $\epsilon_n \geq \epsilon_n^{\text{nocutout}}$ or $|\gamma_m| \geq |\gamma_m|^{\text{nocutout}}$
then fibril tissue damage may propagate

$$LSZ_{E_{muscle}E_{fat}} = \{s; p_a E_{muscle} + q_a E_{fat} + r_a \geq 0 \forall a\}$$

a	p_a	q_a	r_a
1	-0.997	-0.053	0.061
2	0	1	-0.068



$$I_{fm} = 22.92 \quad b = \text{supine} \quad L_a = 8 \quad a_{mid} = 166.63$$

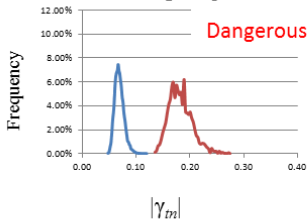
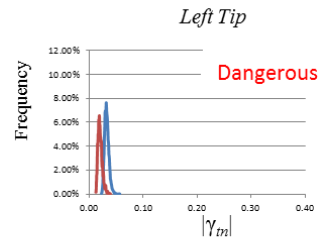
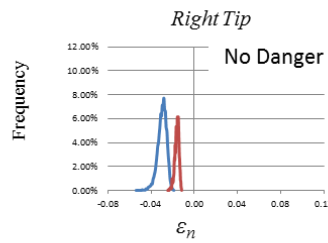
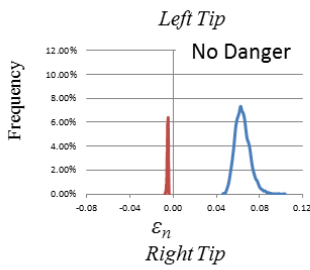


$$EV(\bar{s}_{(100g)}) - EV(\bar{s}_{(100(g-1))}) \leq \frac{SD(\bar{s}_{(100)})}{EV(\bar{s}_{(100)})\sqrt{n_{max}}}$$

with $g = 1, \dots, 100$ and $n_{max} = 10,000$

Converged if satisfied three times continuously

Model is convergence at 2,000 cases



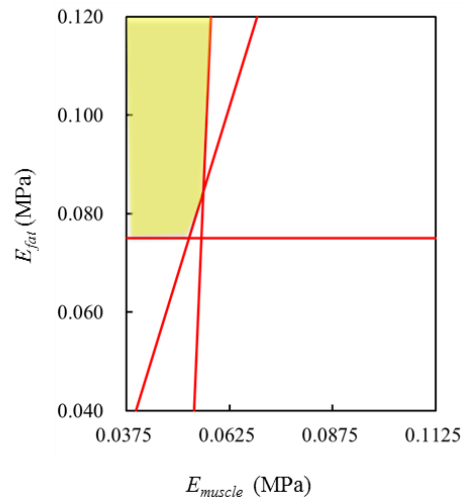
Threshold: $\varepsilon_n^{\text{nocutout}} \quad |\gamma_m|^{\text{nocutout}}$

Target: $\varepsilon_n \quad |\gamma_m|$

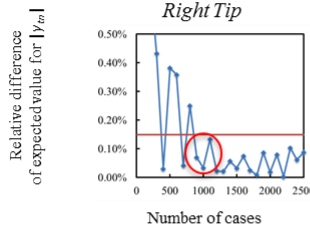
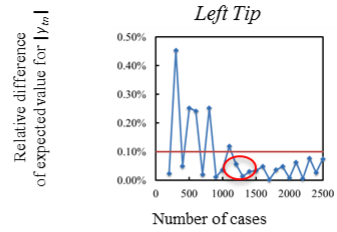
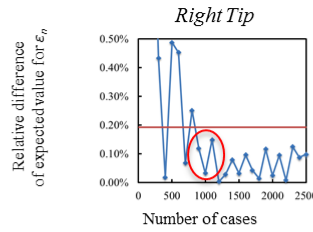
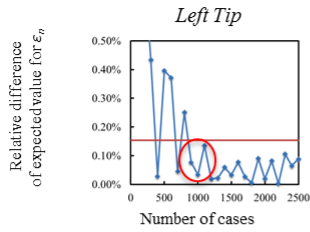
If $\varepsilon_n \geq \varepsilon_n^{\text{nocutout}}$ or $|\gamma_m| \geq |\gamma_m|^{\text{nocutout}}$
then fibril tissue damage may propagate

$$LSZ_{E_{muscle} E_{fat}} = \{s; p_a E_{muscle} + q_a E_{fat} + r_a \geq 0 \forall a\}$$

a	p_a	q_a	r_a
1	-0.939	0.344	0.023
2	-0.997	0.05	0.052
3	0	1	-0.075



$$I_{fm} = 22.92 \quad b = \text{lateral-A} \quad L_a = 4 \quad a_{mid} = 42.23$$

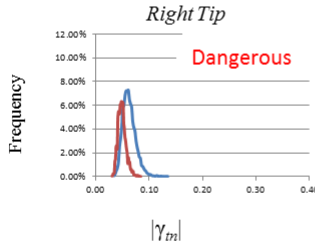
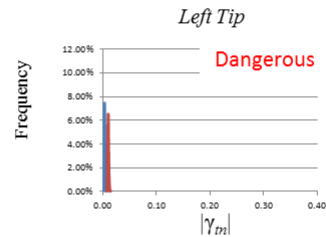
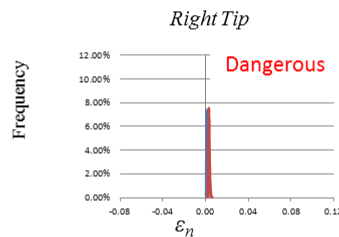
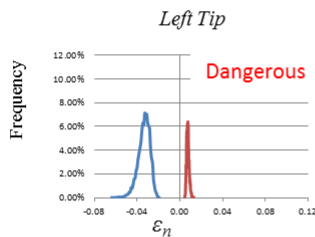


$$EV(\bar{s}_{(100g)}) - EV(\bar{s}_{(100(g-1))}) \leq \frac{SD(\bar{s}_{(100)})}{EV(\bar{s}_{(100)})\sqrt{n_{max}}}$$

with $g = 1, \dots, 100$ and $n_{max} = 10,000$

Converged if satisfied three times continuously

Model is convergence at 1,400 cases



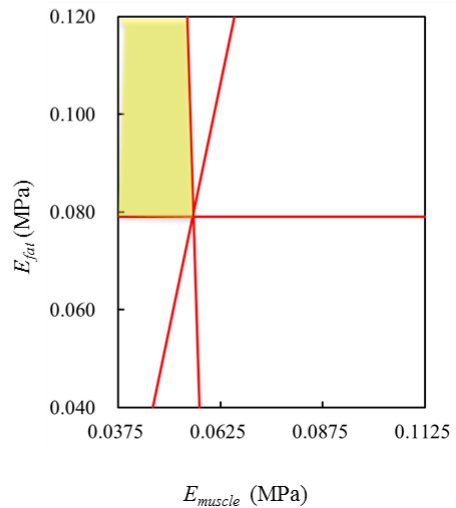
Threshold: $\varepsilon_n^{\text{nocutout}} \quad |\gamma_m|^{\text{nocutout}}$

Target: $\varepsilon_n \quad |\gamma_m|$

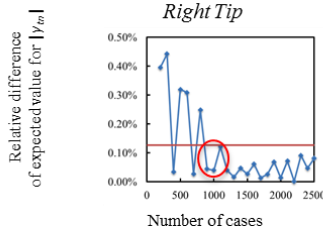
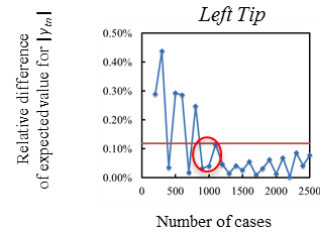
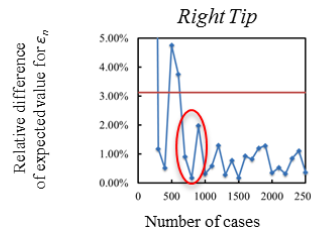
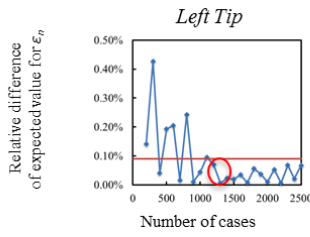
If $\varepsilon_n \geq \varepsilon_n^{\text{nocutout}}$ or $|\gamma_m| \geq |\gamma_m|^{\text{nocutout}}$
then fibril tissue damage may propagate

$$LSZ_{E_{muscle} E_{fat}} = \{s; p_a E_{muscle} + q_a E_{fat} + r_a \geq 0 \forall a\}$$

a	p_a	q_a	r_a
1	-0.998	-0.038	0.059
2	-0.97	0.242	0.035
3	0	1	-0.079



$$I_{fm} = 22.92 \quad b = \text{lateral-A} \quad L_a = 4 \quad a_{mid} = 104.38$$

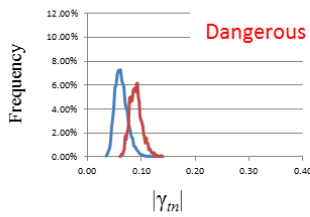
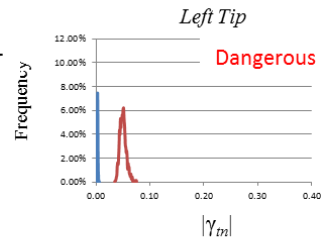
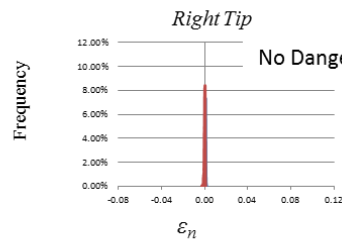
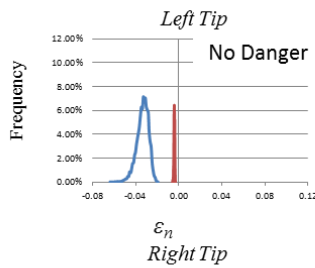


$$EV(\bar{s}_{(100g)}) - EV(\bar{s}_{(100(g-1))}) \leq \frac{SD(\bar{s}_{(100)})}{EV(\bar{s}_{(100)})\sqrt{n_{max}}}$$

with $g = 1, \dots, 100$ and $n_{max} = 10,000$

Converged if satisfied three times continuously

Model is convergence at 1,400 cases



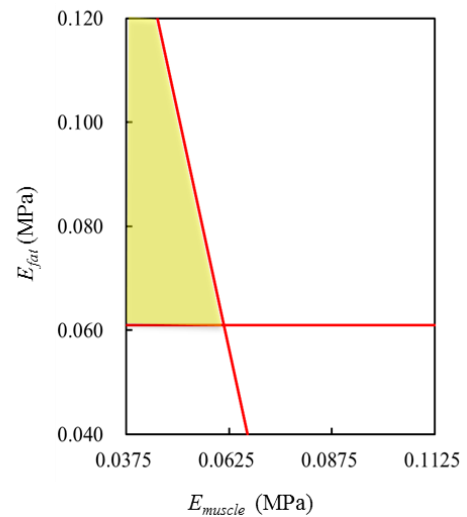
Threshold: $\epsilon_n^{nocutout} \quad |\gamma_m|^{nocutout}$

Target: $\epsilon_n \quad |\gamma_m|$

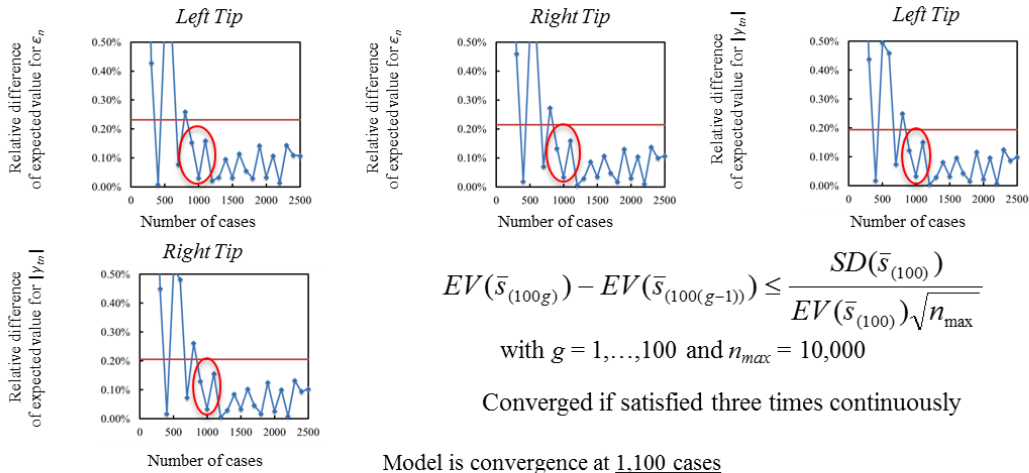
If $\epsilon_n \geq \epsilon_n^{nocutout}$ or $|\gamma_m| \geq |\gamma_m|^{nocutout}$
then fibril tissue damage may propagate

$$LSZ_{E_{muscle} E_{fat}} = \{s; p_a E_{muscle} + q_a E_{fat} + r_a \geq 0 \forall a\}$$

a	p_a	q_a	r_a
1	-0.962	-0.263	0.075
2	0	1	-0.061



$$I_{fm} = 22.92 \quad b = \text{lateral-A} \quad L_a = 4 \quad a_{mid} = 166.63$$

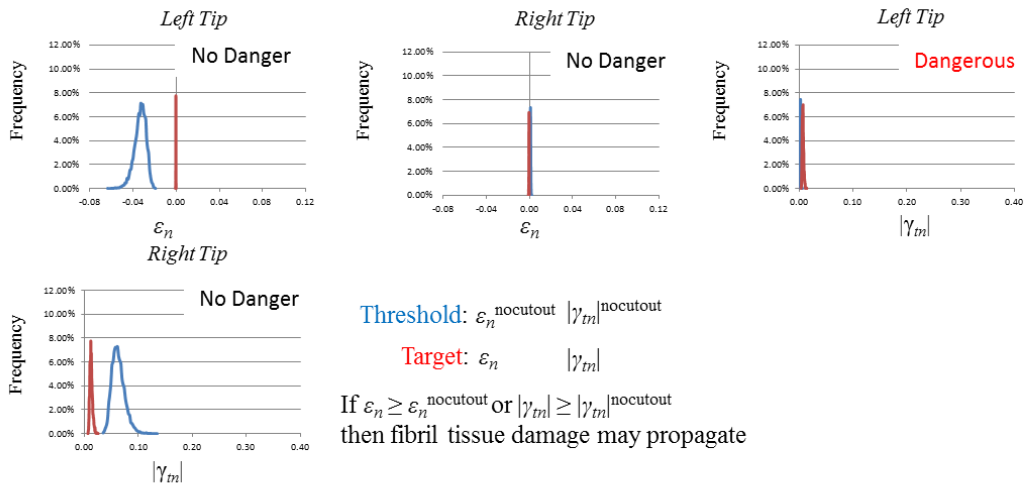


$$EV(\bar{s}_{(100g)}) - EV(\bar{s}_{(100(g-1))}) \leq \frac{SD(\bar{s}_{(100)})}{EV(\bar{s}_{(100)})\sqrt{n_{max}}}$$

with $g = 1, \dots, 100$ and $n_{max} = 10,000$

Converged if satisfied three times continuously

Model is convergence at 1,100 cases



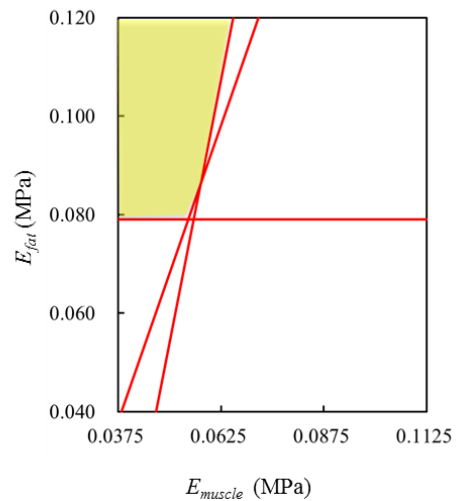
Threshold: $\epsilon_n^{nocutout} \quad |\gamma_m|^{nocutout}$

Target: $\epsilon_n \quad |\gamma_m|$

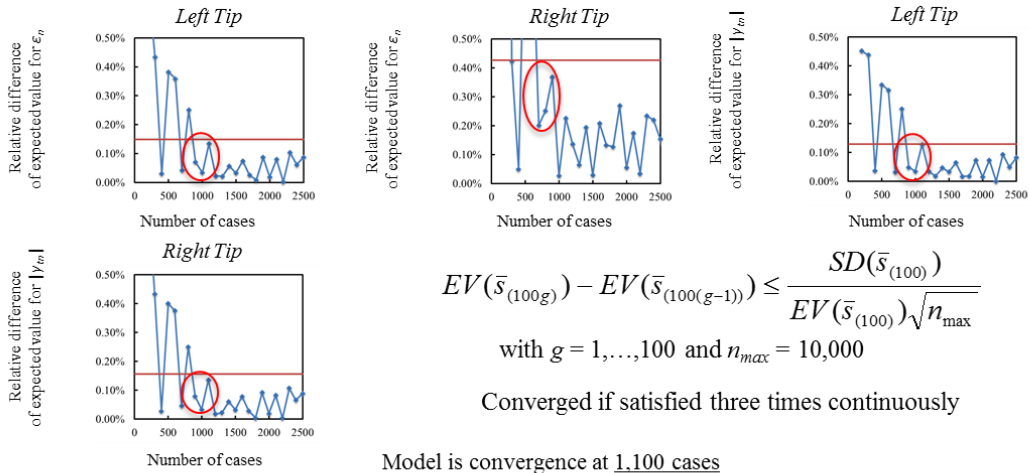
If $\epsilon_n \geq \epsilon_n^{nocutout}$ or $|\gamma_m| \geq |\gamma_m|^{nocutout}$
then fibril tissue damage may propagate

$$LSZ_{E_{muscle} E_{fat}} = \{s; p_a E_{muscle} + q_a E_{fat} + r_a \geq 0 \forall a\}$$

a	p_a	q_a	r_a
1	-0.973	0.23	0.036
2	-0.923	0.385	0.02
3	0	1	-0.079



$$I_{fm} = 22.92 \quad b = \text{lateral-A} \quad L_a = 8 \quad a_{mid} = 42.23$$

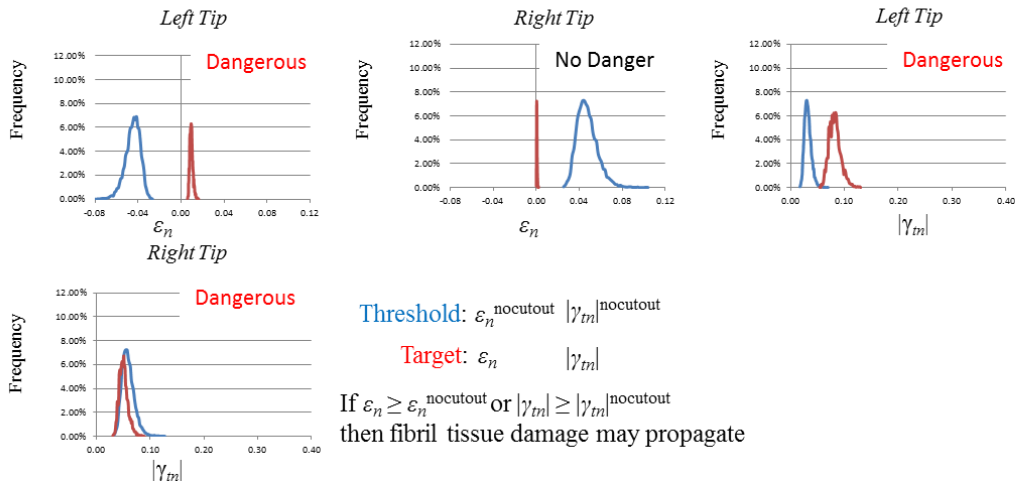


$$EV(\bar{s}_{(100g)}) - EV(\bar{s}_{(100(g-1))}) \leq \frac{SD(\bar{s}_{(100)})}{EV(\bar{s}_{(100)})\sqrt{n_{max}}}$$

with $g = 1, \dots, 100$ and $n_{max} = 10,000$

Converged if satisfied three times continuously

Model is convergence at 1.100 cases



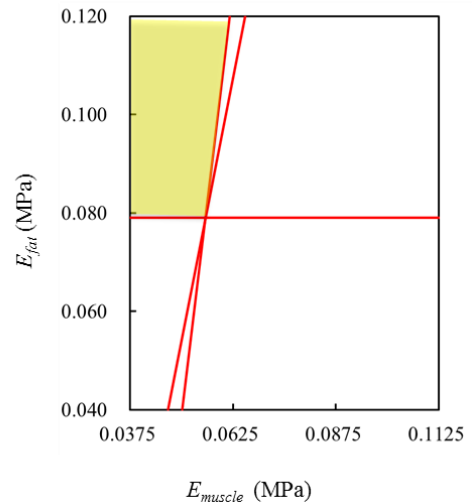
Threshold: $\epsilon_n^{nocutout} \quad |\gamma_m|^{nocutout}$

Target: $\epsilon_n \quad |\gamma_m|$

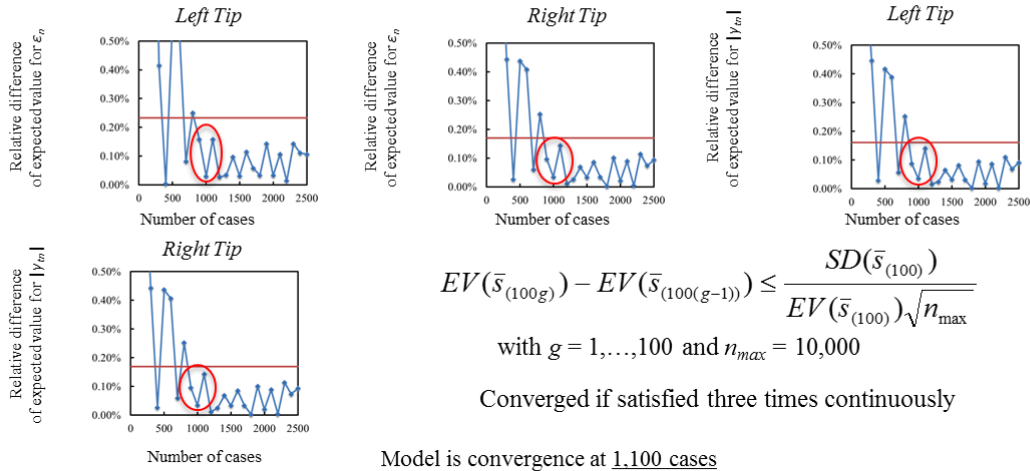
If $\epsilon_n \geq \epsilon_n^{nocutout}$ or $|\gamma_m| \geq |\gamma_m|^{nocutout}$
then fibril tissue damage may propagate

$$LSZ_{E_{muscle}E_{fat}} = \{s; p_a E_{muscle} + q_a E_{fat} + r_a \geq 0 \forall a\}$$

a	p_a	q_a	r_a
1	-0.973	0.23	0.036
2	-0.989	0.143	0.044
3	0	1	-0.079



$$I_{fm} = 22.92 \quad b = \text{lateral-A} \quad L_a = 8 \quad a_{mid} = 104.38$$

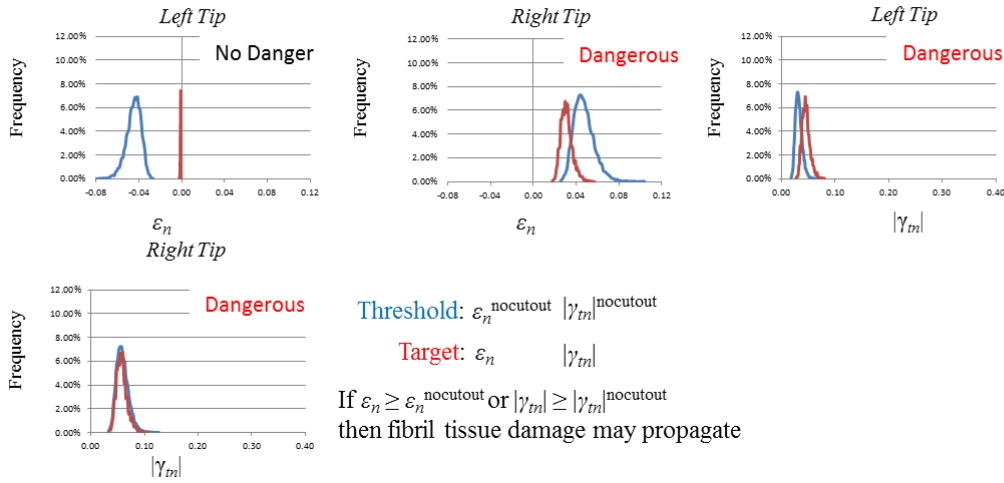


$$EV(\bar{s}_{(100g)}) - EV(\bar{s}_{(100(g-1))}) \leq \frac{SD(\bar{s}_{(100)})}{EV(\bar{s}_{(100)})\sqrt{n_{max}}}$$

with $g = 1, \dots, 100$ and $n_{max} = 10,000$

Converged if satisfied three times continuously

Model is convergence at 1,100 cases



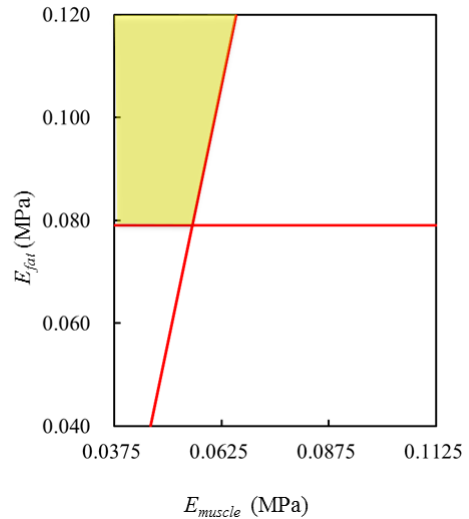
Threshold: $\epsilon_n^{nocutout} \quad |\gamma_{fm}|^{nocutout}$

Target: $\epsilon_n \quad |\gamma_{fm}|$

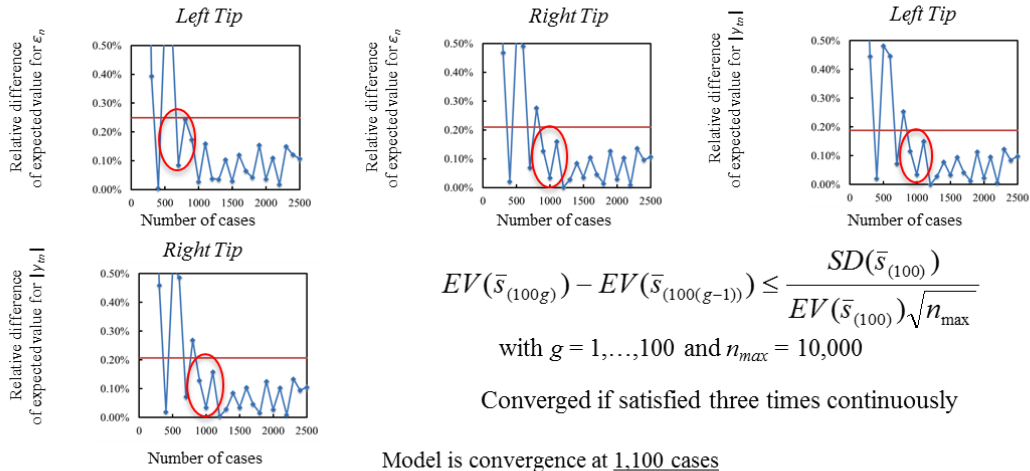
If $\epsilon_n \geq \epsilon_n^{nocutout}$ or $|\gamma_{fm}| \geq |\gamma_{fm}|^{nocutout}$
then fibril tissue damage may propagate

$$LSZ_{E_{muscle} E_{fat}} = \{s; p_a E_{muscle} + q_a E_{fat} + r_a \geq 0 \forall a\}$$

a	p_a	q_a	r_a
1	-0.97	0.242	0.035
2	0	1	-0.079



$$I_{fm} = 22.92 \quad b = \text{lateral-A} \quad L_a = 8 \quad a_{mid} = 166.63$$

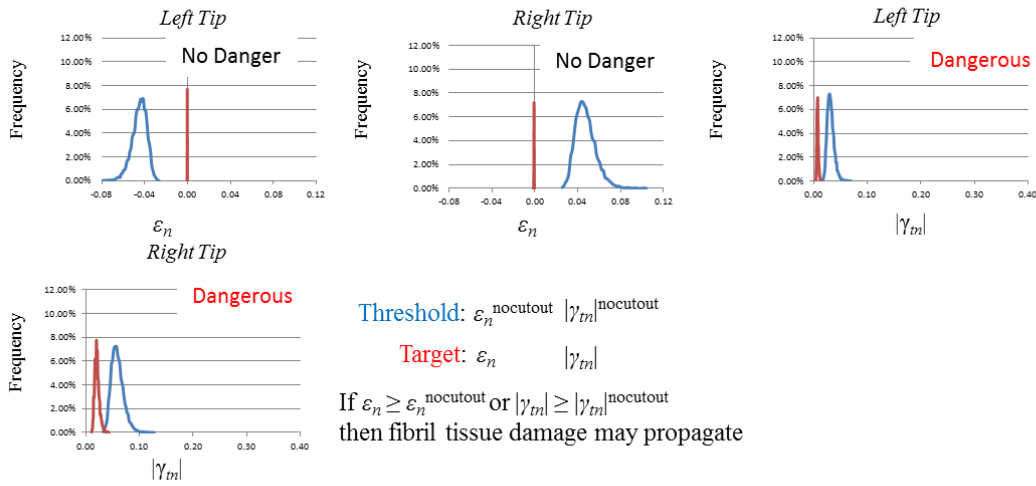


$$EV(\bar{s}_{(100g)}) - EV(\bar{s}_{(100(g-1))}) \leq \frac{SD(\bar{s}_{(100)})}{EV(\bar{s}_{(100)})\sqrt{n_{max}}}$$

with $g = 1, \dots, 100$ and $n_{max} = 10,000$

Converged if satisfied three times continuously

Model is convergence at 1.100 cases



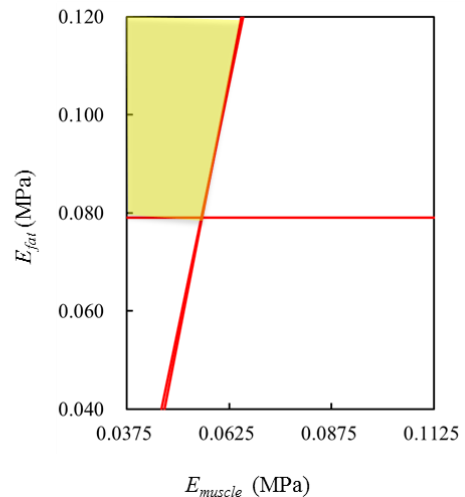
Threshold: $\epsilon_n^{nocutout} \quad |\gamma_m|^{nocutout}$

Target: $\epsilon_n \quad |\gamma_m|$

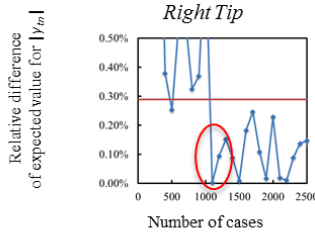
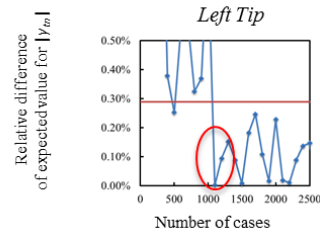
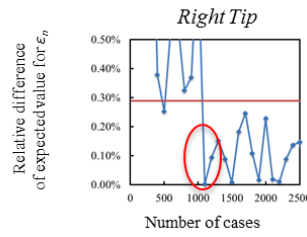
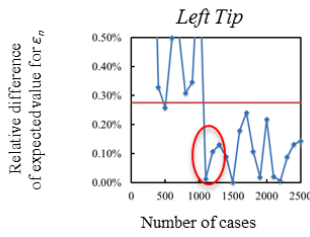
If $\epsilon_n \geq \epsilon_n^{nocutout}$ or $|\gamma_m| \geq |\gamma_m|^{nocutout}$ then fibril tissue damage may propagate

$$LSZ_{E_{muscle} E_{fat}} = \{s; p_a E_{muscle} + q_a E_{fat} + r_a \geq 0 \forall a\}$$

a	p_a	q_a	r_a
1	-0.97	0.242	0.035
2	-0.973	0.23	0.036
3	0	1	-0.079



$$I_{fm} = 22.92 \quad b = \text{lateral-B} \quad L_a = 4 \quad a_{mid} = 42.23$$

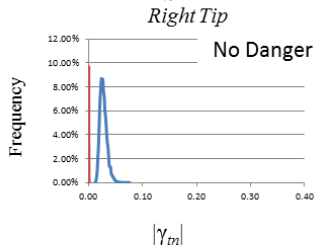
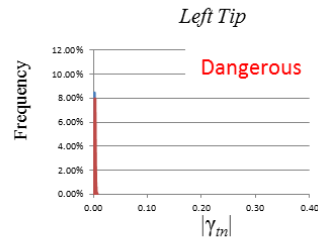
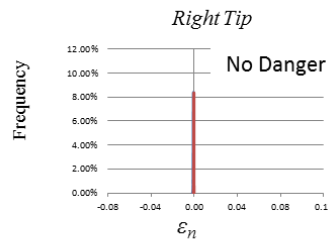
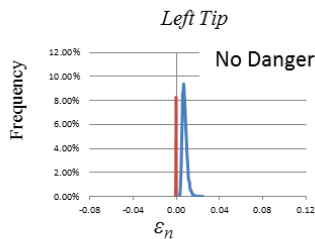


$$EV(\bar{s}_{(100g)}) - EV(\bar{s}_{(100(g-1))}) \leq \frac{SD(\bar{s}_{(100)})}{EV(\bar{s}_{(100)})\sqrt{n_{max}}}$$

with $g = 1, \dots, 100$ and $n_{max} = 10,000$

Converged if satisfied three times continuously

Model is convergence at 1,300 cases



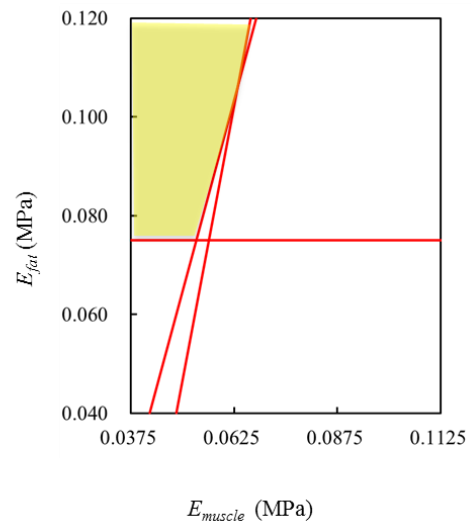
Threshold: $\varepsilon_n^{\text{nocutout}} \quad |\gamma_m|^{\text{nocutout}}$

Target: $\varepsilon_n \quad |\gamma_m|$

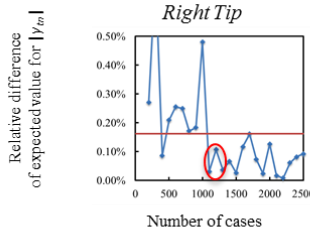
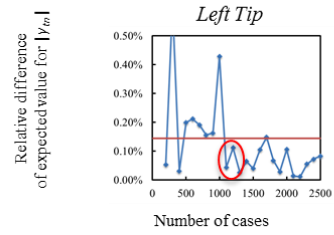
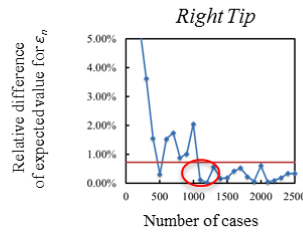
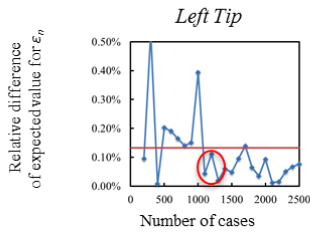
If $\varepsilon_n \geq \varepsilon_n^{\text{nocutout}}$ or $|\gamma_m| \geq |\gamma_m|^{\text{nocutout}}$
then fibril tissue damage may propagate

$$LSZ_{E_{muscle} E_{fat}} = \{s; p_a E_{muscle} + q_a E_{fat} + r_a \geq 0 \forall a\}$$

a	p_a	q_a	r_a
1	-0.952	0.306	0.028
2	-0.975	0.22	0.038
3	0	1	-0.075



$$I_{fm} = 22.92 \quad b = \text{lateral-B} \quad L_a = 4 \quad a_{mid} = 104.38$$

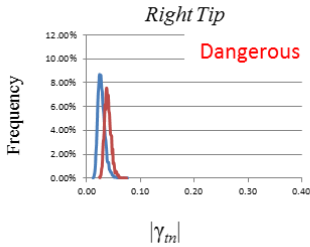
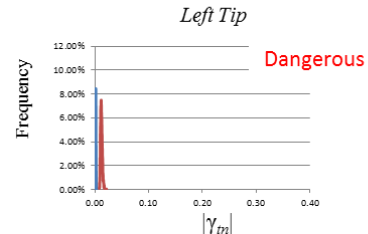
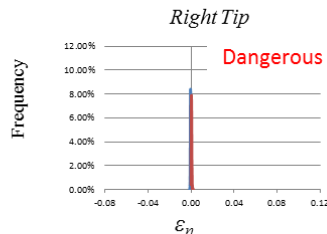
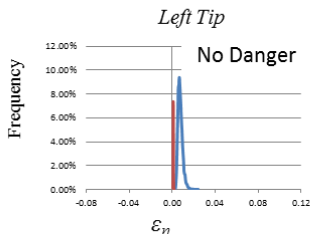


$$EV(\bar{s}_{(100g)}) - EV(\bar{s}_{(100(g-1))}) \leq \frac{SD(\bar{s}_{(100)})}{EV(\bar{s}_{(100)})\sqrt{n_{max}}}$$

with $g = 1, \dots, 100$ and $n_{max} = 10,000$

Converged if satisfied three times continuously

Model is convergence at 1,300 cases



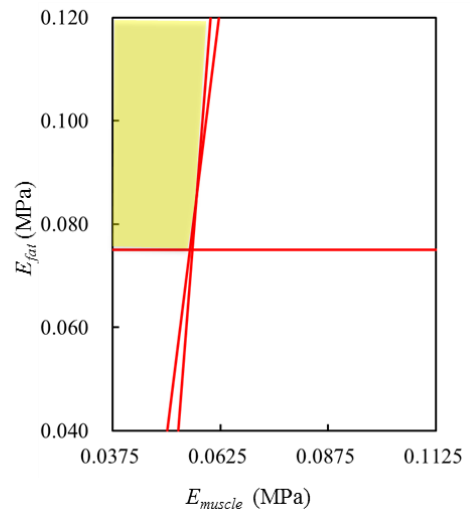
Threshold: $\varepsilon_n^{nocutout} \quad |\gamma_m|^{nocutout}$

Target: $\varepsilon_n \quad |\gamma_m|$

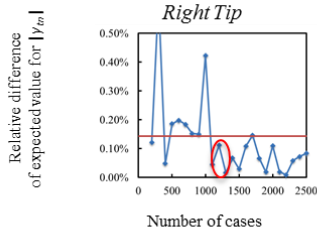
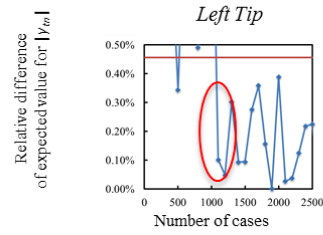
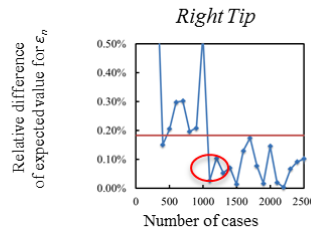
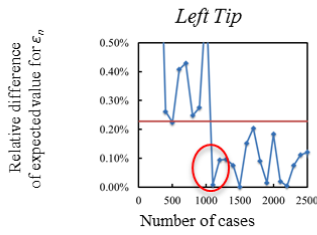
If $\varepsilon_n \geq \varepsilon_n^{nocutout}$ or $|\gamma_m| \geq |\gamma_m|^{nocutout}$
then fibril tissue damage may propagate

$$LSZ_{E_{muscle} E_{fat}} = \{s; p_a E_{muscle} + q_a E_{fat} + r_a \geq 0 \forall a\}$$

a	p_a	q_a	r_a
1	-0.995	0.092	0.049
2	-0.988	0.148	0.043
3	0	1	-0.075



$$I_{fm} = 22.92 \quad b = \text{lateral-B} \quad L_a = 4 \quad a_{mid} = 166.63$$

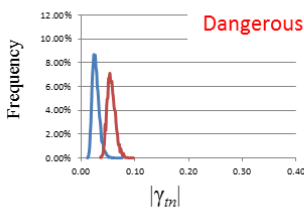
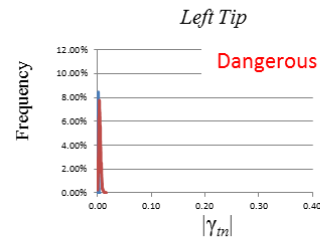
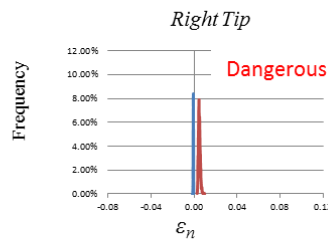
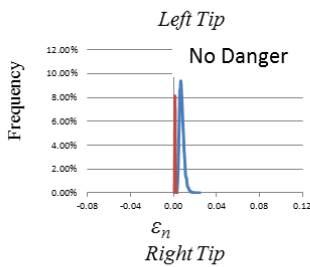


$$EV(\bar{s}_{(100g)}) - EV(\bar{s}_{(100(g-1))}) \leq \frac{SD(\bar{s}_{(100)})}{EV(\bar{s}_{(100)})\sqrt{n_{max}}}$$

with $g = 1, \dots, 100$ and $n_{max} = 10,000$

Converged if satisfied three times continuously

Model is convergence at 1,300 cases



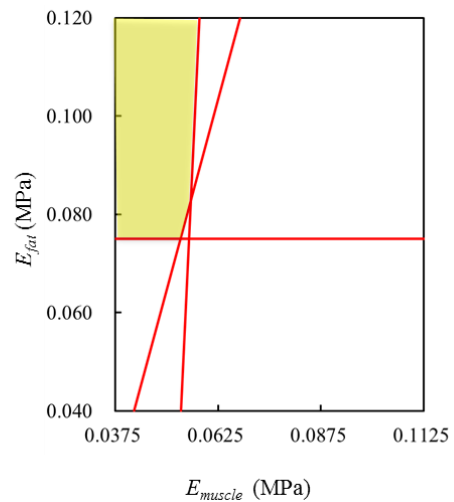
Threshold: $\varepsilon_n^{nocutout} \quad |\gamma_m|^{nocutout}$

Target: $\varepsilon_n \quad |\gamma_m|$

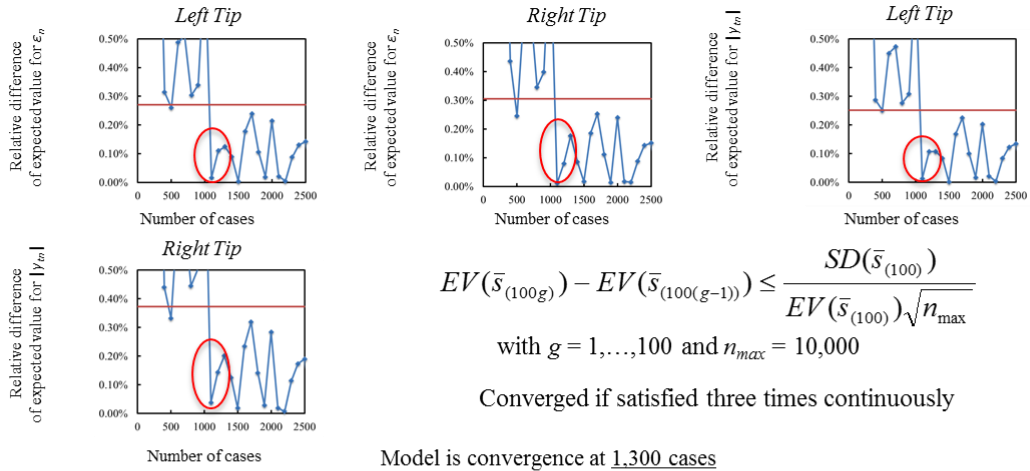
If $\varepsilon_n \geq \varepsilon_n^{nocutout}$ or $|\gamma_m| \geq |\gamma_m|^{nocutout}$
then fibril tissue damage may propagate

$$LSZ_{E_{muscle} E_{fat}} = \{s; p_a E_{muscle} + q_a E_{fat} + r_a \geq 0 \forall a\}$$

a	p_a	q_a	r_a
1	-0.952	0.306	0.028
2	-0.997	0.055	0.051
3	0	1	-0.075



$$I_{fm} = 22.92 \quad b = \text{lateral-B} \quad L_a = 8 \quad a_{mid} = 42.23$$

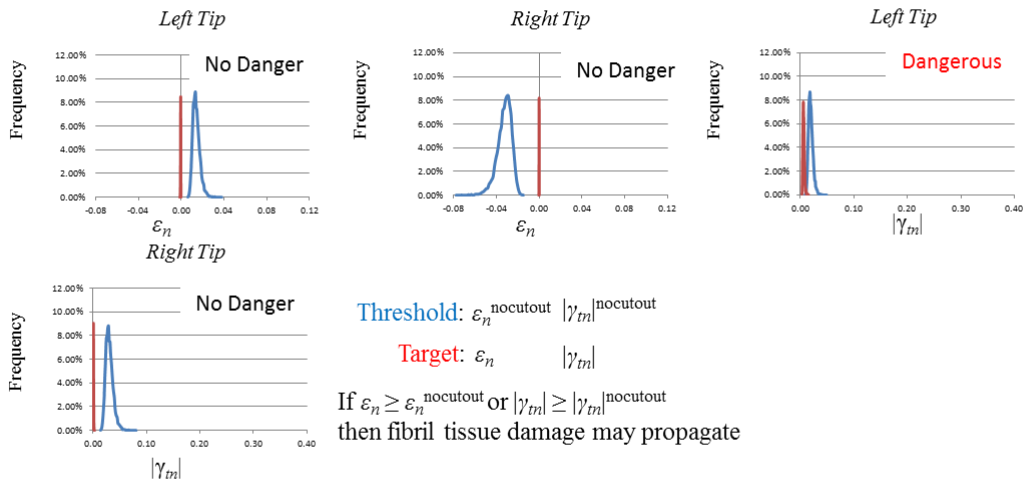


$$EV(\bar{s}_{(100g)}) - EV(\bar{s}_{(100(g-1))}) \leq \frac{SD(\bar{s}_{(100)})}{EV(\bar{s}_{(100)})\sqrt{n_{max}}}$$

with $g = 1, \dots, 100$ and $n_{max} = 10,000$

Converged if satisfied three times continuously

Model is convergence at 1.300 cases



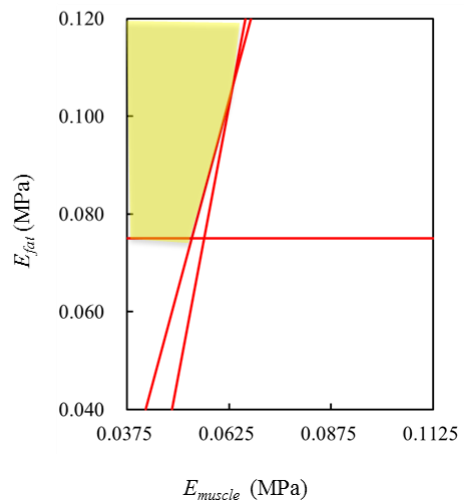
Threshold: $\epsilon_n^{\text{nocutout}} \quad |\gamma_m|^{\text{nocutout}}$

Target: $\epsilon_n \quad |\gamma_m|$

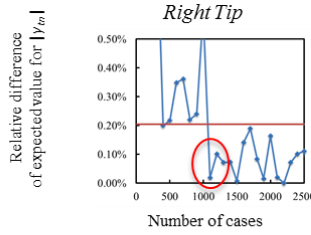
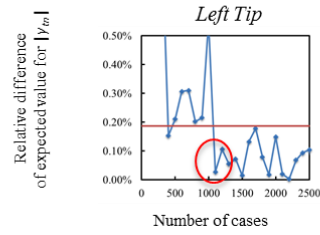
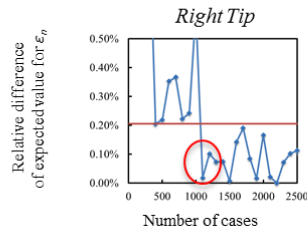
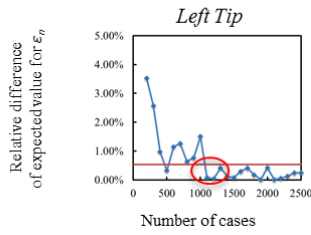
If $\epsilon_n \geq \epsilon_n^{\text{nocutout}}$ or $|\gamma_m| \geq |\gamma_m|^{\text{nocutout}}$
then fibril tissue damage may propagate

$$LSZ_{E_{muscle} E_{fat}} = \{s; p_a E_{muscle} + q_a E_{fat} + r_a \geq 0 \forall a\}$$

a	p_a	q_a	r_a
1	-0.952	0.306	0.028
2	-0.975	0.22	0.038
3	0	1	-0.075



$$I_{fm} = 22.92 \quad b = \text{lateral-B} \quad L_a = 8 \quad a_{mid} = 104.38$$

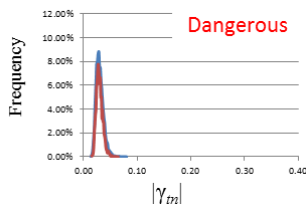
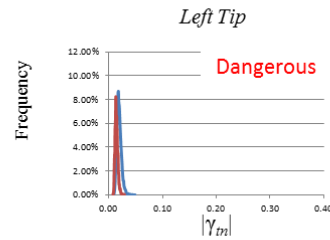
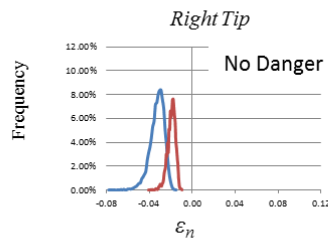
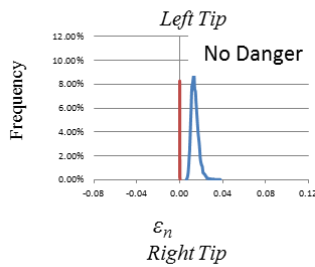


$$EV(\bar{s}_{(100g)}) - EV(\bar{s}_{(100(g-1))}) \leq \frac{SD(\bar{s}_{(100)})}{EV(\bar{s}_{(100)})\sqrt{n_{max}}}$$

with $g = 1, \dots, 100$ and $n_{max} = 10,000$

Converged if satisfied three times continuously

Model is convergence at 1,300 cases



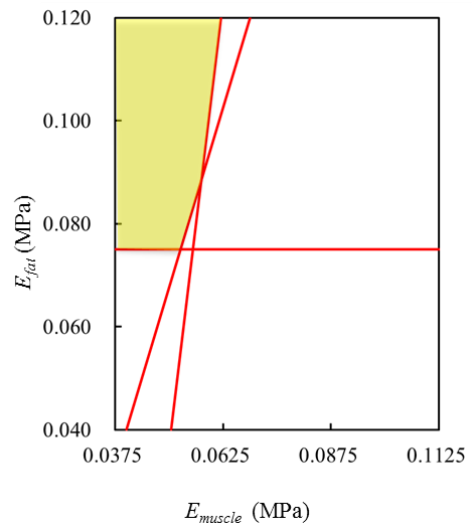
Threshold: $\varepsilon_n^{nocutout} \quad |\gamma_m|^{nocutout}$

Target: $\varepsilon_n \quad |\gamma_m|$

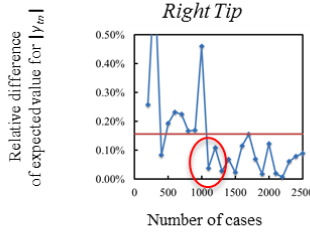
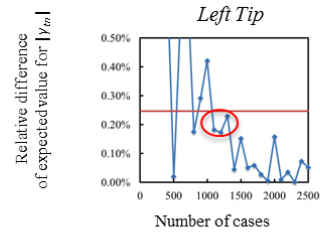
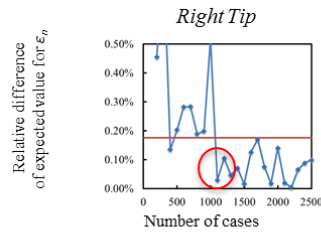
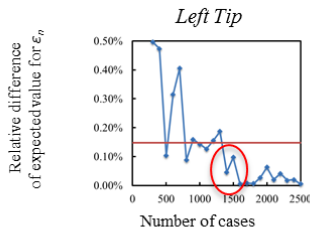
If $\varepsilon_n \geq \varepsilon_n^{nocutout}$ or $|\gamma_m| \geq |\gamma_m|^{nocutout}$
then fibril tissue damage may propagate

$$LSZ_{E_{muscle} E_{fat}} = \{s; p_a E_{muscle} + q_a E_{fat} + r_a \geq 0 \forall a\}$$

a	p_a	q_a	r_a
1	-0.942	0.336	0.024
2	-0.989	0.142	0.044
3	0	1	-0.075



$$I_{fm} = 22.92 \quad b = \text{lateral-B} \quad L_a = 8 \quad a_{mid} = 166.63$$

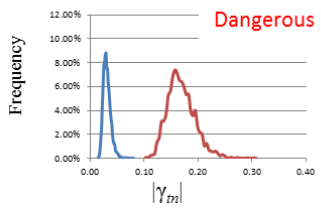
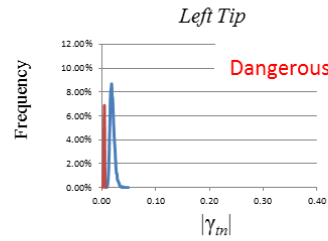
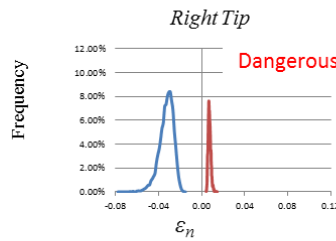
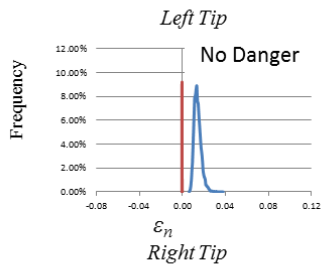


$$EV(\bar{s}_{(100g)}) - EV(\bar{s}_{(100(g-1))}) \leq \frac{SD(\bar{s}_{(100)})}{EV(\bar{s}_{(100)})\sqrt{n_{max}}}$$

with $g = 1, \dots, 100$ and $n_{max} = 10,000$

Converged if satisfied three times continuously

Model is convergence at 1,600 cases



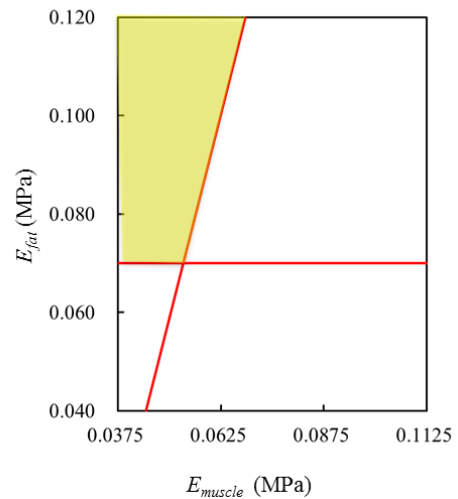
Threshold: $\varepsilon_n^{\text{nocutout}} \quad |\gamma_m|^{\text{nocutout}}$

Target: $\varepsilon_n \quad |\gamma_m|$

If $\varepsilon_n \geq \varepsilon_n^{\text{nocutout}}$ or $|\gamma_m| \geq |\gamma_m|^{\text{nocutout}}$
then fibril tissue damage may propagate

$$LSZ_{E_{muscle}E_{fat}} = \{s; p_a E_{muscle} + q_a E_{fat} + r_a \geq 0 \forall a\}$$

a	p_a	q_a	r_a
1	-0.957	0.287	0.031
2	0	1	-0.065



APPENDIX B

List of Publications

Articles on Periodicals

- 1) Samuel Susanto Slamet, Naoki Takano, Yoshiyuki Tanabe, Asako Hatano and Tomohisa Nagasao, Biomechanics Analysis of Pressure Ulcer using Damaged Interface Model between Bone and Muscle in the Human Buttock, Journal of Computational Science and Technology, 6 (2012) pp.70-80. (Published online: 2012/06/29)
- 2) Samuel Susanto Slamet, Kyouhei Hatano, Naoki Takano and Tomohisa Nagasao, Practical Monte Carlo Simulation Method Highlighting on Tail Probability with Application to Biomechanics Analysis of Pressure Ulcer, Transactions of Japan Society for Computational Engineering and Science, 2014 (2014), Paper No. 20140001. (Published online: 2014/02/07)

Articles on International Conference Proceedings

- 1) Samuel Susanto Slamet*, Naoki Takano and Tomohisa Nagasao, Uncertainty Modeling and Simulation Highlighting on Tail Probability in Biomechanics Study on Pressure Ulcer, CD-ROM Proceedings of the 5th Asia Pacific Congress on Computational Mechanics & 4th International Symposium on Computational Mechanics (APCOM 2013), Singapore, December 11-14, 2013.

Presentations at International Conferences

- 2) Samuel Susanto Slamet*, Naoki Takano and Tomohisa Nagasao, Biomechanics Analysis of Pressure Ulcer using Damaged Interface Model between Bone and Muscle, CD-ROM Proceedings of the 18th Congress of the European Society of Biomechanics (ESB2012), Lisbon, Portugal, July 1-4, 2012.
- 3) Samuel Susanto Slamet*, Naoki Takano, Kyohei Hatano and Tomohisa Nagasao, Local Strain Analysis of Human Buttock for Biomechanics Study on Pressure Ulcer Considering Uncertainty Factors and Tail Probability, CD-ROM Proceedings of the 7th Asian Pacific Conference on Biomechanics (APCB2013), Seoul, Korea, August 29-31, 2013.

Presentations at Domestic Conferences

- 1) Samuel Susanto Slamet*, Naoki Takano and Tomohisa Nagasao, Biomechanics Analysis of Pressure Ulcer Focusing on the Interface Strain between Bone and Muscle in the Buttock Model, 17th Conference of Japan Society of Mechanical Engineers Kanto Branch, Yokohama, March 18-19, 2011.
- 2) Samuel Susanto Slamet*, Naoki Takano and Tomohisa Nagasao, Interface Strain Analysis between Bone and Muscle for Biomechanical Study of Pressure Ulcer, 16th Conference on Computational Engineering and Science JSCES, Chiba, May 25-27, 2011.
- 3) Samuel Susanto Slamet*, Naoki Takano and Tomohisa Nagasao, Biomechanics Analysis of Pressure Ulcer using Damaged Interface Model between Bone and Muscle in the Human Buttocks, JSME 24th Computational Mechanics Conference (CMD2011), Okayama, October 8-10, 2011.

- 4) Samuel Susanto Slamet, Naoki Takano* and Tomohisa Nagasao, Uncertainty Modeling and Sampling Scheme with Focus on Tail Probability Applied to Biomechanics Simulation of Pressure Ulcer, 19th Conference on Computational Engineering and Science JSCES, Hiroshima, June 11-13, 2014.

REFERENCES

- Agache, P. and Humbert, P. (2004). *Measuring the Skin*. Springer.
- American Institute of Aeronautics and Astronautics. (1998). Guide for the Verification and Validation of Computational Fluid Dynamics Simulations. American Institute of Aeronautics and Astronautics, AIAA, AIAA-G-077-1998.
- Basaruddin, K.S., Takano, N. & Nakano, T. (2013). Stochastic multi-scale prediction on the apparent elastic moduli of trabecular bone considering uncertainties of biological apatite (BAP) crystallite orientation and image-based modeling. *Computer Methods in Biomechanics and Biomedical Engineering*, 1–13.
- Bansal, C., Scott, R., Stewart, D. and Cockerell, C. J. (2005). *Decubitus ulcers: a review of the literature*. *International Journal of Dermatology*, 44, 805–810.
- Bieda, B. (2012). *Stochastic Analysis in Production Process and Ecology under Uncertainty*. Springer.
- Brem, H., Lyder, C. (2004). *Protocol for the successful treatment of pressure ulcers*. *The American Journal of Surgery*, 188, 9S–17S.
- Bouten, C.V., Oomens, C.W., Baaijens, F.P., Bader, D.L. (2003). *The etiology of pressure sores: Skin deep or muscle bound?* *Archives of Physical Medicine and Rehabilitation*, 84, 616–619.
- Coleman, H. W. and Stern, F. (1997). *Uncertainties and CFD code validation*. *Journal of Fluids Engineering*, 119, 795–803
- Datta, D. & Kushwaha, H. (2011). Uncertainty Quantification Using Stochastic Response Surface Method Case Study--Transport of Chemical Contaminants through Groundwater. *International Journal of Energy, Information and Communications*, 2, 49–58.
- Dienstfrey, A.M. (2012). *Uncertainty Quantification in Scientific Computing*. Springer.
- Du, X. & Chen, W. (2001). A most probable point-based method for efficient uncertainty analysis. *Journal of Design and Manufacturing Automation*, 4, 47–66.
- Du, X., Chen, W. & Wang, Y. (2010). *Extreme Statistics in Nanoscale Memory Design*. Springer, Boston, MA.

- Elsner, P., Berardesca, E., Wilhelm, K. P. and Maibach, H. I. (2002). *Bioengineering of the Skin: Skin Biomechanics*. CRC Press.
- Gamerman, D. & Lopes, H.F. (2006). *Markov Chain Monte Carlo: Stochastic Simulation for Bayesian Inference*. 2nd Edition. Chapman & Hall.
- Haldar, A. & Mahadevan, S. (2000). *Reliability Assessment using Stochastic Finite Element Analysis*. John Wiley & Sons.
- Hastings, W. (1970). Monte Carlo sampling methods using Markov chains and their applications. *Biometrika*, 57, 97–109.
- Hellen, T. (2004). *A Roadmap of NAFEMS Documents*. NAFEMS Ref. R0087.
- Isukapalli, S.S., Roy, A. & Georgopoulos, P.G. (1998). Stochastic response surface methods (SRSMs) for uncertainty propagation: application to environmental and biological systems. *Risk Analysis*, 18, 351–63.
- Isukapalli, S.S., Roy, A. & Georgopoulos, P.G. (2000). Efficient sensitivity/uncertainty analysis using the combined stochastic response surface method and automated differentiation: application to environmental and biological systems. *Risk Analysis*, 20, 591–602.
- Kikuchi, N. and Oden, J. T. (1988). *Contact Problem in Elasticity: A Study of Variational Inequalities and Finite Element Methods*. SIAM.
- Li, D., Chen, Y., Lu, W. & Zhou, C. (2011). Stochastic response surface method for reliability analysis of rock slopes involving correlated non-normal variables. *Computers and Geotechnics*, 38, 58–68.
- Linder-Ganz, E., Shabshin, N., Itzchak, Y., Gefen, A. (2007). *Assessment of mechanical conditions in sub-dermal tissues during sitting: A combined experimental-MRI and finite element approach*. *Journal of Biomechanics*, 40, 1443–1454.
- Maeda, T. (2006). *Pressure ulcers resulting from earlier and more marked injury in the deeper layers – typical clinical cases and an insight into pocket formation*. *Japanese Journal of Pressure Ulcers*, 8, 195–202 (in Japanese).
- Makhsous, M., Lim, D., Hendrix, R., Bankard, J., Rymer, W.Z., Lin, F. (2007). *Finite element analysis for evaluation of pressure ulcer on the buttock: development and validation*. *IEEE Transactions on Neural Systems and Rehabilitation Engineering*, 15, 517–525.
- McKay, M., Beckman, R. & Conover, W. (2000). A comparison of three methods for selecting values of input variables in the analysis of output from a computer code. *Technometrics*, 21, 239–245.
- Metropolis, M., Rosenbluth, A.W., Rosenbluth, M.N., Teller, A.H. & Teller, E. (1953). Equations of state calculations by fast computing machines. *Journal of Chemical Physics*, 21, 1087–1092.

- Oberkampf, W.L., Trucano, T.G. & Hirsch, C. (2004). Verification, validation, and predictive capability in computational engineering and physics. *Applied Mechanics Reviews*, 57, 345.
- Oomens, C.W.J., Loerakker, S. & Bader, D.L. (2010). The importance of internal strain as opposed to interface pressure in the prevention of pressure related deep tissue injury. *Journal of tissue viability*, 19, 35–42.
- Rauh, A. (2011). *Modeling, Design, and Simulation of Systems with Uncertainties*.
- Reddy, M., Gill, S.S., Rochon, P.A. (2006). *Preventing pressure ulcers: systematic review*. The Journal of the American Medical Association, 296, 974–984.
- Romanelli, M., Clark, M., Cherry, G., Colin, D., Defloor, T. (2006). *Science and practice of pressure ulcer management*. Springer.
- Rubinstein, R.Y. & Kroese, D.P. (2008). *Simulation and the Monte Carlo Method*. 2nd Editio. John Wiley & Sons.
- Sakata, S., Ashida, F. & Iwahashi, D. (2013a). Stochastic Homogenization Analysis of a Particle Reinforced Composite Material using an Approximate Monte-Carlo Simulation with the Weighted Least Square Method. *Journal of Computational Science and Technology*, 7, 1–11.
- Sakata, S., Ashida, F. & Ohsumimoto, K. (2013b). Multiscale Stochastic Stress Analysis of a Porous Material with the Perturbation-Based Stochastic Homogenization Method for a Microscopic Geometrical Random Variation. *Journal of Computational Science and Technology*, 7, 99–112.
- Schenk, C.A. & Schuëller, G.I. (2005). *Uncertainty Assessment of Large Finite Element Systems*. Springer.
- Schoonhoven, L., Defloor, T., Grypdonck, M.H.F. (2002). *Incidence of pressure ulcers due to surgery*. Journal of Clinical Nursing, 11, 479–487.
- Stefanou, G. (2009). The stochastic finite element method: Past, present and future. *Computer Methods in Applied Mechanics and Engineering*, 198, 1031–1051.
- Takano, N., Asai, M. & Okamoto, K. (2012). Monte Carlo Simulation of Dynamic Problem Using Model Order Reduction Technique Highlighting on Tail Probability. *Journal of Computational Science and Technology*, 6, 169–181.
- Takano, N., Onishi, Y., Zako, M., and Nishiyabu, K. (2001). *Microstructure-based deep-drawing simulation of knitted fabric reinforced thermoplastics by homogenization theory*. International Journal of Solids and Structures, 38, 6333–6356.
- Thacker, B.H. (2008). *Why do Probabilistic Finite Element Analysis?* NAFEMS Ref. HT37.

- The American Society of Mechanical Engineers. (2006). *Guide for Verification and Validation in Computational Solid Mechanics*. 10–2006. ASME V&V.
- The American Society of Mechanical Engineers. (2009). *Standard for Verification and Validation in Computational Fluid Dynamics and Heat Transfer*. 20–2009. ASME V&V.
- The American Society of Mechanical Engineers. (2012). *An Illustration of the Concepts of Verification and Validation in Computational Solid Mechanics*. 10.1–2012. ASME V&V.
- The Japan Society for Computational Engineering and Science. (2011a). *A Model Procedure for Engineering Simulation*. JSCES S-HQC002:2011.
- The Japan Society for Computational Engineering and Science. (2011b). *Quality Management of Engineering Simulation*. JSCES S-HQC001:2011.
- Yamamoto, Y., Doi, Y., Akiyama, Y., Izumi, Y., Kimura, H. and Nishijima, S. (2008). *Biomechanical simulation for prevention of pressure ulcers (1.FEM simulation)*. Transactions of Japanese Society for Medical and Biological Engineering, 46, 489–494 (in Japanese).